

AD-A103 070

NAVAL UNDERWATER SYSTEMS CENTER NEWPORT RI
AN EXPERIMENTAL STUDY OF POLYMER DRAG REDUCTION AND BOUNDARY LA--ETC(U)

F/6 20/4

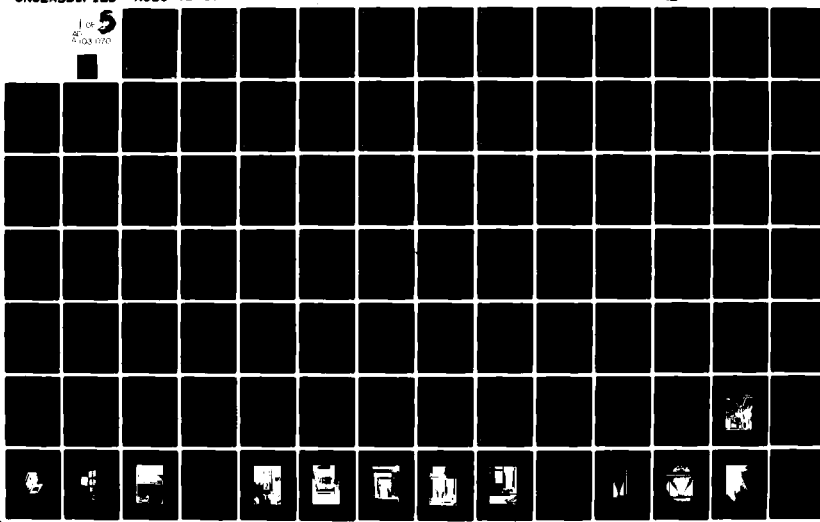
AUG 79 J MIGUEL

UNCLASSIFIED

NUSC-TD-5656

NL

1 of 5
AD-A103 070



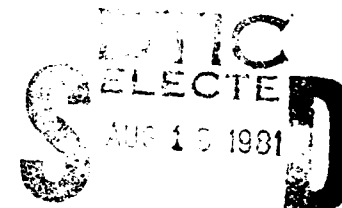
NUSC Technical Document 5456
15 August 1979

(2) BC

AD A103070

An Experimental Study of Polymer Drag Reduction and Boundary Layer Diffusion Characteristics for Incompressible Flow Over a Flat Plate

John Miguel
Weapon Systems Department



FILE COPY

Naval Underwater Systems Center
Newport, Rhode Island 02840

Approved for public release;
distribution unlimited.

81 8 19 031

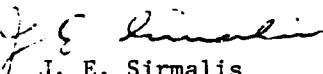
PREFACE

This report was prepared under NUSC Project No. A38500, "Polymer Drag Reduction and Diffusion," principal investigator--John Miguel (Code 36315).

The technical reviewer for this report was Paul E. Gibson (Code 36315).

The author acknowledges the generous assistance of his colleagues at the Naval Underwater Systems Center (Dr. J. E. Sirmalis, R. H. Nadolink, P. E. Gibson, S. P. Tucker, T. A. Galib Jr., J. R. Babiec, R. W. Hoy and S. A. Schneller), and the helpful guidance of Dr. M. P. Wilson, Dr. R. Dowdell and Dr. T. Kowalski (University of Rhode Island).

REVIEWED AND APPROVED: 15 August 1979


J. E. Sirmalis
Head, Weapon Systems Department

Official documents

REPORT DOCUMENTATION PAGE		READ INSTRUCTIONS BEFORE COMPLETING FORM	
1. REPORT NUMBER	TD-5656	2. GOVT ACCESSION NO.	AD-A103 070
3. TITLE (and Subtitle)	AN EXPERIMENTAL STUDY OF POLYMER DRAG REDUCTION AND BOUNDARY LAYER DIFFUSION CHARACTERISTICS FOR INCOMPRESSIBLE FLOW OVER A FLAT PLATE		
4. AUTHOR(s)	John Miguel		
5. PERFORMING ORGANIZATION NAME AND ADDRESS	Naval Underwater Systems Center Newport Laboratory Newport, Rhode Island 02840		
6. PROGRAM ELEMENT, PROJECT, TASK AREA & WORK UNIT NUMBERS	Project No. A-385-00 Subproject No. ZR-000-0101		
7. CONTROLLING OFFICE NAME AND ADDRESS	(11)		
8. MONITORING AGENCY NAME & ADDRESS (if different from Controlling Office)	(12) XK99741		
9. DISTRIBUTION STATEMENT (of this Report)	Approved for public release; distribution unlimited. (17) 2TCC000102		
10. SECURITY CLASS. (of this report)	UNCLASSIFIED		
11. DECLASSIFICATION/DOWNGRADING SCHEDULE	(18)		
12. REPORT DATE	15 August 1979		
13. NUMBER OF PAGES	380		
14. DISTRIBUTION STATEMENT (of the abstract entered in Block 20, if different from Report)			
15. SUPPLEMENTARY NOTES	A thesis submitted to the University of Rhode Island in partial fulfillment of the requirements for the degree of Doctor of Philosophy in Mechanical Engineering (1978).		
16. KEY WORDS (Continue on reverse side if necessary and identify by block number)	Polymer Injection Boundary Layer Flat Plate Drag Reduction Water Tunnel Laser Doppler Anemometry		
17. ABSTRACT (Continue on reverse side if necessary and identify by block number)	<p>Drag reduction by injection of high molecular weight polymers into boundary layers has been demonstrated repeatedly in the past. However, from a volume utilization tradeoff standpoint, the quantities of polymer required make the gain achieved by this process marginal. While indicating reduced polymer requirements for drag reduction, limited data obtained from pipe flow and external boundary layer flow experiments are conflicting and hard to interpret. Ambiguities in measurement techniques due to polymer effects on commonly used instrumentation and opposing features of varied flow facilities have also contributed to making</p>		

20. ABSTRACT (Cont'd)

these earlier works contradictory and difficult to resolve.

Experiments performed in this research indicate that turbulence intensity distributions are altered by the addition of polymer in such a way that the peak of turbulence production is lowered and its location moved away from the wall. The transition region is delayed and extended by the addition of polymer to the boundary layer. The laminar sublayer of boundary layer profiles appears to have thickened due to the addition of polymer. When compared to the law of the wall corrected for developing flow, the velocity profiles also show evidence of a thickened sublayer.

Accepted	_____
FIGTS	_____
DETAIL	_____
UNCLASSIFIED	_____
JUL 1970	1970
FEDERAL AVAILABILITY	
BY	_____
DISTRIBUTOR	_____
Avail	_____
MANUFACTURER	
Dist	Special
A	

TABLE OF CONTENTS

	<u>Page</u>
LIST OF ILLUSTRATIONS	iv
NOMENCLATURE	xix
I. INTRODUCTION	1
General Considerations	1
Scope and Objectives	3
Approach	3
II. LITERATURE REVIEW	5
Historical Background	5
Turbulent Boundary Layer Theory	7
Homogeneous Polymer Flow	18
Polymer Injection Studies	25
Drop Tests, Rotating Disks and Cylinders	44
Review of Experimental Apparatus	47
III. EXPERIMENTAL APPARATUS	52
Flow Facility	52
Initial Attempts	54
Settling Chamber	60
Diffuser	66
Tunnel Design	72
Boundary Layer Probes	74
Polymer Injection System	80
Boundary Layer Concentration Measurements	86
Laser Doppler Anemometer System	96

	<u>Page</u>
Data Processing	126
IV. EXPERIMENTAL PROCEDURE.	130
Polymer Preparation	130
Injection System Calibration.	131
Boundary Layer Sampling	132
Fluorometer Calibration	134
Wall Location	136
Tunnel Characterization	137
Test Series	140
V. ANALYTICAL CONSIDERATIONS	146
Boundary Layer Model.	146
Velocity Profile Relation	146
Skin Friction Relations	148
Effective Reynolds Number Analogy	150
VI. EXPERIMENTAL RESULTS AND DISCUSSION	158
General Remarks	158
Water Flow Boundary Layer Characterization	160
Polymer Flow Boundary Layer	
Characterization	169
Comparison of Analytical Predictions With	
Experimental Results.	193
Clauser Skin Friction Techniques.	202
Polymer Diffusion Patterns.	212

	<u>Page</u>
VII. CONCLUSIONS AND RECOMMENDATIONS	231
General	231
Analytical Prediction Methods	232
Polymer Boundary Layer Characteristics. .	232
Diffusion Characteristics	233
Conclusion Summary.	234
Recommendations	235
APPENDIX A - DEVELOPMENT OF SKIN FRICTION RELATIONS . . .	237
APPENDIX B - COMPUTER PROGRAM DATAPAC AND SAMPLE LISTING	264
APPENDIX C - COMPUTER PROGRAM DATAPAC OUTPUT CURVES, . .	288
APPENDIX D - HYDRODYNAMIC PARAMETER TABULATIONS.	297
APPENDIX E - VELOCITY PROFILE SAMPLES.	321
APPENDIX F - COMPUTER PROGRAM SKINFRIC	328
BIBLIOGRAPHY	334

LIST OF ILLUSTRATIONS

<u>Figure</u>		<u>Page</u>
1.	The Law of the Wall	12
2.	The Velocity Defect Law	14
3.	Pictorial Sketch of Boundary Layer Flow . . .	17
4.	Concentration Profiles in the Intermediate and Final Zones	37
5.	Growth of the Diffusion Boundary Layer Within the Momentum Boundary Layer	42
6.	Experimental Flow Facility	53
7.	Experimental Set-Up Photograph	55
8.	Initial Settling Chamber Photograph	57
9.	Initial Settling Chamber Disassembled Photograph	58
10.	Initial Settling Chamber Corner Flow Photograph	59
11.	Settling Chamber Configuration Photograph . .	61
12.	Rounded Rectangular Tunnel Entrance Photograph	62
13.	Settling Chamber Flow Pattern Photograph . .	63
14.	Rectangular Stand-Off Tunnel Entrance Nozzle Photograph	64

<u>Figure</u>	<u>Page</u>
15. Rectangular Stand-Off Nozzle Flow Pattern	
Photograph	65
16. Transition Nozzle Sideview Photograph . . .	67
17. Transition Nozzle Topview Photograph . . .	68
18. Final Settling Chamber Configuration	
Photograph	69
19. Test Set-Up Schematic	70
20. Rectangular Diffuser Photograph	71
21. Conical Diffuser Inlet Transition Section	
Photograph	73
22. Flat Plate Leading Edge Photograph	75
23. Sand Roughened Leading Edge Photograph . .	76
24. Boundary Layer Probe Rake Photograph . . .	77
25. Disassembled Boundary Layer Probe Rake	
Photograph	78
26. Boundary Layer Probe Rake Tip Close-Up	
Photograph	79
27. Boundary Layer Probe Rake Dimensions . . .	81
28. Boundary Layer Probe Rake Placement	
Photograph	83
29. Boundary Layer Probe Sampling System	
Photograph	84

<u>Figure</u>		<u>Page</u>
30.	Polymer Delivery System Photograph.	85
31.	Fluorometer Schematic	89
32.	G.K. Turner Model 111 Fluorometer Photograph.	91
33.	Calibration Curves for Model 111 Fluorometer Openings 1 and 10	93
34.	Calibration Curves for Model 111 Fluorometer Openings 3 and 30	94
35.	Basic Components of a Laser Doppler Anemometer System	97
36.	Optical Configurations for Laser Doppler Anemometer Systems	100
37.	Polar Scattered Light Intensity Distribution.	101
38.	Fringe Pattern Schematic	103
39.	Fringe Pattern Photograph	104
40.	Photodetector Output Schematic	106
41.	Scattered Light Frequency - Velocity Relationship	107
42.	Measuring Volume Schematic	109
43.	Location of Measuring Volume	112
44.	Doppler Burst From Single Particle Photograph	118
45.	Doppler Burst From Good Particle Distribution Photograph	119

<u>Figure</u>		<u>Page</u>
46.	Doppler Bursts Due to Multiple Particles in Measuring Volume Photograph	120
47.	Count Rate Distribution Photograph	121
48.	Computer Data System Photograph	127
49.	Polymer Injection Flowmeter Calibration Curve	133
50.	Tunnel Velocity Field Map	138
51.	Normalized Turbulence Intensity Distribution	139
52.	Non-Dimensional Velocity Profile	139
53.	Incoming Velocity Profile	141
54.	Axial Velocity Profile Through Transition . .	142
55	Flat Plate Skin Friction Coefficient Curve. .	151
56	Skin Friction vs Reynolds Number as a Function of Polymer Concentration	154
57.	Percent Drag Reduction as a Function of Polymer Concentration	156
58.	Normalized Laminar Velocity Profiles.	161
59.	Non-Dimensional Velocity Profiles at Station $x = 18.0$ inches	162
60.	Transitional Nature of the Velocity Profiles for Water Flow	163
61.	Turbulence Intensity Distribution for Transitional Velocity Profiles	165

<u>Figure</u>		<u>Page</u>
62.	Growth of Boundary Layer for Water Flow	166
63.	Variation of Value of B as a Function of Reynolds Number for Developing Channel Flow. .	167
64.	Law of the Wall for Developing Flow	168
65.	Developing Velocity Profiles for Injected Polymer Concentration $C_i = 100$ WPPM	170
66.	Developing Velocity Profiles for Injected Polymer Concentration $C_i = 200$ WPPM	171
67.	Developing Velocity Profiles for Injected Polymer Concentration $C_i = 400$ WPPM	172
68.	Developing Velocity Profiles for Injected Polymer Concentration $C_i = 500$ WPPM	173
69.	Developing Velocity Profiles for Injected Polymer Concentrations $C_i = 800$ WPPM.	174
70.	Turbulence Intensity Distribution for Injected Polymer Concentrations $C_i = 100$ WPPM.	175
71.	Turbulence Intensity Distributions for Injected Polymer Concentrations $C_i = 200$ WPPM.	176
72.	Turbulence Intensity Distributions for Injected Polymer Concentrations $C_i = 400$ WPPM.	177
73.	Turbulence Intensity Distributions for Injected Polymer Concentrations $C_i = 500$ WPPM.	178

<u>Figure</u>	<u>Page</u>
74. Turbulence Intensity Distributions for Injected Polymer Concentrations $C_i = 800$ WPPM	179
75. Comparison of Non - Dimensionalized Velocity Profiles at Station $x = 18.0$ inches With Theoretical 1/5th Power Law Profile	181
76. Developing Velocity Profiles for Injected Polymer Concentration $C_i = 2,000$ WPPM	182
77. Turbulence Intensity Distribution for Injected Polymer Concentration $C_i = 2,000$ WPPM	184
78. Turbulence Intensity Distribution	186
79. Comparison of the Law of the Wall With Experi- mental Data for Injected Polymer Concentra- tion $C_i = 100$ WPPM	187
80. Comparison of the Law of the Wall With Experi- mental Data for Injected Polymer Concentra- tion $C_i = 200$ WPPM	188
81. Comparison of the Law of the Wall With Experi- mental Data for Injected Polymer Concentra- tion $C_i = 400$ WPPM	189
82. Comparison of the Law of the Wall With Experi- mental Data for Injected Polymer Concentra- tion $C_i = 500$ WPPM	190

<u>Figure</u>		<u>Page</u>
83.	Comparison of the Law of the Wall With Experimental Data for Injected Polymer Concentration $C_i = 800$ WPPM	191
84.	Comparison of Normalize Velocity Profiles With 1/5th Power Law Velocity Profile at Station $x = 18$ Inches	194
85.	Comparison of Experimental Boundary Layer Growth With Analytically Predicted Values for Injected Polymer Concentration $C_i = 100$ WPPM	195
86.	Comparison of Experimental Boundary Layer Growth With Analytically Predicted Values for Injected Polymer Concentration $C_i = 200$ WPPM	196
87.	Comparison of Experimental Boundary Layer Growth With Analytically Predicted Values for Injected Polymer Concentration $C_i = 500$ WPPM	197
88.	Comparison of Experimental Boundary Layer Growth With Analytically Predicted Values for Injected Polymer Concentration $C_i = 800$ WPPM	198
89.	Plot of Clauser Family of Curves for Water Flow	203

<u>Figure</u>		<u>Page</u>
90.	Plot of Clauser Family of Curves for Injected Polymer Concentration $C_i = 100$ WPPM	205
91.	Variation of Local Skin Friction Along the Plate Compared With Experimental Results for Water Flow	206
92.	Variation of Local Skin Friction Along the Plate Compared with Experimental Results for Injected Polymer Concentration $C_i = 100$ WPPM .	207
93.	Variation of Local Skin Friction Along the Plate Compared With Experimental Results for Injected Polymer Concentration $C_i = 200$ WPPM .	208
94.	Variation of Local Skin Friction Along the Plate Compared with Experimental Results for Injected Polymer Concentration $C_i = 400$ WPPM .	209
95.	Variation of Local Skin Friction Along the Plate Compared With Experimental Results for Injected Polymer Concentration $C_i = 500$ WPPM .	210
96.	Variation of Local Skin Friction Along the Plate Compared with Experimental Results for Injected Polymer Concentration $C_i = 800$ WPPM .	211
97.	Effective Reynolds Analogy Values of Local Skin Friction vs Reynolds Number for Injected Polymer Concentration $C_i = 200$ WPPM .	213

<u>Figure</u>		<u>Page</u>
98	Normalized Polymer Wall Concentration	
	Distribution	214
99.	Normalized Polymer Wall Concentration	
	Distribution	214
100.	Axial Velocity Profile at $y = .020$ Inches for	
	Injected Polymer Concentration	
	$C_i = 500$ WPPM Compared With Water	216
101.	Axial Velocity Profile at $y = .020$ Inches for	
	Injected Polymer Concentration	
	$C_i = 2000$ WPPM Compared With Water	216
102.	Normalized Water Diffusion Patterns	218
103.	Normalized Polymer Diffusion Pattern for	
	Injected Polymer Concentration	
	$C_i = 100$ WPPM	219
104.	Normalized Polymer Diffusion Pattern for	
	Injected Polymer Concentration	
	$C_i = 200$ WPPM	220
105.	Normalized Polymer Diffusion Pattern for	
	Injected Polymer Concentration	
	$C_i = 400$ WPPM	221
106.	Normalized Polymer Diffusion Pattern for	
	Injected Polymer Concentration	
	$C_i = 500$ WPPM	222

<u>Figure</u>		<u>Page</u>
107.	Normalized Polymer Diffusion Pattern for Injected Polymer Concentration $C_i = 800$ WPPM	223
108.	Diffusion Boundary Layer Growth as a Function of Polymer Concentration.	226
109.	Diffusion Boundary Layer Growth for $Q_i C_i = 8,000$	227
110.	Diffusion Boundary Layer Growth for $Q_i C_i = 16,000$	227
111.	Diffusion Boundary Layer Growth as a Function of $Q_i C_i$ and Injection Velocity Ratio	228
112.	Diffusion Boundary Layer Growth in the Final Zone.	229
113.	Diffusion Boundary Layer Growth in the Transition Region	230

LIST OF TABLES

<u>Table</u>		<u>Page</u>
1.	Concentrations (WPPM) of Material Required to Achieve 67 Percent Drag Reduction in Pipe Flow of $Re = 14 \times 10^3$ (from Hoyt (1972)).	19
2.	Concentration Sampling Locations in the Boundary Layer.	82
3.	Concentration Measurement Apparatus	95
4.	Laser Doppler Anemometer System Components. .	98
5.	Measuring Volume Parameters	110
6.	Tracking Frequencies	113
7.	Types of Seeding	115
8.	Data System Components	126
9.	Printer Output List	128
10.	Non-Dimensional Locations of Concentration Measurements Stations	135
11.	Injection Parameters	144
12.	Concentration Flux Matrix	145
13.	Comparison of Near Wall Laser Anemometer Measurements in Drag Reducing Flows . . .	192
14.	Comparison of Skin Friction Coefficients for Water Case	199

<u>Table</u>		<u>Page</u>
15.	Comparison of Skin Friction Coefficients for $C_i = 100$ WPPM of Polymer	199
16.	Comparison of Skin Friction Coefficeints for $C_i = 200$ WPPM of Polymer	200
17.	Comparison of Skin Friction Coefficients for $C_i = 400$ WPPM of Polymer	200
18.	Comparison of Skin Friction Coefficients for $C_i = 500$ WPPM of Polymer	201
19.	Comparison of Skin Friction Coefficients for $C_i = 800$ WPPM of Polymer	201
20.	Boundary Layer Parameters for Water Injected at $V_i = .0383$ ft/sec.	298
21	Boundary Layer Parameters for Water Injected at $V_i = .0766$ ft/sec.	299
22.	Boundary Layer Parameters for Water Injected at $V_i = .1532$ ft/sec.	300
23.	Boundary Layer Parameters for Water Injected at $V_i = .3074$ ft/sec.	301

<u>Table</u>		<u>Page</u>
24.	Boundary Layer Parameters for Water Injected at $V_i = .6148 \text{ ft/sec.} \dots \dots \dots \dots$	302
25.	Boundary Layer Parameters for 100 WPPM Polymer Injected at $V_i = .0383 \text{ ft/sec.} \dots \dots \dots \dots$	303
26.	Boundary Layer Parameters for 100 WPPM Polymer Injected at $V_i = .0766 \text{ ft/sec.} \dots \dots \dots \dots$	304
27.	Boundary Layer Parameters for 200 WPPM Polymer Injected at $V_i = .0383 \text{ ft/sec.} \dots \dots \dots \dots$	305
28.	Boundary Layer Parameters for 200 WPPM Polymer Injected at $V_i = .0766 \text{ ft/sec.} \dots \dots \dots \dots$	306
29.	Boundary Layer Parameters for 200 WPPM Polymer Injected at $V_i = .1532 \text{ ft/sec.} \dots \dots \dots \dots$	307
30.	Boundary Layer Parameters for 400 WPPM Polymer Injected at $V_i = .0383 \text{ ft/sec.} \dots \dots \dots \dots$	308
31.	Boundary Layer Parameters for 400 WPPM Polymer Injected at $V_i = .0766 \text{ ft/sec.} \dots \dots \dots \dots$	309
32.	Boundary Layer Parameters for 400 WPPM Polymer Injected at $V_i = .1532 \text{ ft/sec.} \dots \dots \dots \dots$	310
33.	Boundary Layer Parameters for 400 WPPM Polymer Injected at $V_i = .6148 \text{ ft/sec.} \dots \dots \dots \dots$	311
34.	Boundary Layer Parameters for 500 WPPM Polymer Injected at $V_i = .0383 \text{ ft/sec.} \dots \dots \dots \dots$	312

<u>Table</u>		<u>Page</u>
35.	Boundary Layer Parameters for 500 WPPM Polymer Injected at $V_i = .0766 \text{ ft/sec} \dots \dots \dots$	313
36.	Boundary Layer Parameters for 500 WPPM Polymer Injected at $V_i = .1532 \text{ ft/sec} \dots \dots \dots$	314
37.	Boundary Layer Parameters for 500 WPPM Polymer Injected at $V_i = .6148 \text{ ft/sec} \dots \dots \dots$	315
38.	Boundary Layer Parameters for 800 WPPM Polymer Injected at $V_i = .0383 \text{ ft/sec} \dots \dots \dots$	316
39.	Boundary Layer Parameters for 800 WPPM Polymer Injected at $V_i = .0766 \text{ ft/sec} \dots \dots \dots$	317
40.	Boundary Layer Parameters for 800 WPPM Polymer Injected at $V_i = .1532 \text{ ft/sec} \dots \dots \dots$	318
41.	Boundary Layer Parameters for 800 WPPM Polymer Injected at $V_i = .6148 \text{ ft/sec} \dots \dots \dots$	319
42.	Boundary Layer Parameters for 2000 WPPM Polymer Injected at $V_i = .6148 \text{ ft/sec} \dots$	320
43.	Velocity Profiles for Water Injected at $V_i = .0383 \text{ ft/sec} \dots \dots \dots \dots \dots$	322
44.	Velocity Profiles for 100 WPPM Polymer Injected at $V_i = .0383 \text{ ft/sec} \dots \dots \dots$	323
45.	Velocity Profiles for 200 WPPM Polymer Injected at $V_i = .0383 \text{ ft/sec} \dots \dots \dots$	324

<u>Table</u>		<u>Page</u>
46.	Velocity Profiles for 400 WPPM Polymer	
	Injected at $V_i = .0383$ ft/sec	325
47.	Velocity Profiles for 500 WPPM Polymer	
	Injected at $V_i = .0383$ ft/sec	326
48.	Velocity Profiles for 800 WPPM Polymer	
	Injected at $V_i = .0383$ ft/sec	327

NOMENCLATURE

A	=	area	ft^2
A_s	=	ejection slot area	ft^2
a	=	acceleration	ft/sec^2
B	=	law of the wall constant	dimensionless
b	=	Batchelor's Constant	dimensionless
C	=	concentration	WPPM
C_i	=	injected concentration	WPPM
C_f	=	local skin friction coefficient	dimensionless
C_w	=	wall concentration	WPPM
C_w^*	=	critical wall concentration	WPPM
D_e^{-2}	=	diameter of laser beam at $1/e^2$ intensity points	mm
d_l	=	diameter of focused laser beam	mm
d_m	=	diameter of measuring volume	mm
d_f	=	fringe spacing	mm
F	=	force	lb_f
f_D	=	Doppler frequency	1/sec
g	=	gravitational acceleration	ft/sec^2
g_c	=	constant of proportionality	$\text{lb}_m \cdot \text{ft}/\text{lb}_f \cdot \text{sec}^2$
K	=	mixing length constant	dimensionless
L	=	plate length	ft
l_m	=	length of measuring volume	mm
m	=	mass	lb_m
p	=	pressure	lb_f/ft^2

Q	=	volume flow rate	ft^3/sec
Q_i	=	injection rate	ft^3/sec
Re	=	Reynolds number	dimensionless
Re_x	=	$\frac{U_\infty x}{\nu}$	dimensionless
t	=	time	second
T	=	temperature	$^{\circ}\text{F}$
T_i	=	temperature of injected fluid	$^{\circ}\text{F}$
T_w	=	temperature of water	$^{\circ}\text{F}$
U_e	=	velocity at edge of boundary layer	ft/sec
U_∞	=	freestream velocity	ft/sec
u	=	local boundary layer velocity	ft/sec
u^+	=	u/V^* law of the wall variable	dimensionless
u'	=	turbulent velocity component	ft/sec
v	=	velocity	ft/sec
v_i	=	ejection velocity	ft/sec
v_{iy}	=	normal component of injection velocity	ft/sec
V^*	=	characteristic or friction velocity	ft/sec
V_m	=	volume of measuring volume	$(\text{cm})^3$
V_o^*	=	critical shear velocity $= \sqrt{\tau_w / \rho}$	ft/sec
x	=	linear dimension	ft
x^*	=	x/L dimensionless distance	dimensionless
y	=	distance normal to plate	ft
y^+	=	yV^*/v law of the wall variable	dimensionless
\bar{y}	=	mean vertical position of particle	ft

\bar{Y}	=	mean vertical position of single particle	ft
Z	=	defined by equation (58)	dimensionless
α	=	coefficient of polymer term in law of the wall	dimensionless
S	=	Clauser's equilibrium parameter defined by equation (11)	dimensionless
γ	=	exponent of polymer term in law of the wall	dimensionless
ϵ	=	eddy viscosity	$lb_f sec/ft^2$
ΔB	=	polymer constant for law of the wall	dimensionless
δ	=	boundary layer thickness	ft
δ_d	=	diffusion boundary layer thickness	ft
δ_1	=	boundary layer displacement thickness	ft
δ_2	=	boundary layer momentum thickness	ft
ϕ	=	laser beam intersection angle	degrees
λ_2	=	wave length of laser beam	meters
λ	=	$(2/C_f)^{\frac{1}{2}}$	dimensionless
λ_c	=	characteristic height of diffusion boundary layer	dimensionless
ρ	=	density	lb_m/ft^3
μ	=	viscosity	$lb_f sec/ft^2$

τ_w	=	wall shear stress	lb_f/ft^2
ν	=	kinematic viscosity	ft^2/sec
η	=	$y\sqrt{U/\nu x}$ Blasius parameter	dimensionless

I. INTRODUCTION

General Considerations

During the thirty years since B. A. Toms first published his work on the subject, it has been well established that considerably reduced resistance to the turbulent shear flows of liquids may be achieved through the addition of small quantities of high molecular weight polymers into the fluid. This phenomenon of drag reduction is of great importance and has far-reaching implications in the reduction of power required for the pumping of fluids and the transport of bodies through liquids.

Early drag reduction efforts were primarily concerned with well-developed pipe flows, the area in which the first observation was made. Until recently, researchers have directed their efforts toward characterizing the manner in which the boundary layer velocity profiles were affected in an attempt to quantify the effect of polymer additives. Results similar to those achieved in pipe flows have been obtained in investigations dealing with external flows, such as on a flat plate. The magnitude of the turbulent fluctuations in the boundary layer are found by some researchers to decrease with a thickening of the laminar sublayer and a lowering of the wall shear stress. Other

researchers, however, have found no evidence of this thickened sublayer. A limit to the amount of drag reduction achievable with polymer use has been demonstrated and increases in the shear stress have been observed when excess polymer is used. Shear stress reduction for external flows over bodies has been achieved by the ejection of polymer solutions. The exact mechanism of shear stress reductions, however, still remains undefined. Ambiguities in measurement techniques due to polymer effects on commonly used instrumentation and confusing features of varied flow facilities have contributed to making past investigations contradictory and difficult to interpret.

It is evident that a better understanding of the mechanism of drag reduction in developing flows with polymer ejection is required if advantage is to be taken of the phenomenon for practical application. Most cases of interest in external flows would require that a carried polymer supply be used for ejection into the boundary layer. Presently, very little is known about the effect of ejection techniques on polymer distribution in developing boundary layers of external flows and no information is available on the effects of polymer on boundary layer transition phenomena.

Scope and Objectives of Present Study

The object of the research described herein was to: (1) develop a flow facility suitable for the study of polymer flows; (2) perform velocity measurements using non-flow-disturbing laser Doppler anemometry techniques with real-time data processing; (3) develop methods for the prediction of local skin friction values as a function of local polymer wall concentration; (4) determine the effects of ejection techniques on the distribution of polymer in the boundary layer; and (5) determine the diffusion characteristics of a polymer when ejecting it into a laminar boundary layer and also its effect on transition.

Approach

A flow facility was constructed under the constraints of limited funds and practicality of construction. The basic tunnel structure was designed with a width-to-height aspect ratio of 5:1 to minimize the effects of side wall boundary layer growth and corner flows in the rectangularly-shaped channel. Flow delivery was by constant head gravity feed to minimize vibration effects. The polymer delivery system provided minimum mechanical degradation of polymer solutions while allowing variations in polymer concentrations and ejection velocities. Transition from laminar to turbulent flow was achieved at midplate

position allowing ejection of polymer solutions into a developing laminar boundary at the plate leading edge and transitioning to turbulent flow along the plate. Boundary layer velocity profiles through transition to turbulent flow were taken with laser Doppler anemometry techniques, non-disruptive of the flow nor affected by polymer characteristics.

Using boundary layer sampling techniques, polymer diffusion characteristics were measured at five axial wall locations along the plate, as well as at eight positions normal to the plate at each wall station. The ejected polymer concentrations were contaminated with a fluorescent dye, which was later used to analyze the concentrations of the boundary layer samples. Thus it was possible to measure the change in wall concentration and concentration profile in the boundary layer during laminar, transitional, and turbulent flow.

Analytical methods were developed to predict skin friction coefficients as a function of local polymer wall concentrations for comparison with experimentally determined values.

II. LITERATURE REVIEW

Historical Background

B.A. Toms (1949) published the first data on the friction reducing effects of polymers and showed that, for conditions of turbulent flow with constant pressure gradient, the average velocity of monochlorobenzene, flowing in a pipe, increased substantially with the addition of dilute quantities of polymethyl methacrylate. Friction reduction of up to 50% was achieved (as compared with the pure solvent) by the addition of .25% by weight of polymer to the solvent.

Oldroyd (1949) attempted to explain this phenomenon (presently referred to by many as the "Toms effect") as a wall effect due to exclusion of large polymer molecules from a region near the wall due to their size. As a result of studies on the flow of gasoline thickened with aluminum soaps at Edgewood Arsenal during World War II (but not published at that time), Mysel (1949) applied for and received a patent in 1949. He observed that in turbulent flow the pressure loss per unit length of pipe was much lower for thickened gasoline than that of the pure solvent.

The importance of drag reduction seemed to have been overlooked until the late 1950s when Shaver and Merril (1959) and

Dodge and Metzner (1959) published results indicating the low friction factors of non-Newtonian solutions, such as sodium carboxymethylcellulose, in water. Similar observations of reduced friction were made in the oil well industry with the use of the plant derivative, Guar Gum. Solutions of the product were used to suspend sand in the high-pressure, sand-water mixtures utilized in oil well fracturing operations.

These experiences led to U.S. Navy studies in the early 1960's on possible military applications of friction-reducing effects. Among Navy researchers, Hoyt (1963) made the first significant contribution followed by Fabula (1964) who discovered the spectacular friction reducing ability of polyethylene oxide, the most effective friction-reducing material known.

Crawford (1962) and Savins (1961) led the early efforts of industrial research centers. The years that have followed these early efforts have produced an ever-increasing number of international papers, reports, and conferences on the subject.

Excellent summaries of research efforts and results available in the field of drag reduction have been presented by Lumley (1969) and Hoyt (1972). Palyvos (1974), however, prepared the most extensive and detailed review of research efforts to date. This review reveals that after years of active research and the

combined efforts of hydrodynamicists, polymer chemists and rheologists in many countries, there is yet no adequate theoretical explanation for the mechanism of drag reduction, nor is there a satisfactory correlation of the viscoelastic properties of dilute polymer solutions with their friction reduction effect.

Literature pertaining to the current study will be reviewed under four separate categories:

1. Turbulent boundary layer theory
2. Homogeneous polymer flow
3. Polymer ejection studies
4. Experimental facilities .

Turbulent Boundary Layer Theory

The concept of transition from laminar to turbulent flow was first demonstrated in 1880 by Osborne Reynolds in his classic pipe flow experiment. The next major step did not occur until 1904 when, by demonstrating the existence of a thin "boundary layer" in fluid flows, L. Prandtl allowed the reconciliation of viscous flow with classical frictionless hydrodynamic relations. In 1914, by showing that boundary layers could be either laminar or turbulent, Prandtl freed early investigations from the limitation of considering only laminar boundary layers. The

introduction of the "Prandtl mixing length theory" in 1925 was a major contribution toward the understanding of the development of the boundary layer velocity profile. Since that time there have been an ever-increasing number of contributions to the understanding of the flow of fluids.

Many attempts have been made to predict the conditions that govern the transition of laminar to turbulent flow as well as to predict velocity profiles and wall shear. H. Schlichting's classic text, Boundary Layer Theory (1968), remains the most comprehensive treatment of the subject to date. In this work, laminar and turbulent boundary layers in both compressible and incompressible flows over a wide range of application are addressed. However, analyses of the turbulent boundary layer problem still rely heavily on a combination of dimensional analysis, empirical data and flow visualization techniques. Also, during 1968, an attempt was made to introduce order into turbulent boundary layer research. A conference of the world's leading boundary layer researchers was called at Stanford University. Kline (1968) edited the proceedings of that conference, in which some 29 methods and approaches to the analysis of the turbulent boundary layer were presented and discussed.

Viscous Fluid Flow, a text by F.M. White (1974), discusses many of the more significant methods of analysis. Two major

approaches evolved: (1) integral methods averaged across the boundary layer, and (2) finite difference techniques which attempt to solve the full partial differential equations of the boundary layer.

In the last analysis, it remains that the empirical dimensional analysis approach is still the most useful for engineering purposes. The scientific world is indebted to the physical insight of Prandtl and Von Karman for the formulation of the turbulent velocity profile concept. Consideration of regions of influence where the relative importance of viscous shear or turbulent shear dominate led to the formation of the three-layer concept for the velocity distribution in a turbulent boundary layer. The layers are:

Inner Layer: Viscous shear dominates

Outer Layer: Turbulent shear dominates

Overlap Layer: Viscous and turbulent shear equally important.

The mean velocity distribution in a two-dimensional turbulent boundary layer, $u(y)$, depends upon four local parameters: the local wall shear stress, τ_w ; the fluid density, ρ ; the fluid viscosity, μ ; and the boundary layer thickness, δ . For the inner law, Prandtl (1933) deduced that the mean velocity depended on the

wall shear stress, the fluid properties, and the distance y from the wall which led to the following functional relation for the inner law:

$$u = f(\tau_w, \rho, \mu, y). \quad (1)$$

For the outer layer, von Karman deduced that the wall acts only as a source of retardation reducing the local velocity, u , below the freestream velocity, U_e , in a manner independent of the viscosity, μ . The outer law or velocity defect relation, as it is sometimes called, becomes

$$U_e - u = f(t_w, p, y, w). \quad (2)$$

Coles (1954) performed a dimensional analysis on these relationships, where V^* is a characteristic velocity called the wall shear velocity, and is defined as

$$V^* = \sqrt{\frac{\tau_w}{\rho}}. \quad (3)$$

Near the wall, Coles (1954) found that the velocity profile is unaffected by the boundary layer thickness, therefore

$$\text{Inner Law} \quad U^+ = \frac{u}{V^*} = f\left(\frac{yV^*}{V}\right) \quad (4)$$

Far from the wall, viscosity does not affect the velocity distribution. (The viscosity effects are concentrated near the wall.)

$$\text{Outer Law} \quad \frac{\left(\frac{U_e - u}{V^*}\right)}{V} = g(y/\delta) \quad (5)$$

In the overlap region between the inner and outer layers, the commonly known relation for the "law of the wall" (shown in figure 1) may be obtained by equating equations (4) and (5), such that

$$\frac{U}{V^*} = \frac{1}{K} \ln \frac{yV^*}{\nu} + B. \quad (6)$$

The constants K and B have been determined by the data of Nikuradse (1930) to be $K = .40$ and $B = 5.5$.

Coles (1954) presents a correlation of the dimensionless velocity profile, u/V^* , with dimensionless distance from the wall, yV^*/ν , up to a value of about 300. Neglecting separating flows, the data collapse into regions governed by the inner and logarithmic outer laws with the following limits:

Inner Law:

$$\frac{u}{V^*} = \frac{yV^*}{\nu}, \quad 0 < \frac{yV^*}{\nu} < 10 \quad (7)$$

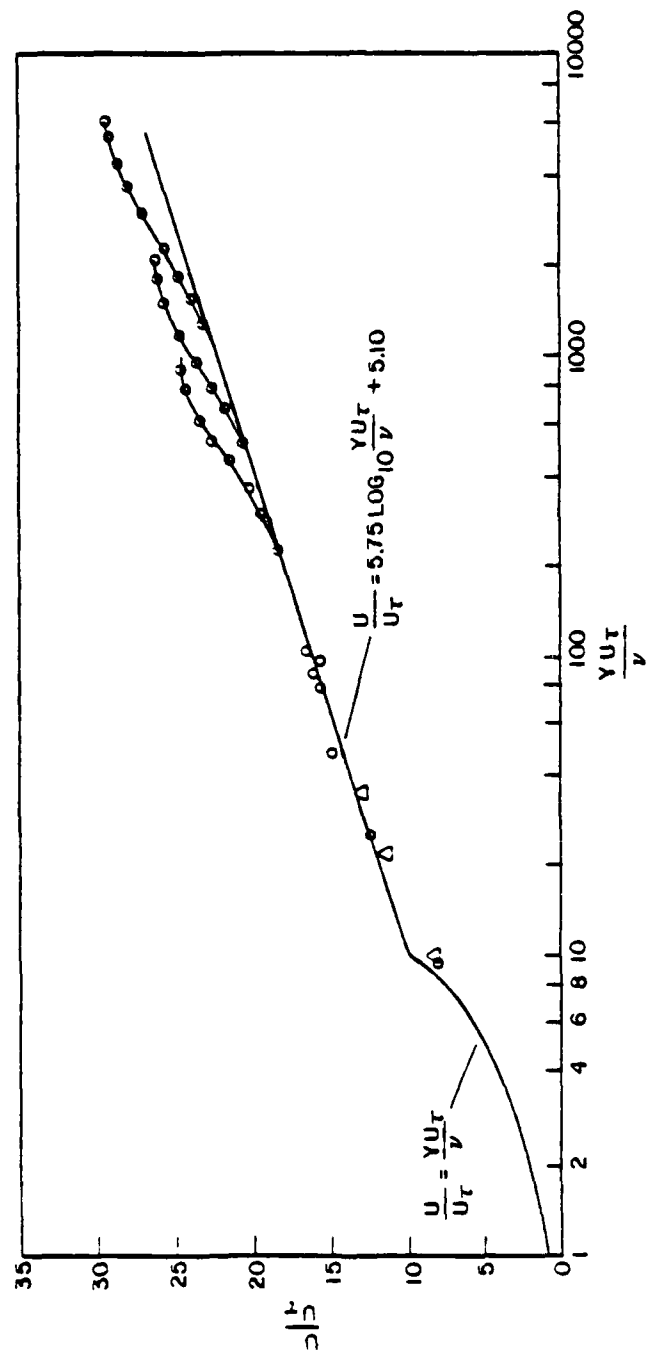


Figure 1. The law of the wall (from Coles (1954))

Logarithmic Law:

$$\frac{u}{v^*} = 2.5 \ln \frac{yV^*}{v} + 5.5, \quad 35 < \frac{yV^*}{v} < 300. \quad (8)$$

For values of $y^+ \equiv \frac{yV^*}{v} > 300$, the viscosity is of negligible importance in the determination of the shape of the boundary layer. The data will then correlate with the velocity defect law (shown in figure 2) in such a way that

$$\frac{u_e - u}{v^*} = f\left(\frac{y}{\delta}, \frac{u}{v^*}\right). \quad (9)$$

In a subsequent paper, Coles (1955) postulates that a two-dimensional boundary layer of an incompressible fluid may be represented by a linear combination of two functions:

$$\frac{u}{v^*} = f\left(\frac{yV^*}{v}\right) + \left(\frac{\Pi}{k}\right) W\left(\frac{y}{\delta}\right). \quad (10)$$

The function $f(yV^*/v)$ is given by equations (7) and (8). Coles refers to the function $W(y/\delta)$ as the "law of the wake." The function, Π , is related to Clauser's (1954, 1956) equilibrium parameter, β , designed as follows:

$$\beta = \frac{\delta}{\tau_w} \cdot \frac{dP_e}{dx}. \quad (11)$$

After additional study, Clauser concluded that the typically fuzzy thickness, δ , should be replaced by the displacement

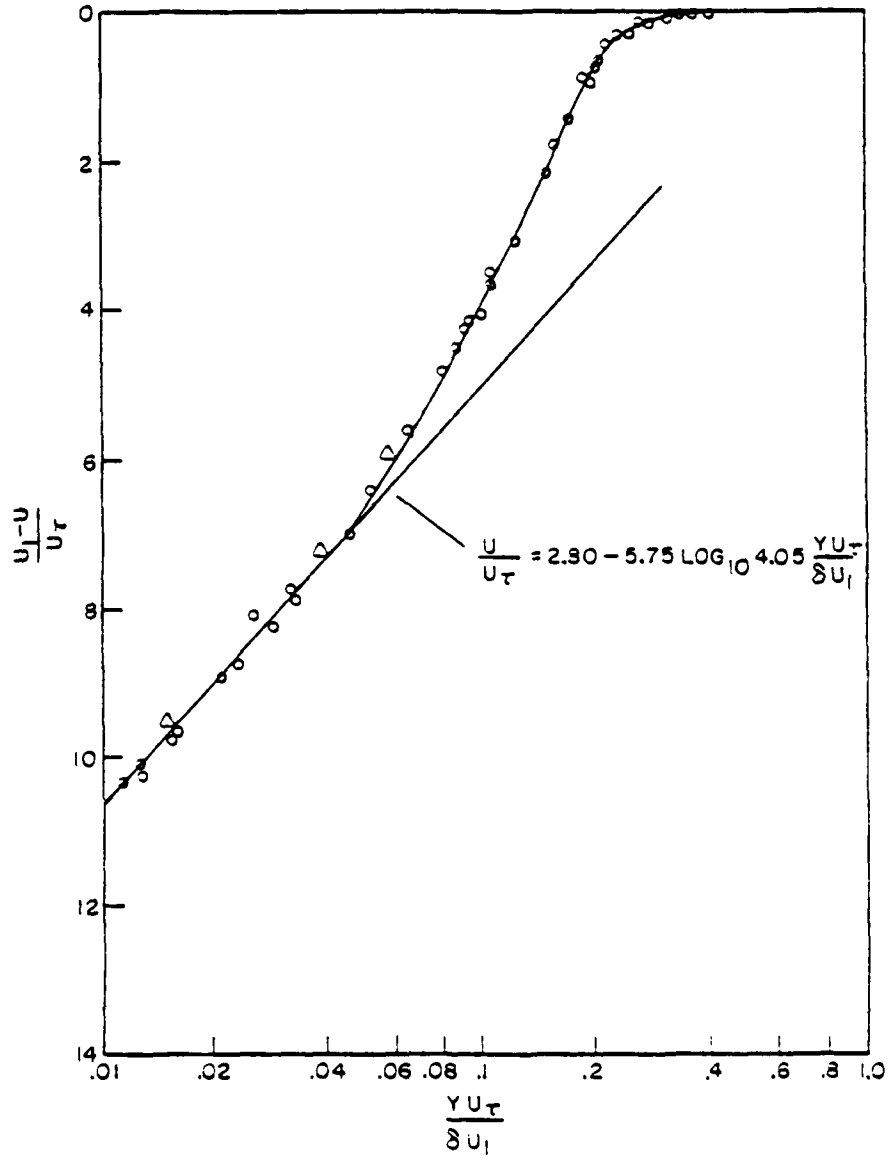


Figure 2. The velocity defect law (from Coles (1954))

thickness, δ_1 , so that the accepted parameter is now

$$\beta = \frac{\delta_1}{\tau_w} \cdot \frac{dP_e}{dx}. \quad (12)$$

The "wake parameter," Π , has a reasonable fit to data when given by the relationship

$$\Pi \approx 0.8(\beta + 0.5)^{0.75}. \quad (13)$$

Coles (1956) proposed the following curve fit for the wake function, W , as

$$W \frac{y}{\delta} \approx 2 \sin^2 \frac{\pi}{2} \cdot \frac{y}{\delta}. \quad (14)$$

Then in Cole's notation for the overlap and other layers, we have the following

$$u^+ = \frac{1}{k} \ln(y^+) + B + \frac{\Pi}{k} W \left(\frac{y}{\delta} \right). \quad (15)$$

It may then be seen that, near the wall, the velocity profile is dominated by friction forces and the function $f(y \cdot u_\tau^+/v)$ controls. Away from the wall, the profile is dominated by inertia forces, with the function $w(y/\delta)$ controlling.

Kline, Runstadler, and Reynolds (1963) visually demonstrated the existence of three regions of turbulent boundary layers, using

a combination of pulsed hydrogen bubble techniques, hot film probes, and dye streak photographs. Shown in figure 3, the flow regions of the turbulent boundary layer model are:

1. A laminar flow region having a near regular, three-dimensional flow pattern for a range of y^+ from $0 < y(u_\tau/v) < 10$.
2. A fully turbulent region of randomly fluctuating eddies. This region, sometimes called the inner turbulent region, exists over a range of y^+ from $10 < y(u_\tau/v) < 370$.
3. An outer turbulent region, or wake region, extending from y^+ of approximately 370 to the outer edge of the boundary layer. In this region, large scale turbulent eddies are found.

Brady (1973) summarized the work of Kline et al. (1963) as follows:

Kline et al. found the 'laminar sublayer' to be made up of a regular structure of low and high velocity longitudinal streaks which meander transverse and normal to the wall. A dimensionless streak spacing $\lambda = \lambda v^*/v = 76.5$ was found for zero pressure gradients. These streaks either break up or randomly burst from the sublayer into the fully turbulent region.

The fully turbulent region is one of intense mixing and high dissipation of energy. Protruding from this region are intermittent large eddies -- visualized as peninsulas of turbulence.

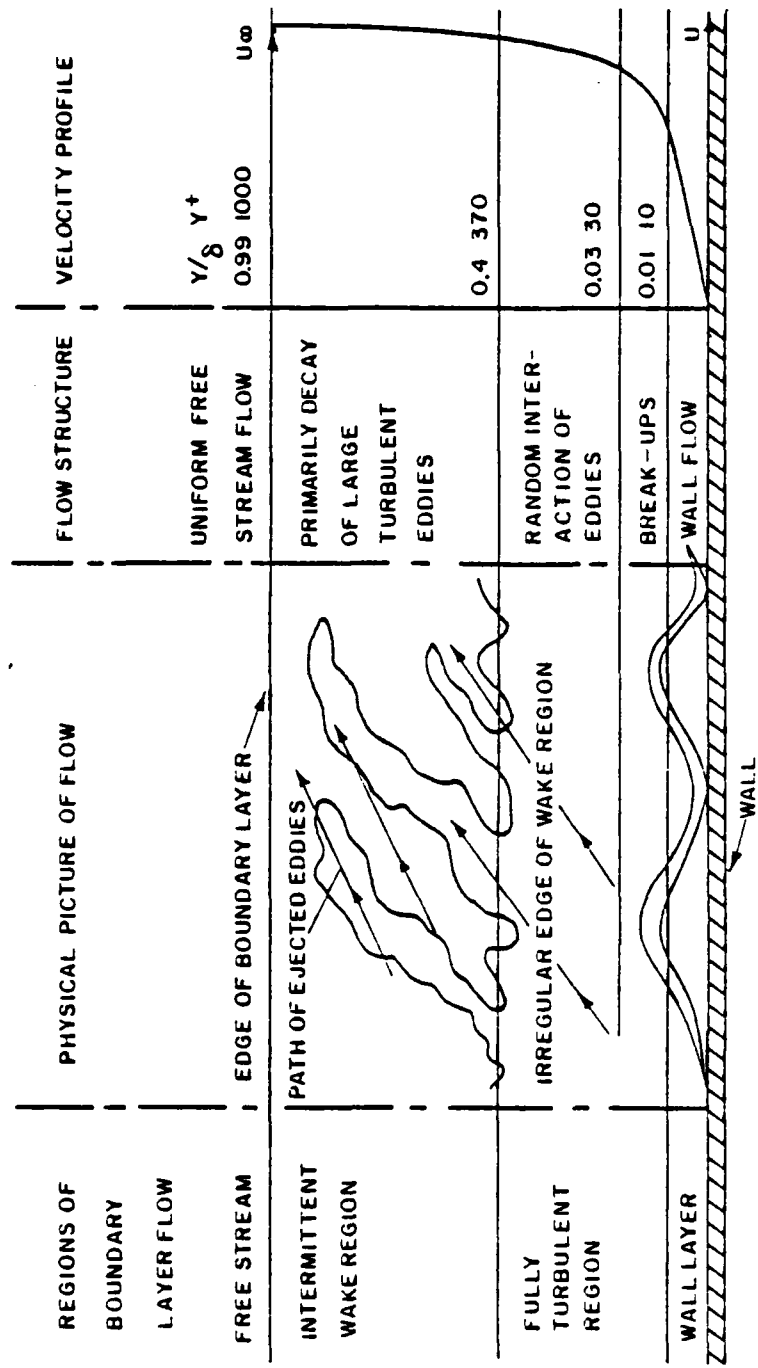


Figure 3. Pictorial sketch of boundary layer flow (from Kline (1963))

The peninsulas of turbulence which extend into the third boundary layer zone -- the outer turbulent region -- gives it a characteristic not unlike the wake behind a cylinder. It has rather large lumps of turbulence at intermittent spacings.

It is clear that the driving force for the entire turbulent boundary layer is the generation of velocity streaks in the sublayer and their subsequent bursting outwards. Kline presents the results of many other investigators, as well as his own, in support of this hypothesis.

Homogeneous Polymer Flow

Since the early work of Toms (1949), Oldroyd (1949), and Mysel (1949), many high molecular weight polymers have been shown to be effective drag reducers. Among the most prominent are: polysaccharides (Guar), polyethylene oxide, polyacrylamides, and sodium carboxymethyl cellulose. For the most part, investigators have considered mainly pipe flows, therefore, this effort will be considered first.

Pipe Flow

Table 1 from Hoyt (1972) shows the effectiveness of small concentrations of polymer on drag reduction. Listed are those concentrations required to achieve 67% drag reduction in pipe flow at $Re = 14 \times 10^3$.

TABLE 1

CONCENTRATIONS (WPPM) OF MATERIAL REQUIRED TO ACHIEVE 67%
 DRAG REDUCTION IN PIPE FLOW OF $Re = 14 \times 10^3$
 (FROM HOYT (1972))

<u>Polymer</u>	<u>Concentration (WPPM)</u>
Gum Karaya	850
Guar	400
Polyacrylamide, Polyhall-250	20
Polyox WSR-301	10

Hoyt and Fabula (1964) and Virk (1971) present data that show a maximum drag reduction asymptote. For a smooth pipe, this asymptote corresponds to 80% of the friction reduction that would be attained if completely laminar flow were sustained at a given Reynolds number.

Meyer (1966) and Elata et al. (1966) have shown that drag reduction in pipes is due to a thickening of the laminar sublayer. It was shown that the constant B in the law of the wall equation (6) remained constant and equal to the Newtonian value until a critical threshold value of the shear velocity, V_o^* , was reached. Thereafter the value of B increased logarithmically with V^* :

$$B = 5.5 + Z \ln \left(\frac{V^*}{V_o^*} \right), \quad (16)$$

$$B = 5.5 + \Delta B, \quad (17)$$

where $\Delta B = Z \ln \left(\frac{V^*}{V_o^*} \right) . \quad (18)$

Using data from several investigators, F.M. White (1968) found that:

$$Z = \alpha C_w^\gamma, \quad (19)$$

$$\text{where } \alpha = 2.3, \text{ and } \gamma = 0.5, \quad (20)$$

with a maximum value of Z of approximately 11. The data further indicated that the critical shear velocity, V_o^* , for the onset of drag reduction was .08 ft/sec. Virk (1966) deduced from experimental data that the onset shear stress is inversely proportional to the polymer molecular radius of gyration. The critical wall shear stress, τ_w^c , which must be exceeded for drag reduction to occur is given by

$$\tau_w^c = \rho (0.624 \times 10^6 \mu / R_G)^2 = \frac{\text{constant}}{R_G^2} \quad (21)$$

where R_G is the rms radius of gyration of the molecule obtained from light scattering data.

Fabula et al. (1969) developed a criteria for the critical wall shear stress at the onset of drag reduction based on molecular deformation times and a molecular characteristic relaxation time. It is thought that individual molecules are too small by several orders of magnitude to interfere with the turbulence structure, indicated by the small value of the ratio of the polymer molecule scale to the scale of turbulent eddies at onset.

To circumvent this problem of length scales, Fabula postulated an interaction between the time scales of the periodic molecular deformation in the viscous sublayer, given by $\dot{\gamma}/2\pi$, where $\dot{\gamma}$ is the shear rate, and a molecular characteristic relaxation time, τ_2 . The molecular characteristic relaxation time, τ_2 , may be determined by the Zimm or Rouse theories which relate a characteristic relaxation time of the solution, τ_2 , to the solvent viscosity, μ_s ; the solution viscosity, μ ; the polymer molecular weight, M ; temperature, T ; and the concentration of polymer, C . It follows then that

$$\tau_2 = \frac{a(\mu - \mu_s)M}{CRT} \quad (22)$$

where a is a constant having a value between .4 and .6.

The resulting criterion for the critical wall sheer stress is given by

$$2\pi(\dot{\gamma}/2\pi) \tau_c = 1$$

or

$$\tau_w^c = \frac{\mu}{\tau_c} = \frac{\mu CRT}{a(\mu - \mu_\sigma)M}. \quad (23)$$

Equation (23) may be written using a relation between intrinsic viscosity, molecular weight, and molecular dimensions yielding:

$$\tau_w^c \approx \frac{\text{constant}}{R_G^3} \approx \frac{1.7 \times 10^{10}}{R_G^3}. \quad (24)$$

Equation (24) of Fabula is similar to Virk's equation (21). The former provides a better estimate of magnitude of onset shear stress whereas the latter is considered more accurate when the constant is determined from test data.

In their work, Kowalski and Brundrett (1974) support Fabula's postulate that the effectiveness of very dilute solution is due to entanglements or "blobs" of macromolecules rather than individual molecules. A formula was developed relating the size of the entangled molecules with the size of a dissipative eddy and are tested to predict the onset of drag reduction in pipe flows of homogeneous polymer solutions.

Darby (1972) reviews drag reduction theories comparing molecular hypotheses, continuum approaches, and conventional boundary layers length scales. Molecular time scale hypotheses are represented by the work of Virk, Fabula, and Kowalski. The continuum approach of Seyer and Metzner concludes that the presence of elastic properties in the dilute solution are sufficient criteria for drag reduction. Elastic properties are represented by a single parameter, the relaxation time, λ , incorporated into a dimensionless group, the Deborah number:

$$N_{De} = \lambda/t_1, \quad (25)$$

where t_1 is a characteristic time of the system. Seyer and Metzner (1969) chose this number to be the reciprocal of the dissipative turbulence frequency, ω_d ,

$$\omega_d = \frac{\bar{V}}{D} N_{Re}^{3/4}. \quad (26)$$

Seyer and Metzner further offer the following phenomena as a possible explanation of drag reduction:

1. Particulate effects due to large molecules or agglomerates which may promote stability of laminar flow or dampen turbulence

2. The solid-like resistance of the fluid to sudden deformation or stretching may suppress the dissipative turbulent frequencies on the generation of turbulence

3. The laminar flow regime may be stabilized so that transition is delayed to higher Reynolds numbers.

Darby (1972) points out that, although Seyer and Metzner favor the second concept, no distinction is made between cause and effect. Dozens of different forms of the Deborah number are presented, illustrating the problems encountered with the present theoretical state of the art.

Boundary layer modification in terms of the Prandtl mixing length theory and law of wall relation indicates a concept of the flow field divided into three regions:

1. A laminar sublayer adjacent to the wall where turbulent fluctuations are absent and momentum transport is by viscous shear only

2. A transition or "buffer" zone adjacent to the laminar sublayer where both viscous shear and turbulent inertial fluctuations contribute to the momentum transport

3. A turbulent boundary layer or "core" outside the buffer zone where transport is dominated by turbulent inertial fluctuations.

Good results for friction factor correlations have been achieved by Elata, Lehner, and Kahanovity (1966) for Guar Gum solutions and Meyer (1966) and Wells (1965) for Polyox.

Many authors have described drag reduction as a "negative roughness effect" since polymers appear to thicken the sublayer while maintaining the same slope of the U^+ versus $\ln Y^+$ curve in the overlap region. Nadolink (1968) demonstrated the existence of the thickened sublayer directly, using a high-speed motion picture camera and a microscope.

White and McEligot (1970), in their work on transition delay from laminar to turbulent flow, found a dependence on where the critical onset shear stress is reached. If the onset shear stress occurs in the laminar flow region, a delay in transition to turbulent flow can occur.

Polymer Injection Studies

Practical application of the phenomena of viscous drag reduction caused by dilute polymer solutions includes increasing

speed or power reduction requirements for naval vessels and increasing the flow through conduits. Realization of these advantages generally requires injection of polymer solutions into a developing boundary layer. Observation that drag reduction is related to changes in the sublayers implies that injecting polymer near the wall affects considerable drag reduction with relatively small amounts of polymer. Literature pertinent to this area of the field will now be reviewed.

Pipe Flows

Wells (1968) suggested uniform injection through a porous wall since it raises the additive concentration to the drag reducing level in the wall region only. Using a Reynolds-Prandtl analogy to analyze the diffusion process, he calculated that distributed injection would require 40 to 140 times less additive than slot injection to maintain equivalent drag reduction. The point was made that a continuously ablating additive coating would yield the maximum performance advantage if it could be made to ablate at the optimum rate.

Wells and Spangler (1967) performed a series of experiments in order to determine whether the presence of the additive only in the wall region could produce significant local shear stress reduction. The experiments utilized centerline injection and

circumferential slot injection of dilute polymer into fully-developed turbulent flow of a Newtonian fluid. It was found that the local pressure loss was reduced by an amount comparable to the flow of a uniform concentration, when the fluid was injected at the pipe centerline. However, no reduction in local pressure loss occurred until the fluid diffused into the wall region.

Maus and Wilhelm (1970) conducted polymer injection tests with a fully-developed flow in a 1.625-inch diameter smooth acrylic pipe. Five circumferential injection slots located 6 inches apart were used. Each slot was 0.050-inch wide and inclined 30° to the pipe centerline. The effects of Reynolds number, injection rate, number of injection points, and concentration of injected solution were studied. It was found that maximum drag reduction occurred when polymer was injected through the furthest upstream slot rather than being distributed over the test length.

Walters and Wells (1971) conducted tests using uniform ejection of polymer solution through a stainless steel porous pipe section into fully-developed turbulent pipe flow. Concentration profiles, velocity profiles, and wall shear stress data were obtained. Fluorometric techniques were used to obtain the concentration profiles. Uranine B was selected as the fluorescent dye over several others, as the laboratory apparatus could be easily decontaminated. The dye was mixed with the injection fluid and

then captured tracer sample concentrations were measured with a fluorometer. Accuracies of the measurement instrumentation of two parts per billion were reported. Uniform polymer injection at the wall appeared to somewhat inhibit turbulent diffusion away from the wall resulting in high wall concentrations. For certain conditions of high polymer mass flux, a wall friction increase was noted, possibly due to the higher viscosity in this region. As compared to water injection, a one to two order of magnitude reduction in total diffusivity in the ejection region was noticed. Downstream of the ejection section, an order of magnitude reduction of total diffusivity was noted along with a significant reduction in wall friction.

Tullis and Ramu (1973) studied the characteristics of mean turbulent flow in the entrance region of a rough pipe for water and for polymer injection into a boundary layer. Polyox WSR-301 was injected through a perforated wall pipe section of a 12-inch diameter, 200-foot-long steel pipe used for the study. Drag reduction of up to 80% in the fully-developed region and 90% in the inlet region were recorded. Comparison of water and dilute polymer ejection showed the polymer concentration profiles developed slower than that of the water alone, indicating lower diffusion of the polymer solution. The inlet length needed for flow to fully develop was found to be greater for polymer injected flows than for the case of no injection. In the fully

developed region, the maximum drag reduction measured was 80% at $C_\infty = 25$ WPPM. Drag reduction in the inlet region appeared to be independent of injection concentration. Fluorescent techniques using rhodamine WT dye were used to measure the small concentration of polymer. Mean flow velocities between 5 and 50 ft/sec. ($R_e = 3 \times 10^5$ to 3×10^6) were used. Injection concentration varied from 100 to 2400 WPPM at rates of 30 to 220 gal/min at a location 3.5 pipe diameters from the pipe inlet.

Sellin (1974) reported drag reduction of 40-50% in large scale tests at R_e of 1.5×10^5 . A Polyox WSR-301 solution was added to water flow in a 203-mm diameter pipeline, 4190 meters in length at the Bristol Sewage Treatment Work at Avonmount, England. Polymer powder, corresponding to a final concentration of 40-60 WPPM, was continuously mixed in a votex chamber and the resulting slurry pumped into the pipeline using a gear pump.

Open Channel Flows

Latto and Shen (1970) performed an experiment of slot injection over a flat plate suspended in a closed loop flume. Concentration of Polyhall-295 from 200 to 600 WPPM were ejected at a 20° angle. Using hot film anemometry it was found that momentum diffusion was less than that for pure water. The flow rate velocity, and angle of ejection of the polymer solution were

also found to be important. Large percentage drag reductions were reported by injecting high concentration aqueous polymer solutions into turbulent boundary layers at low flow rates. It was found that tangential injection at the lowest possible velocity was desirable.

Wetzel and Ripkin (1970) experientially studied the injection of Polyox WSR-301 into a developing boundary layer in a 9-foot, wide open channel. Pitot tubes were located at positions 16, 28, and 60 feet downstream of the injection slot. Polymer injection resulted in much fuller velocity profiles than did water injection. Several methods of polymer concentration determination were investigated including: polarography, the turbidimetric method, and the fluorimetric method. The fluorimetric method was found to give rapid, accurate results. Concentration profiles for water, 1000, 2000, and 3000 WPPM, were found to be in good agreement with the curves developed by Morkorin (1963).

A maximum drag reduction of 25% was experienced over the 40-foot boundary layer length, which resulted in a downstream wall concentration of 30 WPPM. At a distance of 16 feet from the slot, greater drag reduction was attained for the lower concentrations injected than for the larger quantities. At distances further downstream the reverse was true, with better drag reduction attained with the larger injection quantities.

The behavior was attributed to more complete mixing.

Color-dyed polymer injection tests revealed that shortly after injection, the flow organized into a definite pattern of large wavering parallel streaks. This streaking was reported to be a secondary, three-dimensional vortex motion superimposed on the two-dimensional flow.

Fabula and Burns (1970) invoked the negative roughness analogy so that the outer layer mean velocity similarity is unaffected by friction reduction. The similarity law of mixing with polymeric friction is predicted to be the same as without polymeric friction reduction. The velocity defect law of Coles (1956) as well as his value for the law of the wake parameter Π of 0.55 were adopted. A relationship for calculating the local additive concentration at downstream stations along the wall was developed and compared to preliminary data on mixing in an open channel boundary layer injected with Polyox WSR-301.

Latto and Middleton (1970) reported on extensive velocity profile data taken with hot film probes for flow of homogeneous solution of Polyacrylamine MRL-402 over a flat plate suspended in a recirculating flume. Direct drag measurements were made over a period of time for concentrations of 0, 25, 50, and 75 WPPM which indicated no appreciable degradation of the polymer. The turbulent boundary layer profiles appeared "fuller" than corresponding

profiles for pure water. A friction velocity of $U_{\tau}^* \approx 0.074$ ft/sec was found.

Fruman and Tulin (1974) performed a study of diffusion of a thin tangential jet of Polyox WSR-301 solution injected into the turbulent boundary layer of a flat plate vertically suspended in a free-surface, high-speed water channel. Freestream Reynolds numbers of the order of 3.6×10^7 were achieved. Drag measurement by reluctance force gages were taken. Wall concentrations of polymer were taken using a light-intensity, dyed-additive method. The concentration distribution along the wall was found to be represented by two regions.

Within the first region, the wall concentration was practically constant and equal to the injected polymer concentration. In the second region, the concentration varied inversely with the distance from the injection slit. The length of the first zone was found to be 15 to 20 times that of water injection. This extended initial zone appeared to be directly related to the thickening of the viscous sublayer, the reduction of shear stress, and the decrease of molecular diffusivity.

In the region where turbulent diffusivity was predominant, both polymer solution and solvent flows displayed similar behaviors. The distribution of the wall temperature over a flat plate given

by Seban (1960) provided a heat transfer analogy for correlation of data. According to Seban:

$$\frac{T}{T_w} = 25.0 \frac{(\rho_i v_i)^{1.2}}{\sigma u} (X/S)^{-0.8}. \quad (27)$$

Whereas, Tulin indicated $\sigma = \sigma_i$, and therefore

$$\frac{C_w}{C_i} = 17.01 \frac{(v_i)^{1.06}}{U} (X/S)^{-0.711}. \quad (28)$$

Closed Channel Flows

Wu (1969) presented experimental data obtained by injection of various polymer concentrations along a flat plate, and trends similar to Poreh et al. (1971) were noted (lower initial concentrations caused higher drag reductions). The results of Wu indicate poor mixing between the injected fluid and its surroundings. Photographs of submerged jets confirm that additives suppress turbulent diffusion. The flat plate results also suggest that, for efficient drag reduction, the solution injected should be dilute and comparable to the discharge within the inner boundary layer.

Wu and Tulin (1970) performed experiments in a circulating water channel with ejection of various polymer concentrations along smooth and rough plates forming the top of the closed test

section. It was recommended that, for the most effective drag reduction, the slot ejection angle should be small with respect to the flow direction and the slot opening should be comparable to the thickness of the viscous sublayer. Injection rates were also comparable to the normal viscous sublayer discharge. Optimum additional concentrations were found to be $10^2 - 10^3$ WPPM for the smooth plate and an order of magnitude larger for rough surfaces, where mixing due to roughness causes increased dilution of the injected solution.

Poreh and Cermak (1962) studied two-dimensional turbulent mixing of ammonia gas from a line source near a wall. They envisioned a four-zone diffusion process that is worthy of description since the concentration profiles are considered representative of polymer diffusion and for this reason have come under much study. The four zones as described by Poreh and Cermak are:

1. An initial zone - This zone is very close to the source in which a large portion of the diffusion boundary layer is submerged in the viscous sublayer. The length of the region is determined by: the initial condition near the source, relative to the thickness of the sublayer; the injection velocity; and the magnitude of the molecular diffusivity. The extent of

this zone was not determined. Very little reliable data were obtained in this region due to very large velocity and concentration gradients.

2. The intermediate zone - In this zone the diffusion plume is submerged in the momentum boundary layer and its thickness is large when compared to that of the sublayer. The diffusion rate in this region is relatively large and the concentration profiles are found to be approximately similar in the sense that

$$\frac{C}{C_{\text{Max}}} = f(z/\lambda), \quad (29)$$

where λ is a characteristic height of the diffusion boundary layer defined as the distance from the wall where $C/C_{\text{Max}} = 0.5$. Measurements in air indicate that the length of the intermediate zone is 20 to 40 boundary layer thicknesses downstream from the source.

3. The transition zone - In this zone, the diffusion rate is slower due to the lower level of turbulence in the outer portion of the boundary layer.

4. The final zone - The growth of the diffusion boundary layer coincides with that of the momentum boundary layer in

this zone. In this stage the maximum concentration near the wall is inversely proportional to the thickness of the boundary layer and the ambient velocity.

Morkovin (1963) considered the experimental evidence of Poreh and Cermak (1964) for the final two zones of quasi-similarity and concluded that they were consistent with the concepts of eddy diffusivity. He described their data as follows:

$$\text{Intermediate zone: } C/C_w = e^{-0.693} (y/\delta_d)^{1.5} \quad (30)$$

$$\text{Final zone: } C/C_w = e^{-0.693} (y/\delta_d)^{2.15}. \quad (31)$$

Figure (4) displays a plot of the concentration profiles in the intermediate and final zones.

Poreh and Hsu (1971) indicate that the most widely used method to predict gross diffusion patterns in turbulent flow employs an eddy diffusivity model. This model assumes that the flux of the diffused matter by turbulent fluctuation is proportional to an eddy diffusivity term, D_e , times the local concentration gradient:

$$q_y = - D_e (\partial c / \partial y). \quad (32)$$

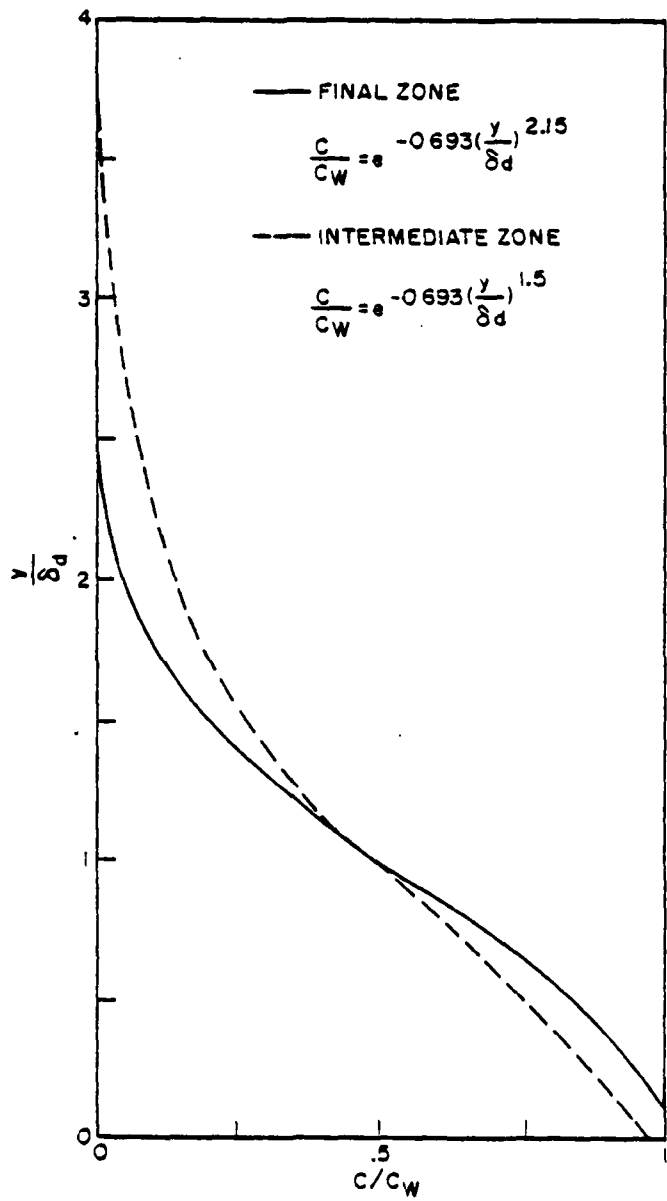


Figure 4. Concentration profiles in the intermediate and final zones

It is further assumed that D_e is a function of the flow field and its value can be specified at a point regardless of the position of the source. They point out that this assumption holds true only at distances from the source that are large compared to the Lagrangian integral scale of turbulence. Measurements made by Poreh and Cermak (1964) indicate that this limitation holds for diffusion in turbulent shear flows. Estimates of the Lagrangian integral scale suggest that it is of the order of boundary layer thicknesses.

Another method for treating diffusion patterns is based on Batchelor's (1957) Lagrangian similarity hypothesis used to predict the turbulent motion of particles in steady, self-preserving shear flows. Cermak (1962) applied the Lagrangian similarity hypothesis to predict diffusion from a continuous point and line source with the conclusion that results from the application of the Langrangian similarity hypothesis were significant for the modeling of diffusion.

Hsu (1971), and Poreh and Hsu (1971) applied these techniques to predict the diffusion boundary layer growth in the intermediate, transition, and final zones for polymer flow. The following equations that resulted describe the change of the mean vertical position, \bar{y} , and the mean longitudinal position, \bar{x} , for an ensemble

of single particle releases, in the logarithmic portion of the boundary layer:

$$\frac{d\bar{v}}{dt} = bV^* \quad (33)$$

where b is Batchelor's constant, and

$$\frac{d\bar{x}}{dt} = u(\bar{y}). \quad (34)$$

It follows, therefore, that

$$\frac{d\bar{v}}{dx} = \frac{bV^*}{u(\bar{y})}. \quad (35)$$

Poreh and Hsu (1971) further conclude that the boundary concentration downstream from a continuous line source may be given by

$$C_{Max} = \frac{Q}{\bar{y} u(\bar{y})} \quad (36)$$

where Q is the discharge of the source per unit width.

Ellison (1959) estimated that Batchelor's constant is given when $b = K$, where K is the Von Karman constant, $1/k = a_\zeta$, in equation (39). His analysis further suggests that \bar{y} (the mean position of particles at a given cross section, x) is equal to \bar{Y} , (the mean position of single particle releases when $\bar{x} = x$). The

mean position of a particle at any cross section, x , may be defined as:

$$\bar{y} = \frac{\int_0^{\infty} cy dy}{\int_0^{\infty} (c) dy}. \quad (37)$$

By replacing y with y/δ_d where δ_d is the value of y when C/C_{Max} is .5, and C by:

$$C/C_{Max} = f(y/\delta_d) \quad (38)$$

equation (37) may be integrated to obtain

$$\bar{y} = a_2 \delta_d. \quad (39)$$

Substituting equation (39) into (35) results in an expression for the diffusion boundary layer developing with distance x , such that

$$a_2 \frac{d\delta_d}{dx} = \frac{bV^*}{u(\bar{y})}. \quad (40)$$

Hsu (1971) observed improved agreement with data when replacing the constant b with the expression

$$b = K(1-\bar{y}/\delta). \quad (41)$$

Figure 5 presents a comparison of experimental data with results from equation (40) for $b = K$, $b = .8K$, and $b = K(1-\bar{y}/\delta)$. The growth of the diffusion boundary layer within the momentum boundary through several zones of diffusion is also shown in this figure.

Sampson (1969) constructed a recirculating water tunnel and an instrumentation system for investigation of turbulent, non-Newtonian, flat plate boundary layers. Non-Newtonian velocity profile data were obtained by laser velocimeter at Reynolds numbers in the region of 10^6 ; the 1/7th power law velocity profile was found to correlate well with the data.

In his studies with concentrations of 100 WPPM of the polymer Separan AP-30, Rudd (1972) found the drag reduction mechanism confined to the viscous sublayer close to the wall. The polymer did not appear to have any significant effect on the central region of flow. A test section of one-half inch square pipe, 7 feet 6 inches long, was used in a recirculating flow system driven by a peristaltic pump.

Velocity measurements were taken with a laser velocimeter. It was found that at concentrations of 100 WPPM, the polymer molecules produced quite a significant amount of light scattering, requiring no additional seeding.

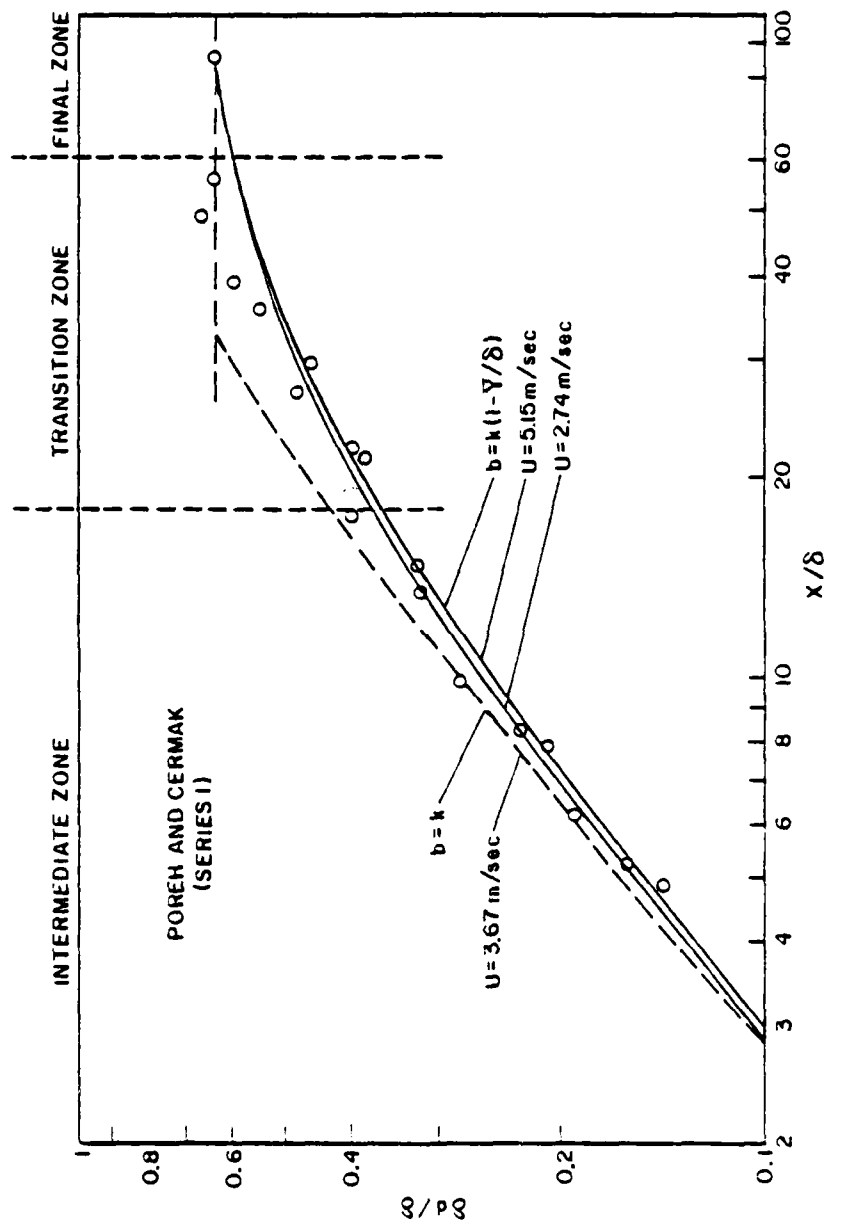


Figure 5. Growth of the diffusion boundary layer within the momentum boundary layer
(from Hsu (1971))

Logan (1972), using a one-half inch square duct under gravity feed, confirmed Rudd's findings of increased streamwise turbulence intensities and decreased spanwise intensities.

Using the recirculating tunnel built by Sampson (1969), Kumor and Sylvester (1973) conducted a series of experiments on the time effects of polymer drag reduction degradation on mean velocity profiles. Sparan AP-30 was the polymer used. The experiments show that the velocity gradient at the wall increases with time, while the sublayer thickness decreases.

Reischman (1973) attempted to correct the flow facility deficiencies of previous investigations. He constructed a unique dimensional turbulent flow channel, in which the side walls were slightly bowed, to allow good spatial resolution at the wall in the center of the channel. The flow channel was constructed of 1/4-inch Plexiglas with a cross section of 1 inch by 12 inches (an aspect ratio of 12:1) and a length of 70 inches. Velocity measurements in homogeneous 100 WPPM solution of Magnifloc 837-A, Sepman AP 273, and Polyox WSR-301 were made using a laser Doppler anemometer measuring individual realizations. For drag reductions of 40% or less for the near wall velocity measurements, the viscous sublayer (indicated by a linear velocity profile) was found to be of the same extent as for a comparable solvent flow. Reischman found no evidence of a thickened sublayer.

Drop Tests, Rotating Disks and Cylinders

Crawford and Pruitt (1963) were among the first to observe the increased velocity of steel spheres falling in a solution of Guar Gum as compared to their velocity in plain water. Ruszczycky (1965), using steel spheres of a diameter up to 1 inch, performed tests in concentrated solutions of Guar Gum and Polyox WSR-301 up to 15,000 WPPM. For the 1-inch spheres, the maximum drag reduction observed was approximately 28% at Guar Gum concentration of 5000 WPPM and a Polyox concentration of 7500 WPPM.

Lang and Patrick (1966) found that the drag of spheres falling in Polyox WSR-301 was reduced by about 70% while the drag of other shapes, such as cones and cylinders, was only slightly reduced. Dyed-wake photographs of falling spheres indicated a significant change in the shape of the wake, with the laminar separation point being shifted rearward (Re range 6×10^3 to 2.5×10^5).

Hoyt et al. (1965, 1964) showed that addition of Guar Gum lowers the torque by as much as 70% for concentrations of 300 to 400 WPPM for turbulent rotating disk flow.

Using a multiple disk apparatus, Whitsitt et al. (1969) showed that rough disks gave higher torque reduction of about 60%

in Guar Gum solution at 250 WPPM than did smooth disks. A polyacrylamide solution lost its torque-reducing ability very quickly. However, the work of Huang and Santelli (1972) showed that polyacrylamide solutions were more resistant to shear degradation when compared to polyethylene oxide.

Sirmalis (1974) conducted an extensive study of drag reduction on axisymmetric torpedo-shaped bodies having 6° and 12° spherical tail cones. During the study, experiments covering a range of Reynolds numbers from one to five million in plain water and polymer oceans of 1 to 60 WPPM of Polyox WSR-301 were conducted. Photographic studies revealed that, at very low concentrations, (2.5 WPPM), the fine structured turbulence was absent and only large scale turbulence remained. Computer routines tended to overpredict boundary layer thickness while indicating proper growth shapes. No shift in the boundary layer separation region was noted.

Testing in fresh water with polymer ejection from the body showed similar results but with better visual representation at the higher polymer concentration. Dyed water ejection tests displayed the characteristic coarse and fine turbulence structure. Ejection of 50 WPPM dyed polymer solution eliminated most of the fine structured turbulence leaving only the coarse structure. Dye streaking was apparent at the higher concentration levels. The streak spacing, consistent with laminar sublayer streaks,

was also in agreement with the number of ejection holes in the screen ejector in the nose of the body. A maximum of 70% reduction in skin friction was achieved with the 6° tail body in a polymer ocean of 20 WPPM.

Polymer diffusion tests were conducted at a fixed rate of 20.6 in/sec and a nominal velocity of 27 ft/sec. Wall samples and boundary layer samples at .025 inch and .055 inch were taken and analyzed by fluorometric techniques. Tests were conducted with water and concentrations of 5, 10, 20, 50, 500, and 1000 WPPM of polymer. All polymer tests displayed a drastically reduced diffusion resulting in an extended initial mixing zone. Similarity concentration profiles were found to have like forms, and therefore

$$\frac{C}{C_w} = e^{-0.693(y/\delta_d)K_3}. \quad (41)$$

Profile coefficient, K_3 , has an experimentally determined value of 0.75. Sirmalis indicates that the true value is believed to be below this value, since data were not obtained in the critical region of within approximately 0.010 inch of the wall. These results were considered significant in that they imply substantially reduced polymer quantities may be required with proper ejection techniques.

Review of Experimental Apparatus

The vast number of investigations concerning the phenomena of drag reduction, and the continuing attempts to conduct a definitive experiment, indicate the scientific community's interest in the problem and the difficulties involved. From these studies, it is known that drag reduction additives include soap solutions, algae, plant derivatives, and high molecular weight polymers. Additionally, a maximum drag reduction asymptote of approximately 80% has been shown. In spite of these efforts, the exact nature of the phenomena of drag reduction remains elusive to the various techniques applied to its study.

Flow visualization experiments have provided some insight from a qualitative view point, while pressure drop-flow rate experiments have contributed an indication of the magnitude and scope of the phenomena. The bulk of these efforts are, however, still contradictory and difficult to interpret due to the confusing features of the flow facilities and ambiguities in the measurement instrumentation employed.

Reischman (1975) points out that, in general, experimental techniques for velocity measurement may be separated into four groups: pitot tubes, bubble tracing, hot-film probes, and laser Doppler anemometers.

Pitot probe investigations comprise the largest group and are subject to errors requiring complex corrections. Smith et al. (1967) have demonstrated that measurements in identical flow situations made by various size pitot probes yield different results. Metzner and Astaria (1967) attribute these errors to the influence of additional viscoelastic normal stress terms. Corrections for pitot probe techniques are generally omitted, however, as being too complicated. In spite of this, Tomita (1970) applied viscoelastic corrections to his pitot probe measurements.

Hot film probes, the next largest group, depend upon the heat transfer characteristics of the medium. Frieche and Schmartz (1969) have shown that hot-element sensors are difficult to calibrate because polymer additives alter the heat transfer characteristics of the medium and collect on the sensors. It is pointed out that the calibration drift problem is particularly severe in dilute polymer solutions where the sensitivity of the probe to velocity changes is lower than it is in the water alone.

Donohue et al. (1972) point out that bubble tracing techniques are hampered by large uncertainties as well as being an extremely tedious process.

The fourth group comprise laser Doppler anemometer efforts. A relatively new discovery by Yeh and Cummings (1964), the laser Doppler anemometer is a linear, non-interfering instrument which does not depend on the rheological or intensive properties of the working fluid. The laser anemometer was first used in drag reducing flows during four investigations almost simultaneously: Chung and Graebel (1969), Goldstein et al. (1967), Rudd (1969), and Shankan (1969). The measurements of Shankan (1969) have insufficient sample size, however, for accurate results, while Goldstein et al. (1967) only made measurements on the tube center-line.

Chung and Graebel (1969) experimented in a small, .47-inch diameter pipe where the spatial resolution of their laser anemometer was very poor. Subsequently, five researches have made acceptable laser velocimetry measurements in drag-reducing flows. This group consists of Rudd (1969), Logan (1972), Sampson (1969), Kumor and Sylvester (1973), and Reischman (1975). Of these experiments, all were conducted in a square cross-section apparatus, except the work of Reischman who used a 12:1 aspect ratio tunnel. Rudd and Logan utilized a one-half inch square duct and Sampson, and Kumor and Sylvester, used an 8-inch square tunnel with a submerged off-center flat plate. White law (1973) has shown that non-symmetric secondary flows are significant in square duct flows.

Sampson (1967) reported that pump vibrations were significant, prohibiting meaningful tests at higher flow rates and that the effect of these vibrations on the laser system were unknown. Additionally, accommodations in both equipment and system design were necessary to minimize costs of the construction of the laser system. Although the electronic output was noisy with a relatively poor signal-to-noise ratio, usable data were obtained by use of a storage oscilloscope.

Kumor and Sylvester utilize the same facility as Sampson but offer no water data to allow verification of the suitability of this facility.

Reischman avoided the detrimental recirculation aspects of the previous researchers by using his flow facility in a blow down mode. In contrast to the previous researchers, Reischman used an individual realization-type laser Doppler anemometer, which measures the period for 10 cycles of a Doppler burst scattered from a single particle. However, the orientation of the laser light beam optical system was in an undesirable side scatter mode where scattered light intensity is predictably weak. The singular results of Reischman, indicating that the viscous sublayer does not thicken, were obtained in an improved flow facility under weak signal conditions for homogeneous polymer flow.

This is in direct conflict with the conclusion of all previous investigators.

Rudd, Logan, and Sampson used continuous wave anemometers employing a frequency tracker which converts Doppler frequency to an analog signal proportional to the instantaneous velocity.

To date, all of the work using laser Doppler anemometers has been performed with homogeneous polymer flows, not with ejection of polymer solutions. A goal of the present work was to improve the deficiencies of previous researchers and obtain data on velocity profiles, with and without injection of polymer solutions into the boundary layer on a submerged flat plate in a high aspect ratio, rectangular water tunnel. Laser Doppler anemometry velocity measurements in this experiment were made in the forward scatter mode where scattered light intensity distributions are strongest.

III. EXPERIMENTAL APPARATUS

The experimental apparatus in this research consists of a flow facility and water tunnel, a polymer ejection system, a laser Doppler anemometer system for velocity measurement, a fluorometer to measure boundary layer concentration profiles, and a minicomputer for real-time data processing. The characteristics of each element are discussed in detail in the sections that follow.

Flow Facility

The overall flow facility designed for this experimental effort is shown schematically in figure 6. Filtered water is fed to a 15,000-gallon capacity water tank having a constant head overflow, providing 5 psi flow head for the tunnel. Various filter cartridges allow filtration of particles ranging in size from 5 microns to .5 micron. A high pressure steam heat exchanger allows deaeration of the water by heating. The flow rate of water from the storage tank to the tunnel is measured by a Cox Instruments Co. turbine flowmeter and controlled by a manual ball valve in the exit line. A round to rectangular transition section provides entrance to a rectangular diffuser. The flow is then straightened in a settling chamber designed to form small scale turbulence of uniform distribution. The flow enters the water

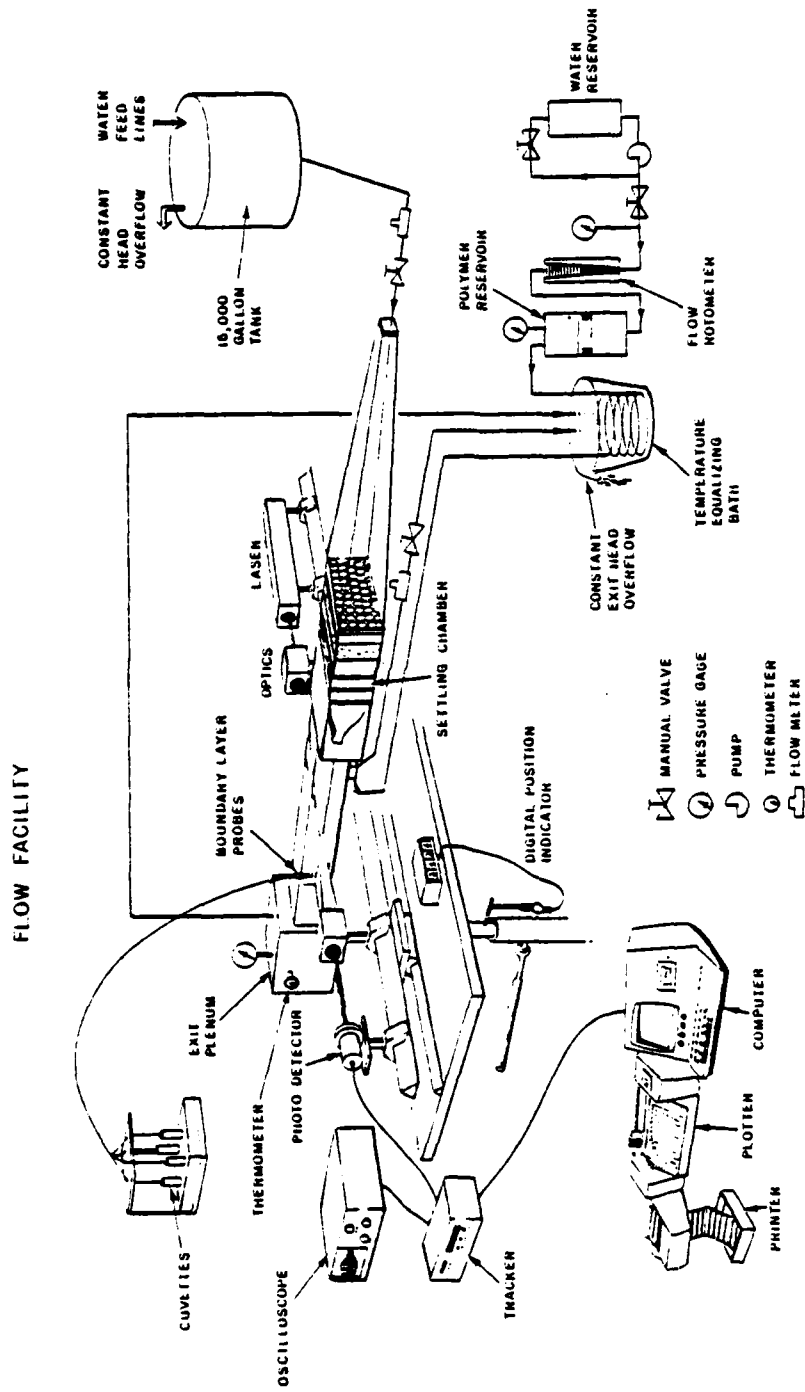


Figure 6. Experimental flow facility

tunnel through a specially designed transition nozzle. The flat plate is attached to the floor of the tunnel allowing wall samples to be taken through the bottom wall of the tunnel. The boundary layer approaching the flat plate is bled off through a suction port ahead of the leading edge of the flat plate. Boundary layer sampling probes are lowered through ports in the tunnel ceiling. Velocity measurements are taken throughout the entire internal volume without disturbing the flow using the laser Doppler anemometer techniques and a three-dimensional traversing system. The flow then exits the tunnel through an exit plenum. Constant tunnel exit pressure is provided by exiting the flow into a container with constant exit head overflow. The boundary layer bleed flow is also exited into this container. Polymer solutions, for ejection over the flat plate, pass through a delivery line coiled in the exit flow container. The temperature of the polymer solution then approaches the temperature of the water flowing through the tunnel. Figure 7 is a photograph of the actual test setup.

Initial Attempts

In order to avoid the design of a round to rectangular transition diffuser and because axial length was at a premium in the test setup, a relatively large cross-section settling

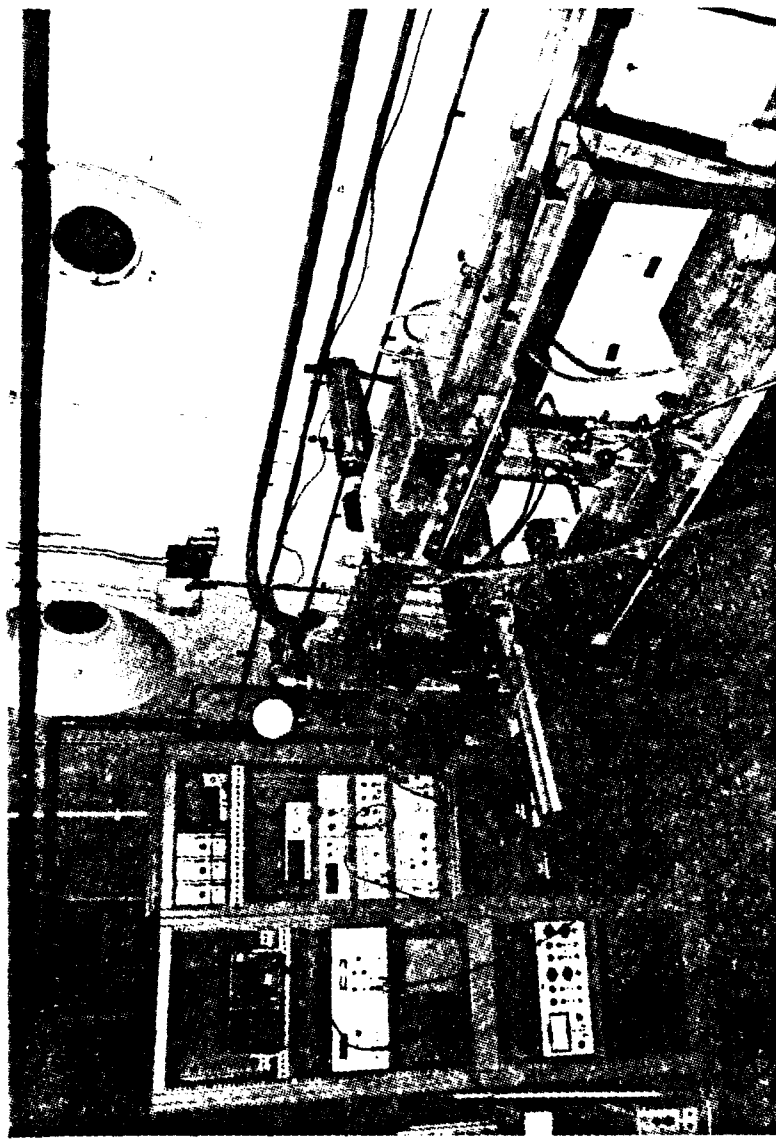


Figure 7. Experimental set-up photograph

chamber was designed and built of anodized aluminum as shown in figures 8 and 9. The dimensions were: width, 8.25 inches; height, 6.5 inches; and length, 11 inches. The top and rear side were made of Plexiglas for measuring and photographing the flow. Dye probe access ports were located in the top and the flow entered through a 3/4-inch fitting. Two overlapping perforated plates (0.25-inch diameter holes and 48% open area) were thought to distribute the flow, followed by 1/8-inch HEXCELL honeycomb (1 inch long) for flow straightening and four screens (24-mesh, .007-inch diameter wire of 67.4% open area) for the even distribution of fine, small-scale turbulence. A rounded edge slot formed the tunnel entrance.

The perforated plates were totally ineffectual as a high-speed central core water jet maintained itself well into the settling chamber. An impact distribution plate was attached to the inlet fitting. This fix transformed the high-speed core flow into violent turbulent recirculating flows. In addition, corner vortices formed in the exit flow, as shown in figure 10. At this juncture it became evident that a diffuser would be necessary to decelerate the flow and an entrance nozzle to the tunnel would also be required to eliminate the formation of corner vortices. A redesign of the settling chamber to provide equal contraction ratio in the horizontal and vertical planes was also performed in an attempt to further minimize the formation of corner vortices.

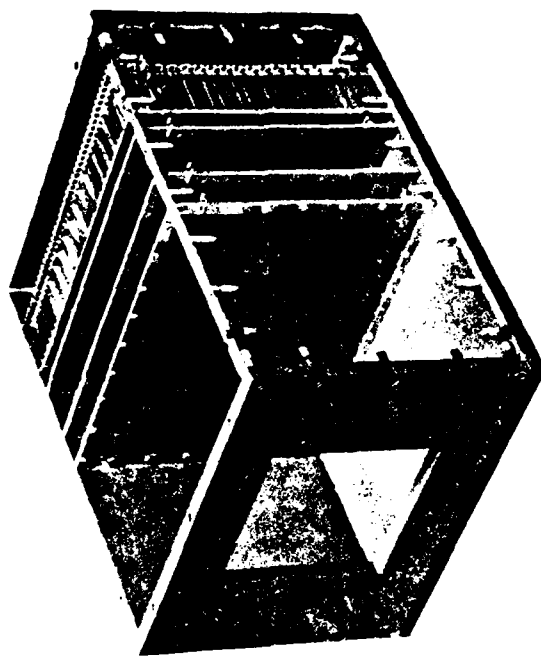


Figure 8. Initial settling chamber photograph

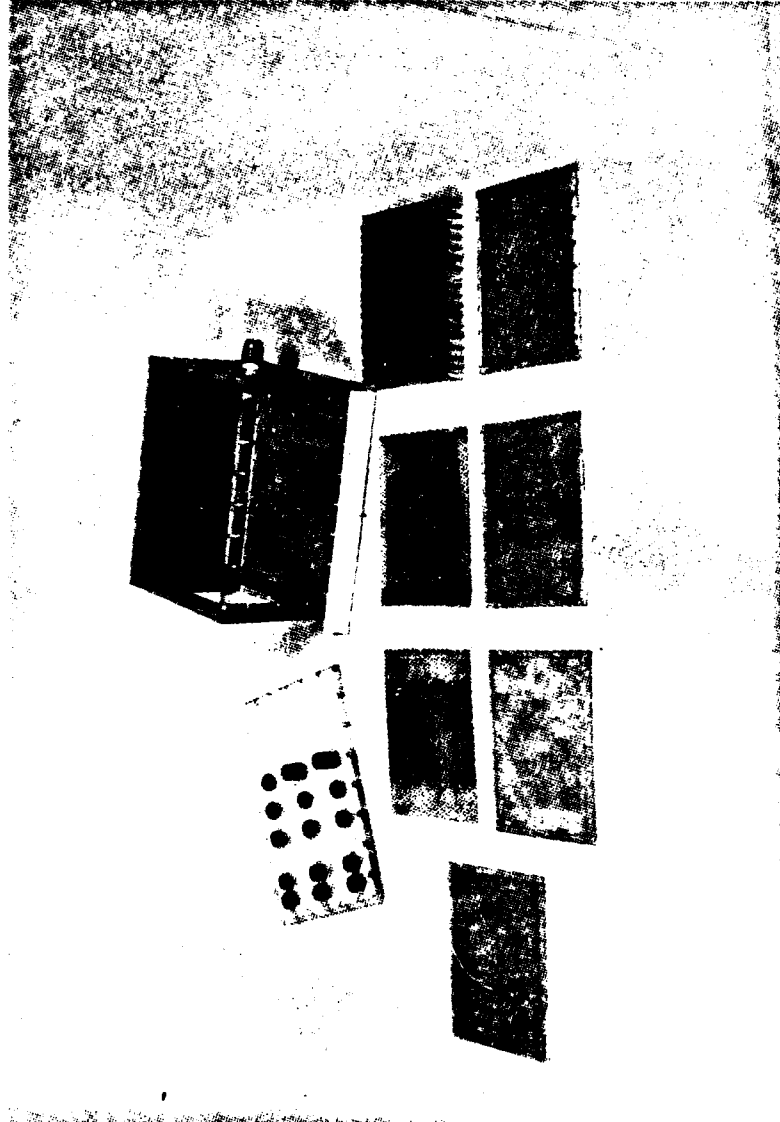


Figure 9. Initial settling chamber disassembled photograph

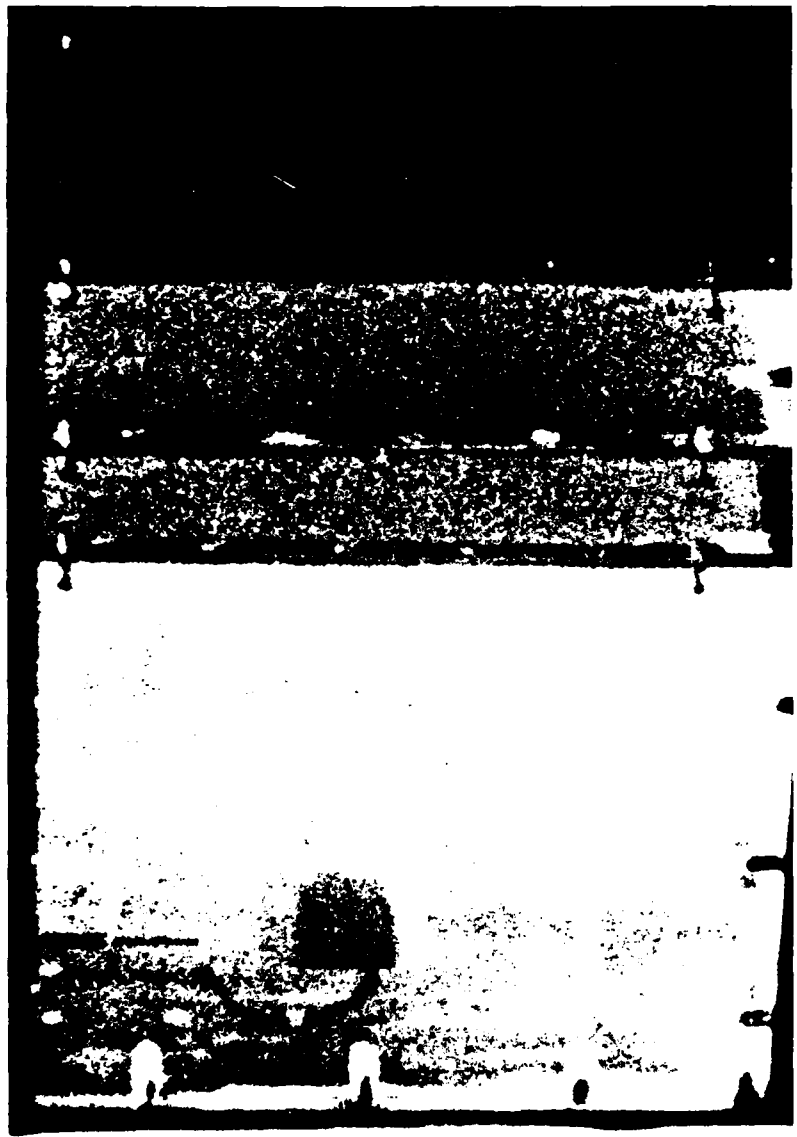


Figure 10. Initial settling chamber corner flow photograph

Settling Chamber

The second settling chamber design dimensions now remained firm at a width of 8.25 inches, a height of 2.75 inches, and a length of 18.5 inches. The contraction ratios from settling chamber to tunnel were fixed at 3.67 in both the horizontal and vertical planes, providing an overall contraction of 13.5:1. The settling chamber was constructed entirely of Plexiglas and had an internal configuration, shown (in order) in figure 11, consisting of a perforated plate, two screens, a honeycomb, and four additional screens, spaced at 1-inch intervals with 2 inches upstream of the honeycomb. The entrance to the tunnel was a well-rounded rectangular hole, shown in figure 12.

The configuration straightened the flow; however, corner vortices at the tunnel entrance remained (figure 13). A standoff rectangular nozzle was designed and tested with no success, as shown in figures 14 and 15. In addition, small flow oscillations appeared due to intermittent stall in the diffuser.

The corner vortices were finally eliminated by the design and fabrication of a transition nozzle in the form of a ninth order polynomial whose first four derivatives are zero at each end. The polynomial coordinates were placed on paper tape and used to cut templates for the vertical and horizontal contours in

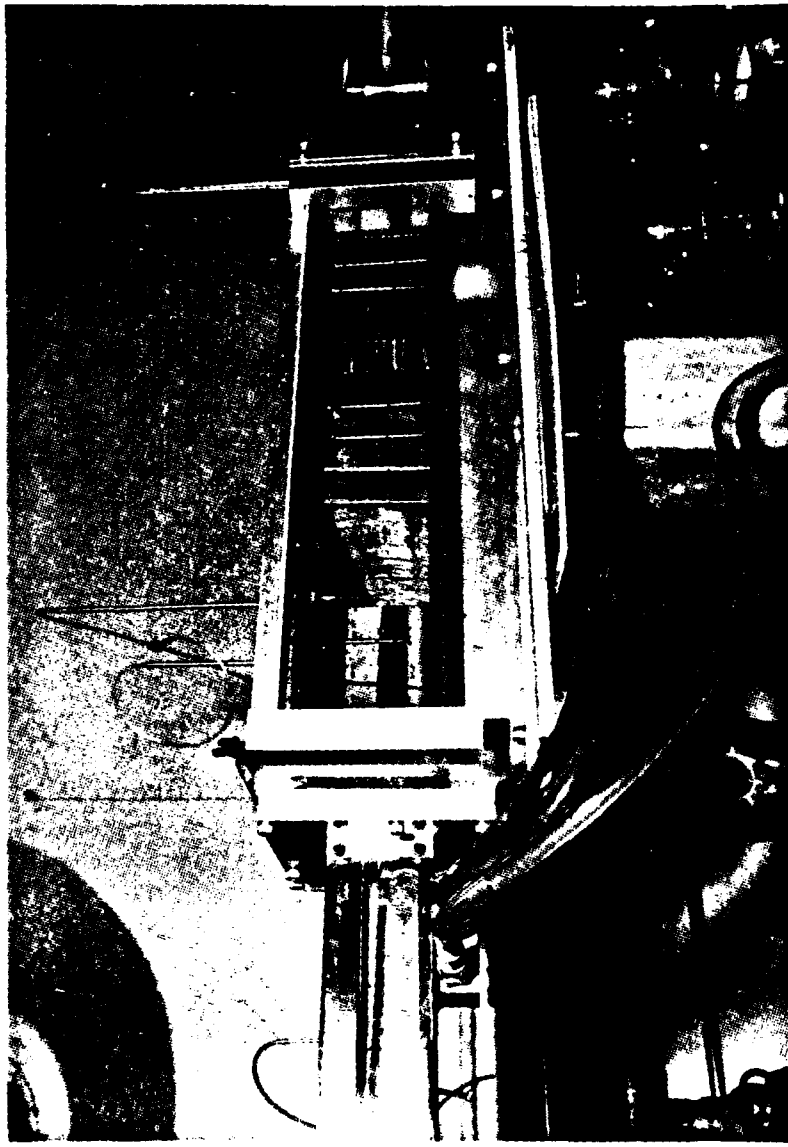


Figure 11. Settling chamber configuration photograph

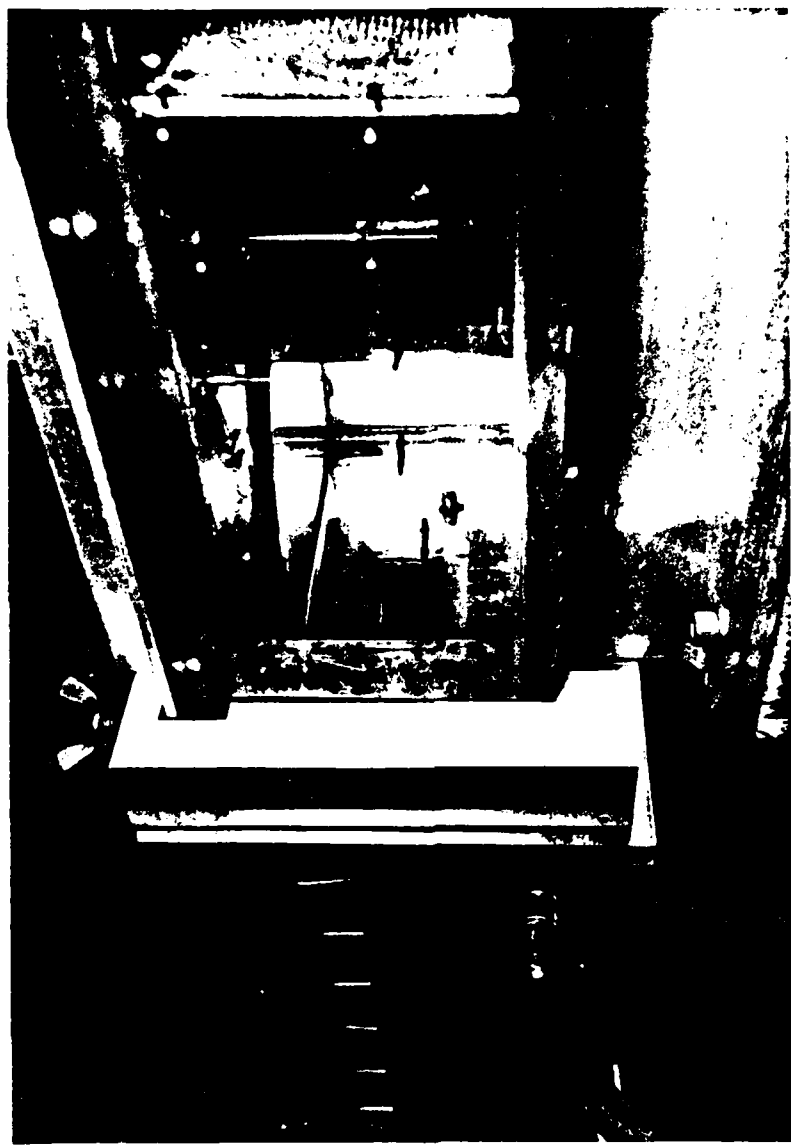


Figure 12. Rounded rectangular tunnel entrance photograph

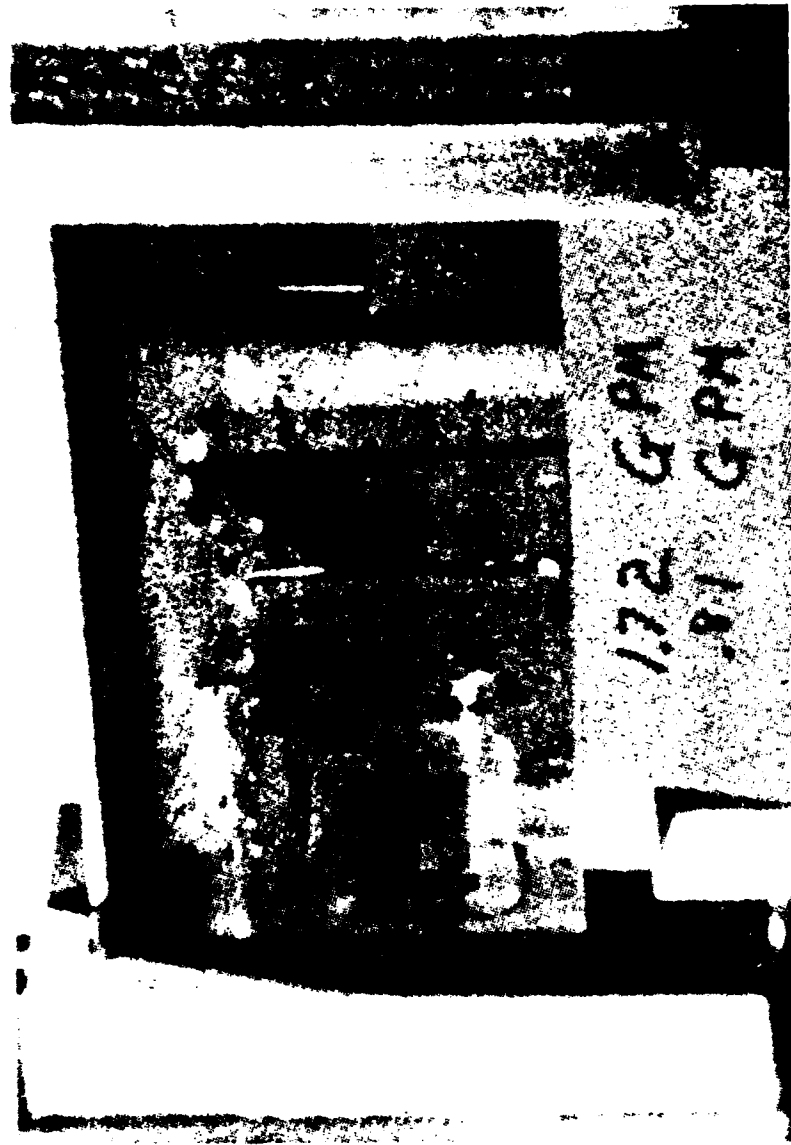


Figure 13. Settling chamber flow pattern photograph

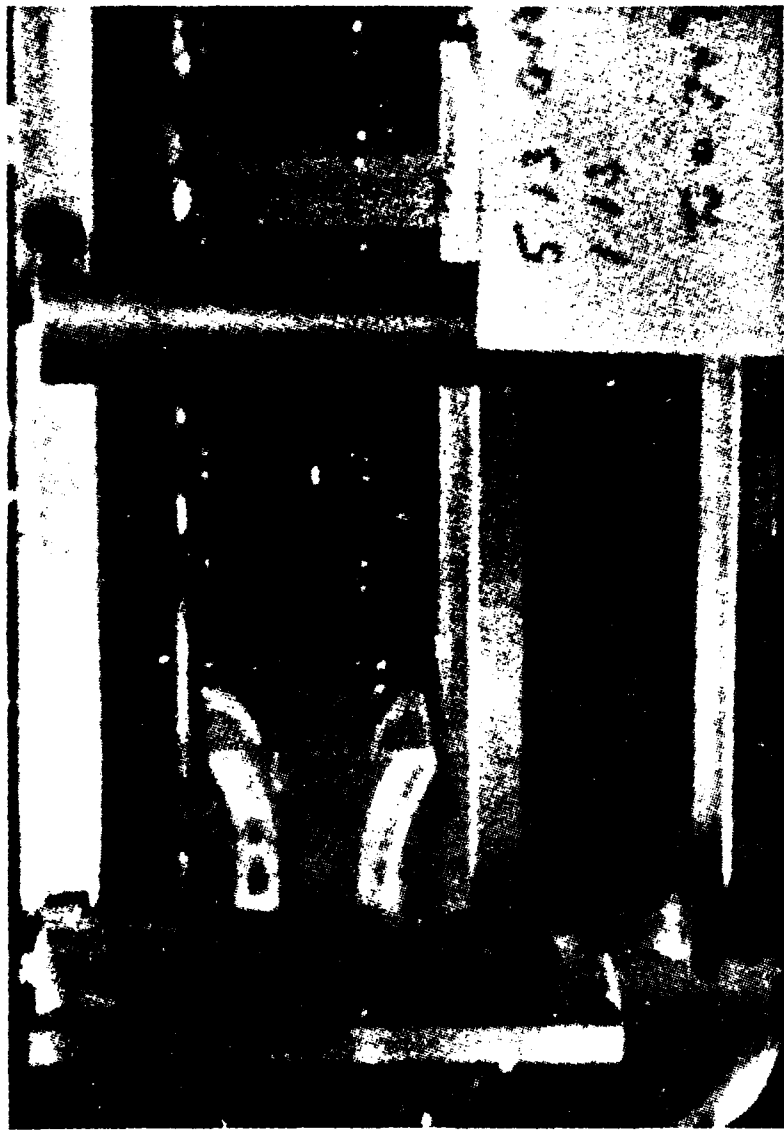


Figure 14. Rectangular stand-off tunnel entrance nozzle photograph



Figure 15. Rectangular stand-off tunnel entrance nozzle flow pattern photograph

a tape-driven automatic milling machine. These templates were used to cut a mandril from a cast block of epoxy resin. This mandril was placed in a casting box of the same internal dimensions as the settling chamber. The transition nozzle block was then cast over the mandril. Removal of the mandril after an appropriate curing time yielded a block with proper internal flow passage configuration that fit into the settling chamber. The transition nozzle used is shown in figures 16 and 17.

Discussions on the internal configurations of the settling chamber, with Drs. Andrew Chawat and Steven Barker at the University of California at Los Angeles, provided the key element for the removal of the final obstacle for flow conditioning. A 3-inch length of reticulated Scott foam quieted and steadied the flow, removing any remaining flow disturbances.

The final settling chamber design consisting of a perforated plate, Scott foam, honeycomb, two screens and a transition nozzle is shown in figure 18 and schematically in figure 19.

Diffuser

A 36-inch long rectangular Plexiglas diffuser (figure 20) was designed having no appreciable stall, according to Kline (1959). The entrance dimensions were 0.75 inches by 0.75 inches with rectan-

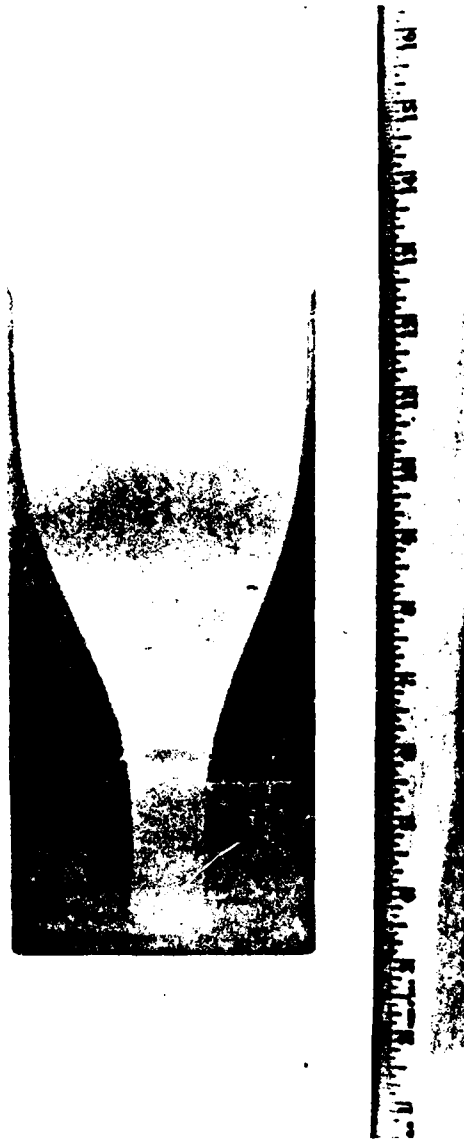


Figure 16. Transition nozzle side view photograph

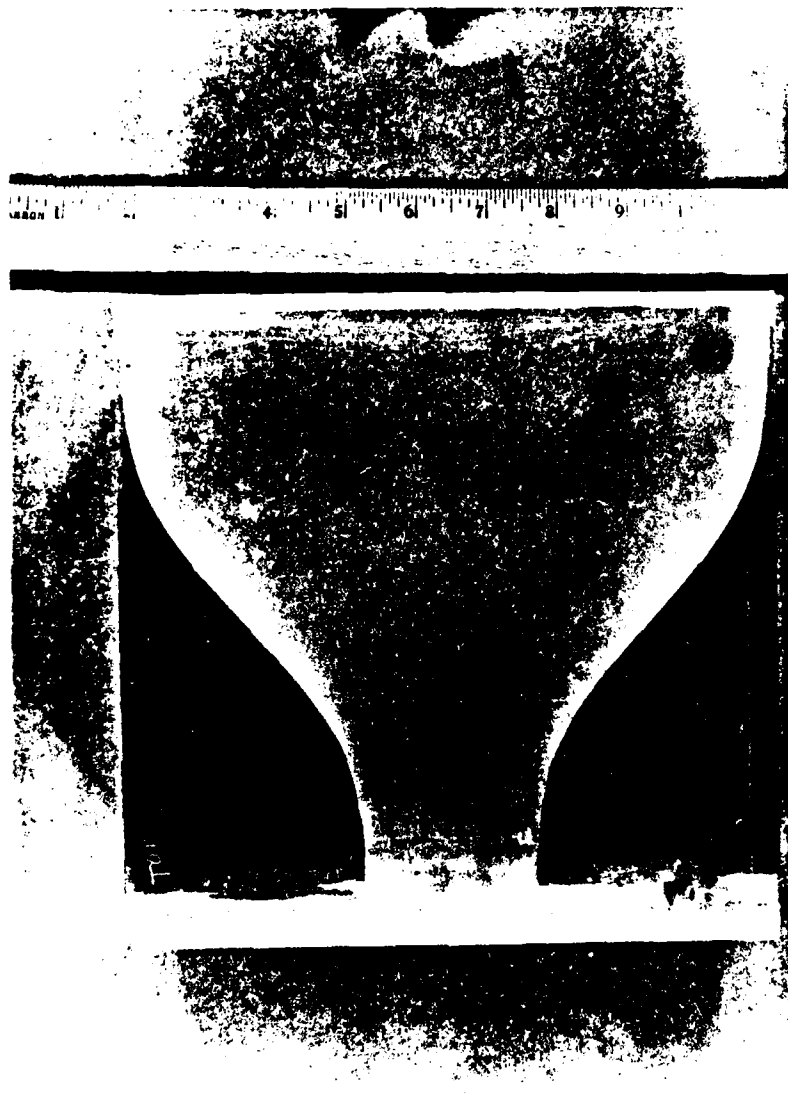


Figure 17. Transition nozzle top view photograph

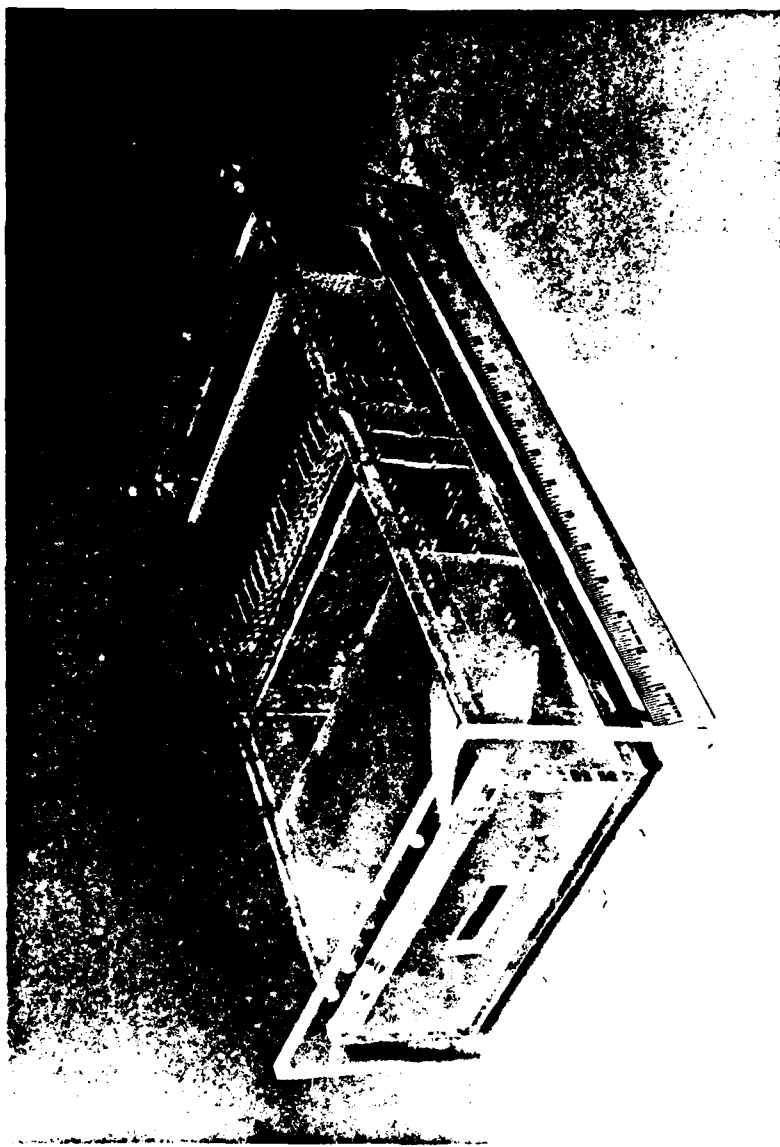


Figure 18. Final settling chamber configuration photograph

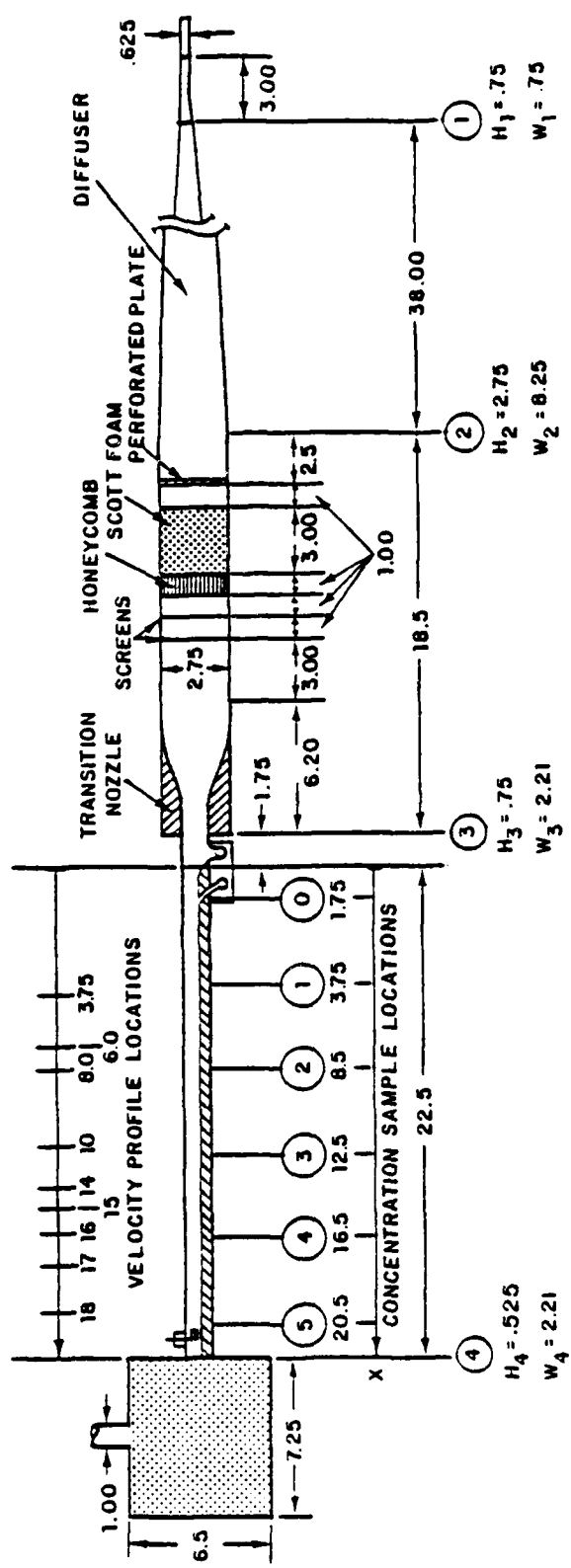


Figure 19. Test set-up schematic

AD-A103 070

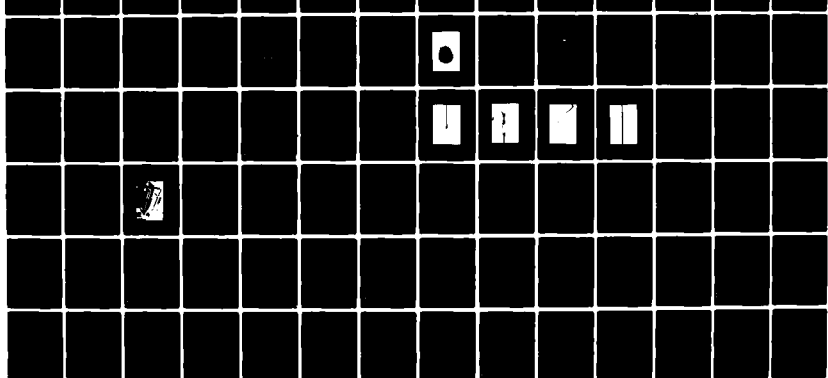
NAVAL UNDERWATER SYSTEMS CENTER NEWPORT RI
AN EXPERIMENTAL STUDY OF POLYMER DRAG REDUCTION AND BOUNDARY LA---ETC(U)
AUG 79 J MIGUEL
NUSC-TD-5656

F/6 20/4

UNCLASSIFIED

NL

2 or
302010



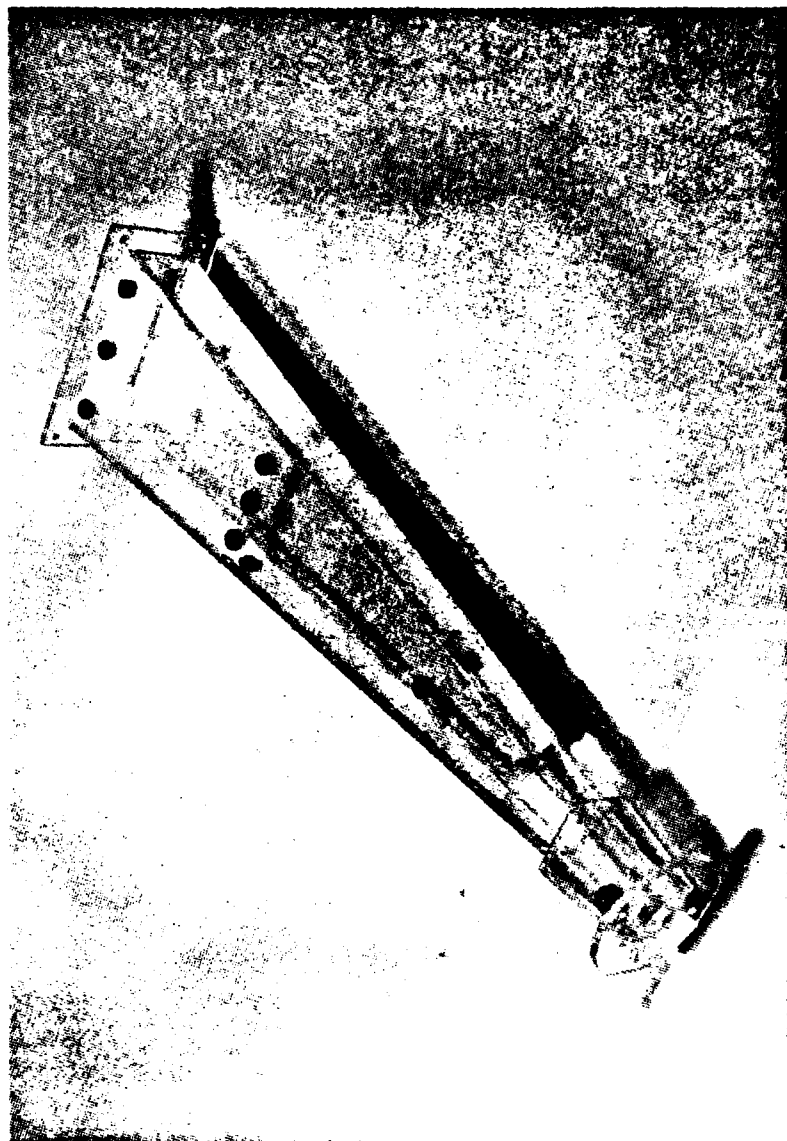


Figure 20. Rectangular diffuser photograph

gular exit dimensions of 8.25 inches in width and 2.75 inches in height to match the new settling chamber dimensions. In order to minimize separation effects in going from .625-inch (inside diameter) round pipe to a .75-inch square cross section, a special transition section was fabricated. The walls at the entrance of the diffuser were thickened with extra layers of Plexiglas and a round entrance hole of a diameter equal to the diagonal of the entrance was drilled. The interfaces where the round hole broke through the interior walls were hand-blended smooth. A conical transistion section from the .625-inch (inside diameter) inlet pipe to the rounded diffuser inlet was made and is shown in figure 21. A screen was incorporated to aid in maintaining flow distribution.

Tunnel Design

The tunnel is constructed of .375-inch thick Plexiglas walls and inverted aluminum channel sections forming the top and bottom of the tunnel. The interior dimensions are: height, .75 inches; width, 2.21 inches; and length, 24.25 inches. Ten access ports along the top of the tunnel allow insertion of boundary layer sampling probes into the tunnel flow. The five stations used in this experiment are shown in figure 19.



Figure 21. Conical diffuser inlet transition section photograph

Starting 1.75 inches from the entrance to the tunnel, an anodized aluminum flat plate is fixed to the floor of the tunnel. A one-half inch suction slot at the upstream edge of the flat plate allows the incoming boundary layer to be bled off and a new boundary to be started in the flat plate. An axially adjustable leading edge allowed the ejection slot height to be varied up to 0.050 inches in the horizontal, x, direction. Boundary layer wall concentration sampling holes (.030 inch in diameter) were drilled at locations corresponding to the probe sampling planes. The polymer ejection slit was located 1.75 inches from the leading edge and slanted at an angle of 15° to the flow.

Eight different leading edges, shown in figure 22, were tried in an attempt to obtain transition in the center portion of the plate. Of all the leading edges tried, the most effective one (figure 23) consisted of an epoxied sand surface (average grain size 0.020 inch) sloped at 7.5°.

Boundary Layer Probes

Boundary layer probe rakes were fabricated and are shown assembled in figure 24 and as an exploded view in figure 25. The mounting fixture has a slot machined in its side to allow the rake to be retracted up into the roof of the tunnel out of the flow passage. Figure 26 is a close-up of the probe tips showing their



Figure 22. Flat plate leading edge photograph



Figure 23. Sand roughened leading edge photograph

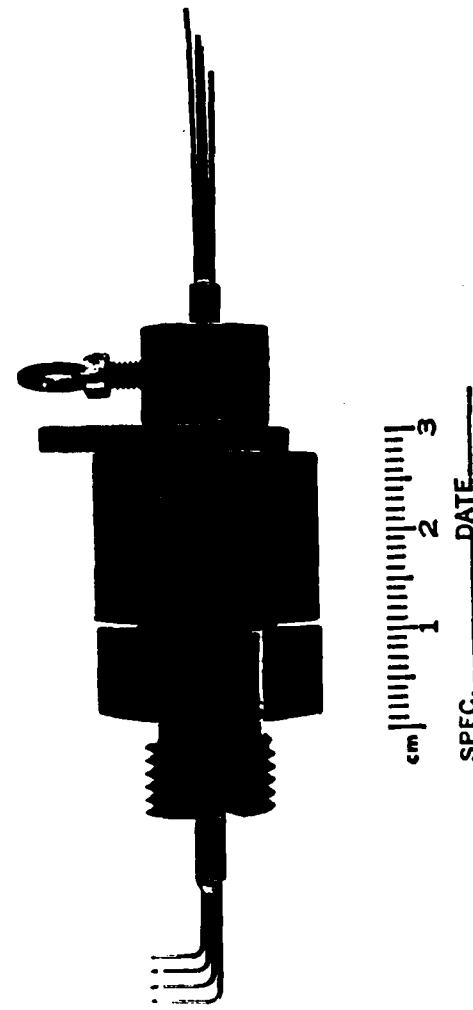


Figure 24. Boundary layer probe photograph

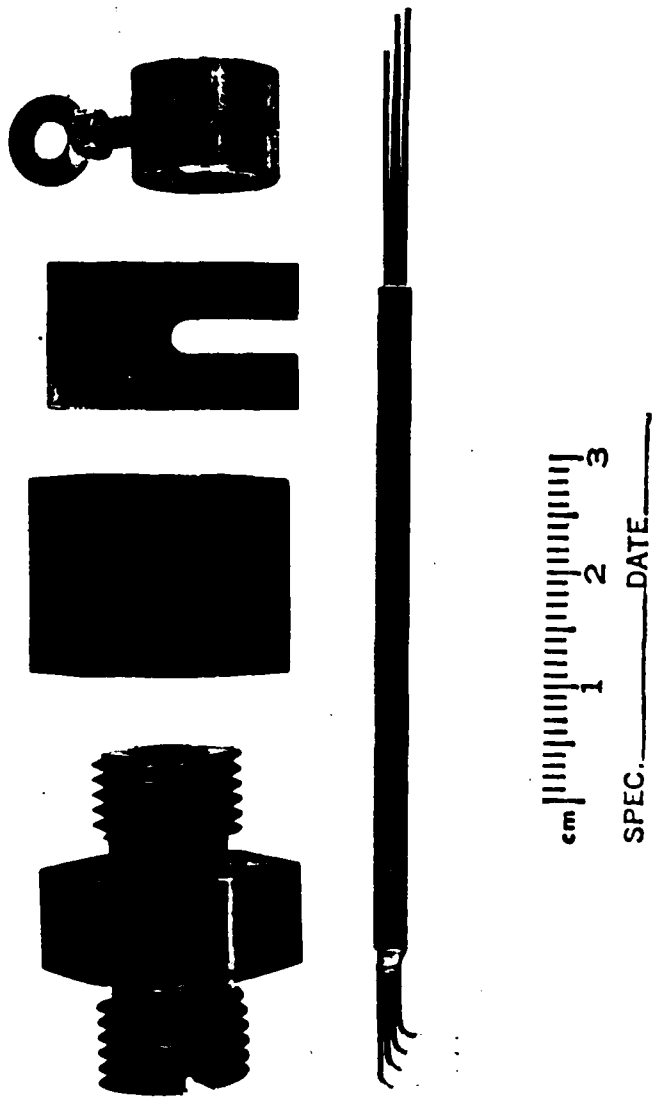


Figure 25. Disassembled boundary layer probe photograph

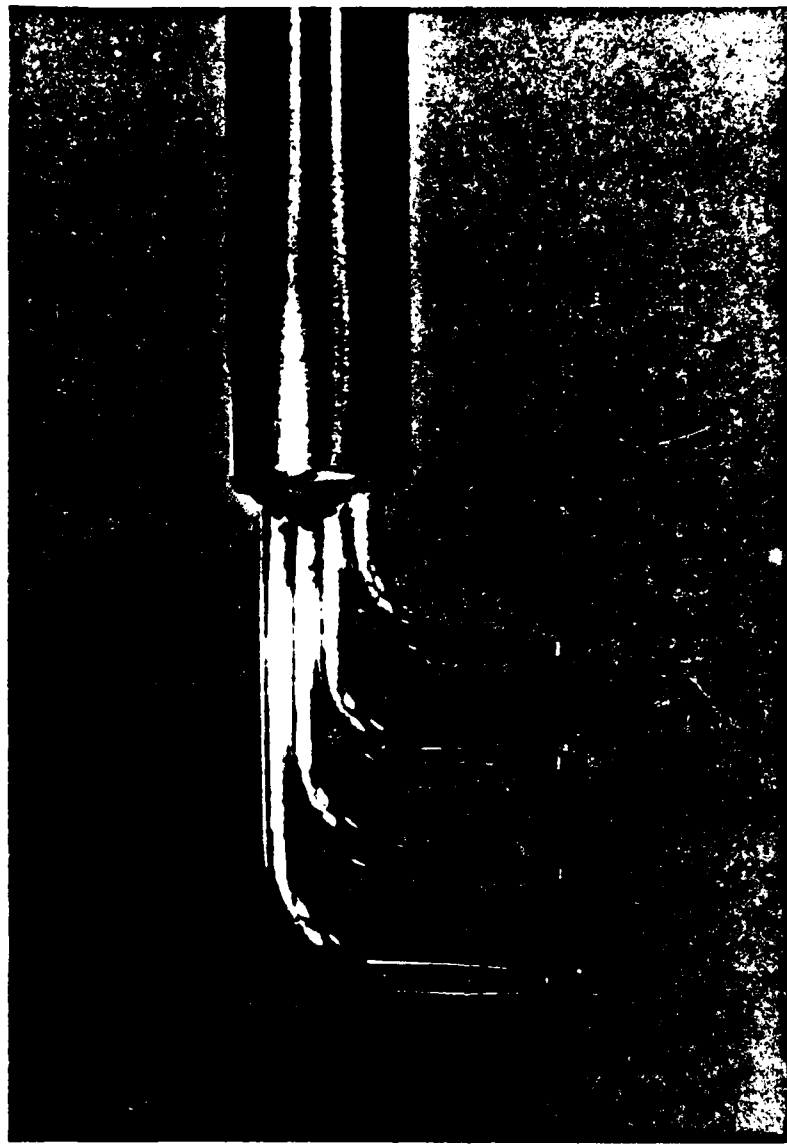


Figure 26. Boundary layer probe rake tip close-up photograph

tapered rectangular shape of .005 inch high by .015 inch wide. Figure 27 presents probe dimensions and table 2 presents the location of the sampling points with and without the spacers used to reposition probes in the vertical, y, direction. The boundary layer samples would pass through the probe and along a 36-inch by .020-inch diameter flexible tube to a sampling stand containing six cuvettes. Figures 28 and 29 show this arrangement with reservoirs in place of the cuvettes in the sampling stands.

Polymer Injection System

The polymer injection system was designed to minimize polymer degradation during the delivery process. As shown in figure 6, water is recirculated to a water reservoir. Part of the water flow is bypassed through a water-calibrated rotometer to the polymer reservoir. The polymer reservoir contains 13 liters of polymer solution above a separation piston. The water flow pushes the piston upwards. This action in turn pushes the polymer mixture out of the reservoir into the delivery line to the tunnel. The delivery line is coiled in the constant exit head container and submerged in a bath of tunnel exit flow water to equalize the polymer flow temperature with that of the main tunnel flow.

Figure 30 is a photograph of the polymer delivery system.

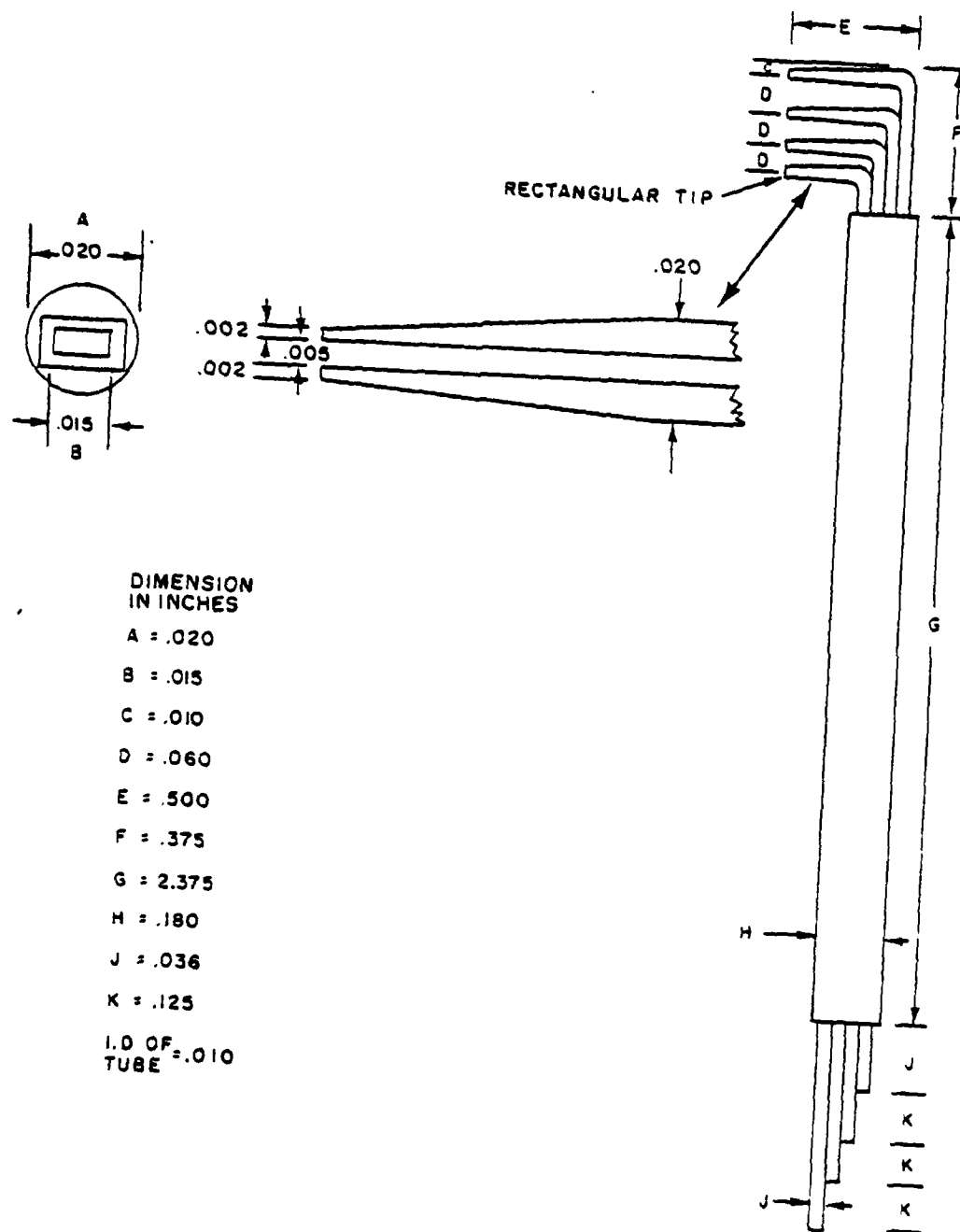


Figure 27. Boundary layer probe rake dimensions

TABLE 2
CONCENTRATION SAMPLING LOCATIONS IN THE BOUNDARY LAYER

Probe Sample	Y_c (Spacer .020-inch)	Y_c (Spacer .103-inch)
0	0	0
1	.010	.010
2	.030*	.072
3	.072	.113*
4	.092*	.134
5	.134	.175
6	.154*	.196
7	.196	.237*
8	.216*	.299*

* Spacer in place



Figure 28. Boundary layer probe rake placement photograph

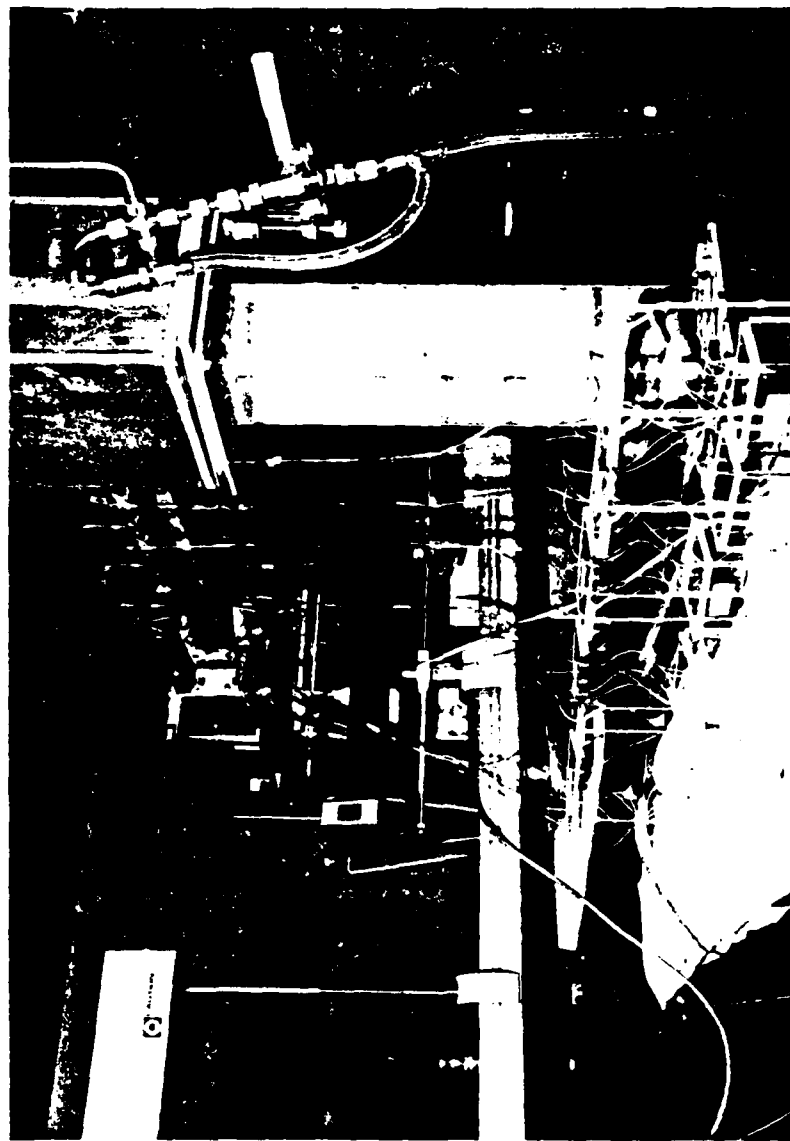


Figure 29. Boundary layer probe sampling system photograph

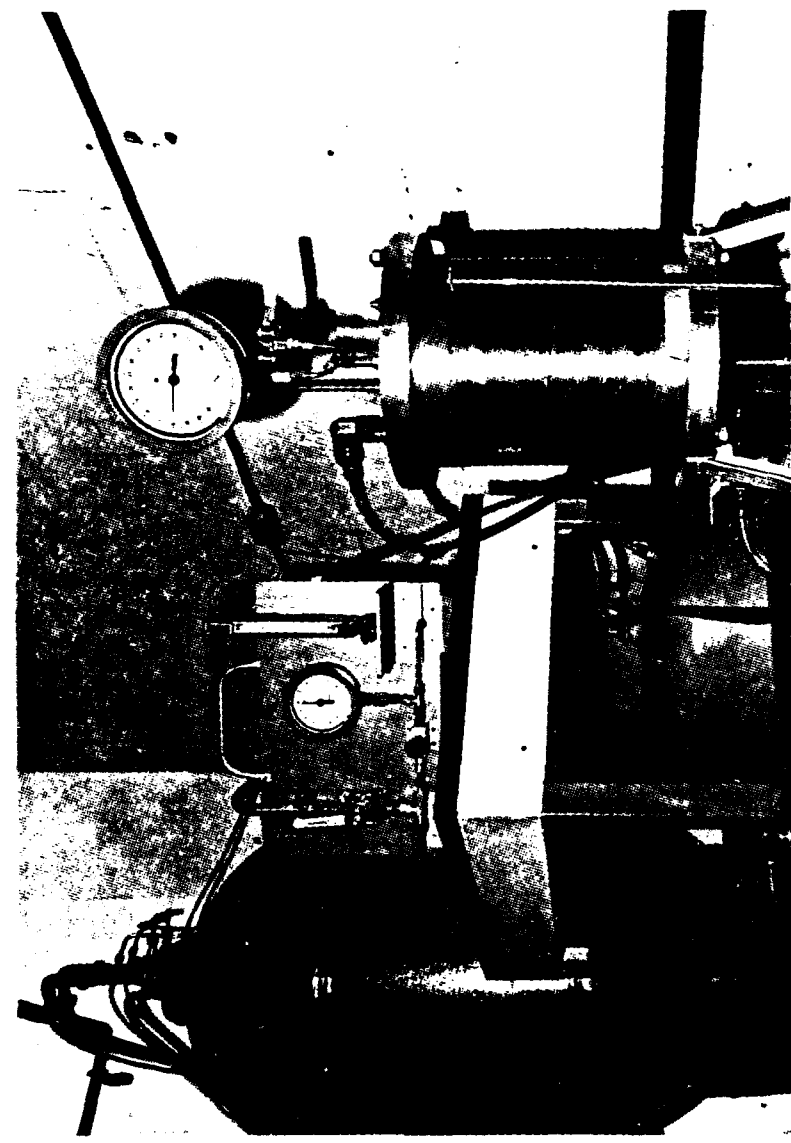


Figure 30. Polymer delivery system photograph

Boundary Layer Concentration Measurements

The methods used for the measurement of concentration distributions of polymers in solution include: polarographic (investigated by Goren (1965)); turbidity (investigated by Ruch et al. (1965)); and opaqueness and fluorometric techniques. Wetzel and Ripkin (1970) present a complete discussion of all but the opaqueness method, which was used by Fruman and Tulin (1974).

Fruman and Tulin (1974) constructed a specially-built light absorption system utilizing photocells and a recording oscillograph. The intensity of the light source was chosen in order to achieve the maximum possible output readings between zero dye and a dye concentration corresponding to practically zero light transmission. This dye concentration was chosen to be 1250 WPPM of India ink in tap water. The voltage output of the photocell was 40.0 mV and the equivalent spot displacement on the recorder was 12.0 cm. When a continuously-running sample provided a steady state output, the reading was compared to previous readings obtained during the calibration of the system. The scatter in the data was attributed to stability problems with the light intensity and galvanometer of the recording oscillograph.

The method selected for use in this study is the fluorometric method. This method has been used successfully by Wetzel and

Ripkin (1970), Walters and Wells (1971), Tullis and Ramu (1973), and Sirmalis (1974). The method consists of injecting a tracer dye into the fluid being analyzed and capturing a sample of the fluid for analysis in a fluorometer.

Fluorescence, the basic phenomenon being measured, is the instantaneous emission of light from a molecule or atom that has absorbed light. Consideration of the equation of fluorescence in dilute solution shows that

$$F_m = K I_o \epsilon C d \phi \quad (42)$$

where

F_m is the meter reading,

K is the amplification factor of the photodetector,

I_o is the intensity of the exciting light,

ϵ is the extinction coefficient of the compound

(a constant for any given wavelength of I_o),

C is the concentration to be measured,

d is the path length (a constant),

ϕ is the quantum yield (a constant),

indicates that decreasing concentration, C, may be compensated by increasing the amplification factor, K, or the light intensity, I_o .

This is done in fluorometry, yielding larger scale readings for lower concentration. The fundamental principle of fluorescence

measurement is shown in figure 31, a simplified schematic of a fluorometer taken from Turner (1972). The intensity of the exciting light is controlled by a range selector having four apertures or sensitivity ranges. The desired wavelength of exciting light is selected by a primary monochromator or filter placed between the light source and the sample. Emitted by the sample, the wavelength of light to be measured is selected by a second filter placed between the sample and a photodetector. The output of the photodetector, a current proportional to the intensity of the fluorescent light, is amplified to give a reading on a meter or recorder.

In operation, a standard sample is placed in the fluorometer and the sensitivity or intensity of exciting light adjusted to a desired reading. Unknown samples and a blank are then read. The net readings of the standard and unknown samples, with the blank subtracted, are in the same proportion as their concentration. Standard linear curves may be prepared and the concentrations of samples read directly from the curve.

The basic assumption made in all polymer solution studies is that the diffusion of the tracer dye is identical to that of the boundary layer mixture. This is a reasonable assumption based on data comparing various measurement methods by Wetzel and Ripkin

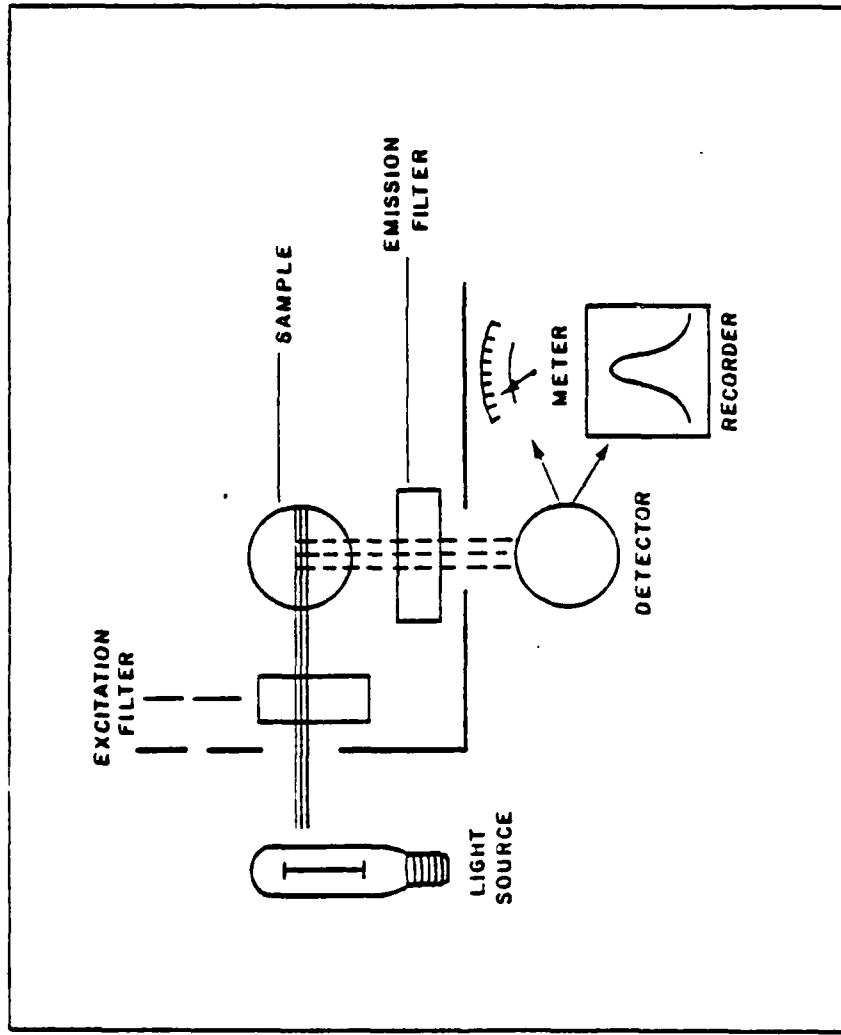


Figure 31. Fluorometer schematic

(1970). Tests of two widely used fluorescent trace dyes, Rhodamine and Uranine-B, found both to be compatible with Polyox. The solutions were stable and their drag-reducing properties were unaffected when tested in a capillary tube blowdown rheometer similar to Hoyt (1966).

Selection of the fluorometric method for the present experiment was based on the accuracy, ease, and rapidity in determining dye concentrations reported by previous authors and the availability of a G.K. Turner Model 111 Fluorometer, figure 32. The use of a fluorometer of the type utilized by previous investigators should minimize data correlation problems due to apparatus and technique differences.

Although it is easy to use, the Rhodamine dye was rejected because it is very difficult to clean off the apparatus. The Uranine-B dye was selected, however, since it is readily adaptable to laboratory use and gave a reproducible reading to 1 part in 10^9 on a weight basis. This range was adequate as the dye concentration of the injected solution could be adjusted to produce samples along the plate sufficiently above the background blank levels to give reproducible results. Calibration curves were experimentally developed for the fluorometer using known concentrations of Uranine-B dye in the type water to be used in the experiment.

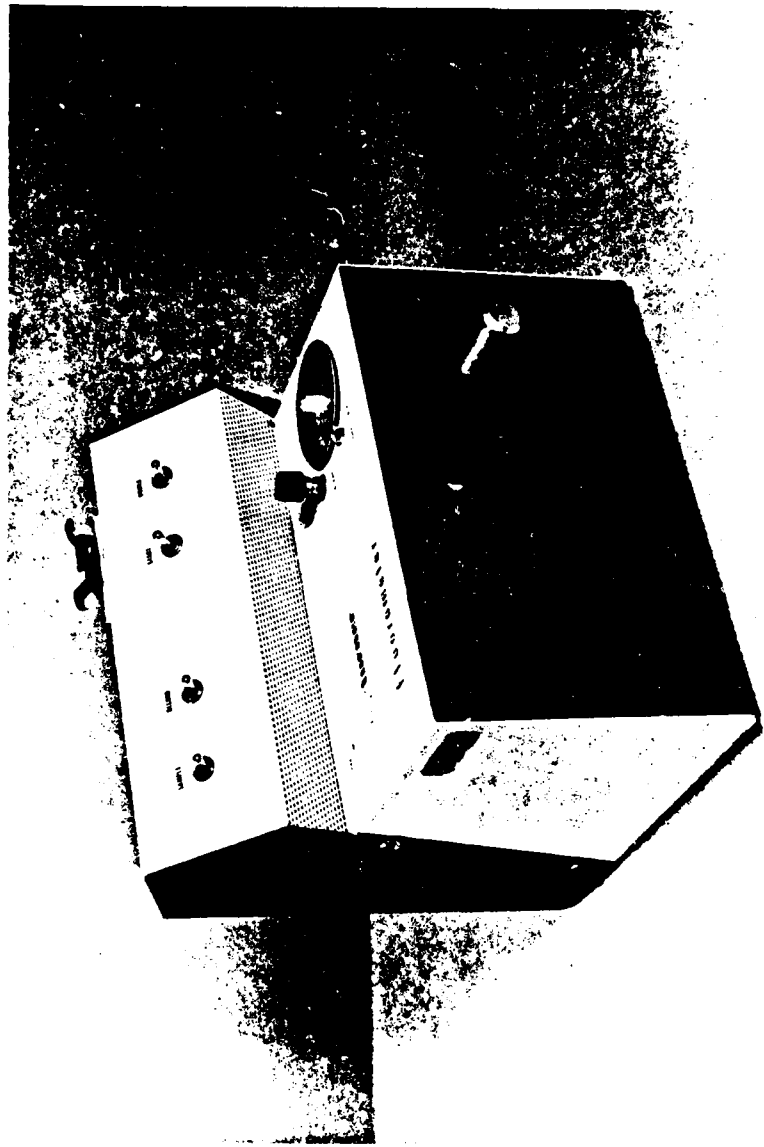


Figure 32. G.K. Turner model 111 fluorometer photograph

The G.K. Turner Model 111 Fluorometer has four sensitivity aperture settings allowing calibration curves to be drawn over a range of about 1 part per 10^6 to 1 part per 10^9 on a weight basis. For concentrations greater than the lower value, controlled dilution prior to measurement was performed. The calibration curves used in this experiment are shown in figures 33 and 34. Sample sizes of approximately 3.5 to 4.5 ml are required for measurement.

The sample is placed in a small test tube called a cuvette and inserted in the instrument. The measurement is automatically taken when the door is closed. Cleanliness must be observed and care taken to wipe the outside of the cuvette prior to measurement as fingerprints affect the reproducibility of the sample readings. Wiping the exterior of the cuvette with a clean paper towel was found to be sufficient. All samples were allowed to achieve room temperature prior to reading.

Table 3 provides a list of apparatus used in the concentration measurements.

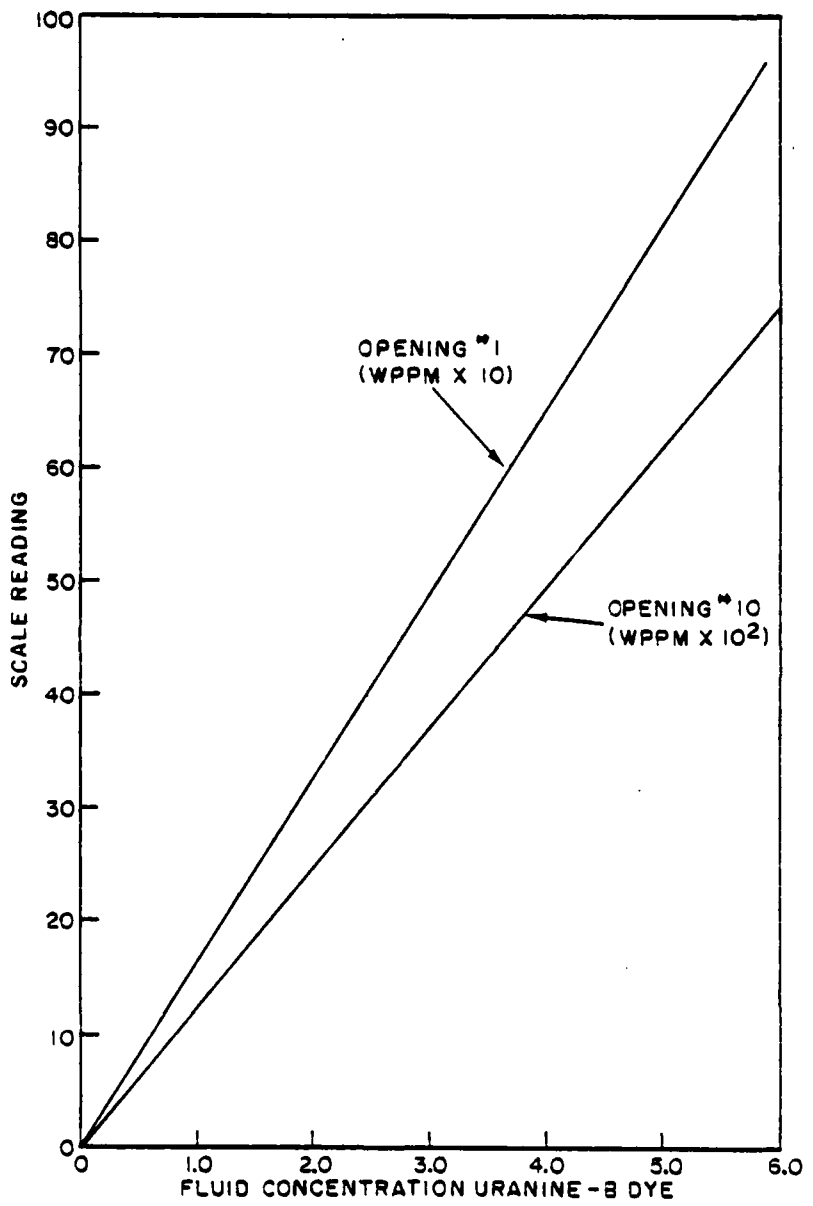


Figure 33. Calibration curves for model 111 fluorometer opening 1 and 10

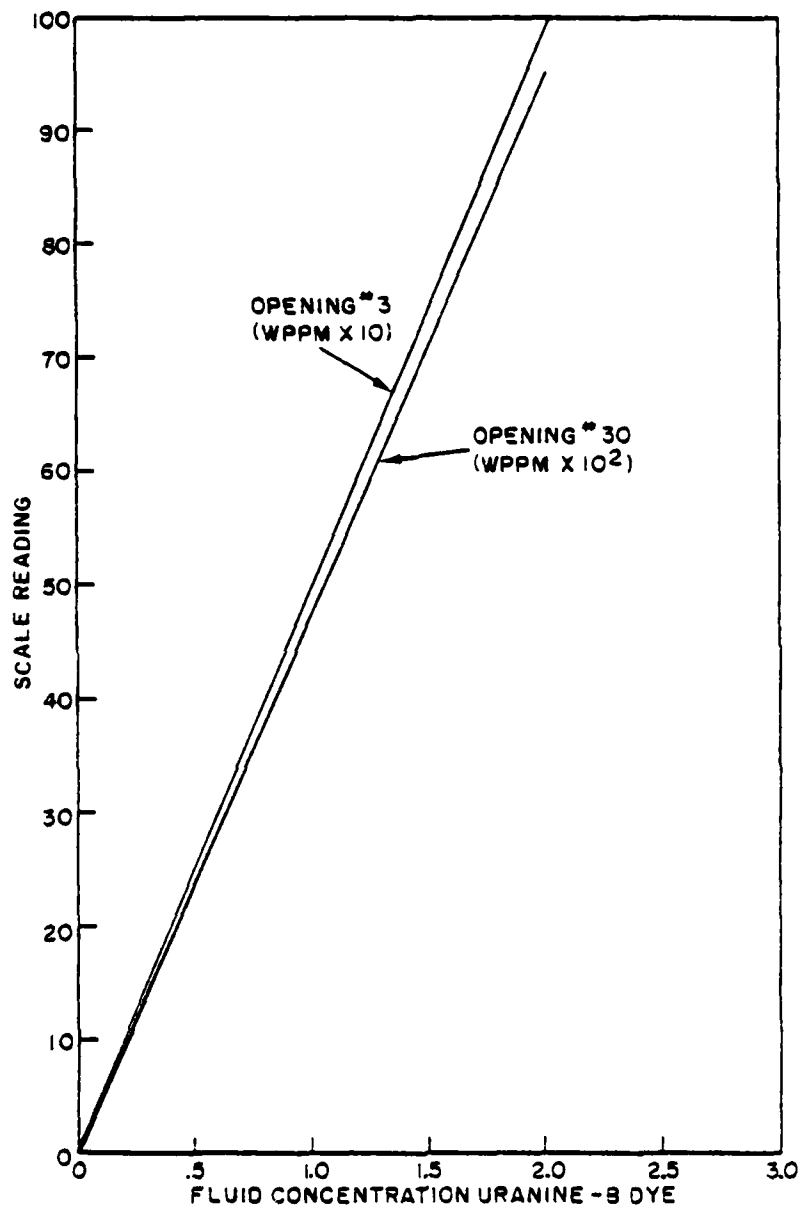


Figure 34. Calibration curves for model 111 fluorometer openings 3 and 30

TABLE 3
CONCENTRATION MEASUREMENT APPARATUS

Component	Specification
<u>Fluorometer</u>	G. K. Turner Model 111
<u>Excitation lamp</u>	G.E. # G4T4/1
Primary filter	2A (closet to lamp) 47B Together these filters transmit only light at 435 nm wave length.
Secondary filter	2A-12 This filter only passes light at wavelengths greater than 500 nm.
Cuvettes	Matched cuvettes Fisher Scientific No. 14-385-900A
Dye	Uranine-B Fluoresces at 470 nm and 515 nm

Laser Doppler Anemometer System

The velocity measurements in this experiment were taken with a laser Doppler anemometer. (LDA will be used as short form terminology. Operation of an LDA system is based on the principle that coherent laser light scattered from a particle in a moving fluid will be Doppler shifted in frequency. The basic components of an LDA system, shown in figure 35, include a laser, transmitting optics, receiving optics, photodetector, and signal processing equipment. Table 4 presents a list of the laser Doppler system components used in this experiment.

Among the advantages of LDA systems are the following:

1. The flow is not disturbed
2. No flow calibration is required
3. There is excellent spacial resolution due to small measuring volume
4. High frequency response occurs.

Constraints on the use of LDA systems require (1) an optically clear medium, (2) a window to the flow (two windows are preferred), and (3) particles in the flow. Because the LDA measures particle velocity and not fluid velocity, there must be sufficient concentration of particles of the proper size and density to provide the

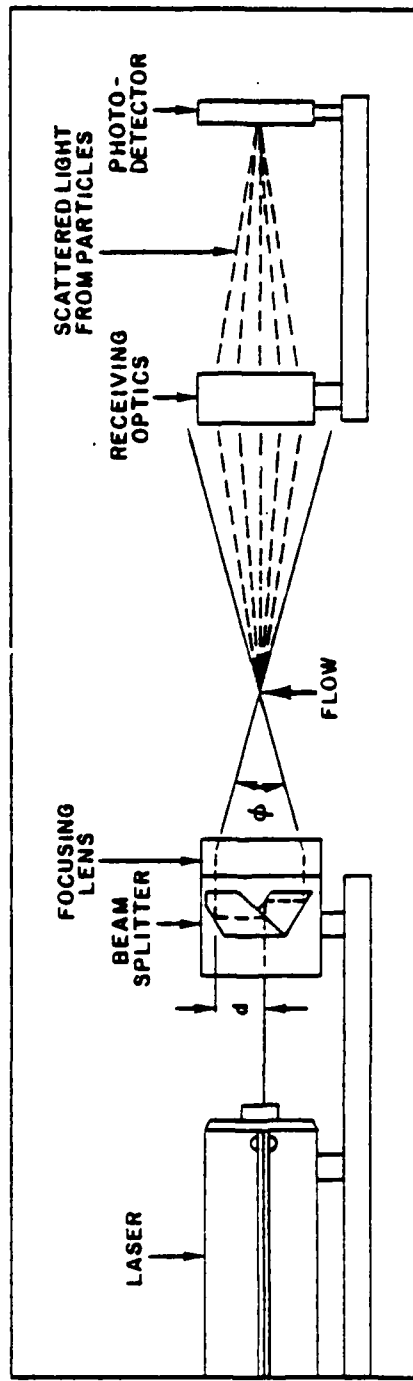


Figure 35. Basic components of a laser doppler anemometer system

TABLE 4
LASER DOPPLER ANEMOMETER SYSTEM COMPONENTS

Component	Specification
• Laser:	Spectra Physics model 120 Helium-Neon laser power - 5 milliwatts beam diameter - .8 millimeters (at 1/e ² point) wavelength - 632.8 x 10 ⁻⁹ meters
• Transmitting Optics:	TSI Model 910
Lens I:	Model 917 Focal length 103. mm Beam intersection angle 25.0°
Lens II:	Model 918 Focal length 241. mm Beam intersection angle 11.58°
Lens III:	Model 919 Focal length 598. mm Beam intersection angle 4.71°
• Beam separation:	50 mm
• Receiving Optics:	TSI Model 930
Lens I:	Model 937 Focal length 102. mm
Lens II:	Model 938 Focal length 242.2 mm
Lens III:	Model 939 Focal length 577.2 mm
• Photodetector:	TSI Photodiode model 960 Bandwidth 100 Mhz
• Aperture diameter:	0.25 dia mm
• Signal Processor:	TSI tracker model 1090
• Frequency response:	2kHz to 50 MHz

required signal while closely following turbulent fluctuations in the flow.

In general, LDA systems are characterized by the arrangement of their optical components as shown schematically in figure 36.

In the "forward scatter" arrangement, the receiving optics and photodetector are located opposite the laser to receive light scattered in the forward direction. This is the most favorable mode as the majority of incident light is scattered by the particles in the forward direction. A typical polar scattered light intensity distribution predicted by the Mie scattering theory for micron size particles is shown in figure 37. The scattered light intensity in the forward direction is typically of order 10^3 times greater than the backscattered light intensity. Requiring two windows on the flow, the forward scatter mode is ideal for water tunnel measurements. Lower laser power and particle concentrations may be used due to increased light intensity.

The "backscatter" arrangement has the receiving optics and photodetector located on the same side of the flow as the laser light source. This arrangement requires only one window on the flow. However, higher laser power, shorter focal lengths, increased particle concentration and/or size are required due to decreased light intensity scattered in the backwards direction.

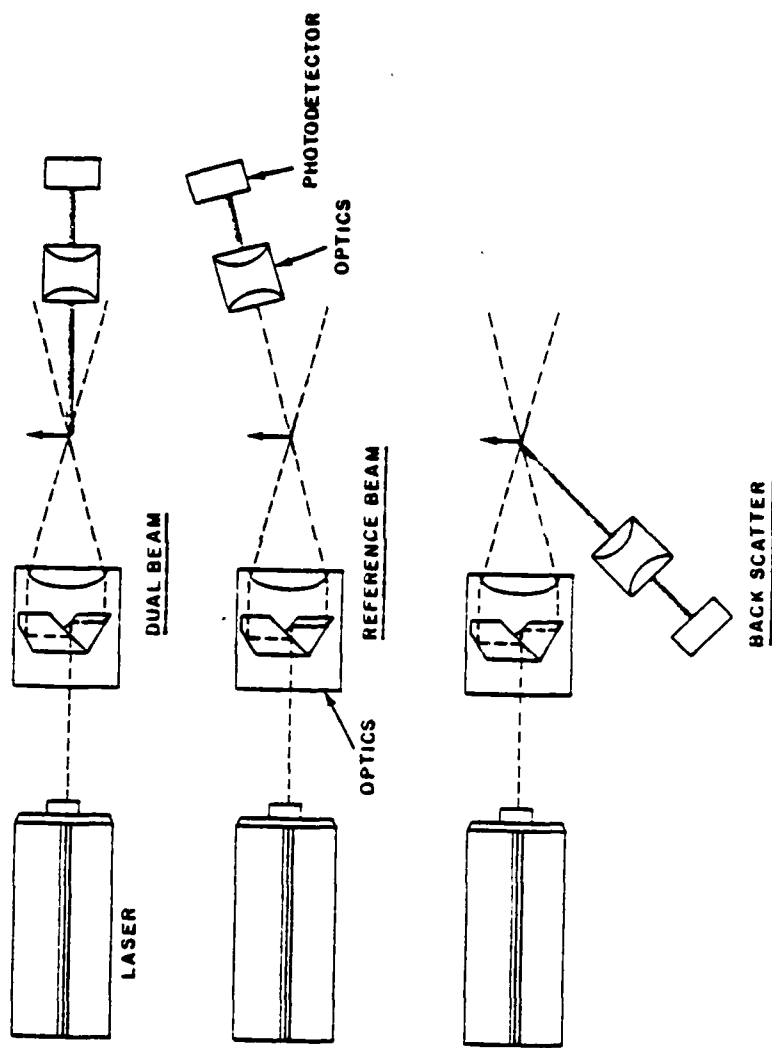


Figure 36. Optical configurations for laser doppler anemometer systems

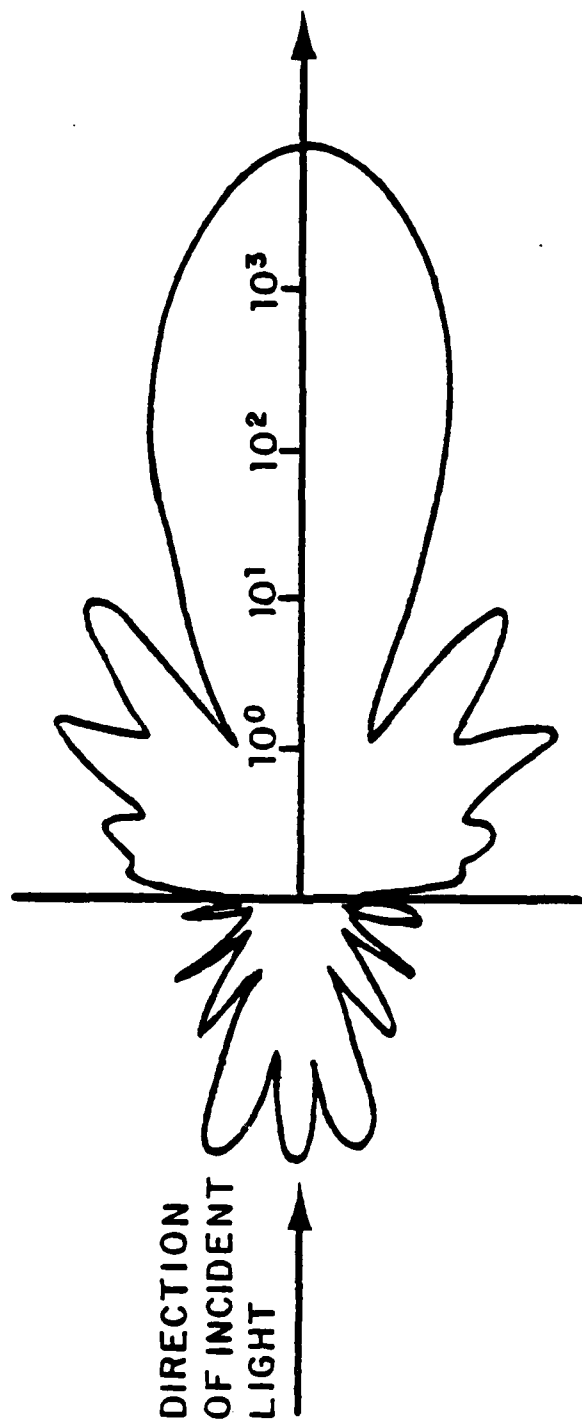


Figure 37. Polar scattered light intensity distribution

"Reference beam" mode refers to a single observed light beam, whereas the "dual beam" mode refers to the system where the light from two crossed beams is observed. Although the reference beam mode in forward scatter was developed first, the dual beam mode will be discussed in detail here as it is the actual mode used and the easiest to conceptualize.

In the dual beam mode, the laser beam is split into two beams of equal intensity, equidistant from the original beam. The beams are then focused at a crossover point where they interfere with each other to form a fringe pattern, shown schematically in figure 38. These fringes are caused by the interaction of the light in the two beams cancelling and reinforcing each other to form a standing electromagnetic interference pattern. The crossover region where the two beams are focused is called the measuring volume. Figure 39 is an actual photograph of a plane of this measuring volume magnified 600 times, containing over 100 fringes. A particle moving through the measuring volume in the plane of the two beams then passes through alternating regions of low light intensity (light cancelling) and regions of high light intensity (light reinforcing).

Light scattered from particles passing through the measuring volume is focused by the receiving optics onto a photodetector

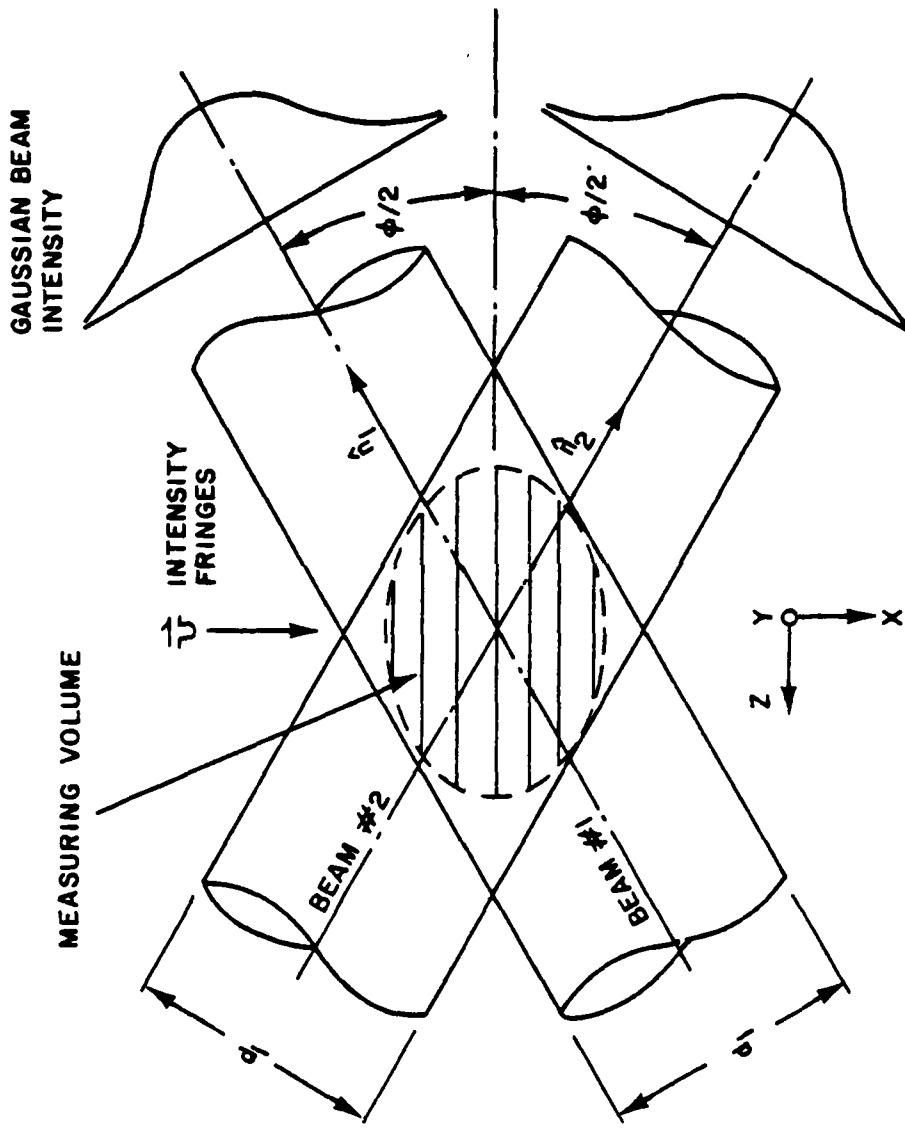


Figure 38. Fringe pattern schematic

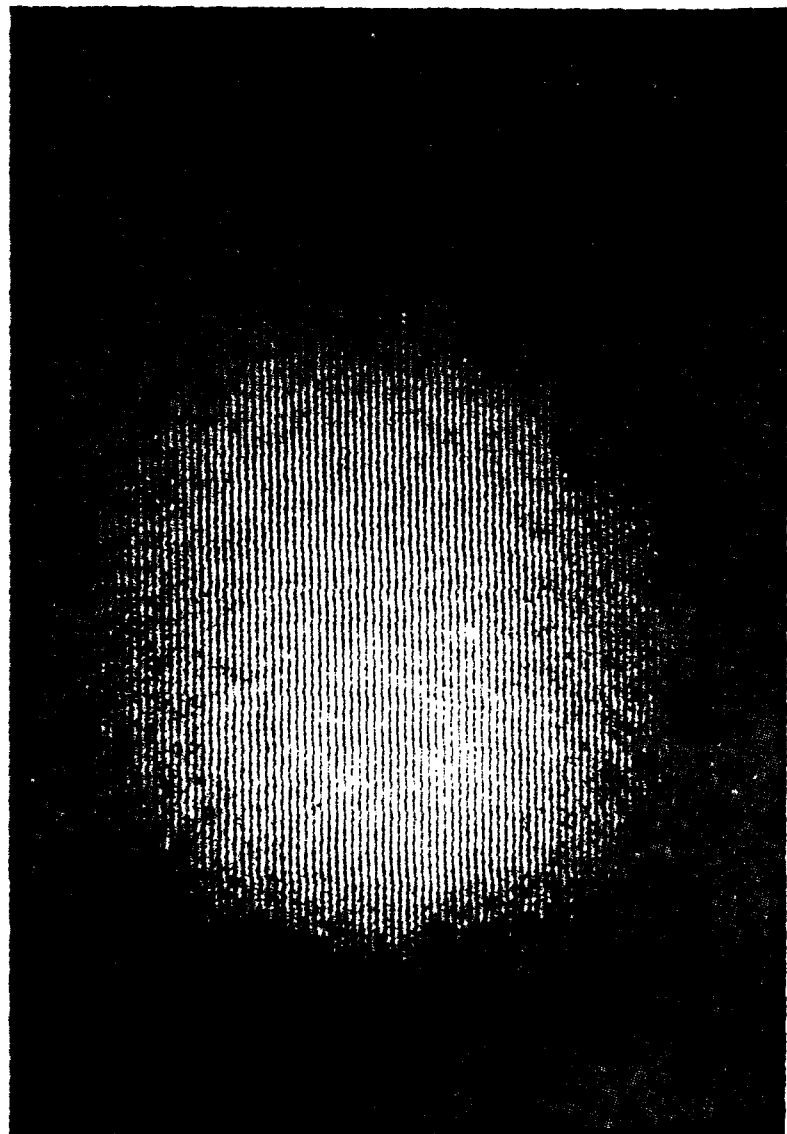


Figure 39. Fringe pattern photograph

whose output signal is shown schematically in figure 40. An aperture is placed in front of the photodetector, blocking light from locations other than those from the beam crossover region. Due to the Gaussian intensity distribution, the amplitude will vary with a maximum occurring in the center of the measuring volume. The frequency, f_D , of this signal, produced by the scattered light pulses from a particle travelling through the measuring volume, is linearly proportional to the velocity with which the particle is moving across the fringes (figure 41). This frequency is determined by the frequency tracker of the LDA system. The distance between fringes, d_f , is a function of the laser wavelength and the angle of beam intersection only, such that

$$d_f = \frac{\lambda}{2 \sin(\theta/2)}. \quad (43)$$

The velocity of the particle may then be given by

$$U = f_D \cdot d_f. \quad (44)$$

Conversion of frequency to velocity requires only that the laser wavelength and angle of beam intersection be known. A flow direction ambiguity of 180° does exist, however, in that the fringe system cannot distinguish reverse flow from forward flow. The problem may be resolved for reversing flow by frequency shifting.

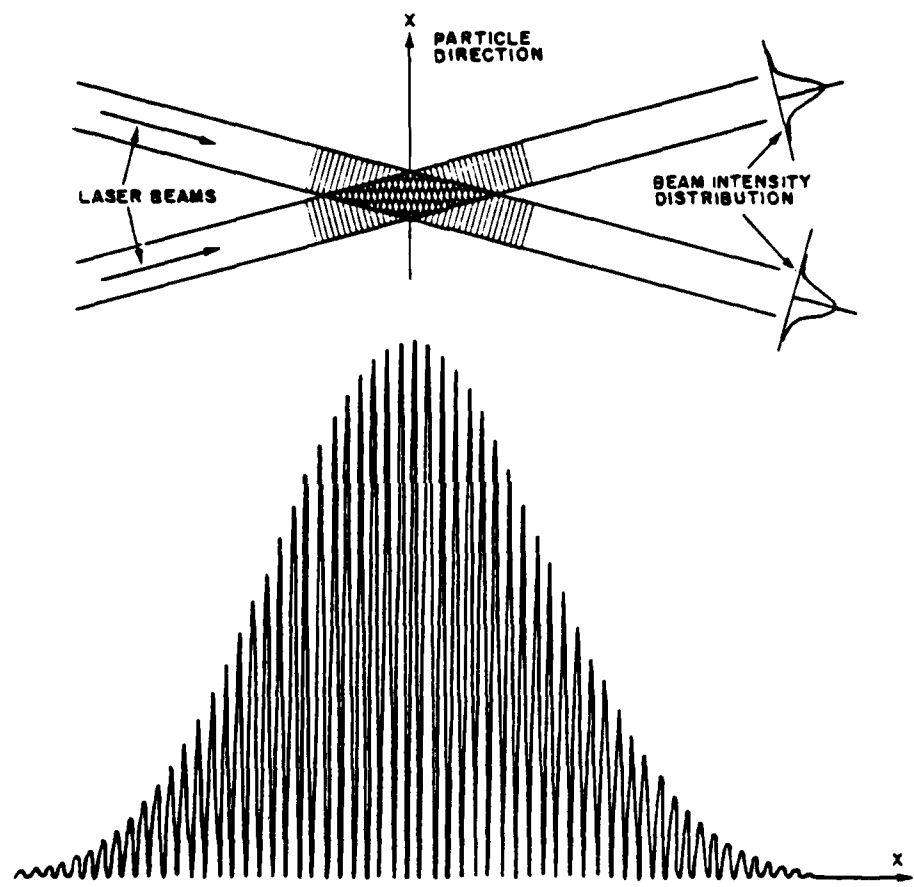


Figure 40. Photodetector output schematic

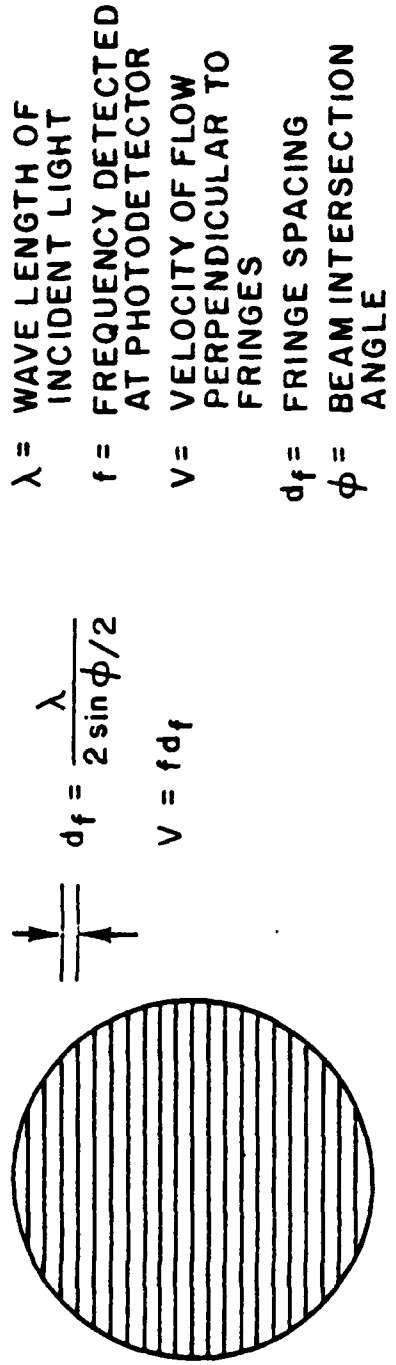


Figure 41. Scattered light frequency-velocity relationship

The fringes may be considered to be moving if one beam is frequency shifted relative to the other. If the difference in frequency between the two beams is 40 MHz, then a stationary particle in the measuring volume will yield a 40-MHz signal from the photodetector. A particle travelling in the same direction as the fringes will produce a lower frequency while a particle moving in the opposite direction will raise the frequency. Frequency shifting provides a zero offset or bias allowing bidirectional measurements. Techniques for frequency shifting include Bragg cells (40 MHz-shift) and rotating diffraction gratings (a few MHz shift).

The region of the beam crossover point called the measuring volume may be considered shaped as shown in figure 42. The diameter of the measuring volume, d_m , and the length of measuring volume, l_m , are expressed in terms of the diameter of the laser after focusing, d_ℓ , and the beam intersection angle θ as follows:

$$d_\ell = \frac{4\lambda F}{\pi D_e - 2} , \quad (45)$$

$$d_m = \frac{d_\ell}{\sin \theta/2} , \quad (46)$$

$$l_m = \frac{d_\ell}{\cos \theta/2} . \quad (47)$$

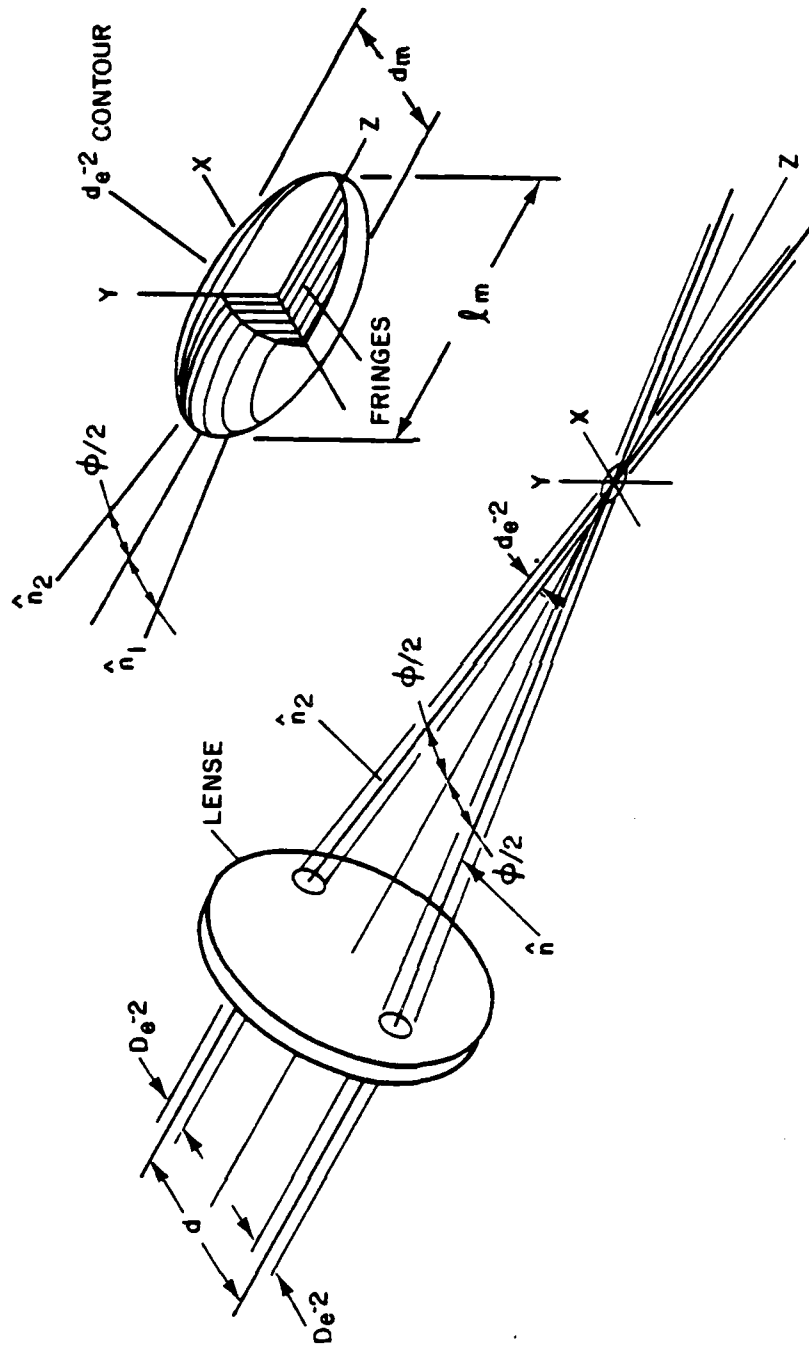


Figure 42. Measuring volume schematic

The volume of the measuring volume is given by equation (48)

$$V_m = \pi(D_e^{-2})^3 / 6 \cos(\theta/2) \sin(\theta/2). \quad (48)$$

The laser beam diameter, D_e^{-2} , is defined as that region where the light intensity is greater than $1/e^2$ (about 14%) of the center-line beam intensity. Table 5 shows typical values of these terms.

TABLE 5
MEASURING VOLUME PARAMETERS

Parameter	Values		
F (mm)	103	241	598
θ ($^\circ$)	25.0	11.58	4.71
D_e^{-2} (mm)	.8	.8	.8
d_L (mm)	.104	.243	.602
d_m (mm)	.106	.244	.603
l_m (mm)	.479	2.406	14.657
d_f (mm)	1.462×10^{-3}	3.136×10^{-3}	7.700×10^{-3}
N_{FR}	73.0	77.0	78.0
V_m (cm^3)	2.766×10^{-6}	74.600×10^{-6}	$2,785.900 \times 10^{-6}$

The position of the measuring volume, when making measurements in a liquid flow, will be different as compared to that in

air flow. Figure 43 shows the location of the measuring volume relative to the wall in terms of the parameters of Snell's law equation, such that

$$\lambda_1 n_1 = \lambda_2 n_2 . \quad (49)$$

The position of the measuring volume may be determined with the use of equations (50) and (51) as follows:

$$n_1 \sin \frac{\theta_1}{2} = n_2 \sin \frac{\theta_2}{2} , \quad (50)$$

$$a = \frac{b}{2} \cot \frac{\theta_2}{2} . \quad (51)$$

Photodetector

The quantum efficiency, a measure of the photodetector's efficiency to convert light energy to electrical current, is typically higher for photodiodes than for photomultiplier tubes. However, photomultiplier tubes make up for this lack of efficiency with internal gains of from 10^4 to 10^7 . In general, the selection of a photodetector depends on signal intensity, with low scattered light levels requiring photomultiplier tubes; high light levels require photodetectors. The photomultiplier also has higher frequency response than photodiodes making them more applicable to frequency shifted systems.

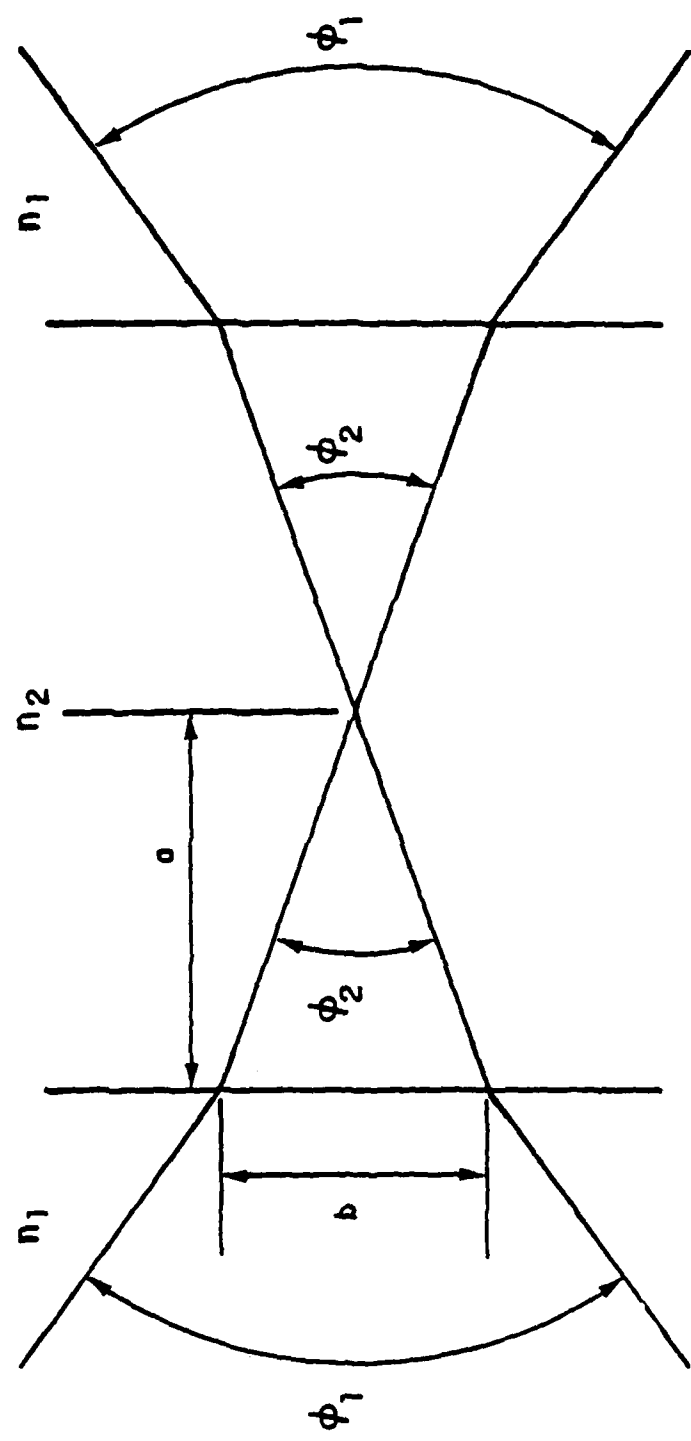


Figure 43. Location of measuring volume

Signal Processor

The signal processor used is of the tracker type. Basically, it consists of a combination of tracking filter and frequency-to-voltage converter, with provision for signal validation and retention of the last valid reading when no signal is present. The fundamental limitation of a tracker is the capture range. Should the change in velocity between one particle and the next exceed the capture range, the unit will not track the new value and any succeeding values that remain outside the capture range. However, the tracker system will return the last valid reading until a new reading occurs within the captive bandwidth. Table 6 indicates the range of tracking frequencies available with this system.

TABLE 6
TRACKING FREQUENCIES

Frequency Range	Tracking Range (MHz)	Output (FS=10V DC)	Capture Window
High frequency	0.5 - 50	0.2V/MHz	5 MHz
Mid frequency	0.02 - 5	2.0V/MHz	0.5 MHz
<u>Low frequency</u>	<u>0.002 - 0.5</u>	<u>20V/MHz</u>	<u>0.05 MHz</u>

Particles

Particles in the flow form the basic requirement for the application of LDA techniques. The relative relationships between mode of operation and direction of maximum scattered light intensity have been discussed previously. The types of particles and their concentration are also related to the mode of LDA operation as well as the fluid medium to be measured.

For gas flows, the diameter of particles should be of the order of 0.1 to 1 micron while liquid flows generally required 1 to 10 micron particles. Excellent results have also been attained with natural contaminants in water flows. If possible the water used should be filtered to remove large particles providing a uniform dispersal of contaminants and lessening the chance of large particles saturating the photodetector output.

Nelling (1971) has shown that 1-micron sized particles are able to follow flow fluctuation of up to 10 kHz in air with an accuracy of 1.0%. Table 7 presents a list of types of seeding and the medium in which they are used.

TABLE 7
TYPES OF SEEDING

Medium	Seed
Water	Polystyrene beads
	Milk, cream powder
	Natural pigment
Hydraulic oil	Paint pigment
Air	Ammonium chloride
	Magnesium oxide
	Silicon oil droplets
	Smoke
	Water vapor
	Dioctyl phthalate
	Aluminum oxide
Burning gas	Silicon dioxide
	Magnesium oxide
	Silicon oil droplets
	Dibutyl phthalate

Laser Power

A determination of laser power required to attain a desired signal-to-noise ratio (SNR) requires precise information on the configuration, characteristics of the fluid, properties, and concentration of the scattering centers as well as characteristics of the photodetector. This selection is quite complex and beyond the scope of this work. However, the following general remarks by Fingerson (1976) may be used as a general laser selection guide.

In forward scatter with focal lengths up to 250 mm for subsonic flows containing scattering centers above 0.1 micron in size, a 5-mW laser is adequate and generally of the He-Ne type.

In the backscatter mode with short focal distances of 120 mm or less and favorable conditions, a 15-mW laser is the minimum. For long focal lengths, especially in backscatter, 1-W lasers of the Argon-Ion type are generally used. For these applications, a variable power adjustment feature is desirable in matching laser power to actual conditions.

In general a 5-mW or 15-mW He-Ne laser is adequate for most laboratory experiments particularly where forward scatter can be used. For increased focal length, increased velocity, backscatter

or dual component velocity measurements, a larger laser such as Argon-Ion is desirable.

An oscilloscope photograph of the photodiode output due to the reflected light from a single particle travelling through the measuring volume is shown in figure 4. The total Doppler burst consists of approximately 100 fringes indicating a particle travelling close to the center of the measuring volume. Figure 45 represents good particle distribution, providing nearly continuous signal output due to sequential occupancy of the measuring volume by individual particles. Multiple particles in the measuring volume at the same time are to be avoided. This type of output is shown in figure 46. Although providing nearly continuous signal, the relatively high background noise level, caused by varying phase and amplitude, affects the accuracy of the apparent frequency measurement. The accepted term for this is Doppler ambiguity. A count rate distribution of 2.7×10^3 particles/second corresponding to figure 45 is shown in figure 47. Each spike contains a Doppler burst envelope for a single particle.

Errors in Laser Doppler Average

Edwards et al. (1971), and George and Lumley (1973) treat laser anemometry measurement errors in detail. Limitations of a theoretical nature include:

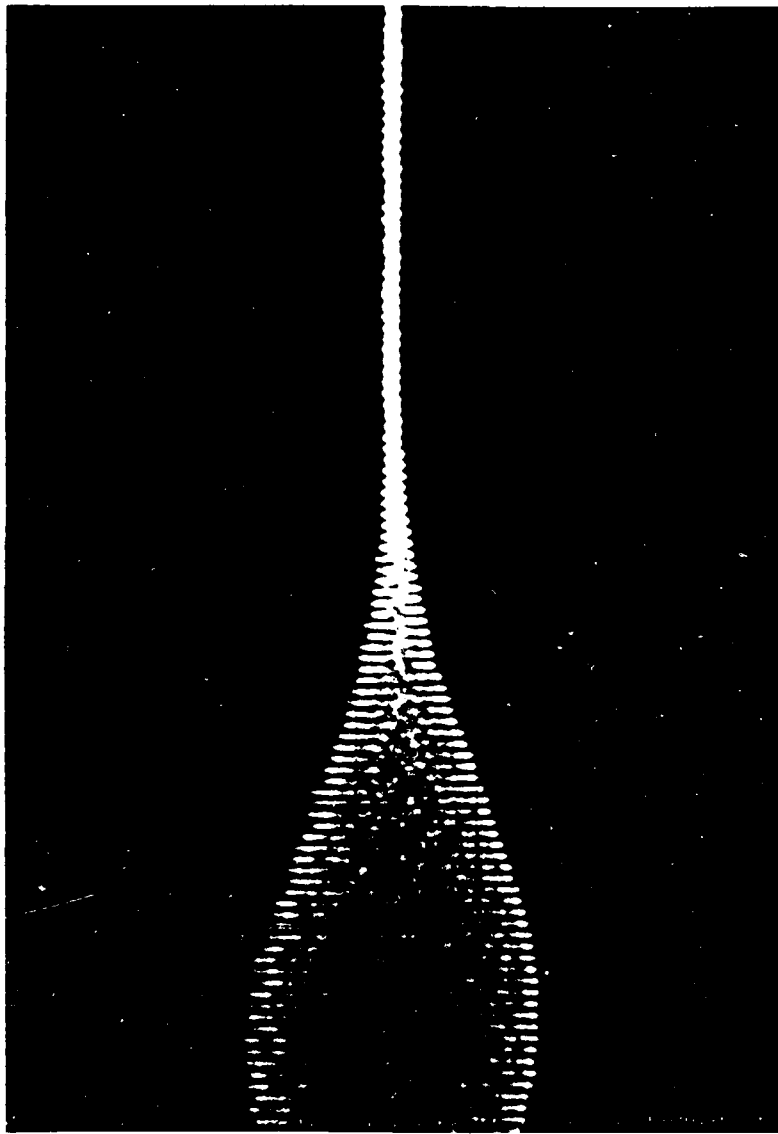


Figure 44. Doppler burst from single particle photograph

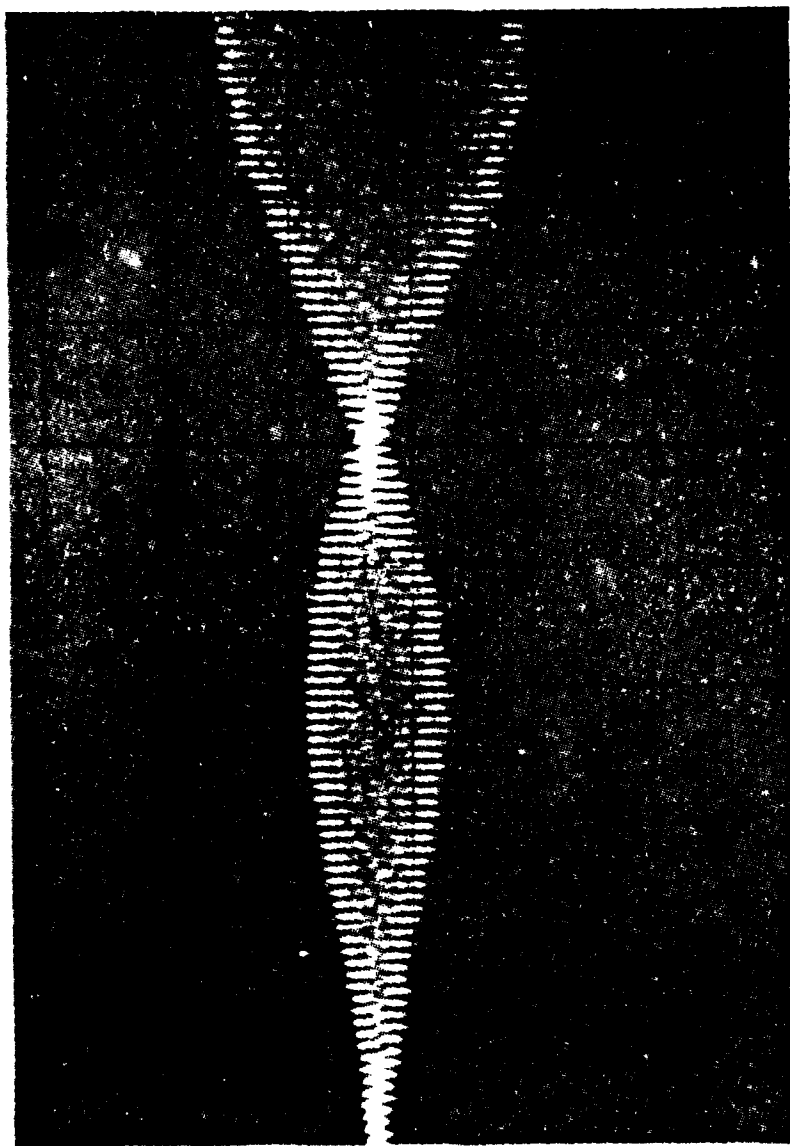


Figure 45. Doppler burst from good particle distribution photograph

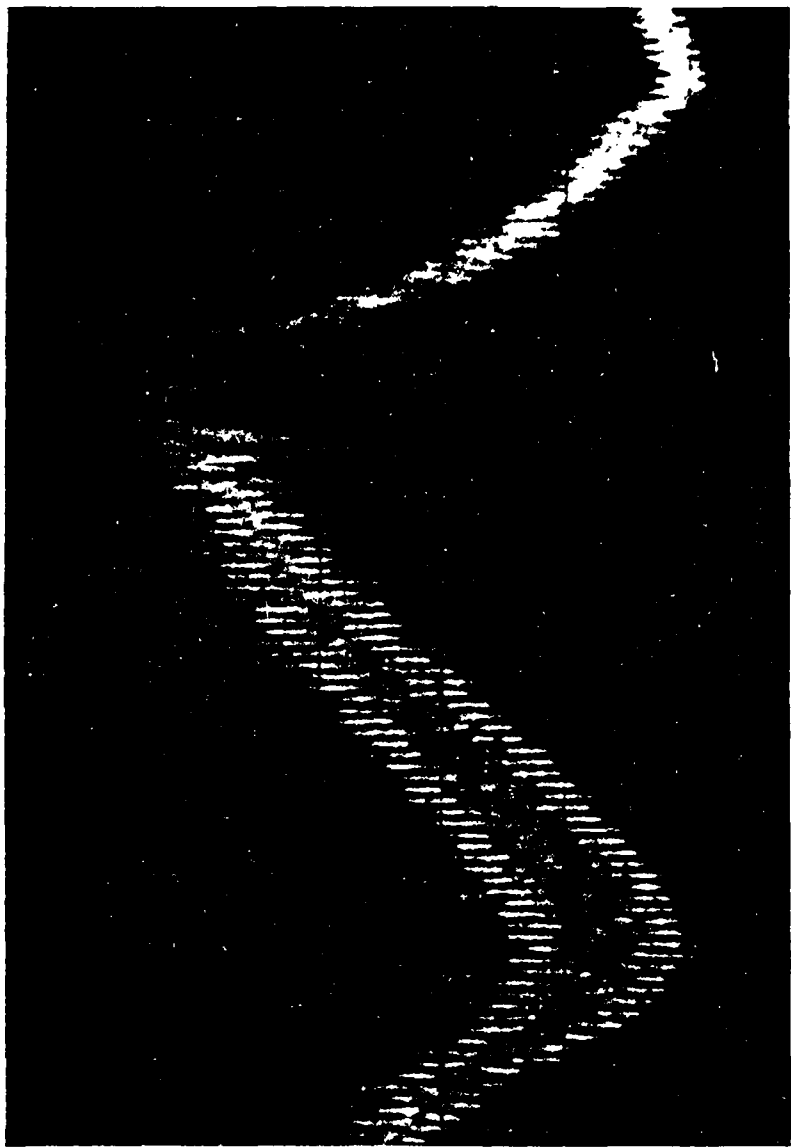


Figure 46. Doppler bursts due to multiple particles in measuring volume photograph

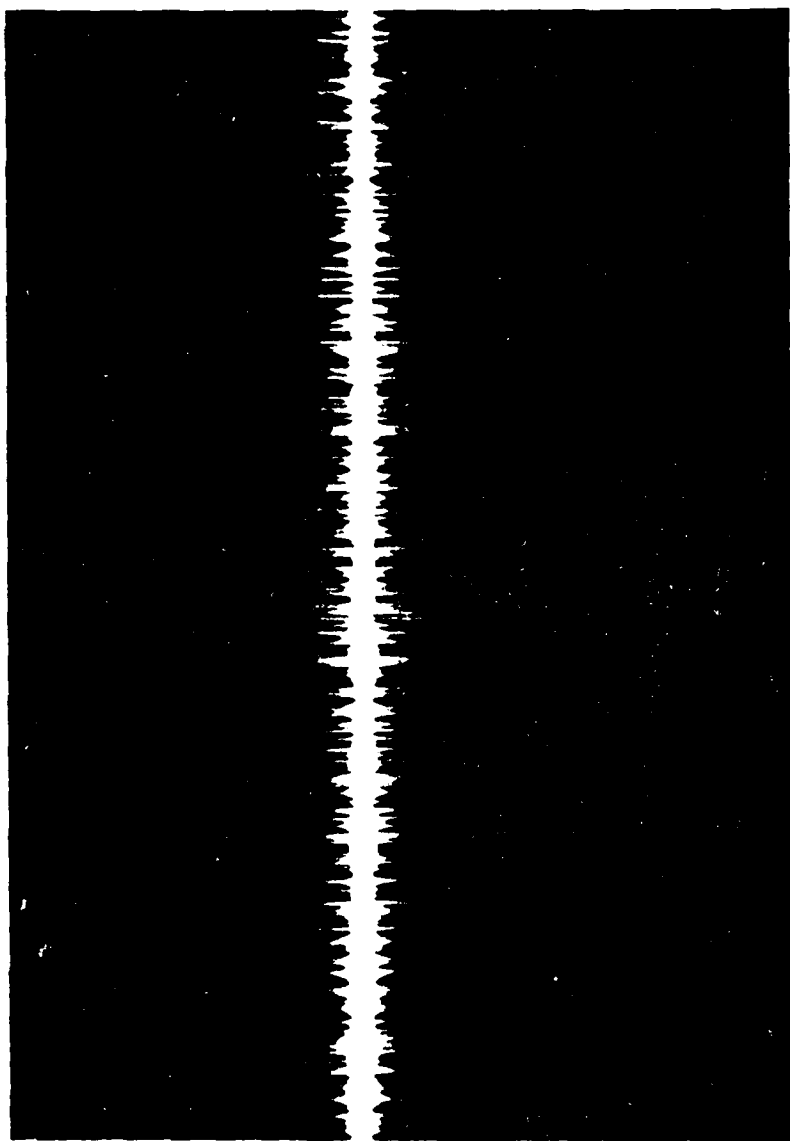


Figure 47. Count rate distribution photograph

1. Velocity fluctuations in the measuring volume
2. Mean velocity gradients across the volume
3. Effect of the finite transit time of the particles through the volume.

The finite measuring volume of the laser anemometry has an effect on mean flow measurements in steep velocity gradients.

Turbulent particle movement within the measuring volume can also influence resulting turbulence data. Since the Doppler signal from a single particle has a beginning and an end, higher frequency variations are generated appearing as spectral broadening (even in laminar flow). This spectral broadening gives a minimum turbulence intensity which can be measured.

Doppler ambiguity caused by phase and amplitude modulation of the Doppler signal is a source of inherent noise. This noise is not a problem at low particle concentrations but becomes significant where the probability of multiple particle in the measuring volume is high. However, interpretation of spectral broadening and its effects on signal processor remains controversial.

Even under the most ideal conditions, there are certain errors associated with laser Doppler anemometry. These errors are frequently called "broadening errors" since, in the frequency

domain, they would cause the frequency to be broadened into a distribution with a finite width. In a tracker, this broadening translates into a voltage fluctuation in the output. The major sources of broadening are

1. σ_F - finite transit time broadening
2. σ_T - small scale turbulence fluctuations
3. σ_G - mean velocity gradient broadening
4. σ_I - instrument broadening

If it is assumed that each of the broadening components has a Gaussian distribution, the output variance may be written as

$$\left(\frac{\bar{e}^2}{E^2} \right)_b = \left(\frac{\bar{e}^2}{E^2} \right)_F + \left(\frac{\bar{e}^2}{E^2} \right)_T + \left(\frac{\bar{e}^2}{E^2} \right)_G + \left(\frac{\bar{e}^2}{E^2} \right)_I. \quad (52)$$

If a measurement in a laminar flow with no velocity gradient is considered, then the broadening reduces to

$$\left(\frac{\bar{e}^2}{E^2} \right)_{b, \text{ laminar}} = \left(\frac{\bar{e}^2}{E^2} \right)_F + \left(\frac{\bar{e}^2}{E^2} \right)_I. \quad (53)$$

The second term on the right hand side, the instrument broadening, may be determined by entering a constant amplitude, constant frequency, voltage fluctuations as the tracker input, and observing the corresponding voltage fluctuation at the output. This gives

the level of the instrument broadening. Comparison with the results of the laminar flow measurement allow the finite transit time broadening to be determined.

The transit time broadening, σ_F , comes about as a result of the signal from any one particle existing for only a finite time. If there is more than one particle in the control volume at a given time, then there will be voltage and phase variations due to "old" particles leaving the control volume and "new" particles entering it. The finite transit time broadening is a strong function of control volume geometry and many discussions of its cause and effects may be found in the bibliography.

An estimate of the velocity gradient broadening is given by Durst (1976) as

$$\frac{\sigma_g^2}{W_D^2} \approx \frac{\sigma_3^2}{U_0^2} \left(\frac{dU}{dx_3} \right)_0^2 \quad (54)$$

where the velocity in the vicinity of $x_3 = x_{30}$ has been approximated by

$$U = U_0 + (x_j - x_{30}) \left(\frac{dU}{dx_3} \right)_0 + \frac{(x_3 - x_{30})^2}{2} \left(\frac{d^2U}{dx_3^2} \right)_0 + \dots, \quad (55)$$

and σ_3 ≡ scattering volume dimension in the direction of the velocity gradient, and W_D ≡ Doppler frequency.

The previous approximation shows the desirability of keeping the smallest dimension of the control volume in the direction of the velocity gradient in order to minimize gradient effects.

The final source of broadening is usually the parameter of interest. In some measurements the turbulence variation has been taken as the difference between the variance measured in turbulent flow and that measured in laminar flow under the same conditions.

Data Processing

A modest real-time computer data system was used in conjunction with the laser Doppler anemometer. The data system components shown in figure 48 are listed in table 8.

TABLE 8
DATA SYSTEM COMPONENTS

Laser Doppler Anemometer	TSI Model 1090-1
Display Keyboard	Wang Model 2220
Central Processing Unit (CPU)	Wang Model 2200-72
Plotter	Wang Model 2272-2
Printer	Wang Model 2231W
Data Interface	NUSC

The data system provides a printout of seven variables and functions of variables, a plot of normalized velocity ratio versus position, and a cassette recording of four data functions. Table 9 lists printer output.

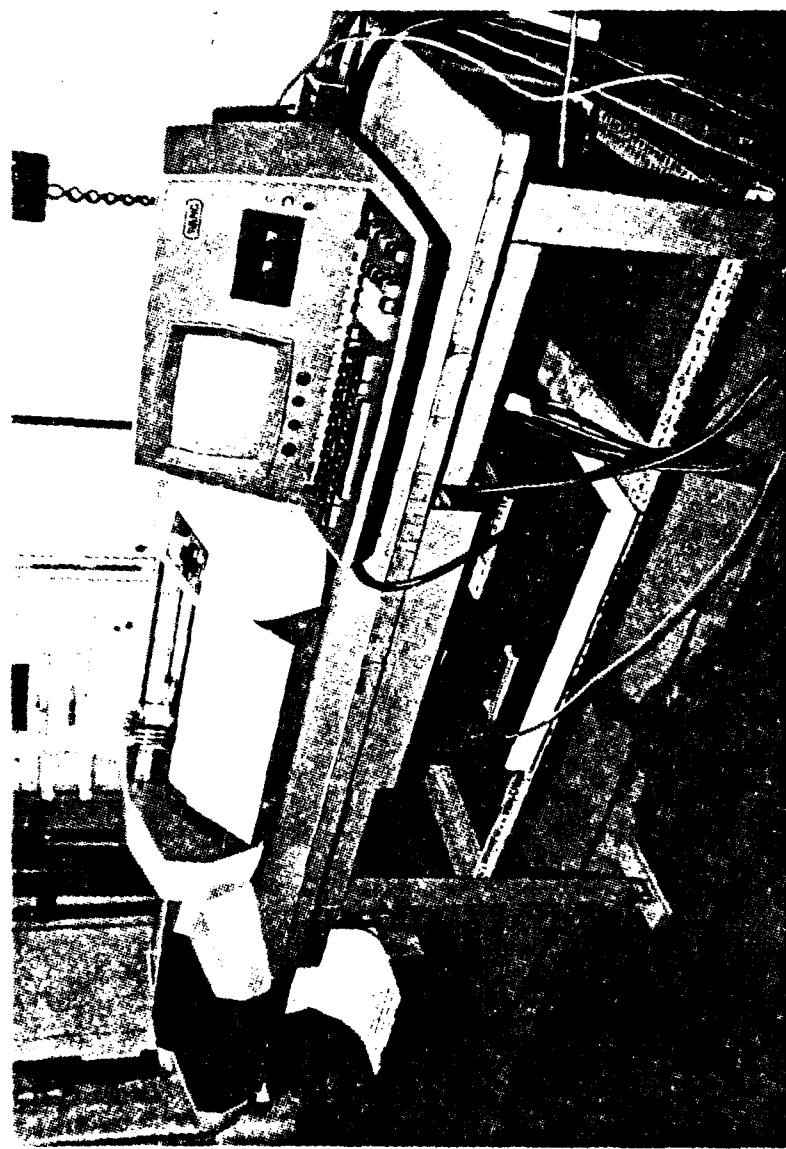


Figure 48. Computer data system photograph

TABLE 9
PRINTER OUTPUT LIST

<u>Variables</u>	<u>Variable Functions</u>
y (inches)*	Height above plate
u (ft/sec)*	Velocity
u^1 (ft/sec)*	Velocity fluctuation
u/UFS^*	Normalized velocity ratio
u^1/u	Local turbulence level
u^1/UFS	Relative turbulence level
<u>volts</u>	<u>Tracker output</u>

* stored on tape cassette.

The program "DATA" selects 61 data points from each channel of input and computes their average for computational use. The four channels of input include velocity and rms of the velocity fluctuation from the LDA system output, position y from the digital position indicator, and a counter channel.

From listings and laboratory data, x station and velocity profile data were key punched as input to a comprehensive data processing program called "DATAPAC." This program calculated hydrodynamic parameters, listed data, plotted data, and theoretical curves using a high-speed Calcomp plotter. Appendix B

presents a copy of program DATAPAC and a sample output listing.
Typical output curves from one velocity profile are shown in
appendix C.

IV. EXPERIMENTAL PROCEDURES

Three types of tests were performed in this research. These were: (1) tunnel characterization tests, (2) water injection boundary layer sampling tests, and (3) polymer injection boundary layer sampling tests. The preparations for these experiments will be discussed first.

Polymer Preparation

The polymer used in this experiment was polyethylene oxide (Polyox WSR-301) of approximate molecular weight 6×10^6 . This polymer was selected due to its availability and widespread use among researchers, thereby minimizing data correlation problems due to use of polymers of different molecular weight.

As the experimental program called for solutions of 1000 WPPM or less to be tested, a master solution was prepared at 2000 WPPM and diluted to the required concentrations.

The master solution was prepared using the same procedure as Sirmalis (1974). Premeasured Polyox powder was sifted onto the surface of the carefully weighed water, which was slowly stirred by a magnetic mixing bar. After a clear solution resulted (1 hour),

the solution was left to stand for approximately 40 hours to minimize the high viscoelastic effects of freshly mixed solution and to assure homogeneity. The master solution was kept in a dark, cool place after initial mixing to reduce the auto-oxidation problem with polyethers. When required, the proper amount was pipetted out of the master solution and diluted to the required concentration. These dilute solutions were used within 24 hours of the makeup time.

The Uranine master solution was prepared in a similar manner. When a test solution was required, the proper amount of each constituent was added to enough water to make one liter of solution. This solution was poured back and forth into the container ten times to assure complete mixing and then let to stand for 1 hour to achieve homogeneity. A series of calibration tests with the fluorometer indicated that this procedure provides accurate results.

Injection System Calibration

The polymer injection system was designed to minimize mechanical degradation of the polymer concentration and avoid polymer effects on the flow measuring device. This was accomplished by using water, bypassed from a recirculatory loop to

displace polymer from a reservoir. The reservoir contained a free-sliding piston with O-ring seals and was thoroughly cleaned after each test to prevent alteration of the next concentration to be tested. The water flow passed through a Fisher Scientific Company variable area flowmeter with tube number 448-225. The float diameter was 1/8 inch and made of stainless steel.

The calibration curve for the flow range of 20, 40, and 80 cm³ per minute is shown in figure 49. The accuracy of the curve applied to the delivery system was confirmed by the capture of polymer solution in a graduated cylinder. There were no oscillations of the float in the variable area tube indicating the steadiness of delivery.

Boundary Layer Sampling

Five boundary layer sampling stations were used in these experiments, located at axial distances of 3.75, 8.5, 12.5, 16.5, and 20.5 inches from the leading edge of the plate. All probe rakes were retracted up into the ceiling of the tunnel out of the flow at the start of the test. The rake furthest downstream was lowered to the plate first and a set of samples captured in the cuvettes. The wall sample was not taken through the hole in the plate at this time to prevent probe interferences. When

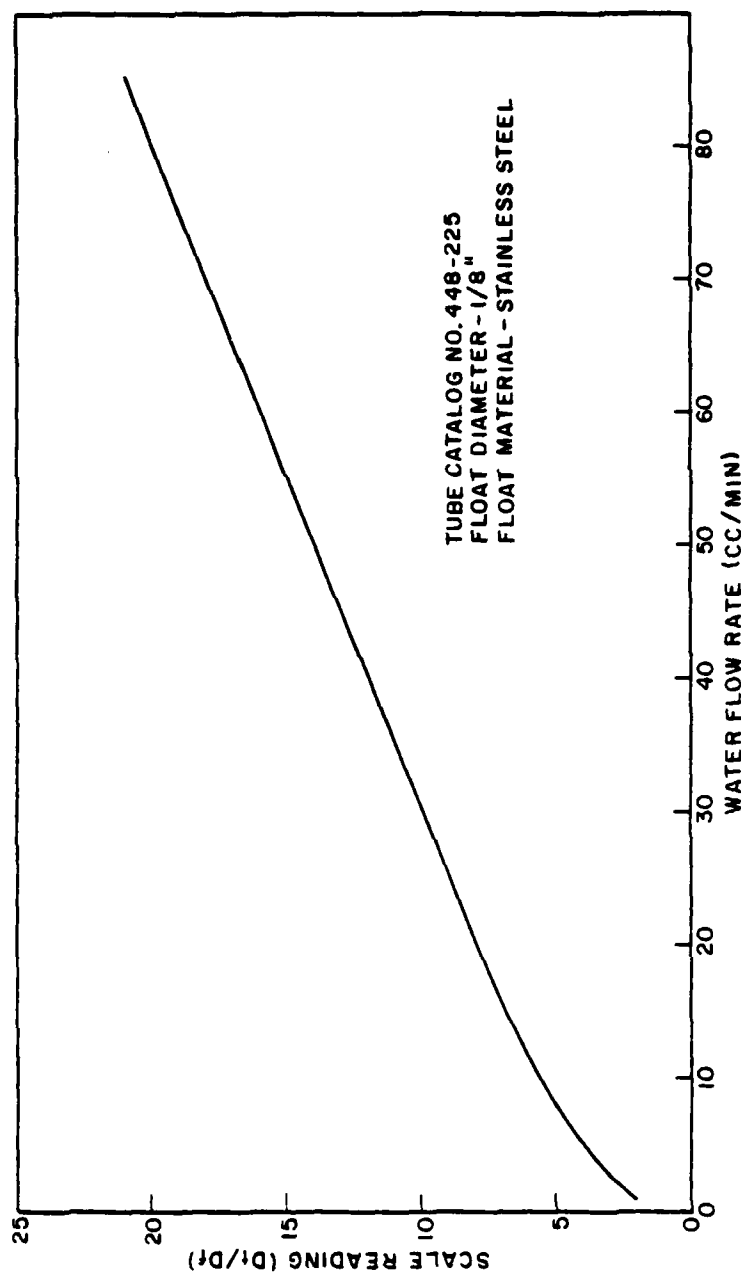


Figure 49. Polymer injection flowmeter calibration curve

a sufficient sample volume was captured, at approximately 8 to 10 minutes, the sample lines were transferred to a reservoir and the probe rake raised to position number 2. The new position was determined by a gage block inserted between a collar on the rake body and the top of the tunnel fitting. Using the reservoir and placing the probes in the next position allowed the lines to purge themselves while the next set of cuvettes was being readied. When the probe was raised to position number 2, the wall sample was taken. After all the samples were taken at the station, the rake was retracted up into the ceiling of the tunnel, out of the flow. The upstream probe stations were used, in order, until all the samples were taken. All samples were expelled under internal tunnel pressure. No suction was used to avoid interference effects between probes during sampling. Volume rates of sampling were based on the slowest velocity in the boundary layer that allowed all the samples to be taken within the capability of the delivery system. Table 10 presents the non-dimensional locations of each of the stations at which concentration measurements were taken.

Fluorometer Calibration

The fluorometer used in these tests is a G.K. Turner Model 111 Fluorometer. Uranine-B dye was selected since it was readily adaptable to laboratory use, compatible with polymer flows, and

gave reproducible readings to about 1 part in 10^9 on a weight basis. This range was more than sufficient for the experiment to

TABLE 10
NON-DIMENSIONAL LOCATIONS OF CONCENTRATION MEASUREMENTS STATIONS

<u>Station</u>	<u>X (Inches)</u>	<u>X/L (L=22.5 Inches)</u>	<u>X/S (S=.020 Inches)</u>	<u>X/S (S=.005 Inches)</u>
0	1.75	.078	87.5	350.0
1	3.75	.167	187.5	750.0
2	8.50	.378	425.0	1700.0
3	12.50	.556	625.0	2500.0
4	16.50	.773	825.0	3300.0
5	20.50	.911	1025.0	4100.0

be performed as the dye concentration in the solution to be ejected could be adjusted, thus producing samples along the plate sufficiently above background levels to give reproducible results. The Model 111 Fluorometer has four sensitivity settings allowing

calibration curves to be drawn over a range of about 1 part per 10^6 to 1 part per 10^9 , on a weight basis. For concentrations greater than the lower value, dilution prior to measurement was performed. The calibration charts for this experiment are shown in figures 33 and 34. Approximately 3.5 to 4.5 ml of sample is required for measurement. The sample, contained in a cuvette (a small test tube), is placed in the instrument and the measurement is taken. Cleanliness was found to be a key factor in the technique as fingerprints, body oils, and trace contamination could affect readings. All cuvettes were carefully wiped with soft laboratory paper towels and handled only by the upper edge. All samples were allowed to achieve room temperature prior to reading.

Wall Location

The location of the plate surface was determined with use of the laser beam. The beam of diameter $d_m = .0096$ inches was lowered until two visual effects were observed. First, surface imperfections were observed, highlighted by the laser beam as it approached the plate. Secondly, with the aid of a viewing telescope, observation of the measuring volume at the beam crossover point showed the reflection of the intersected beams from the plate surface as a second image. When the second image blended

with the original image, the beams were considered on the surface. The center of the measuring volume was then about 0.0048 inch off the surface of the plate. The beams were lowered to that distance and the vertical height digital indicator set at zero. The measurements were all considered to be made at a height corresponding to the center of the measuring volume above the surface of the plate.

Tunnel Characterization

To determine the suitability of the water tunnel for the experiment, a velocity field map of the tunnel was made using the LDA system. (The two-dimensional character of the tunnel is shown in figure 50.) Additional tests downstream and at higher flow rates also showed that corner flow effects, although present, were removed from the center of the tunnel.

Velocity profiles and turbulence intensity distributions were taken and are presented in comparison with the work of Laufer (1951) as figures 51 and 52. These curves are in excellent agreement.

A critical requirement for this experiment was that transition be effected on the plate, preferably at its mid-length to allow observation of laminar, transitional, and turbulent flow

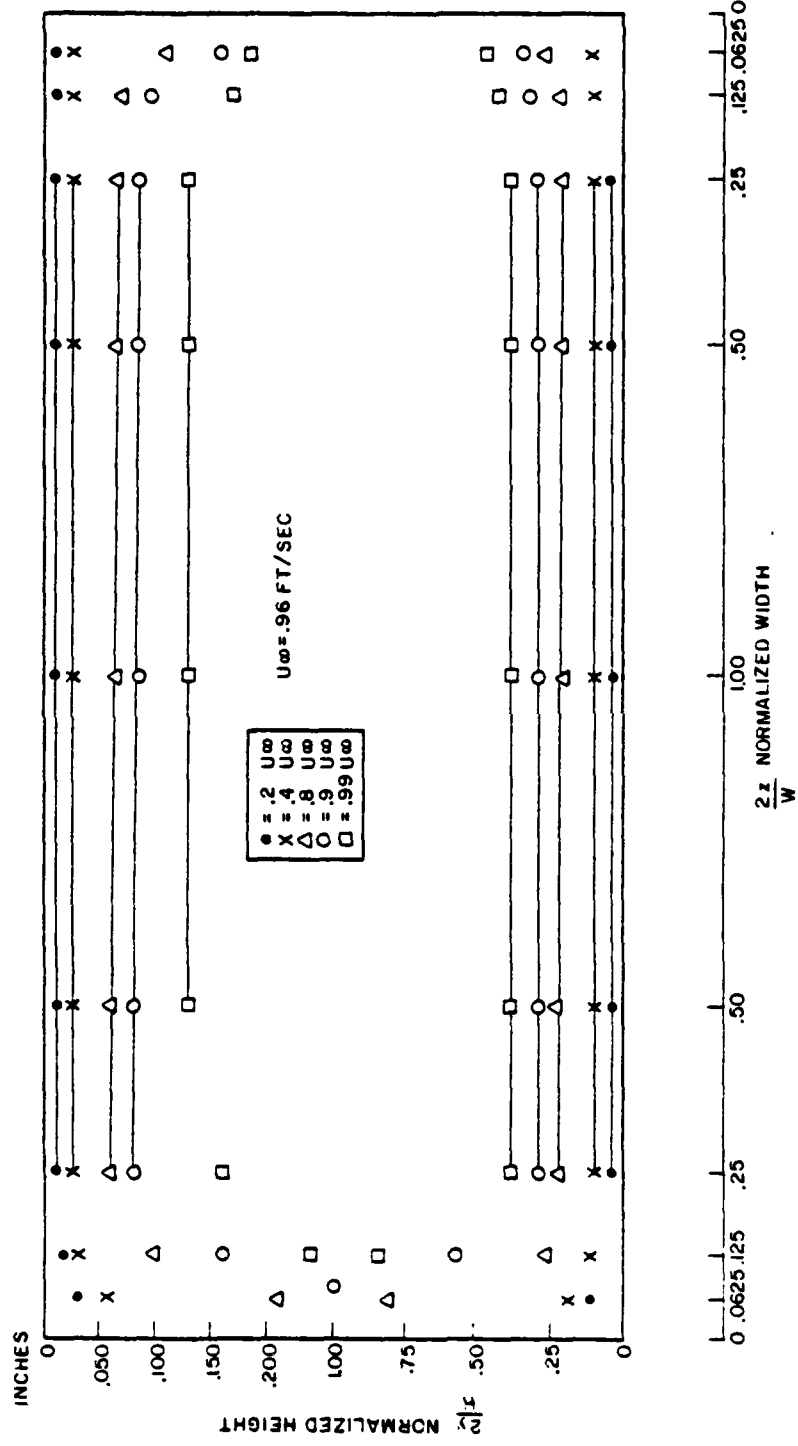


Figure 50. Tunnel velocity field map

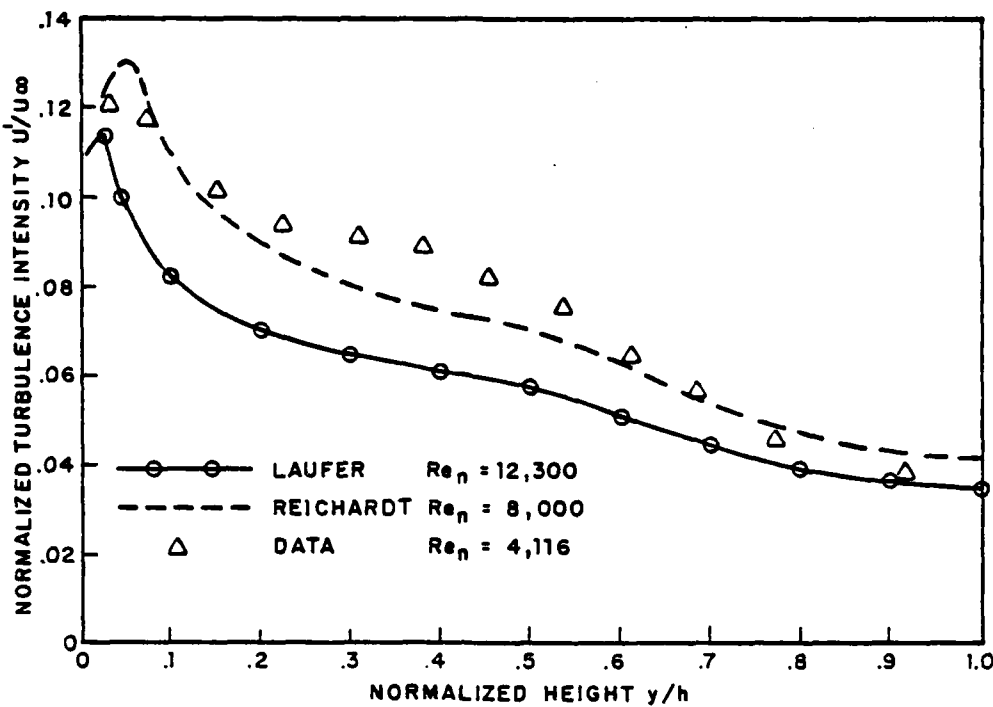


Figure 51. Normalized turbulence intensity distribution

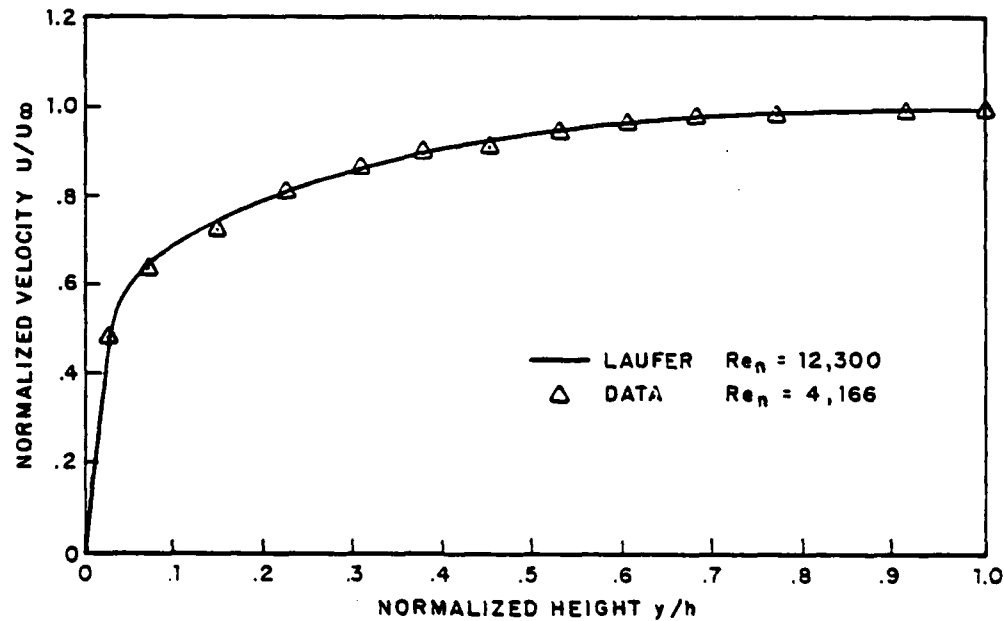


Figure 52. Non-dimensional velocity profiles

boundary layers. The incoming velocity profile is shown in figure 53. Velocity profiles at axial distances of 3.75, 14, and 18 inches, presented in figure 58, are also laminar, transitional, and turbulent. Ejection of a dye onto the surface of the plate showed turbulent bursting occurring at $X = 6.00$ inches.

Application of a laser Doppler technique to locate transition on a flat plate as developed by P. E. Gibson of the Naval Underwater Systems Center, Newport, Rhode Island, is shown in figure 54. From laminar and turbulent velocity profiles, the height above the plate which yielded the greatest corresponding velocity difference was determined. The laser measuring volume was then set at that height and transversed the length of the tunnel, producing a plot of axial velocity distribution. This technique confirmed that transition was occurring on the plate.

Test Series

The test program consisted of two parts: (1) water ejection tests, and (2) polymer ejection tests. All tests were run at a constant tunnel flow of 8 gal/min and an average velocity, V_{avg} , of 2.2 ft/sec. Volumetric flow rates, Q_i , of 20, 40, and 80 cm^3/min were selected to be injected through two slot openings, s , of 0.020 and 0.005 inch. Table 11 lists the injection parameter

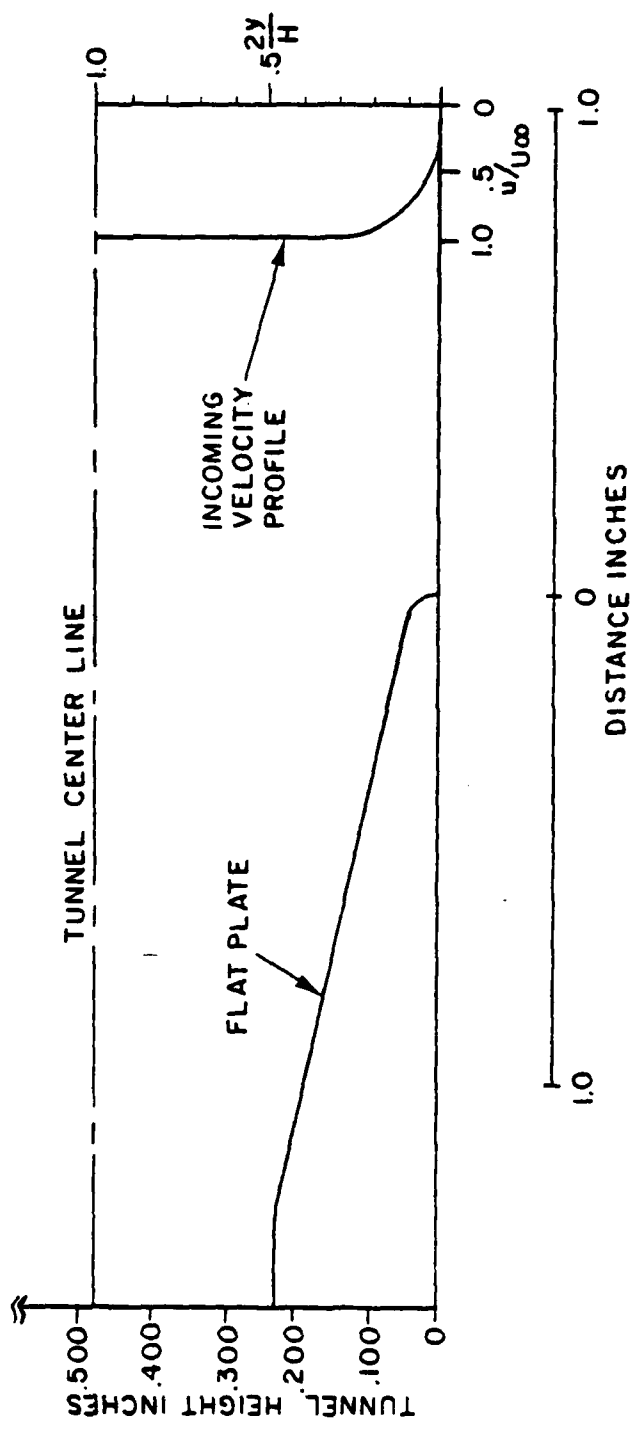


Figure 53. Incoming velocity profile

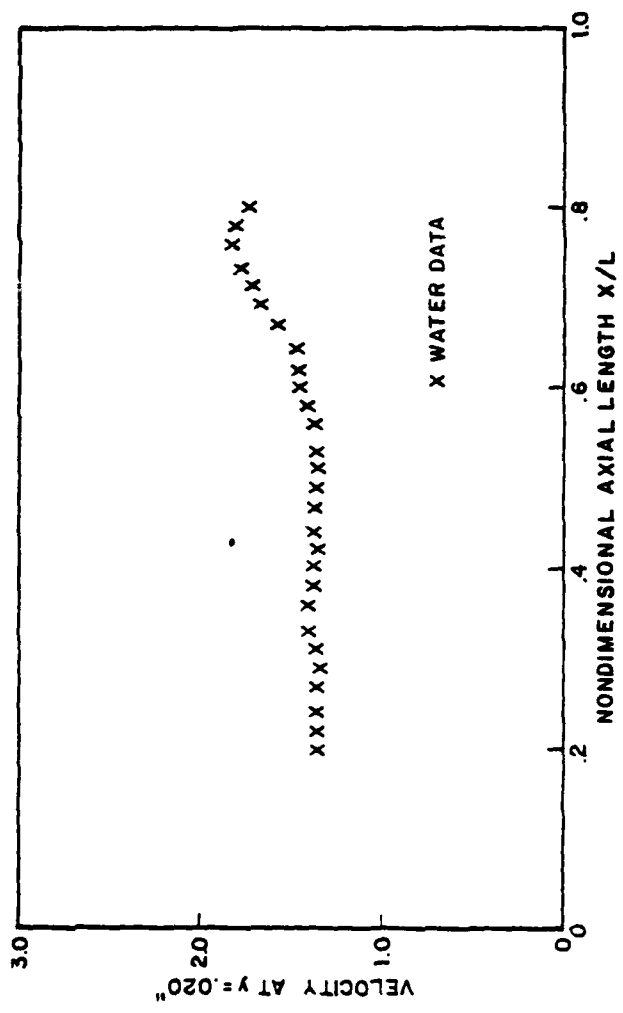


Figure 54. Axial velocity profile at $y = .020$ inches through transition

used. At a given velocity of ejection determined by the combination of slot area and volumetric ejection flow rate, various concentrations of polymer were ejected. Table 12 presents the concentration flux matrix tested.

TABLE 11
INJECTION PARAMETERS

S(in)	$A_g (\text{in})^2$	$Q_i (\text{cc/min})$	$V_i (\text{ft/sec})$	$V_{iy} (\text{ft/sec})$	Normal Component		Velocity Ratio	Velocity Ratio
					Slot Height	Slot Area	of Injection Velocity	Velocity
.020	.04424	20	.0383	.0099			.0174	.00451
.020	.04424	40	.0766	.0198			.0348	.00901
.020	.04424	80	.1532	.0396			.0696	.01802
.005	.01106	20	.1537	.0398			.0699	.01809
.005	.01106	40	.3074	.0795			.1398	.03614
.005	.01106	80	.6148	.1591			.2795	.07233

TABLE 12
CONCENTRATION FLUX MATRIX

Slot	.020 Inch	.020 Inch	.020 Inch	.005 Inch
Q_i	20 cc/min	40 cc/min	80 cc/min	80 cc/min
$C_i Q_i$				
100	2,000	4,000	8,000	-
200	4,000	8,000	16,000	-
400	8,000	16,000	32,000	32,000
500	10,000	20,000	40,000	40,000
800	16,000	32,000	64,000	64,000
2000	-	-	-	160,000

V. ANALYTICAL CONSIDERATIONS

Boundary Layer Model

This section presents an analytical approach for developing turbulent flow over a submerged flat plate with polymer injection. A model is developed for predicting growth of the boundary layer, diffusion of polymers, and prediction of skin friction coefficients and transition as a function of local wall polymer concentrations.

In the analysis that follows, the velocity profile, continuity equation, momentum equation, and an expression for polymer wall concentration from a regression analysis which, in turn, was obtained from experimental data are combined with an effective Reynolds number analogy. This combination yields expressions for the growth of the boundary layer and the skin friction coefficient as a function of the local polymer wall concentration.

Velocity Profile Relation

Meyer (1966) provided a ΔB correction for the law of the wall accounting for polymer effects

$$u^+ = \frac{1}{K} \ln y^+ + B + \Delta B. \quad (56)$$

An alternate method of accounting for the polymer effect would be by adjustment of the mixing length constant, according to Virk (1971). In his work on maximum drag reduction along the ultimate asymptote line, he noted that a change in K by a factor of up to 5 is possible and in full agreement with data. However, from his studies, Meyer concluded that drag reduction in pipes is due to thickening of the laminar sublayer. The mixing length constant, K , which equals approximately 0.4, is apparently unaffected by dilute concentrations of additive. Meyer further correlated the constant B and showed it to remain constant at the Newtonian value of 5.5 until the friction velocity reached a threshold value, v_o^* , after which B increased logarithmically with v^* ,

$$B = Z \ln(v^*/v_o^*). \quad (57)$$

The term Z is a dimensionless constant dependent on the type of polymer additive and the concentration. A constitutive relation for Z is suggested by White (1968) from simple curve fit expressions as

$$Z = \alpha(C_w)^{\gamma}, \quad (58)$$

where $\alpha = 2.3$ and $\gamma = 0.5$. (59)

Skin Friction Relations

The boundary layer continuity, and momentum equations for flow over a submerged flat plate with zero pressure gradient as applied to the polymer flow case studied are given as

$$\frac{\partial(\rho u)}{\partial x} + \frac{\partial(\rho v)}{\partial y} = 0 \quad (60)$$

and

$$\rho u \left(\frac{\partial u}{\partial x} \right) + \rho v \left(\frac{\partial u}{\partial y} \right) = - \frac{\partial \tau}{\partial y}. \quad (61)$$

Upon changing independent variables x and y to x , y^+ , and C_w , the x derivatives must be handled by the chain rule, since the parameters y^+ and C_w are functions of x in the law of the wall. Thus, the substitute is

$$\frac{\partial}{\partial x} = \frac{\partial y^+}{\partial x} \left(\frac{\partial}{\partial y^+} \right) + \frac{\partial C_w}{\partial x} \left(\frac{\partial}{\partial C_w} \right) . \quad (62)$$

As may be noted in equation (62), concentration derivatives are added. The fluid properties of density, ρ , and viscosity, μ , are assumed constant and equal to those of the solvent water in this analysis.

The resultant boundary layer equation, after considerable algebraic manipulation, is

$$\int_{x_0}^x \frac{U}{v} dx = \int_{\lambda_0}^{\lambda} \left[\delta^+ \left(\left\{ z \ln \left(\frac{v^*}{v_o} \right) \left[\frac{2}{K} (\ln \delta^+ - 1) + 2B + z \ln \left(\frac{v^*}{v_o} \right) \right] \right\} \right. \right. \\ \left. \left. + \left\{ \frac{2}{K} (\delta^+ - 1) (B - \frac{1}{K}) + \frac{1}{K^2} (\ln \delta^+)^2 + (B)^2 \right\} \right) \right] d\lambda \\ - \int_{C_{w0}}^{C_w} \delta^+ \lambda \left\{ \frac{z}{C_w} \ln \left(\frac{v^*}{v_o} \right) \left[1 + \frac{1}{K^2} (\ln \delta^+ - 1) + B - \frac{1}{K} \right] \right\} dC_w \quad (63)$$

where

$$\lambda = \frac{U}{v^*} = \sqrt{\frac{2}{C_f}} \quad (64)$$

and

$$\delta^+ = e^{K(\lambda-B)} \left[\left(\frac{v^*}{v_o} \right)^{-Kz} \right]. \quad (65)$$

Appendix A presents a complete development of the equations related to this method.

With elimination of the polymer terms, equation (63) compares favorably with the classical skin friction relations of Prandtl-

Schlichting and Schultz-Grunow, as well as the simplified relation of F. White. This comparison is presented in figure 55.

Prior to the solution of equation (63) and (65), it is necessary to determine a means of calculating C_w . A regression analysis was performed on all of the data for the slowest injection rate of 20 cc/min and injection concentrations of $c = 100, 200, 400, 500,$ and 800 WPPM. Equation (66) represents the results of that analysis which successfully correlates 88% of the data obtained, so that

$$\frac{C_w}{C_i} = .8343 + 2.3033\left(\frac{X}{L}\right) - 7.385\left(\frac{X}{L}\right)^2 + 4.2855\left(\frac{X}{L}\right)^3. \quad (66)$$

Equation (66) is valid for $X/L > .27$. For $X/L < .27$, equation (67) holds true. It follows then that

$$\frac{C_w}{C_i} = 1.0. \quad (67)$$

Effective Reynolds Number Analogy

White (1968) rearranged the friction factor relation derived by Meyer (1966) and evolved the following effective Reynolds number analogy. The friction factor in the presence of polymer may be considered equal to the Newtonian friction factor evaluated at an effective Reynolds number given by

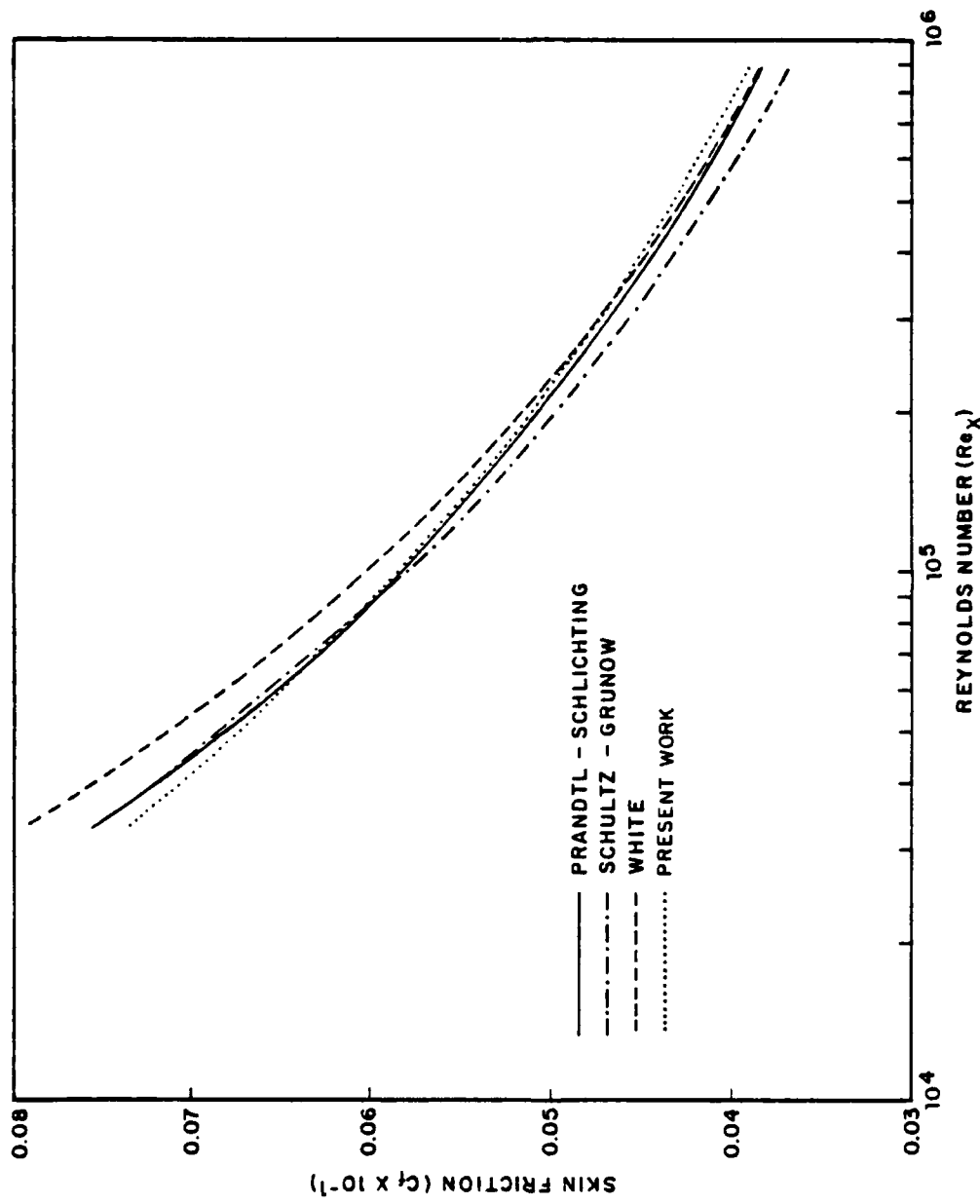


Figure 55. Flat plate skin friction coefficient curve

$$Re_p = Re \left(\frac{V^*}{V_o} \right)^{Kz} . \quad (68)$$

Thus, the polymer has the effect of increasing the Newtonian Reynolds number, Re , and thereby yielding the lower polymer solution friction factor. For constant freestream velocity and assuming constant polymer ocean flow, skin friction versus Reynolds number curves may be obtained as follows:

1. Calculate Reynolds number at given X ,

$$Re_x = \frac{Ux}{v} . \quad (69)$$

2. Calculate initial skin friction value using White's simplified relation,

$$C_f = \frac{.455}{[\ln(.06 Re_x)]^2} . \quad (70)$$

3. Calculate initial shear velocity,

$$V^* = U_\infty \sqrt{\frac{C_f}{2}} . \quad (71)$$

4. Calculate effective polymer Reynolds number,

$$Re_p = Re_x \left(\frac{V^*}{V_o} \right)^{Kz} , \quad (72)$$

where

$$z = \alpha C_w^\gamma \text{ for } C_w \leq C_w^* \quad (73)$$

$$z = \alpha (C_w^*)^\gamma \text{ for } C_w > C_w^*$$

5. Calculate polymer skin friction,

$$C_{f,p} = \frac{.455}{[\ln(.06 Re_p)]^2} . \quad (74)$$

6. Calculate shear velocity,

$$V^* = U_\infty \sqrt{\frac{C_f}{2}} . \quad (75)$$

Equations (72) through (75) should be repeated until the shear velocity does not change by more than 0.5%. This iterative procedure yields skin friction values as a function of Reynolds numbers. A new value of x along the plate should be selected and the procedure should be repeated. Figure 56 presents curves of skin friction versus Reynolds number for concentrations of 5, 10, 15, 20, and 25 WPPM as well as turbulent and laminar flow skin friction curves given by equations (70) and (76) for water flow only,

$$C_f = \frac{.664}{\sqrt{Re_x}} . \quad (76)$$

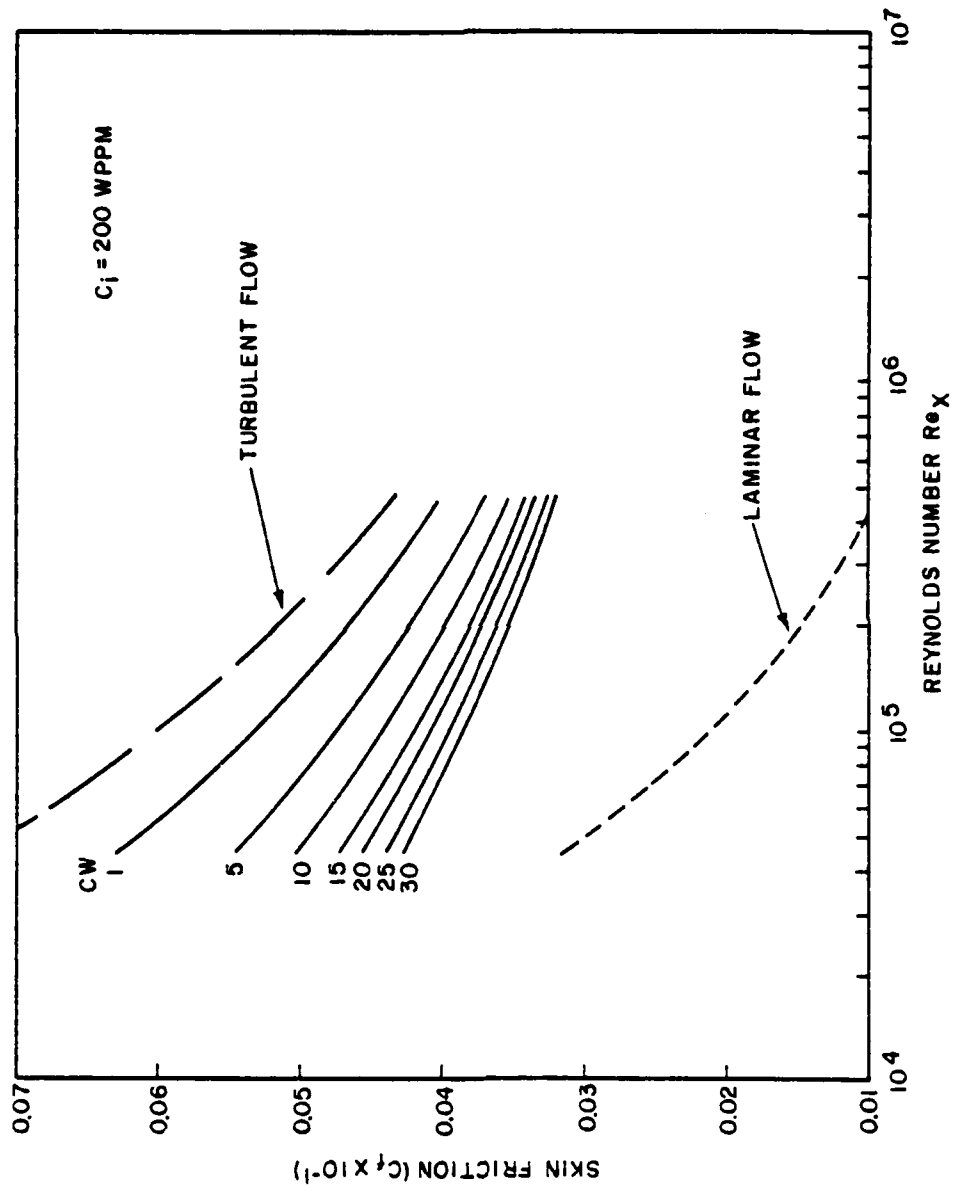


Figure 56. Skin friction versus reynolds number as a function of polymer concentration

Using the concept of the effective Reynolds number analogy and the variation in the wall concentration of polymer determined from the regression analysis performed on the experimental data, it is possible to numerically integrate the right hand side of equation (63) and compare it with the resulting Reynolds number obtained from integration of the left hand side of equation (63).

The computational procedure is presented in appendix F as a listing of computer program SKINFRIC. The model allows for an initial laminar flow over the plate, changing to turbulent flow at $x = x_t$. The integrations are performed from initial values of x where injection occurs, an initial wall concentration equal to the injected concentration of polymer and an initial value of λ determined from laminar flow conditions given by equation (76). This is based on the assumption that small concentrations of polymers do not affect laminar flow. The work of Hoyt and Fabula (1964) showed that non-Newtonian is a misnomer applied to low concentrations of polymers. They found that these solutions were of constant viscosity and greater magnitude than that of the solvent. White (1968) determined the limiting value of λ to be approximately 11.0 by single curve fitting of data. Application of the maximum drag reduction concentration for Polyox of $C_w^* = 30$ WPPM as determined by Hoyt and Fabula (1964), and shown in figure 57, allowed the limiting value of λ to be taken as 12.6.

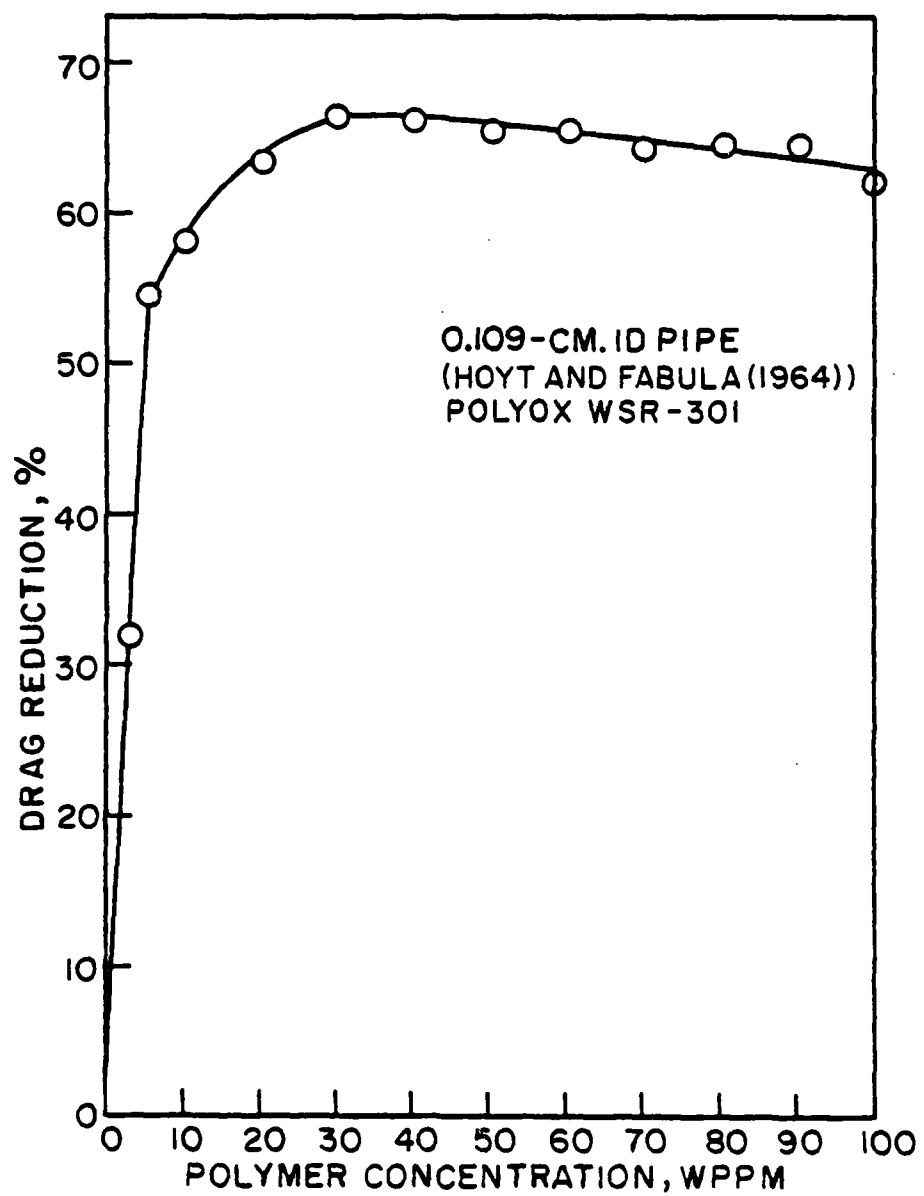


Figure 57. Percent drag reduction as a function of polymer concentration

It is further assumed that the effective Reynolds number analogy is a solution to equation (63). Values of λ are then used in the numerical integration of the right hand side of equation (63). Values of the polymer wall concentration, equation (66), from the regression analysis are also used. The integration proceeds from $X_0 = 0$ at the point of injection of the polymer and neglects leading edge effects. Laminar flow equations give the flow over the initial region of flat plate until the preset transition point is reached at $x = x_t$, after which turbulent effective Reynolds analogy parameters apply. Comparison of the difference between integrand 1 and integrand 2 on the right hand side of equation (63) with the left hand side Reynolds number is made at the end of the plate. If they are not within 1%, the location of the point of transition is adjusted and the procedure repeated until the results are within the set tolerance limits. The transition region is defined as starting at the transition point and ending at the distance where the Reynolds number equals 350,000. In this zone a linear intermittency factor is assumed and an appropriately proportioned friction factor calculated.

Typical plots of skin friction coefficient versus Reynolds number for various polymer concentrations injected at $Q_1 = 20$ cc/min are shown in figures 92 through 96. Boundary layer growth over the length of the plate is presented in figures 85 through 88 and compared with experimental data.

VI. EXPERIMENTAL RESULTS AND DISCUSSION

General Remarks

The experimental program was conducted at a constant tunnel flow of 8 gallons per minute. Injection into the boundary layer was performed through two different size slots of width, $s = .020$ inch, and $s = .005$ inch, at injection rates of 20, 40, and 80 cc/min. These six injection velocity ratios were tested with dyed water injection. Polymer concentrations of 100, 200, 400, 500, and 800 WPPM were injected at 20, 40, and 80 cc/min through the $s = .020$ inch slot and at 80 cc/min. through the $s = .005$ -inch slot, producing injection velocity to average freestream velocity ratios of 0.0174, 0.0348, 0.0696 and 0.2795, respectively.

Velocity profiles were taken at nine stations along the plate corresponding to axial distances of $x = 3.75, 6, 8, 10, 14, 15, 16, 17$, and 18 inches. Concentration measurements were taken at five stations along the plate corresponding to axial distances of $x = 3.75, 8.5, 12.5, 16.5$, and 20.5 inches. At each concentration measuring station, nine samples were taken throughout the boundary layer including a wall sample. Table 2 indicates the relative heights in the boundary layer at which the concentration samples

were captured according to which spacer was used in conjunction with the sampling probe.

In total, 243 velocity profiles and 130 concentration profiles were measured. Space limitations prohibit the complete listing of the data file; however, copies of the data file are available from the author at the Naval Underwater Systems Center, Newport, Rhode Island. The focus of the discussion will concentrate on the 20 cc/min injection rate through the .020-inch slot which yielded an injection velocity ratio of 0.0174. This slowest injection velocity was selected as providing minimum boundary layer disturbance at the point of injection. Previous investigations such as Sirmalis (1976), Fruman and Tulin (1976), Wu (1968), and Wells (1968) have recommended minimization of the injection velocity. The hydrodynamic parameters for the tests discussed are presented in appendix D with velocity profiles presented in appendix E.

Water Flow Boundary Layer Characterization

Velocity profiles for the laminar flow region are presented in figure 58 and compared with the classical Blasius profile. The slight variation from the classical form may be attributed to the effects of the small pressure gradient at the leading edge of the plate and due to its shape and roughness. Displacements among the data themselves are due to the effects of injection velocity, with minimum injection velocity approaching the theoretical profile.

Downstream, at a station $x = 18$ inches, the velocity profiles follow a $1/6$ th power law turbulent flow shape as shown in figure 59. Patel (1968) has shown that in developing flows the velocity profiles go through various power law shaped profiles until a $1/7$ th power law profile is achieved for fully-developed turbulent flow. The measured profiles are in agreement with Patel's findings as fully-developed turbulent flow was not totally achieved due to the length of the plate used.

The transitional nature of the velocity profiles from laminar to turbulent flow for the case of 20 cc/min injection at a velocity of injection, $V_i = .0383$ ft/sec, is shown in figure 60.

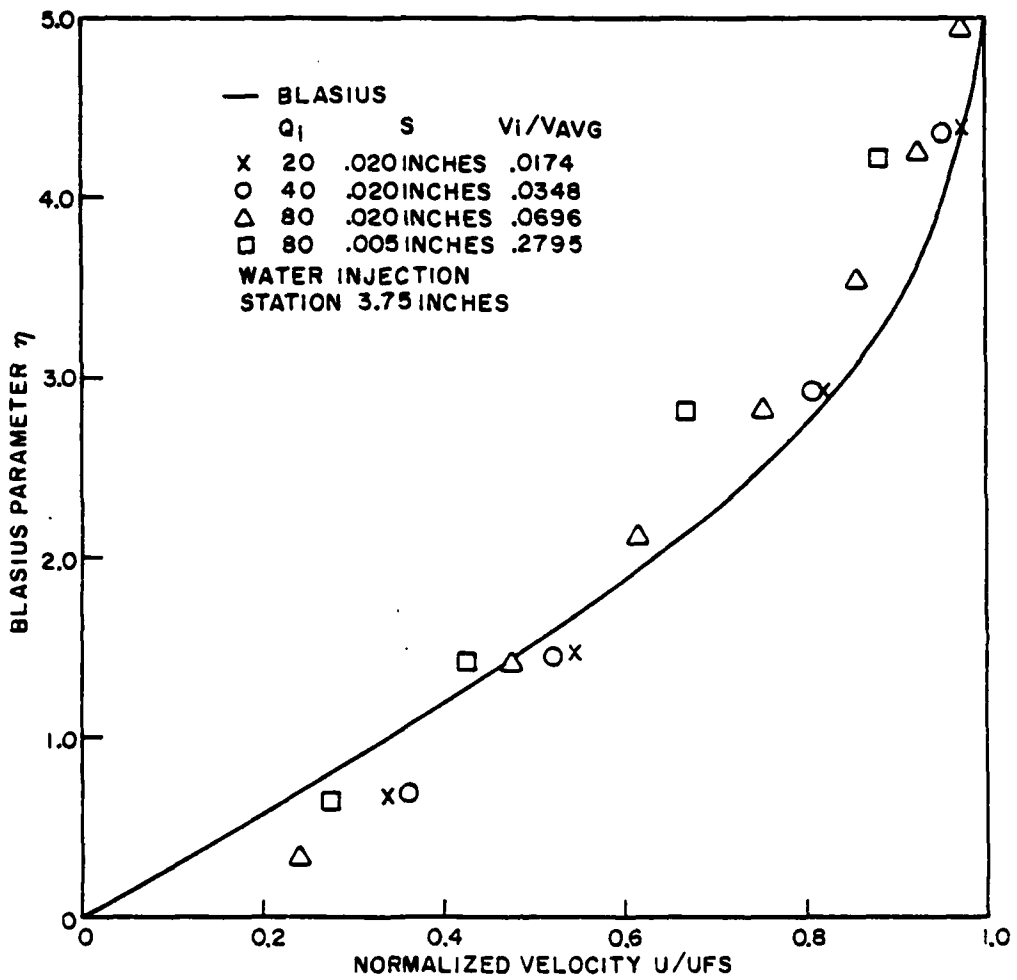


Figure 58. Normalized laminar velocity profiles

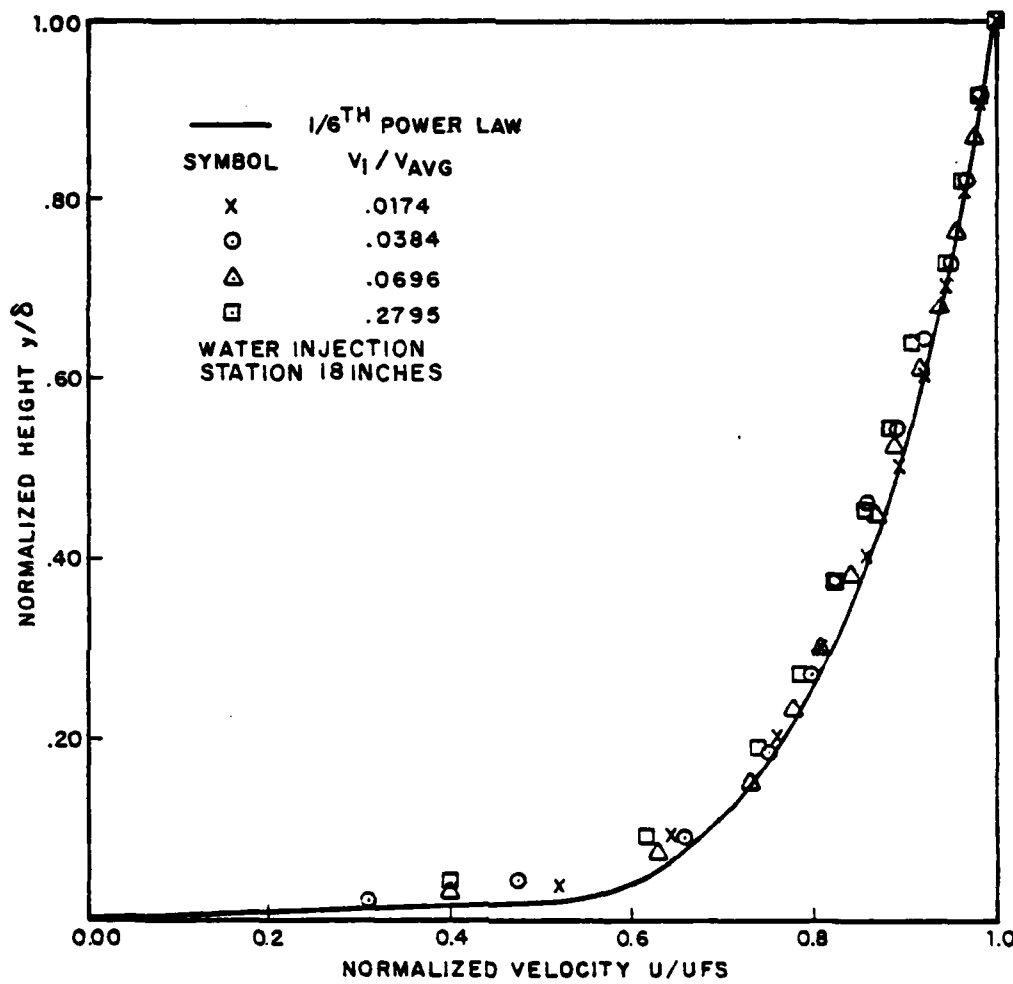


Figure 59. Non-dimensional velocity profiles at station
 $x = 18.0$ inches

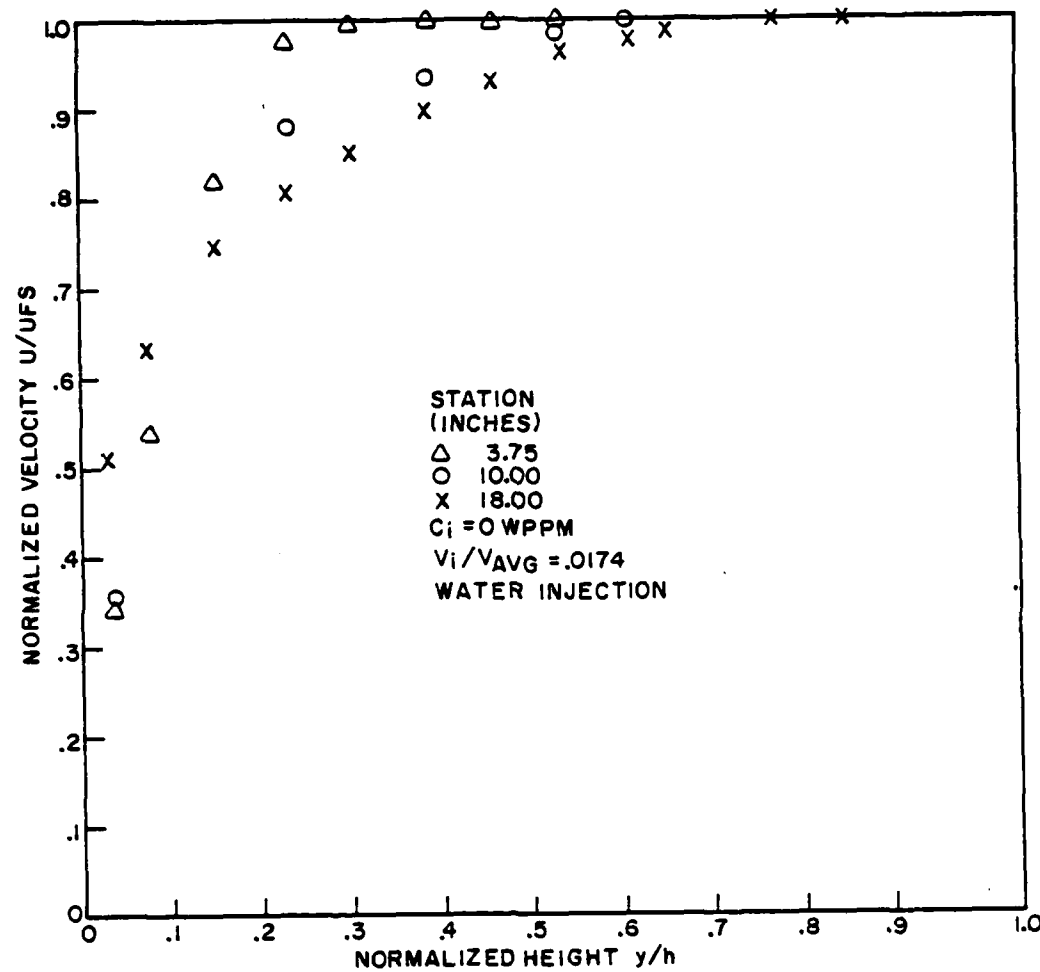


Figure 60. Transitional nature of the velocity profiles for water flow

The turbulent intensity distributions for these stations are presented in figure 61. As shown by Schubauer and Klebanoff (1955), the velocity becomes greater closer to the wall as the flow becomes turbulent. Transition to turbulent flow is generally observed by a sudden, rapid growth in the height of the boundary layer. The growth of the boundary layer for water injection is shown in figure 62 and reveals this characteristic.

An additional criterion to characterize turbulent flows is that the velocity distribution in the wall region should follow the well known law of the wall, such that

$$u^+ = A \ln y^+ + B,$$

where A and B are universal constants having the value of 2.5 and 5.5, respectively. Patel (1968) indicates that, for developing flow, the value of B decreases until the value of 5.5 is achieved for fully-developed turbulent flow. Application of this concept to the channel flows under discussion revealed the variation in the value of B as shown in figure 63 as a function of length Reynolds number. A representative value of $B = 7.2$ was used in this study for the turbulent flow region which is not fully developed. Figure 64 presents a plot of the law of the wall in inner variables

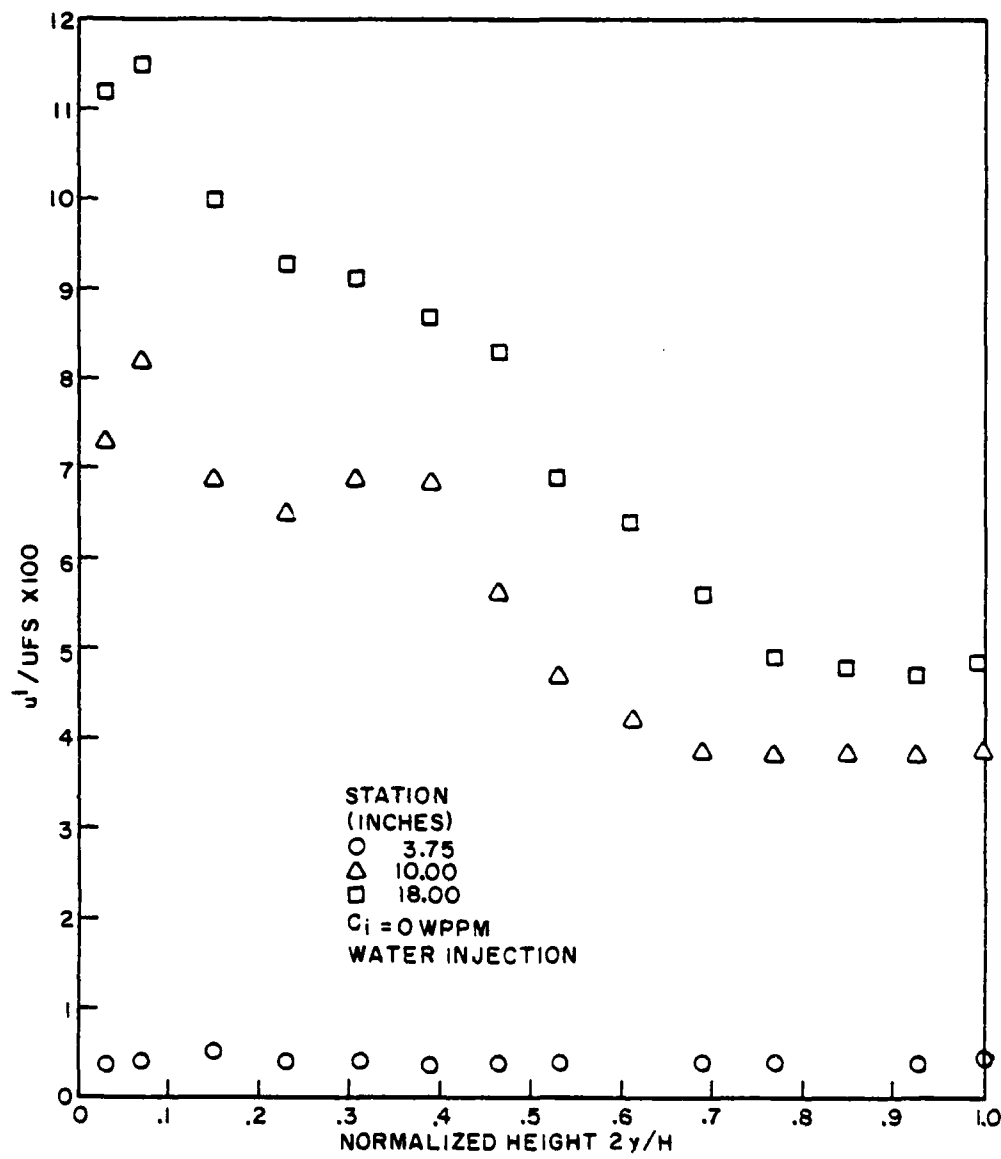


Figure 61. Turbulence intensity distributions for transitional velocity profiles

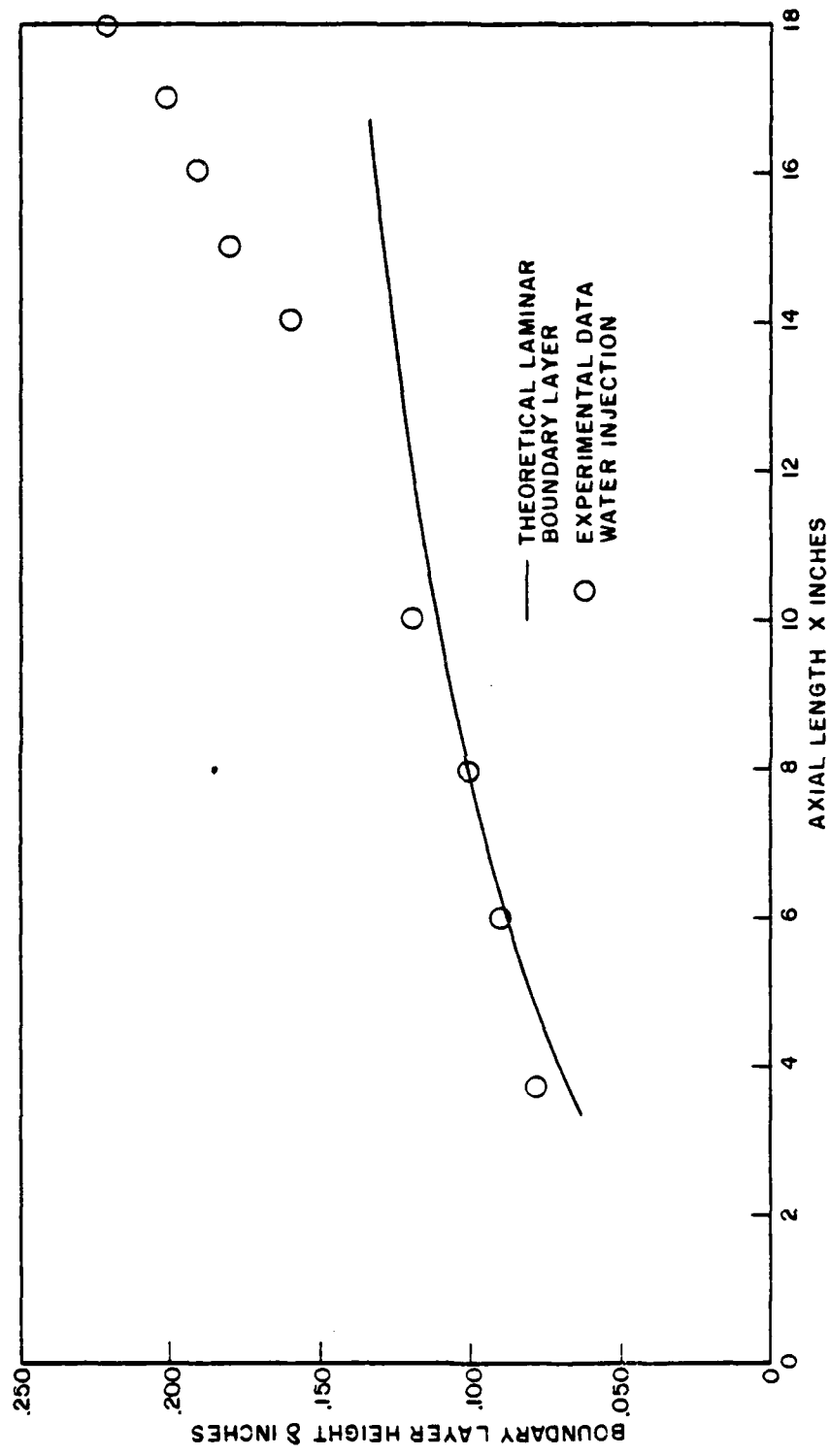


Figure 62. Growth of boundary layer for water flow

AD-A103 070

NAVAL UNDERWATER SYSTEMS CENTER NEWPORT RI
AN EXPERIMENTAL STUDY OF POLYMER DRAG REDUCTION AND BOUNDARY LA--ETC(U)

F/6 20/4

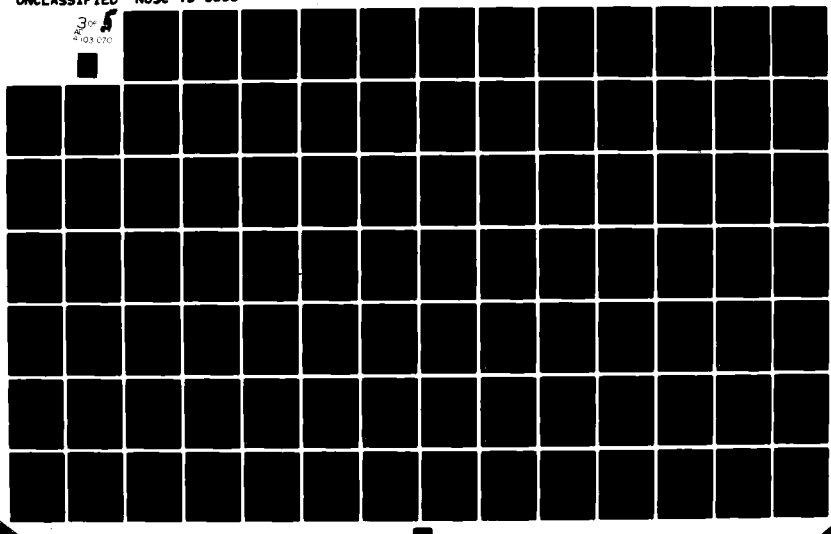
AUG 79 J MIGUEL

UNCLASSIFIED

NUSC-TD-5656

NL

3 of 4
AD-A103 070



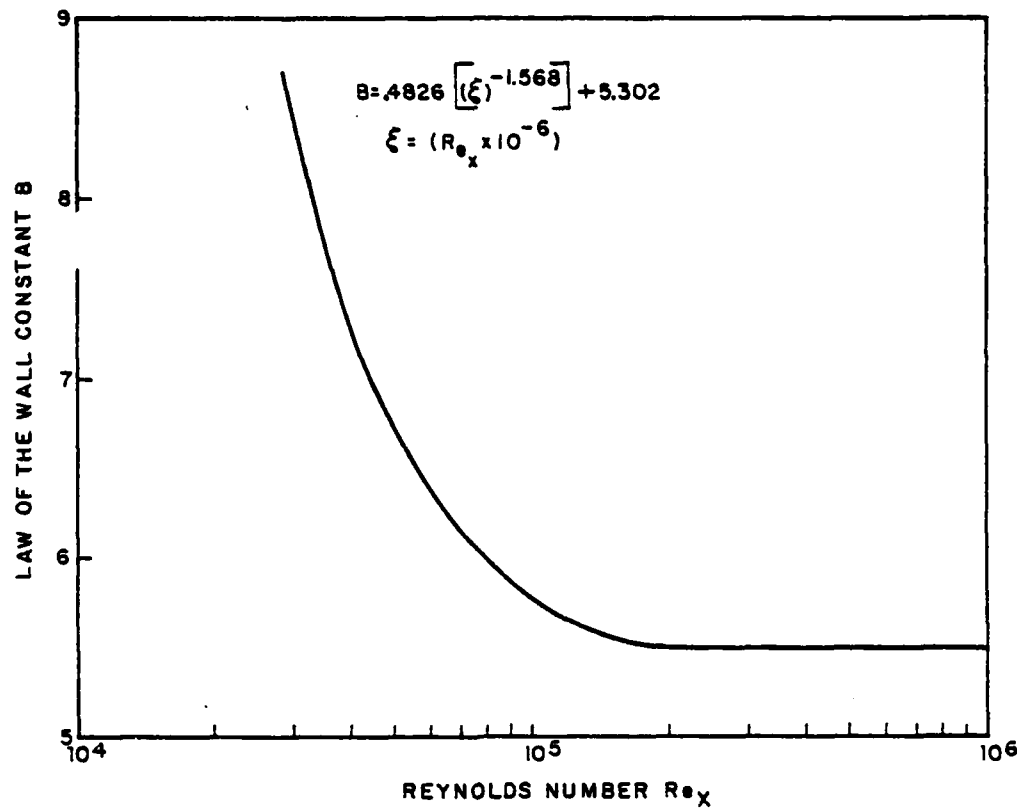


Figure 63. Variation in value of B as a function of Reynolds number for developing channel flow

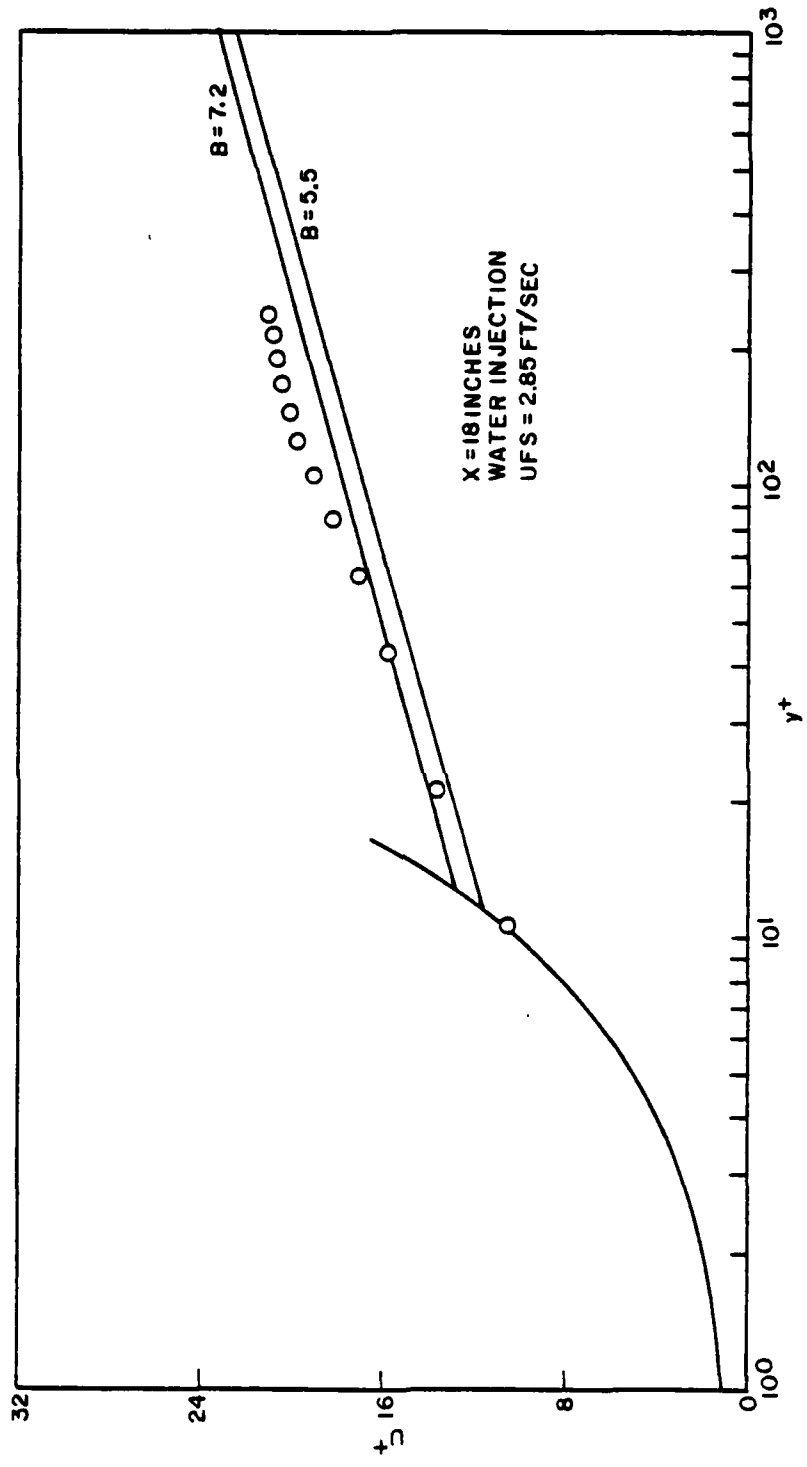


Figure 64. Law of the wall for developing flow

y^+ and u^+ for $B = 5.5$ and 7.2 . A comparison is also made with experimental data showing excellent agreement with the value of $B = 7.2$. The value of $B = 7.2$ is therefore used in the expression for the law of the wall to account for the developing velocity profile aspect of the flow.

Polymer Flow Boundary Layer Characterization

Developing velocity profiles for injected polymer concentrations of $C_i = 100, 200, 400, 500$, and 800 WPPM are presented in figures 65 through 69. The profiles are from stations $x = 3.75, 10.0$, and 18.0 inches representing laminar, transitional, and turbulent flow regions. The characteristic increasing fullness of the velocity profiles over the length of the plate is evident in each test sequence.

Turbulence intensity distributions for these profiles are plotted in figures 70 through 74. The freestream turbulence intensity was .3% for the tests where water and polymer concentrations equal to $100, 200$, and 400 WPPM were injected. For the injection of polymer at 500 and 800 WPPM, the freestream turbulence level was .4% and .5%, respectively.

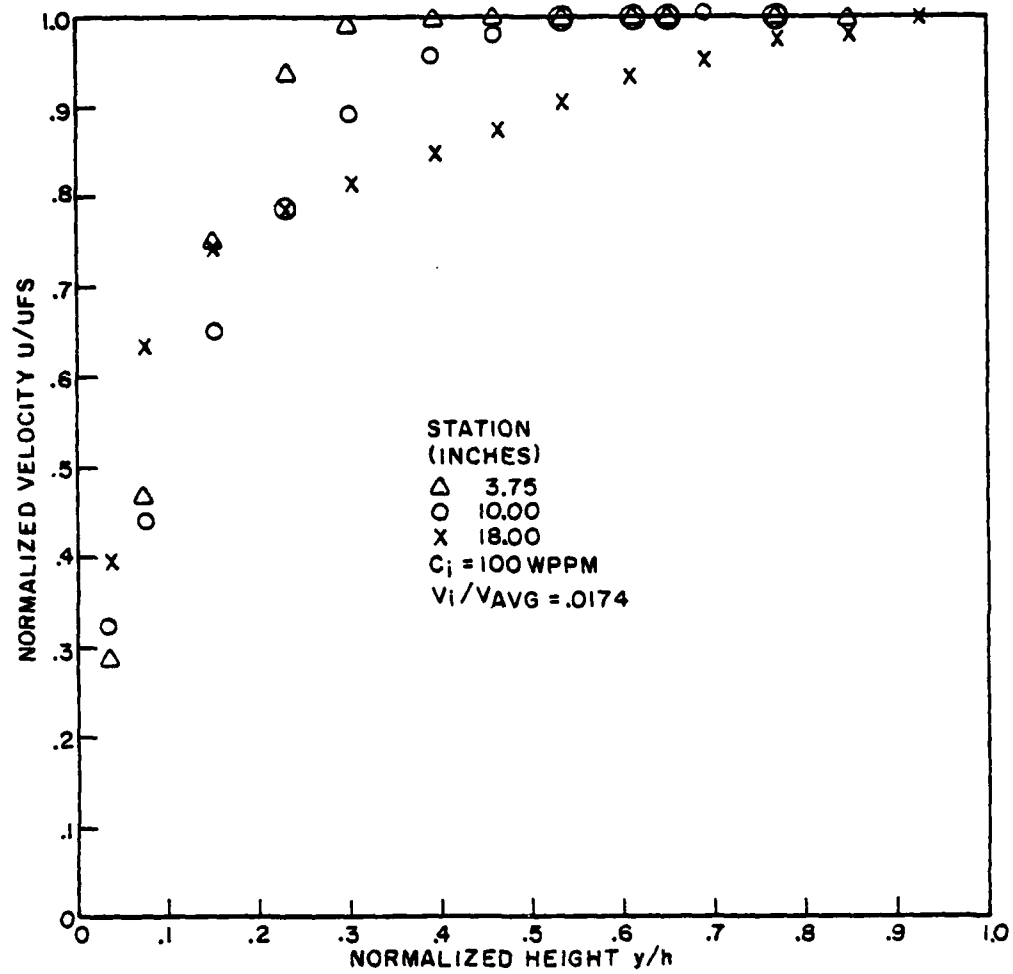


Figure 65. Developing velocity profiles for injected polymer concentration $C_i = 100$ WPPM

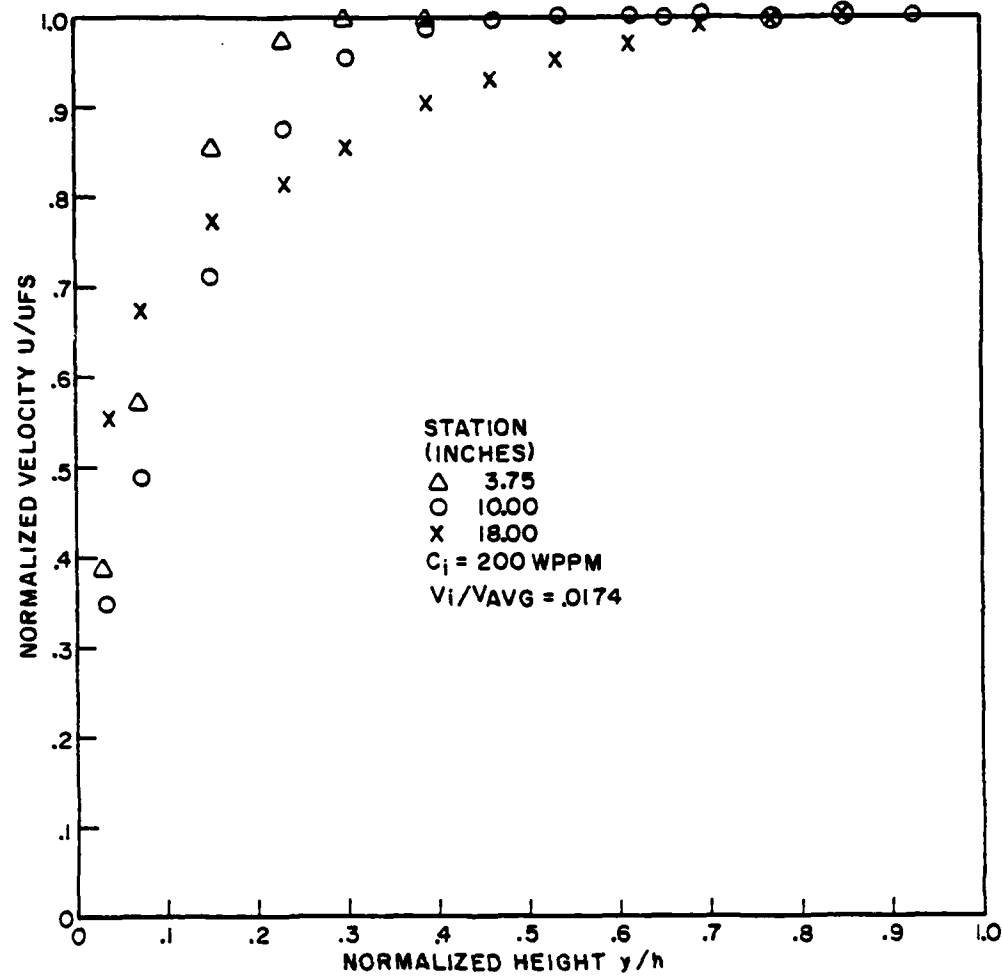


Figure 66. Developing velocity profiles for injected polymer concentration $C_i = 200$ WPPM

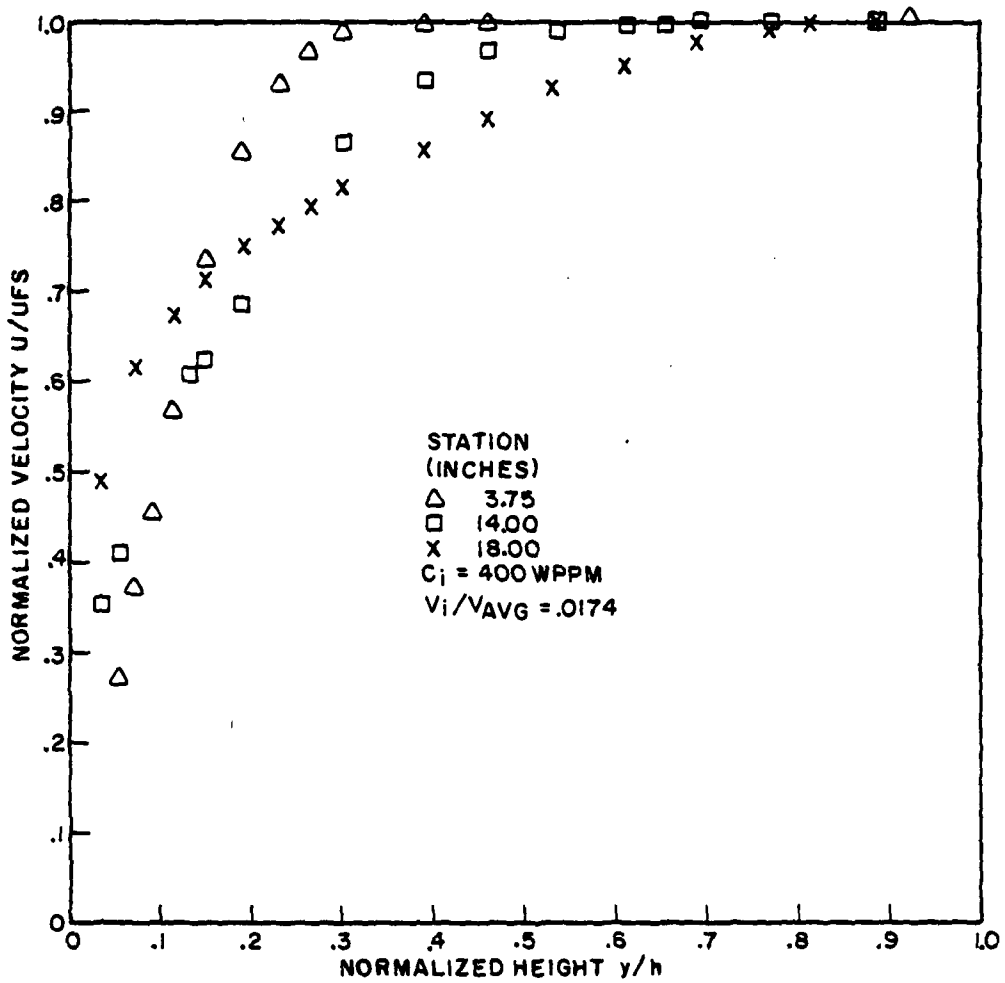


Figure 67. Developing velocity profiles for injected polymer concentration $C_1 = 400 \text{ WPPM}$

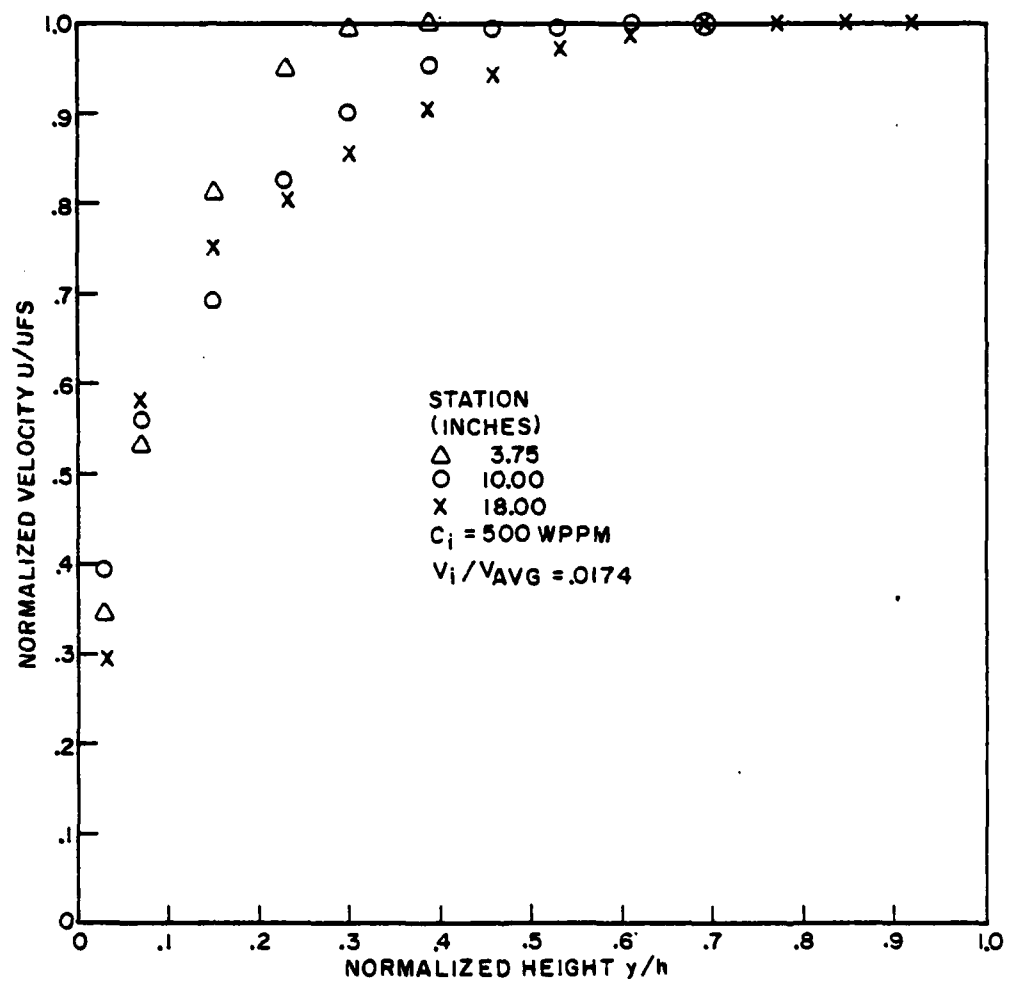


Figure 68. Developing velocity profiles for injected polymer concentration $C_i = 500 \text{ WPPM}$

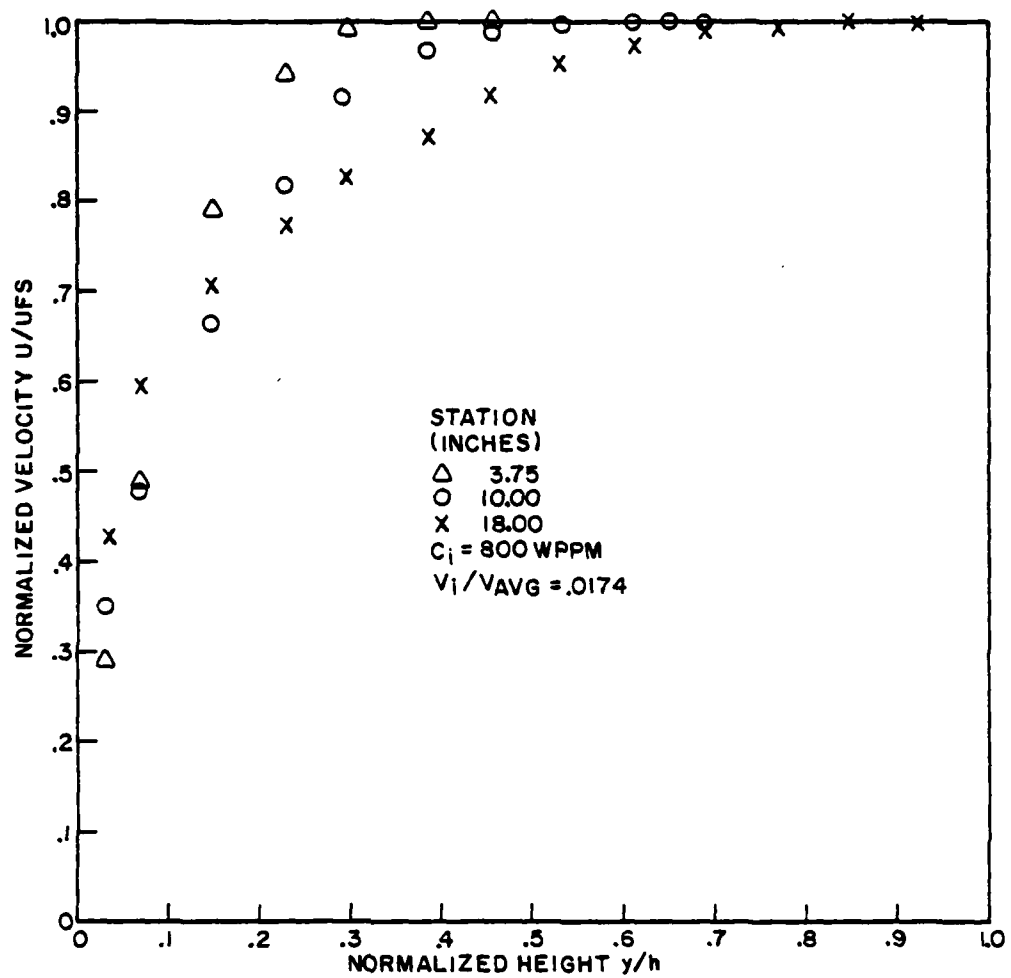


Figure 69. Developing velocity profiles for injected polymer concentration $C_i = 800 \text{ WPPM}$

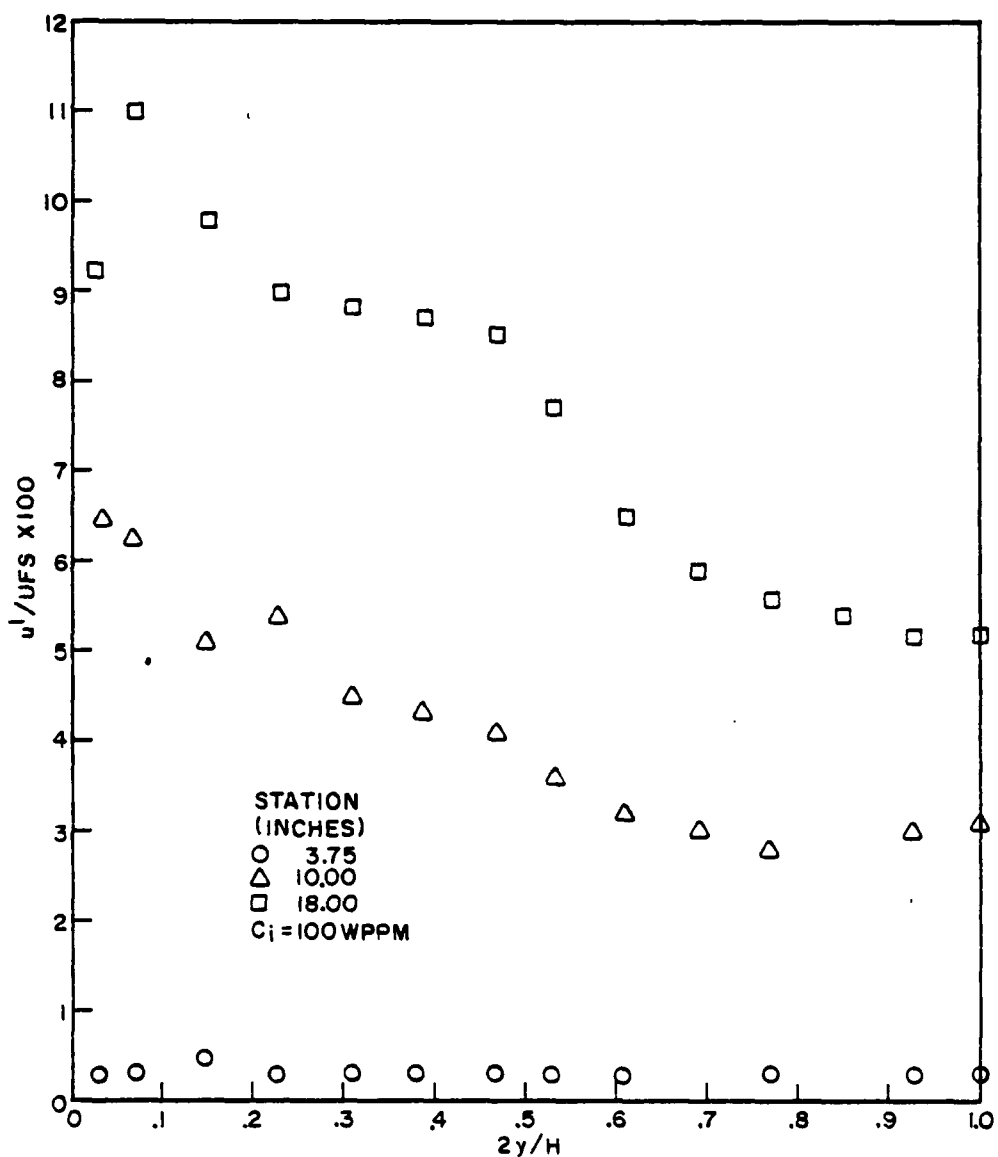


Figure 70. Turbulence intensity distribution for injected polymer concentration $C_i = 100$ WPPM

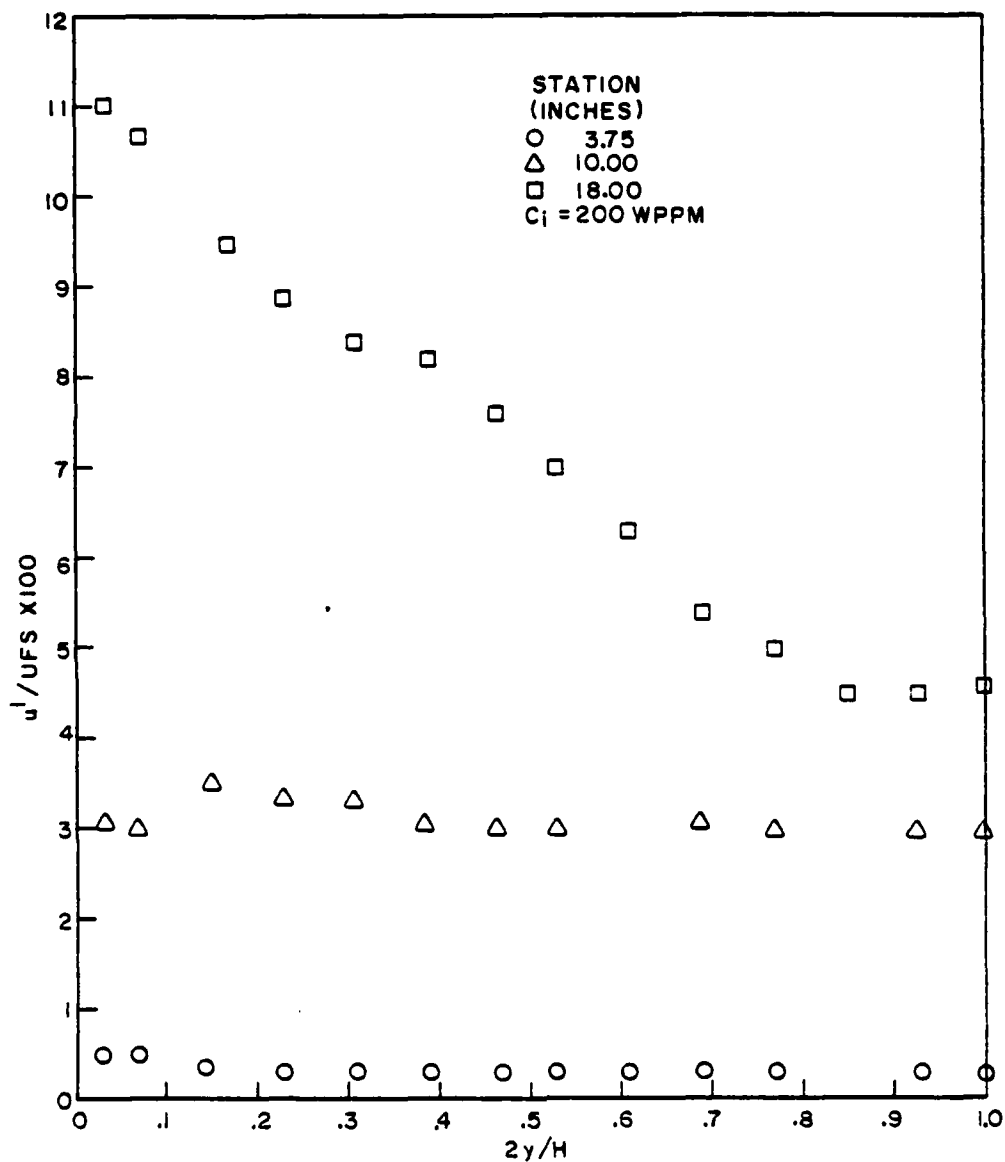


Figure 71. Turbulence intensity distribution for injected polymer concentration $C_1 = 200$ WPPM

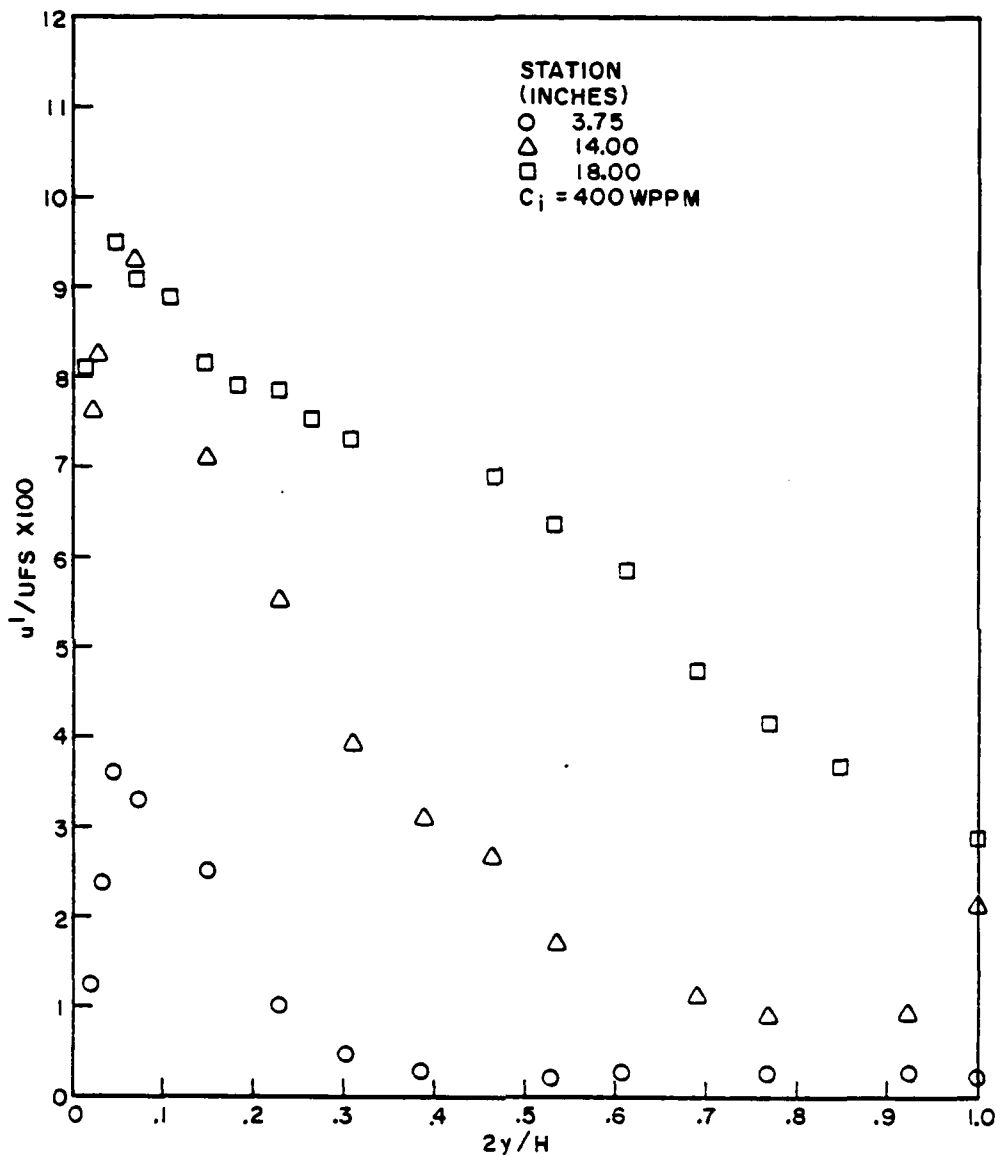


Figure 72. Turbulence intensity distribution for injected polymer concentration $C_i = 400 \text{ WPPM}$

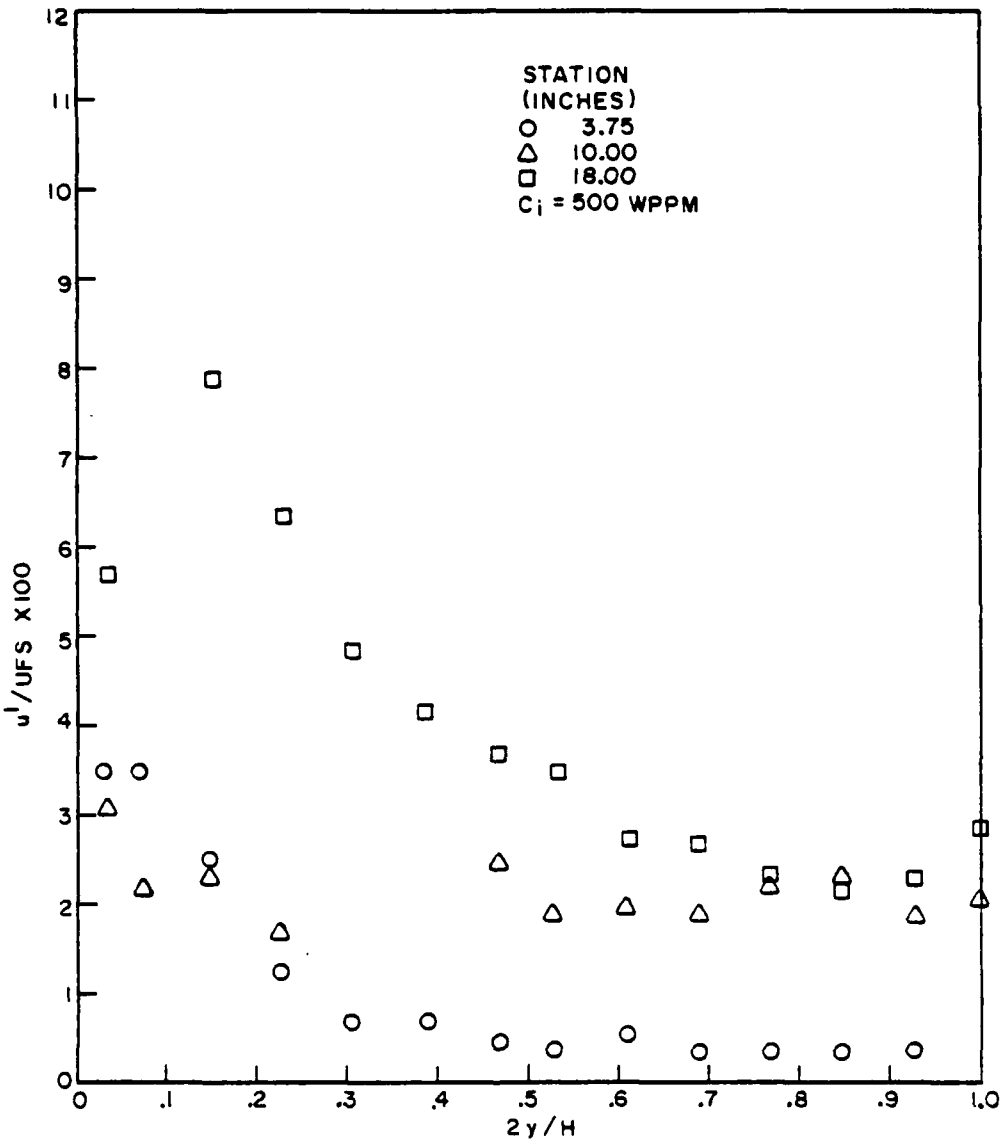


Figure 73. Turbulence intensity distribution for injected polymer concentration $C_i = 500$ WPPM

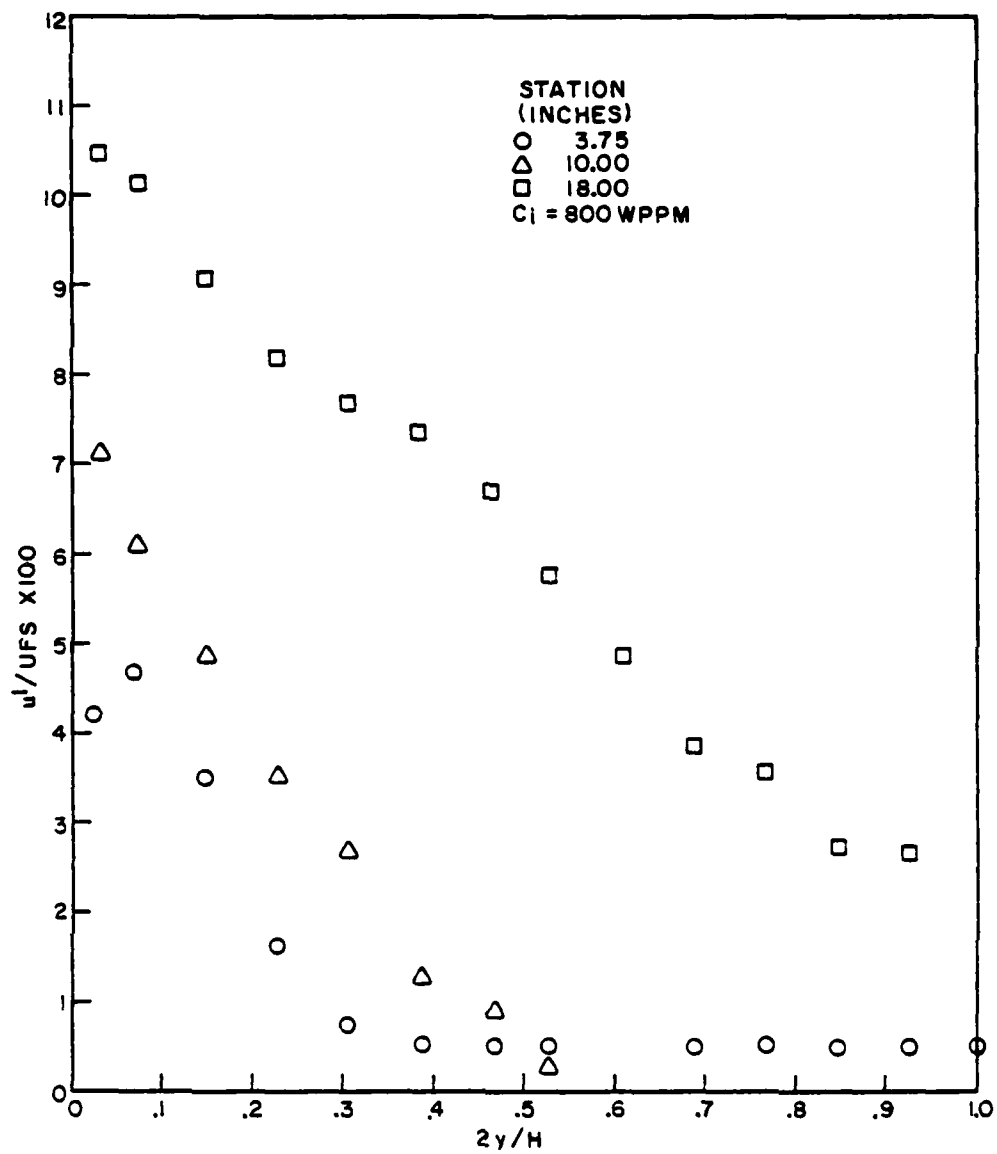


Figure 74. Turbulence intensity distribution for injected polymer concentration $C_1 = 800$ WPPM

The velocity profiles at $x = 3.75$ inches are all laminar in shape. At $x = 10$ inches, the velocity profiles appear less turbulent than the water case. This characteristic is also shown in the lower turbulence intensity distributions at this station for all concentrations injected. The polymer causes a reduction in the peak value of turbulence intensity and shifts the position further away from the wall. The entanglement or "hand holding" of the long chain polymers may act as a woven blanket to dampen or suppress turbulence.

A comparison of velocity profiles at $x = 18$ inches, normalized with respect to boundary layer thickness and freestream velocity compared with a 1/5th power law velocity profile in figure 75 shows good agreement for the $C_i = 400$ WPPM injection case. The $C_i = 500$ WPPM injection data also plotted on this figure indicate a lesser developed profile and a possible thicker sublayer.

When 2000 WPPM was injected through the .005-inch wide slot at a velocity ratio $U/U_{avg} = .280$, the freestream turbulence intensity was 3.0%. Figure 76 presents a comparison of the velocity profile development for the 2000 WPPM injection case with the comparable water injection case. These data, taken at $x = 3.75$ inches (2 inches downstream from the injection slot), indicate a disturbance effect due to the higher injection velocity for

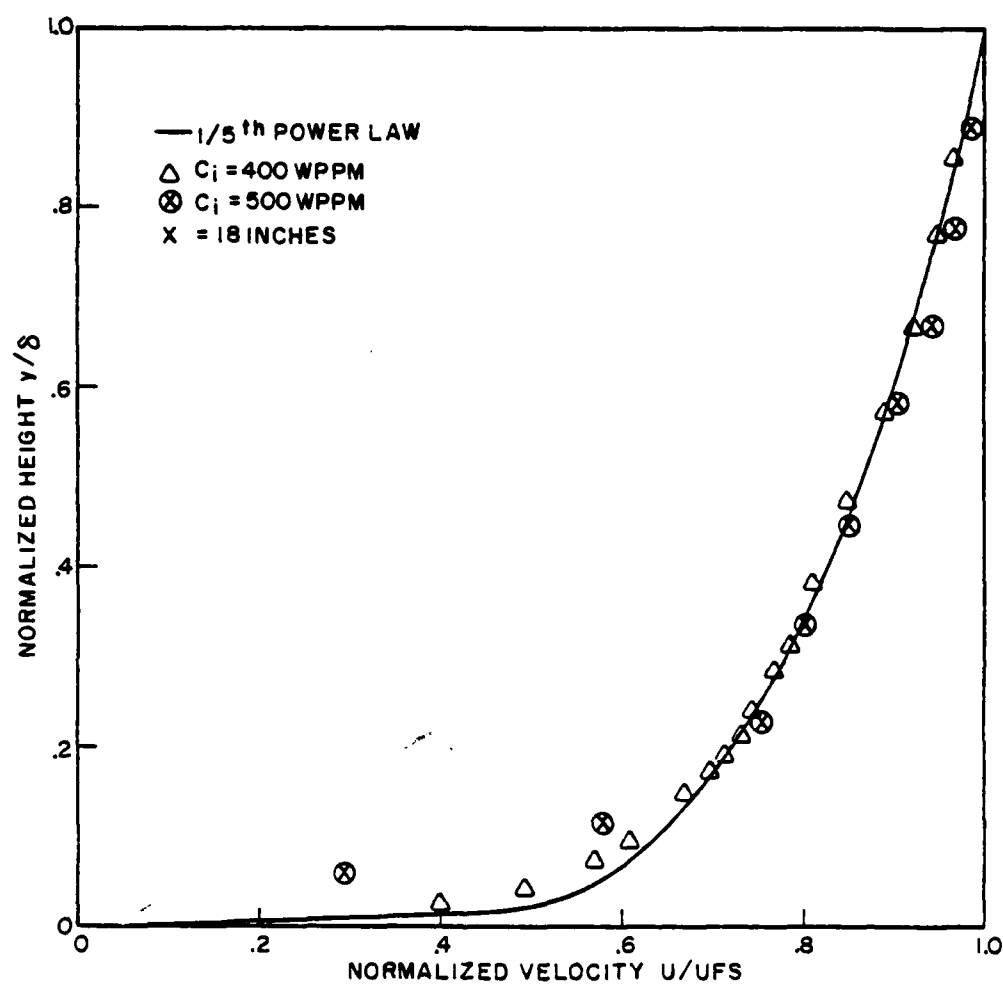


Figure 75. Comparison of non-dimensionalized velocity profiles at station $x = 18$ inches with theoretical $1/5^{\text{th}}$ power law profile

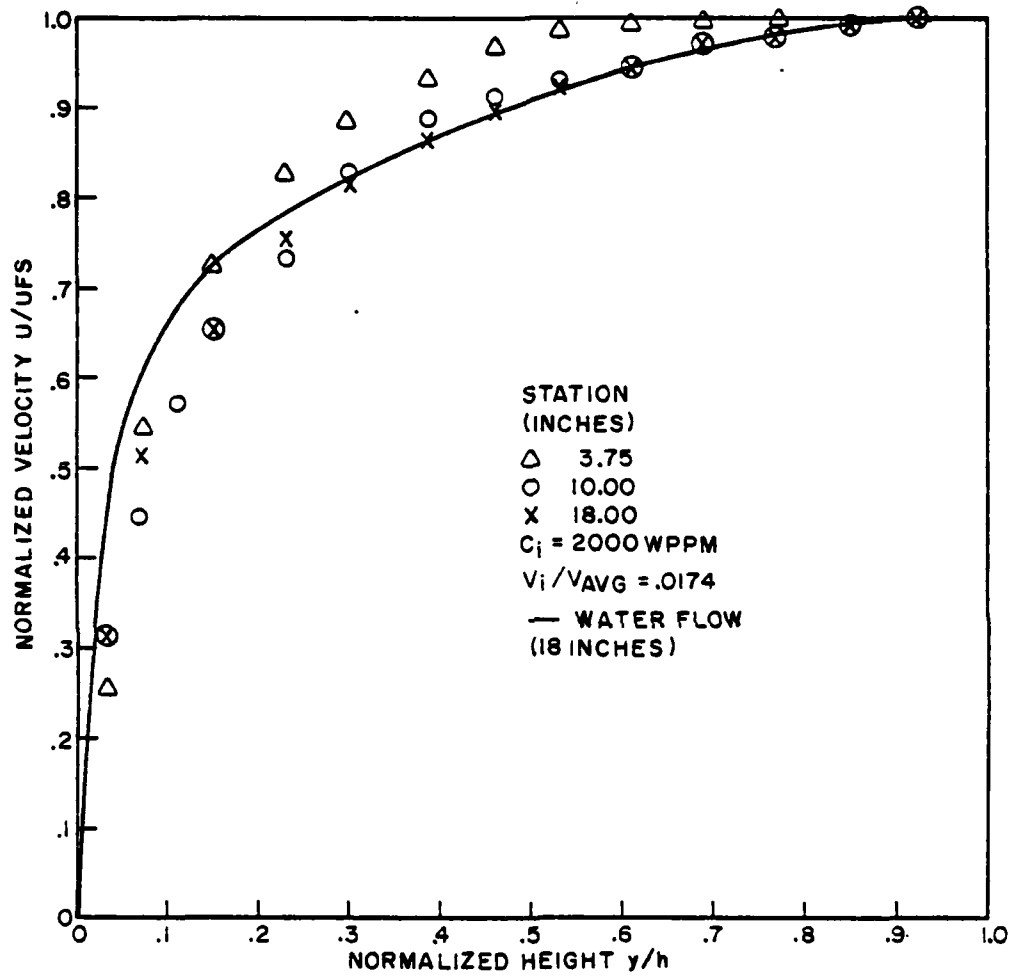


Figure 76. Developing velocity profiles for injected polymer concentration $C_i = 2000 \text{ WPPM}$

the narrow slot. The tendency of the thick 2000 WPPM injection concentration to stay together, coupled with the high injection velocity, contribute to the disturbance of the boundary layer.

Here again, at $x = 18$ inches, the polymer velocity profile compares well with the water turbulent velocity profile in the outer region of the boundary layer. Closer to the wall, the polymer velocity profile departs from the water profile and is less full. This anomaly in the near wall region may be due to a thickening of the laminar sublayer.

Figure 77 presents a comparison of the turbulence intensity distributions at $x = 18$ inches for the 2000 WPPM polymer injection case and a similar water case at the same injection velocity ratio ($(V_i/V_{avg} = .280)$ and slot width ($s = .005$ inches)). The characteristic lowering of the peak value of the turbulence intensity and shifting of its location away from the wall are also shown.

The lowering and redistribution of the primary turbulent activity into a broader band found in this study is supported by the work of Reischman (1973). However, due to experimental differences only qualitative comparisons can be made with the work of previous researchers. Rudd's data, typical of Logan's and Kumor and Sylvester's measurements, are presented in figure

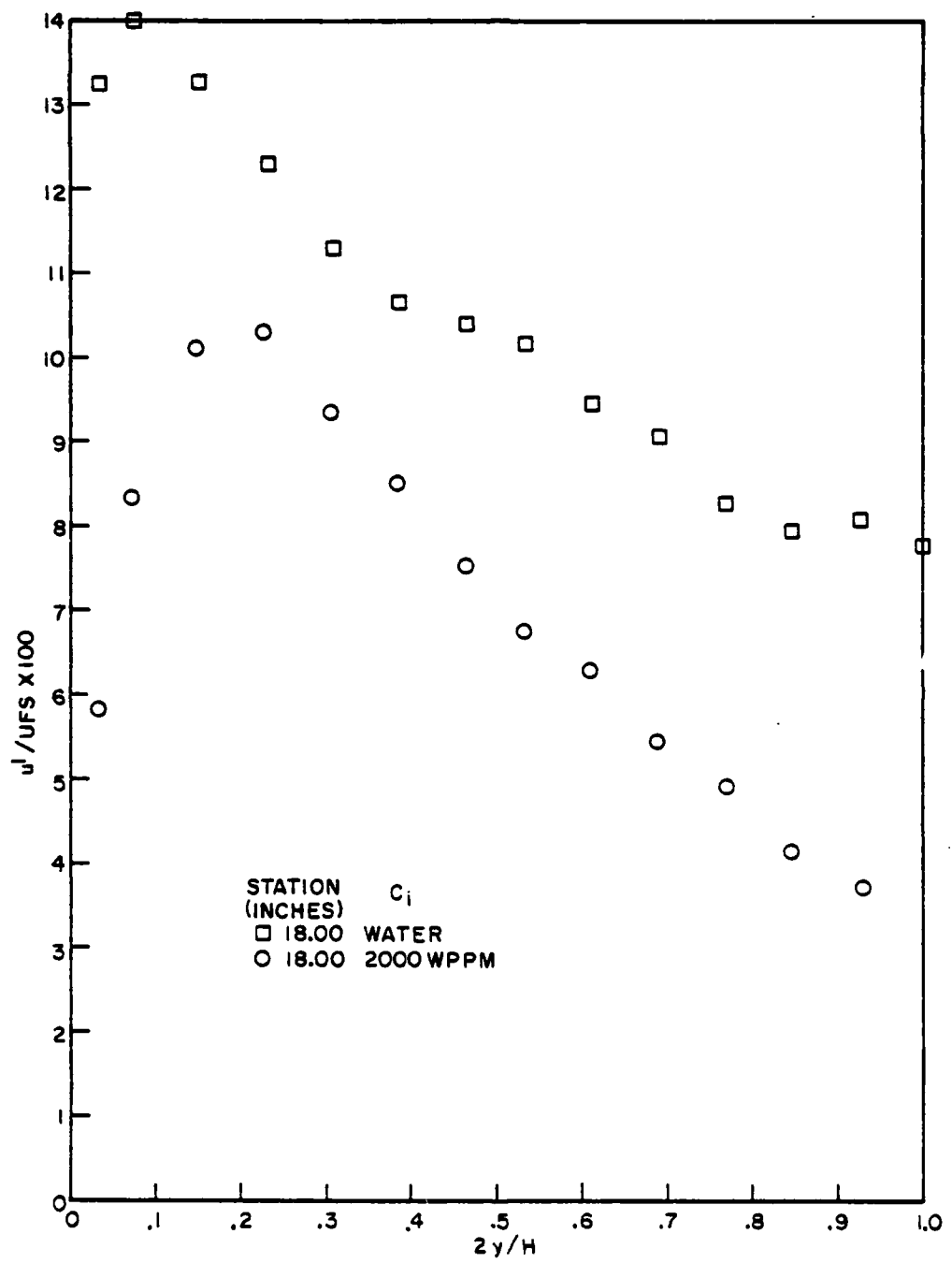


Figure 77. Turbulence intensity distribution for injected polymer concentration $C_1 = 2000$ WPPM

78 taken from Reischman (1973). However, Reischman used a rectangular channel while the others conducted their experiments in a square duct.

A controversy exists concerning the so-called "sublayer thickening" which is represented by the velocity profile remaining linear to a y^+ value of 15 to 20 instead of the solvent value of 8 to 9. There have been five investigations (including this one) that have made velocity measurements at $y^+ < 10$. Table 13 from Reischman (1973) indicates the extent of the linear curve and the lowest y^+ location at which velocity measurements were made in each prior investigation. Data from this investigation have also been included. Reischman alone concluded that the sublayer does not thicken based on the maximum value of y^+ for which $u^+ = y^+$. Previous results achieving larger values of y^+ which indicated a thicker sublayer were held in serious question due to experimental facilities and technique. This problem was discussed in section II which reviewed experimental facilities. It has been found that in the rectangular channel used in this research linear values of y^+ up to 15 have been achieved with Polyox WSR-301. Figures 79 through 83 present velocity profiles plotted in terms of inner variables and compared to the law of the wall. It is recommended that future investigations concentrate their efforts in the region of y^+ from 7 to 50 to provide additional data at the interface of the sublayer and the buffer region or elastic

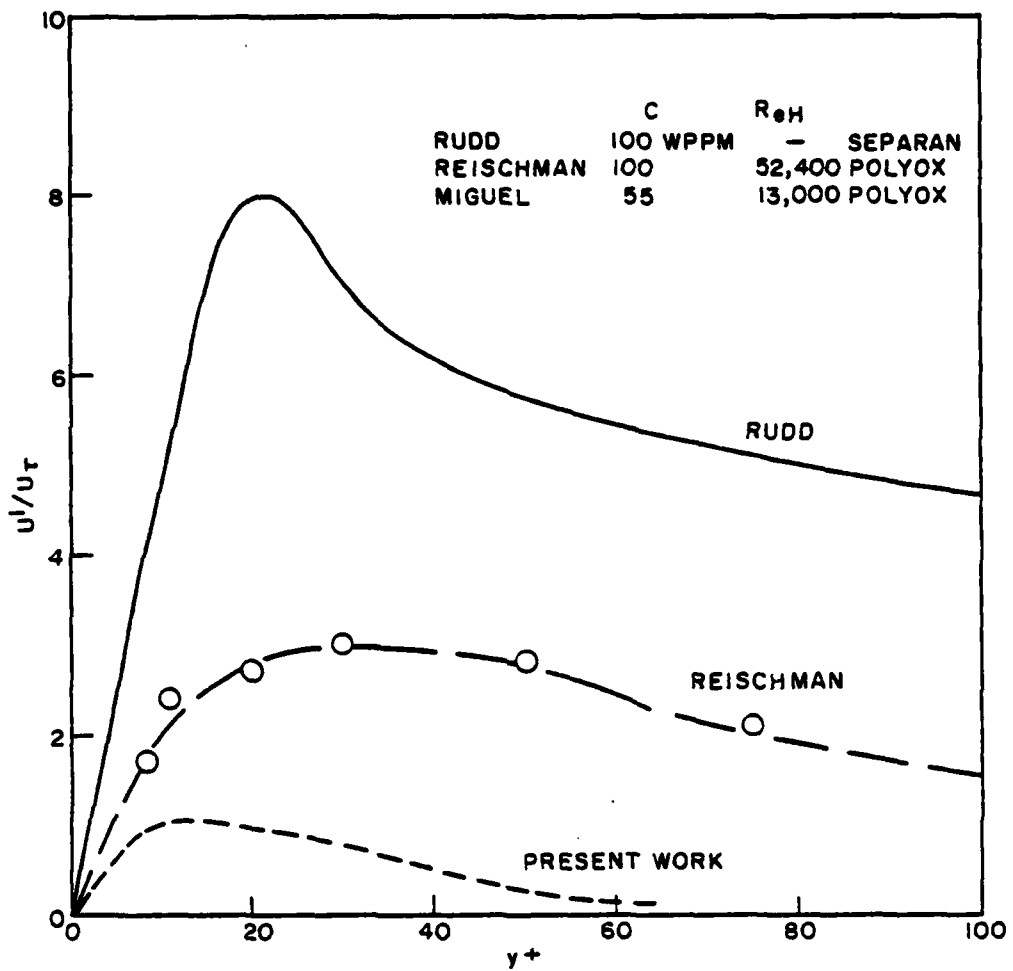


Figure 78. Turbulence intensity distribution

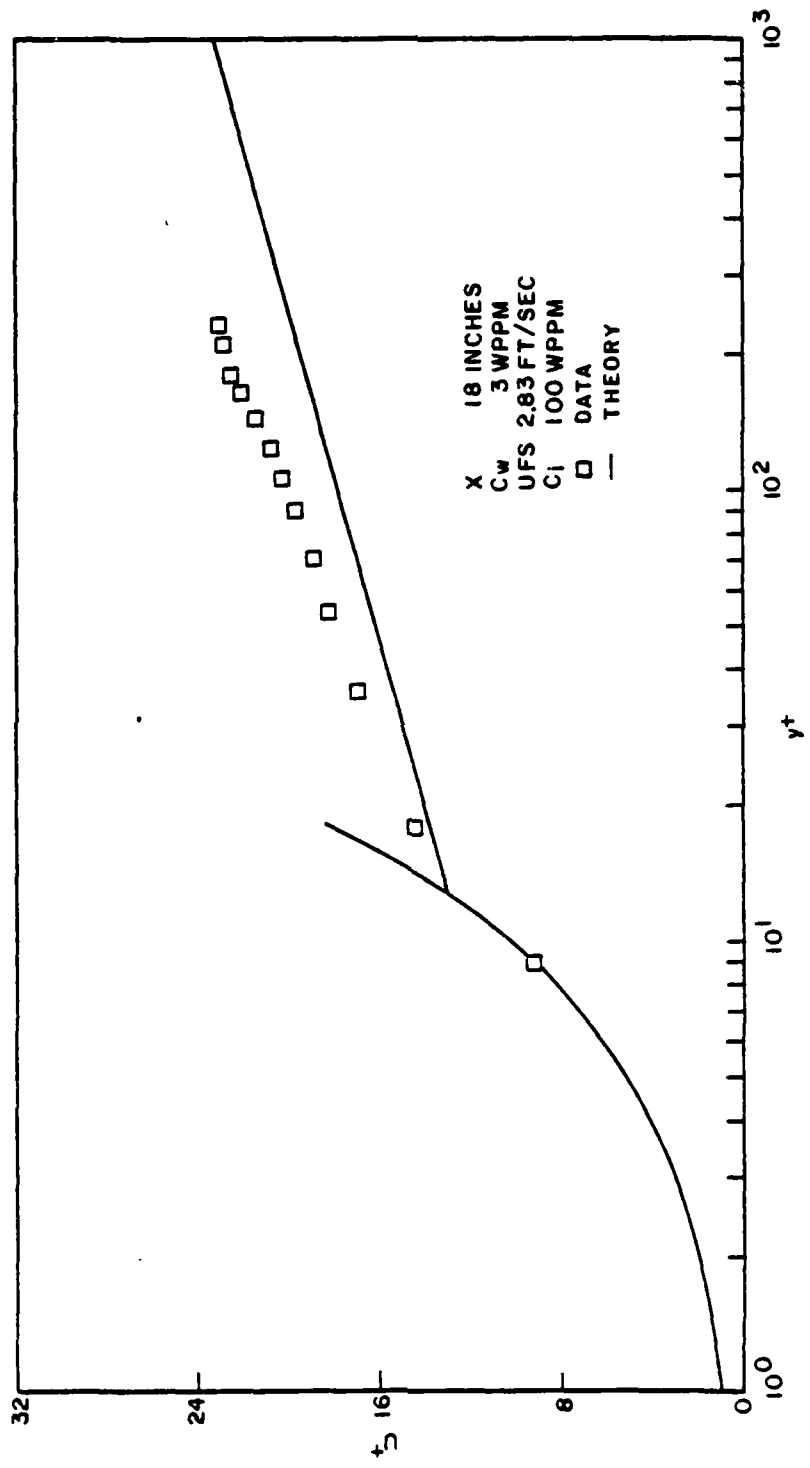


Figure 79. Comparison of the law of the wall with experimental data for injected polymer concentration $C_1 = 100$ WPPM

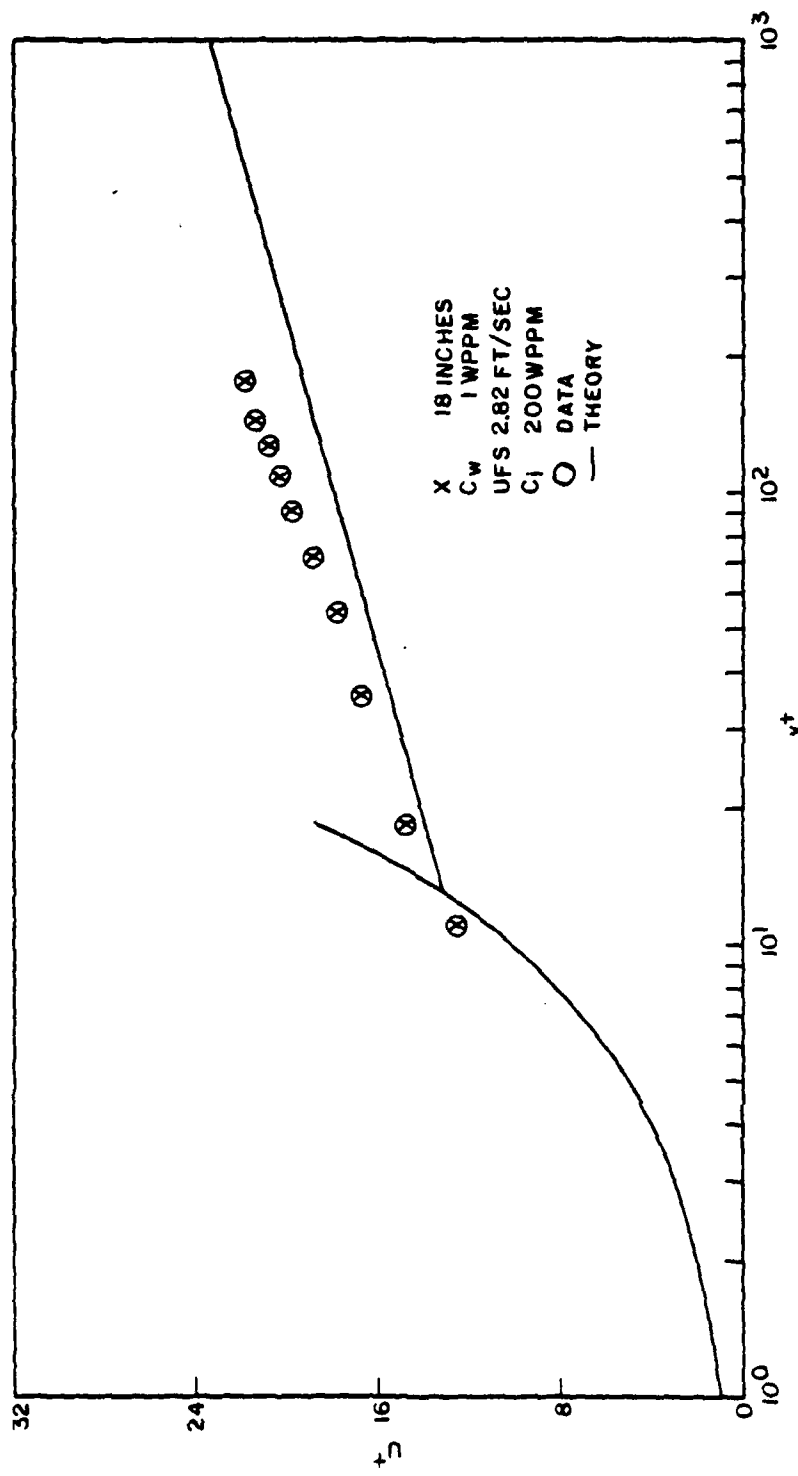


Figure 80. Comparison of the law of the wall with experimental data for injected polymer concentration $C_1 = 200$ WPPM

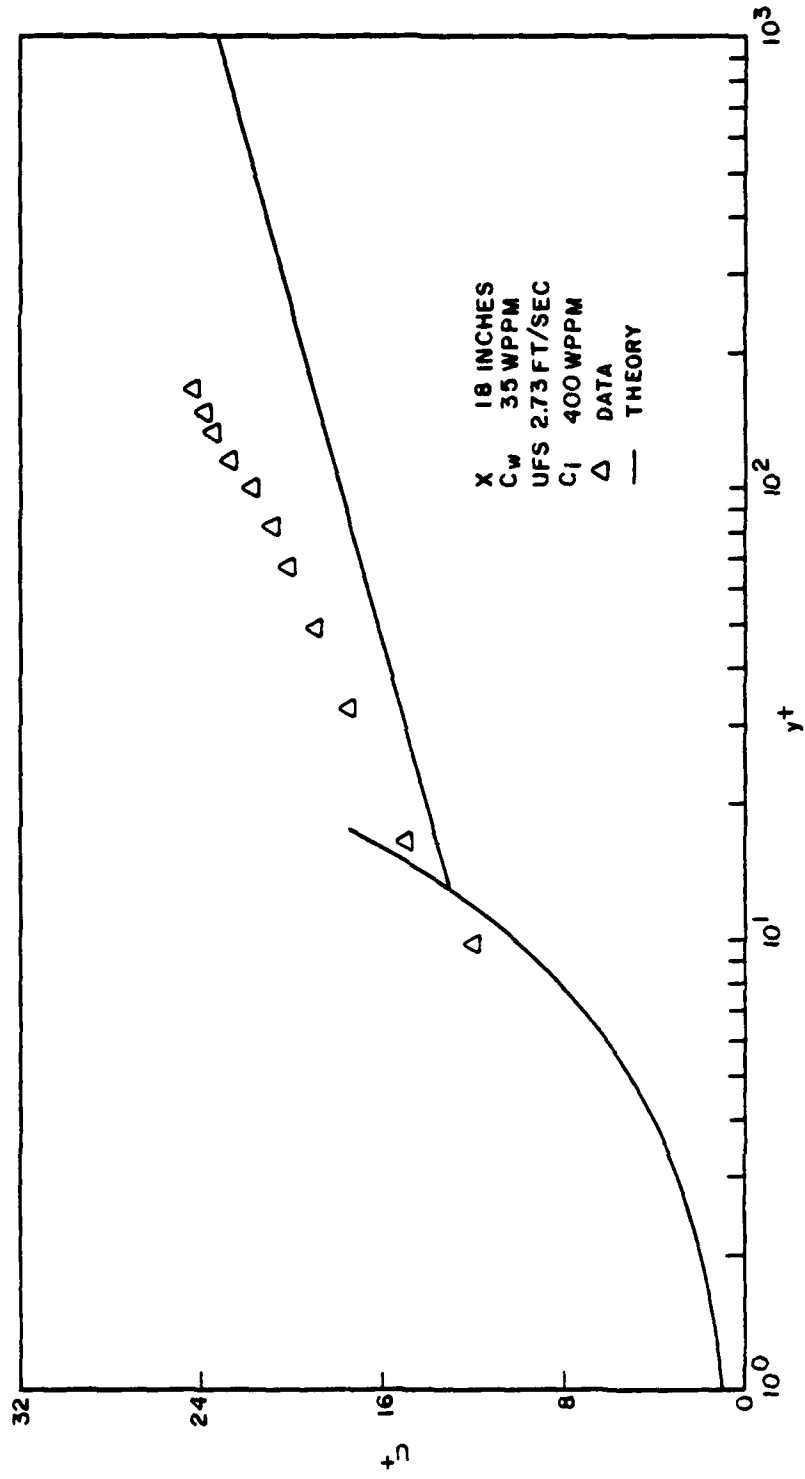


Figure 81. Comparison of the law of the wall with experimental data for injected polymer concentration $C_1 = 400$ WPPM

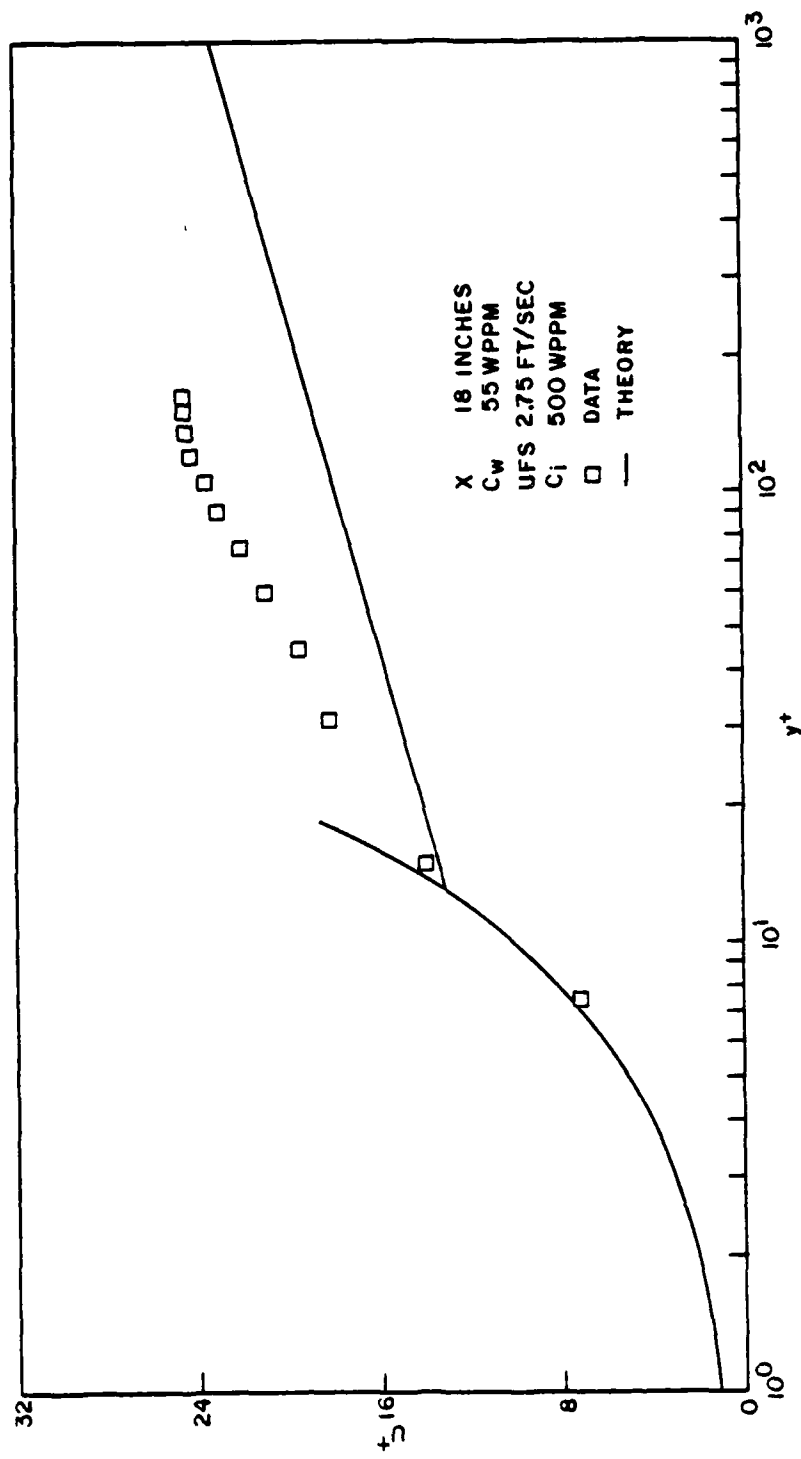


Figure 82. Comparison of the law of the wall with experimental data for injected polymer concentration $C_1 = 500$ WPPM

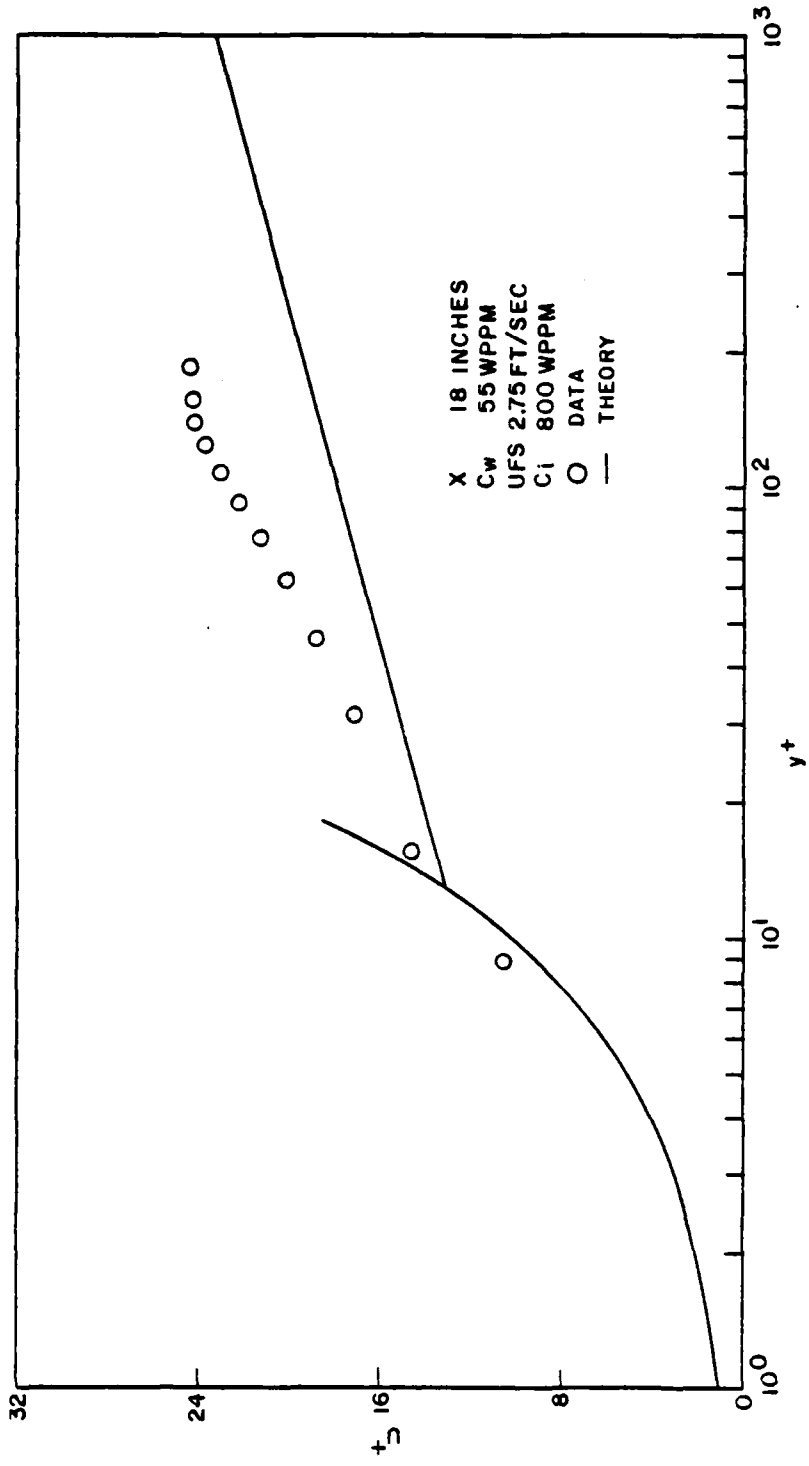


Figure 83. Comparison of the law of the wall with experimental data for injected polymer concentration $C_1 = 800$ WPPM

TABLE 13

COMPARISON OF NEAR WALL LASER ANEMOMETER
MEASUREMENTS IN DRAG REDUCING FLOWS

Author	Maximum y_+^+ for Which $u = y_+^+$	Lowest y_+^+ Measurements
Lazar	10	10
Rudd	19	8
Kumor & Sylvester	16	3
Reischman	9	3
Present Work	15	7

sublayer which joins the viscous sublayer and the elevated log region. Figure 84 indicates the large variation in the velocity profile in this region. Profiles in the outer region tend toward the turbulent while becoming more laminar close to the wall.

Comparison of Analytical Predictions With Experimental Results

Typical boundary layer growth patterns are presented in figure 85 through 88 for various concentrations injected at a constant rate of $V_i/V_{avg} = .0174$. There is excellent agreement between the experimental data and the theoretical profile predicted by the mathematical flow model utilizing the effective Reynolds number analogy. The gradual increase in the boundary layer height for the 500 WPPM injection case may be explained in terms of the water temperature and associated solvent viscosity. For this case, the water temperature was the coldest at 57° F. The resulting higher kinematic viscosity resulted in lower axial Reynolds number affecting transition and the growth of the boundary layer.

Skin friction calculations as a function of local polymer wall concentration were based on three techniques: (1) slope of the velocity profile, (2) Clauser technique, and (3) flow model. The results, indicating good agreement, are presented in tables 14 through 19. Skin friction computation from the slope of the velocity profile at the wall is relatively straightforward and will not be discussed in detail. This method is sensitive, however, to the value of the velocity near the wall. Velocity measurements must be made in the vicinity of the laminar sublayer and are susceptible to velocity gradient biasing in the laser measuring volume.

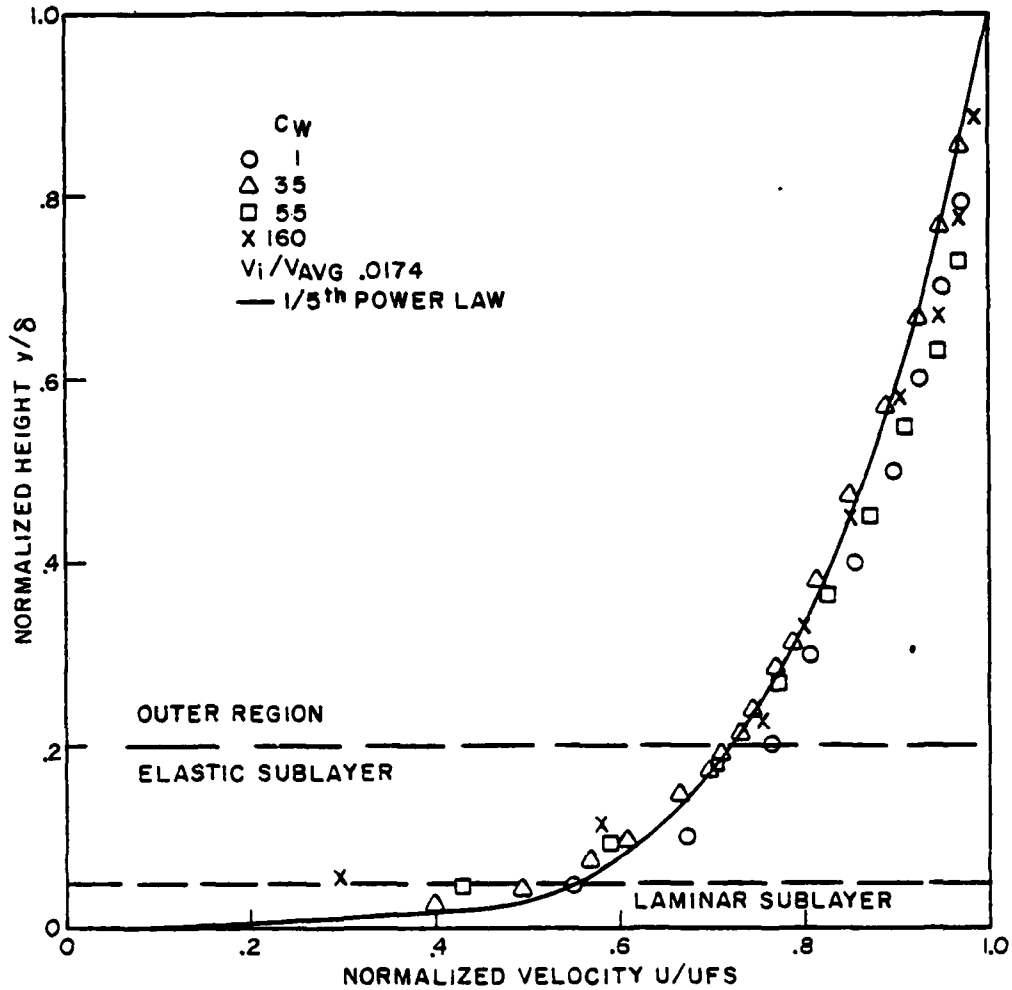


Figure 84. Comparison of normalized velocity profiles with 1/5th power law at station $x = 18$ inches

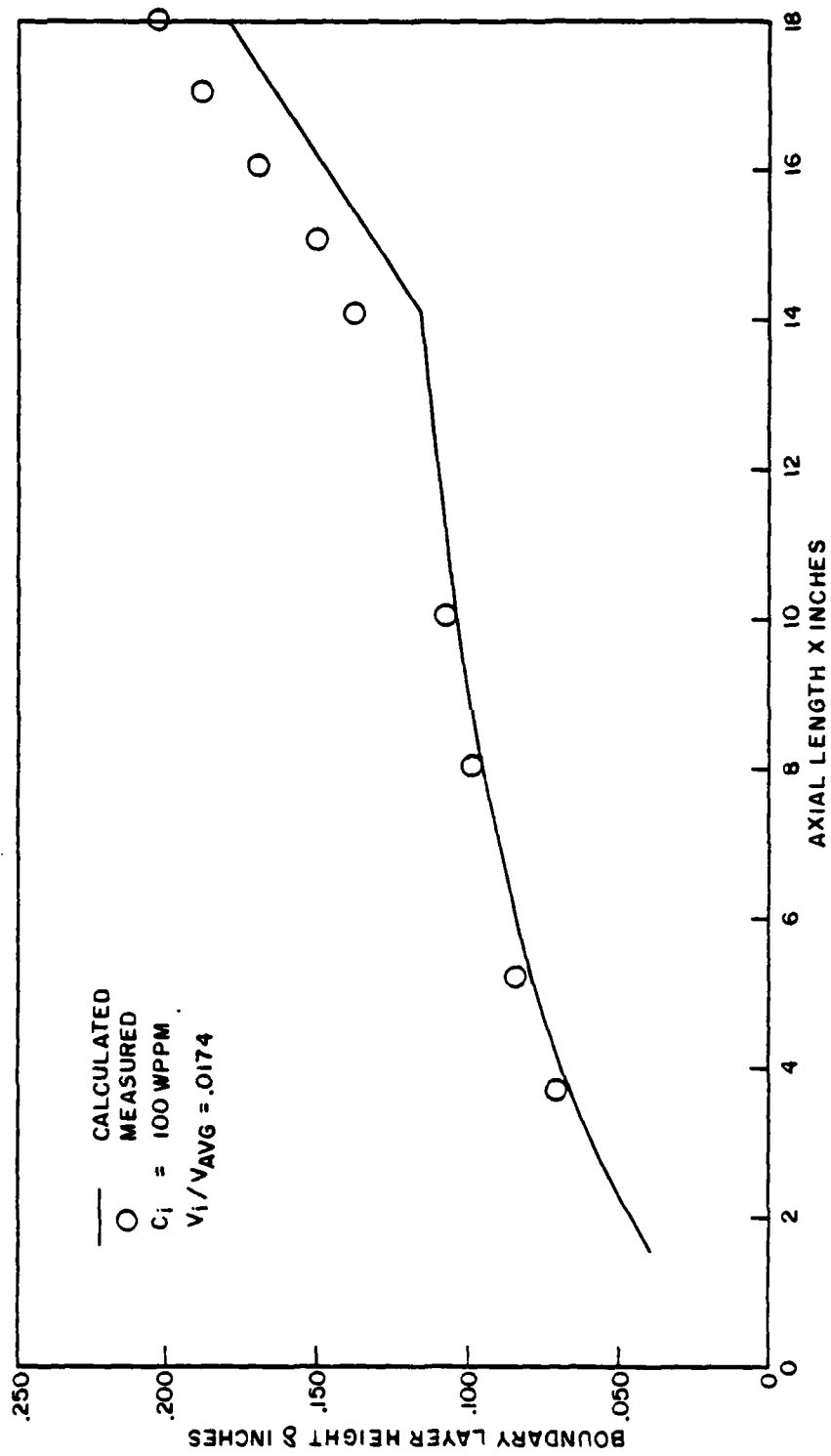


Figure 85. Comparison of experimental boundary layer growth with analytically predicted values for injected polymer concentration $C_1 = 100 \text{ WPPM}$

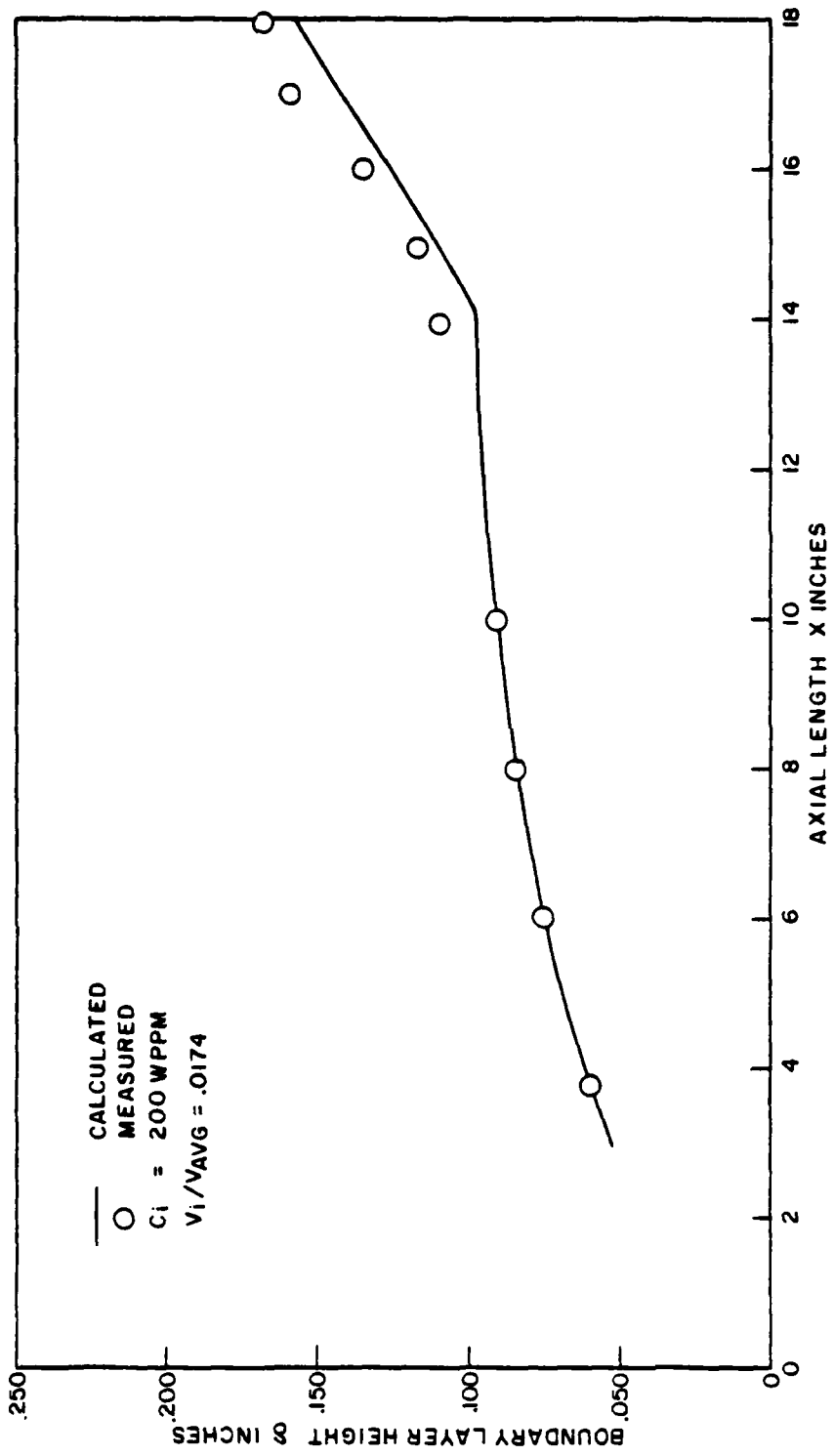


Figure 86. Comparison of experimental boundary layer growth with analytically predicted values for injected polymer concentration $C_1 = 200 \text{ WPPM}$

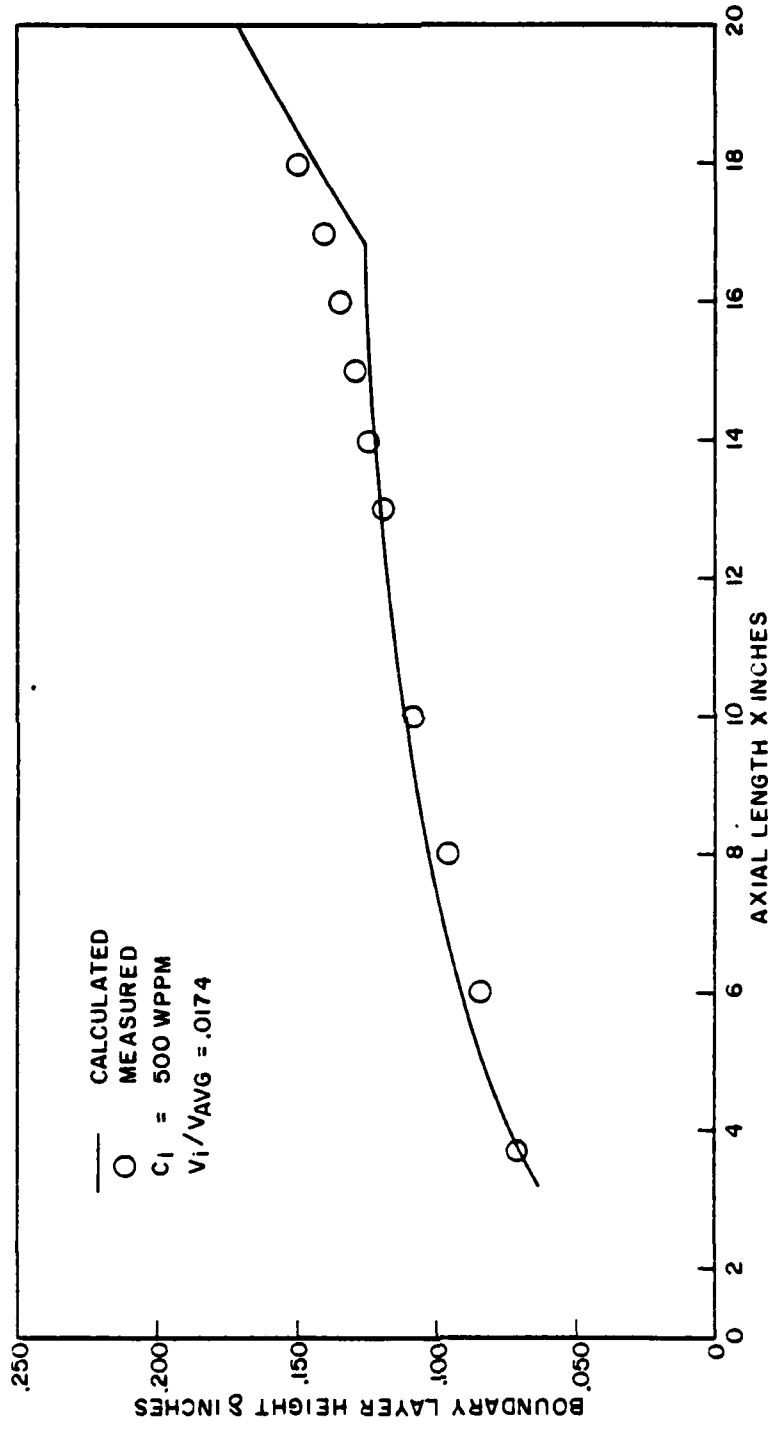


Figure 87. Comparison of experimental boundary layer growth with analytically predicted values for injected polymer concentration $C_1 = 500 \text{ WPPM}$

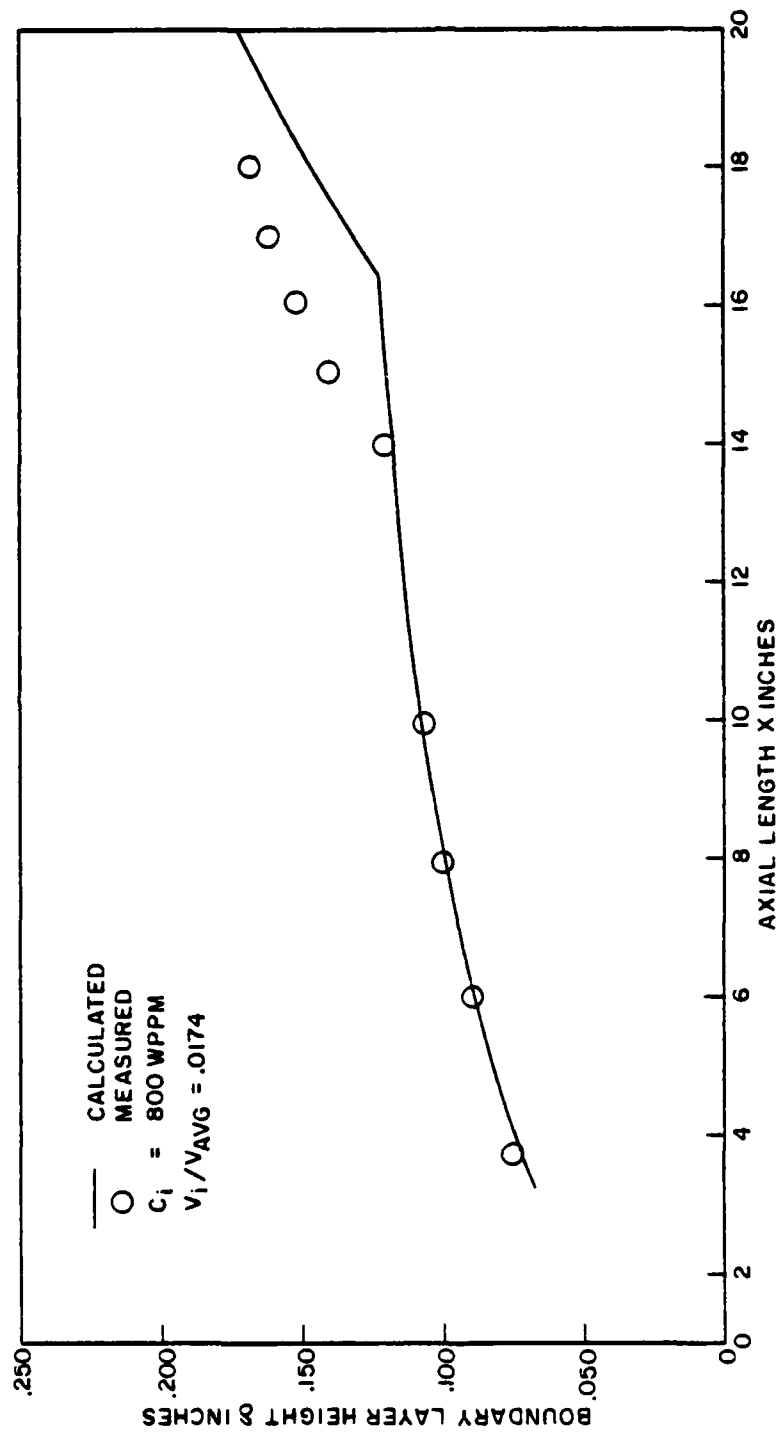


Figure 88. Comparison of experimental boundary layer growth with analytically predicted values for injected polymer concentration $C_i = 800 \text{ WPPM}$

TABLE 14

COMPARISON OF SKIN FRICTION COEFFICIENTS FOR WATER CASE

x(inches)	16	17	18
R_{ex}	354252	376793	402064
C_f (Model)	.00458	.00453	.00447
C_f (Clauser)	.00450	.00440	.00425
C_f (Velocity Profile)	.00497	.00478	.00461
C_w	0	0	0

TABLE 15

COMPARISON OF SKIN FRICTION COEFFICIENTS FOR
 $C_1 = 100$ WPPM OF POLYMER

x (inches)	16	17	18
R_{ex}	330,812	352,991	375,215
C_f (Model)	.00347	.00380	.00426
C_f (Clauser)	.00325	.00335	.00350
C_f (Velocity Profile)	.00405	.00406	.00424
C_w	10	4.6	3

TABLE 16

COMPARISON OF SKIN FRICTION COEFFICIENTS FOR
 $C_i = 200$ WPPM OF POLYMER

x (inches)	16	17	18
R_{ex}	345601	346215	365801
C_f (Model)	.00327	.00345	.00359
C_f (Clauser)	.00300	.00340	.0040
C_f (Velocity Profile)	.00356	.00395	.00420
C_w	15	5	1

TABLE 17

COMPARISON OF SKIN FRICTION COEFFICIENTS FOR
 $C_i = 400$ WPPM OF POLYMER

x (inches)	16	17	18
R_{ex}	322,476	343262	365,325
C_f (Model)	.00337	.00354	.00350
C_f (Clauser)	.00220*	.00265*	.00280*
C_f (Velocity Profile)	.00345	.00354	.00374
C_w	80	60	35

* Clauser skin friction values only valid for values of $C_i \leq 200$ WPPM polymer.

TABLE 18

COMPARISON OF SKIN FRICTION COEFFICIENTS FOR
 $C_i = 500$ WPPM OF POLYMER

x (inches)	16	17	18
R_{ex}	291,816	311,736	331,261
C_f (Model)	.00302	.00318	.00336
C_f (Clauser)	.00280*	.00290*	.00310*
C_f (Velocity Profile)	.00265	.00279	.00294
C_w	250	210	160

TABLE 19

COMPARISON OF SKIN FRICTION COEFFICIENT FOR
 $C_i = 800$ WPPM OF POLYMER

x (inches)	16	17	18
R_{ex}	301,196	321,545	341,454
C_f (Model)	.00314	.00332	.00351
C_f (Clauser)	.00250*	.00260*	.00290*
C_f (Velocity Profile)	.00307	.00332	.00347
C_w	110	80	55

* Clauser skin friction values only valid for values of $C_i \leq 200$ WPPM polymer.

Clauser Skin Friction Techniques

The Clauser technique, presented in 1954, and discussed by C.C. Lin (1959), bears some discussion. Utilizing the law of the wall and expressions (77), (78), and (79), Clauser obtained a family of curves of U/U_{FS} versus $\log (Re_y)$ with the skin friction, C_f , as a parameter, so that

$$U_\tau = \frac{U_e}{\sqrt{\frac{2}{C_f}}} \quad (77)$$

$$\frac{U}{U_\tau} = \frac{U}{U_e} \sqrt{\frac{2}{C_f}} \quad (78)$$

and

$$y^+ = \frac{U_\tau y}{v} = \frac{U_e y}{v} \sqrt{\frac{C_f}{2}} \quad (79)$$

This family of curves for water flow utilizing the value of $B = 7.2$ is shown in figure 89. Application of this figure to a determination of C_f merely requires the placing of a measured velocity distribution thereon and reading off the value of C_f , interpolating where necessary. Adapting this technique to polymer flows requires that the appropriate form of the law of the wall be used, resulting in

$$\frac{U}{U_{FS}} = \sqrt{\frac{C_f}{2}} \left[5.6 \left(\log \sqrt{\frac{C_f}{2}} + \log \frac{(U_{FS})y}{v} \right) + 7.2 + 2 \log \frac{U_{FS} \sqrt{\frac{C_f}{2}}}{U_\tau^*} \right] \quad (80)$$

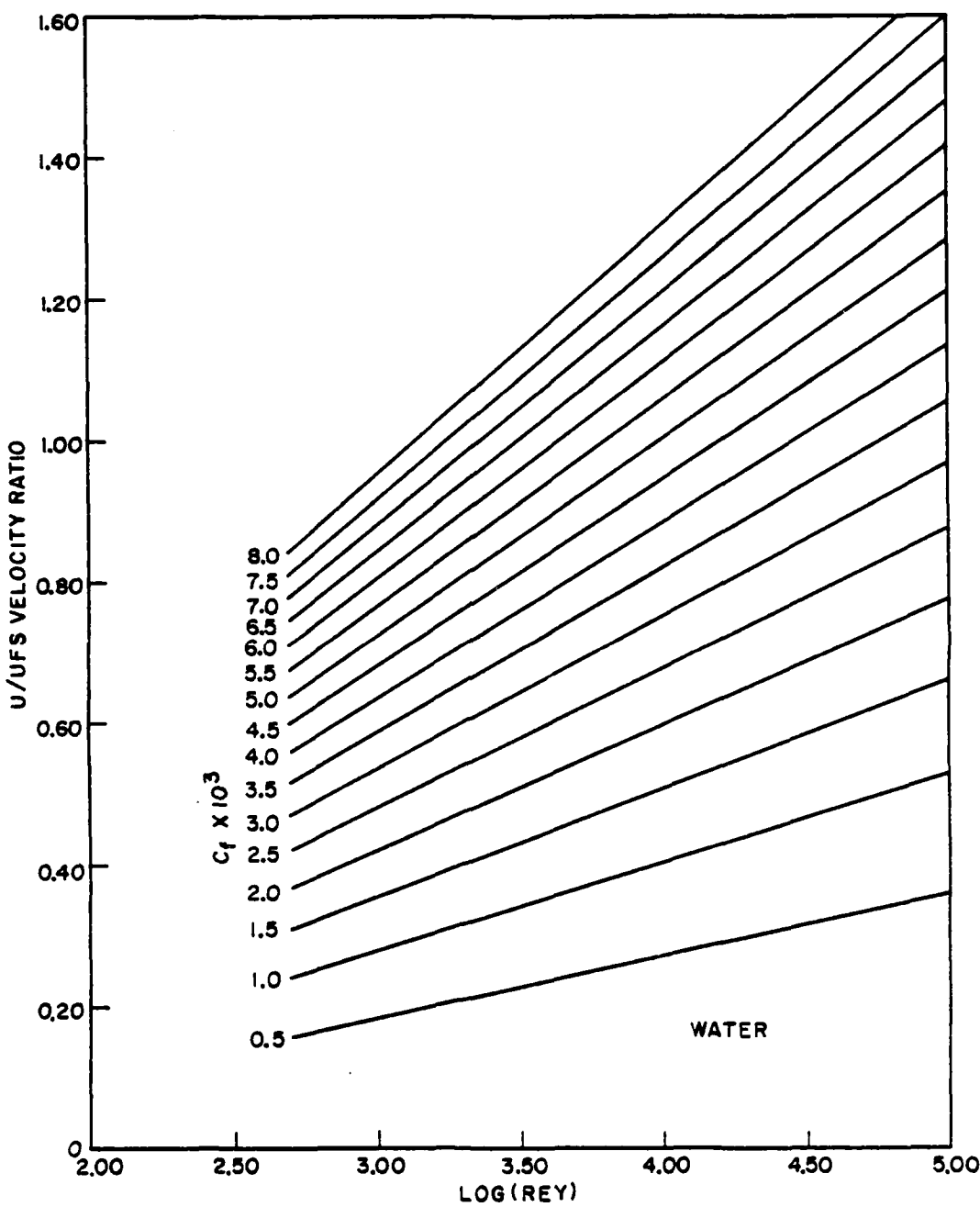


Figure 89. Plot of Clauser family of curves for water flow

where $z = \alpha C_w^{\gamma}$. (81)

Figure 90 demonstrates the application of this technique to polymer flows. A new family of curves must be obtained for each polymer concentration considered.

Designed for fully-developed turbulent flow, application here has been attempted for developing flow. Additionally the ΔB shift for polymer flow is assumed to be of the form given by equation (81). For this reason, the skin friction values are presented for comparison purposes only. Additional experimentation with fully-turbulent flows over a range of polymer concentrations should be performed to further develop this technique since the present data indicate much promise.

Figures 91 through 96 present variations in the value of the local skin friction along the plate for various injection polymer concentrations as predicted by the flow model. Also plotted on these figures are values of skin friction determined from data taken at the plate. The comparative agreement is excellent. The lower values of C_f determined by the modified Clauser technique may be attributed to the developing aspect of the velocity profiles and their near-wall anomaly due to the polymer. The flow model prediction compares very well with the velocity profile data in all cases. During transition, a linear intermittency function

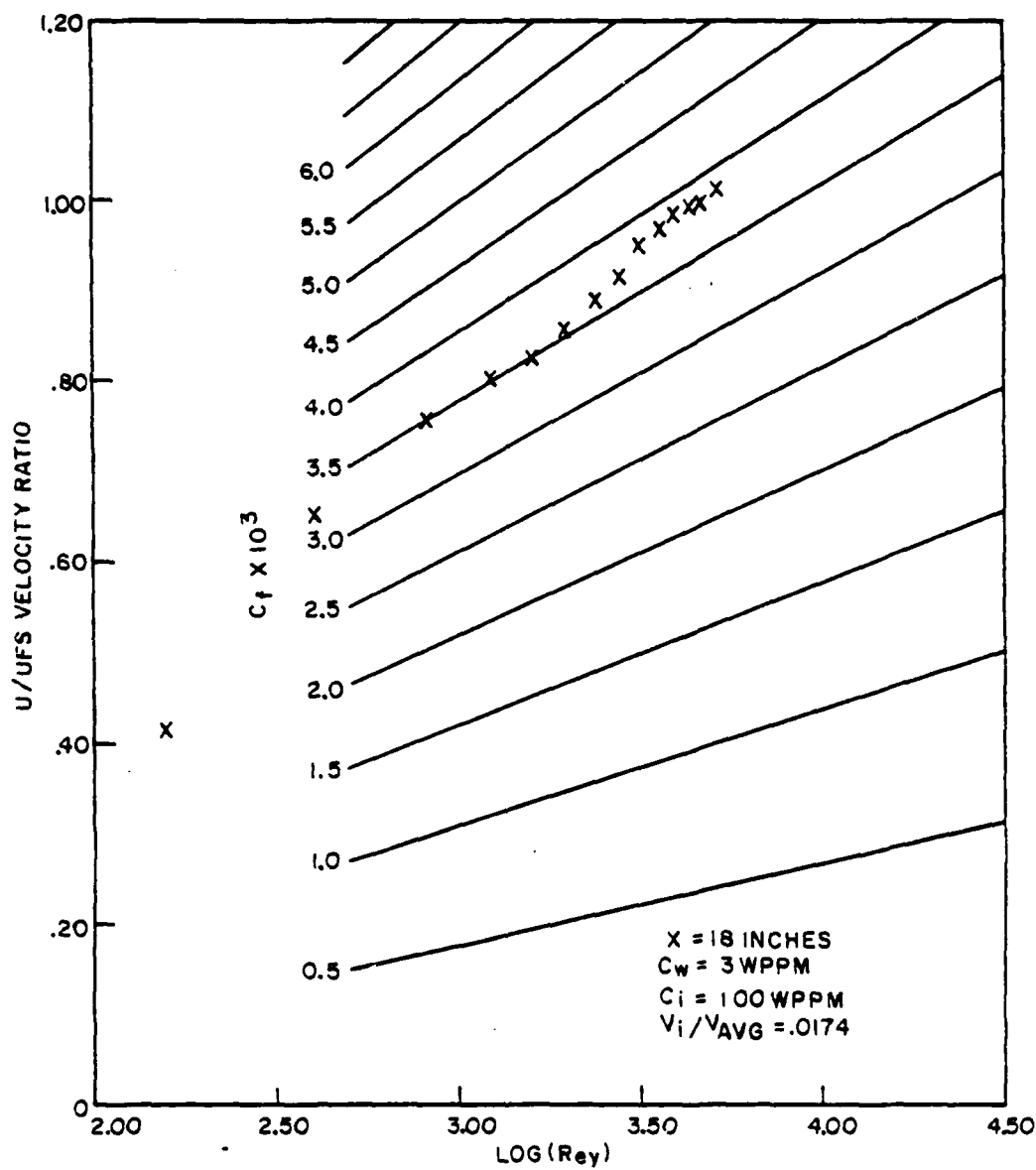


Figure 90. Plot of Clauser family of curves for injected polymer concentration $C_i = 100$ WPPM

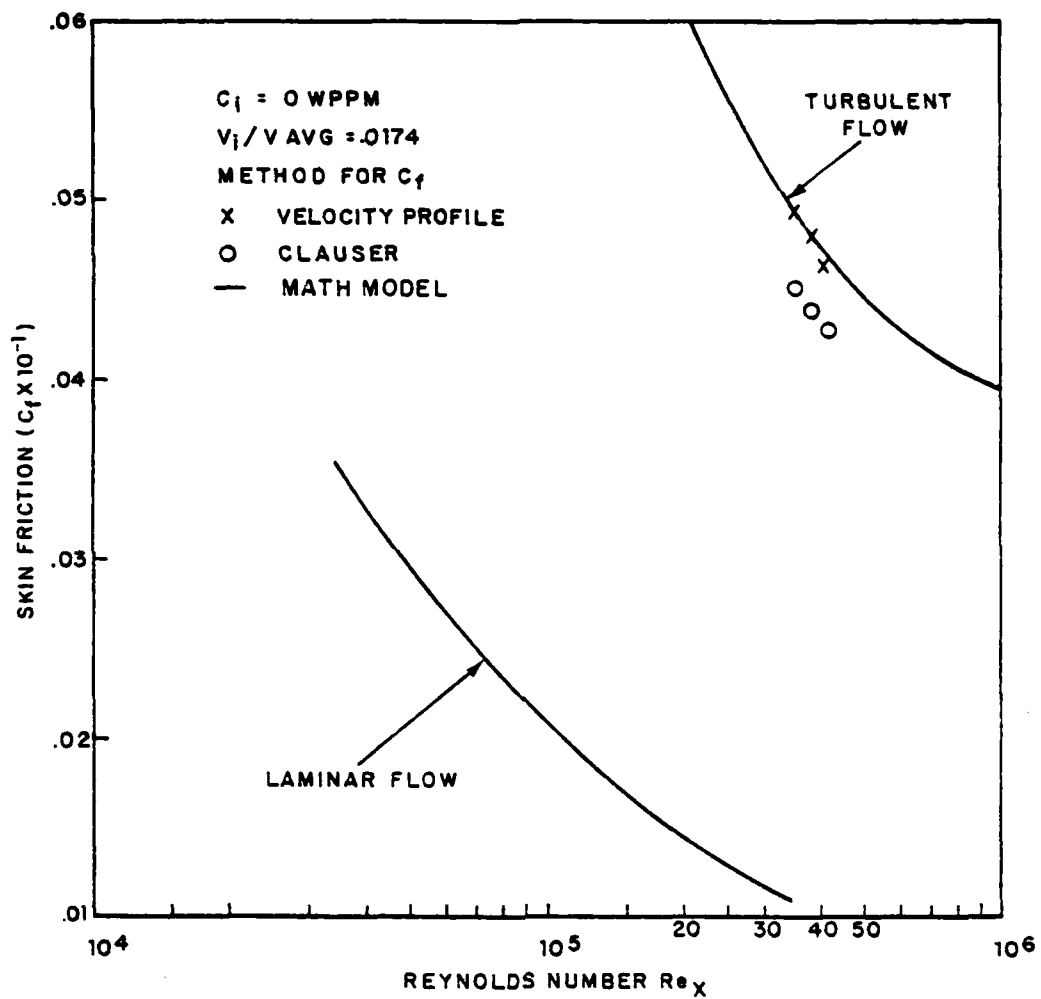


Figure 91. Variation of local skin friction along the plate compared with experimental results for water flow

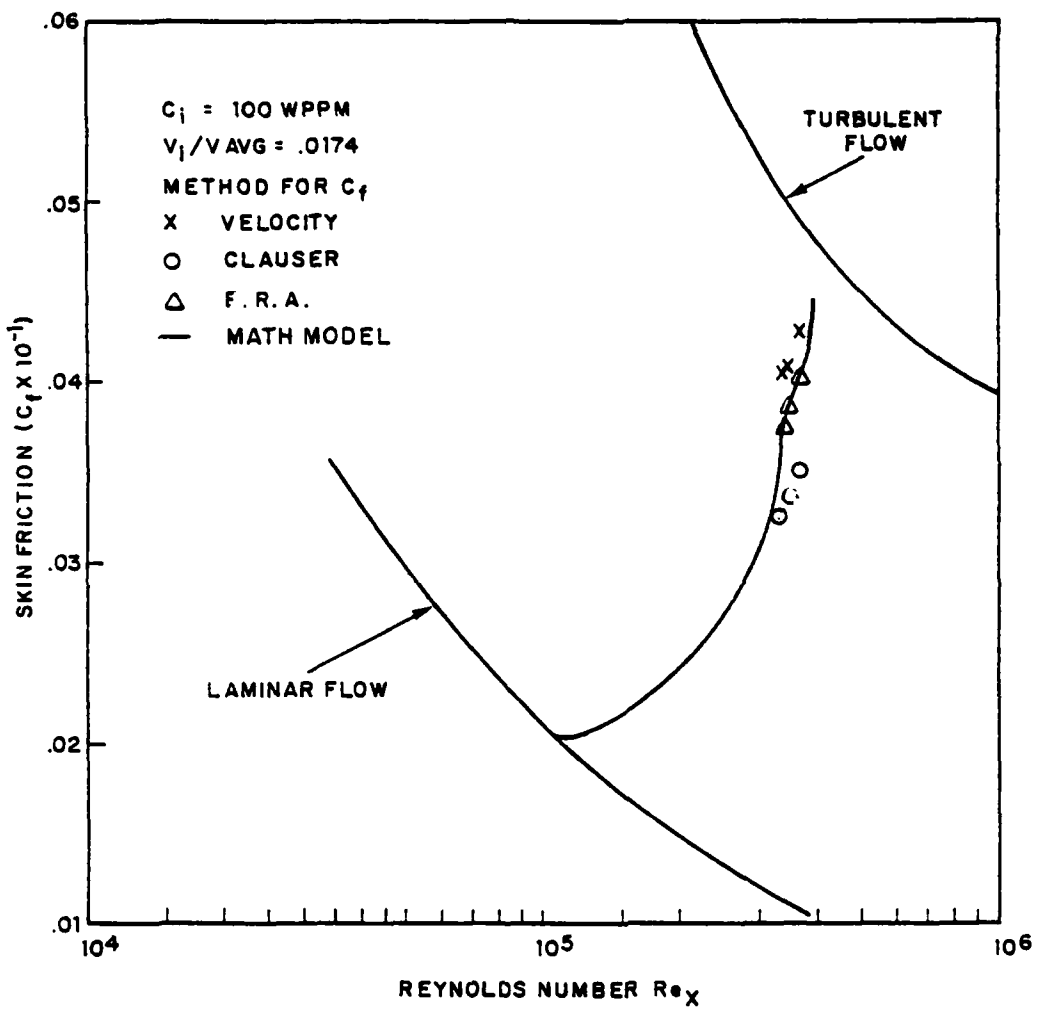


Figure 92. Variation of local skin friction along the plate compared with experimental results for injected polymer concentration $C_1 = 100$ WPPM

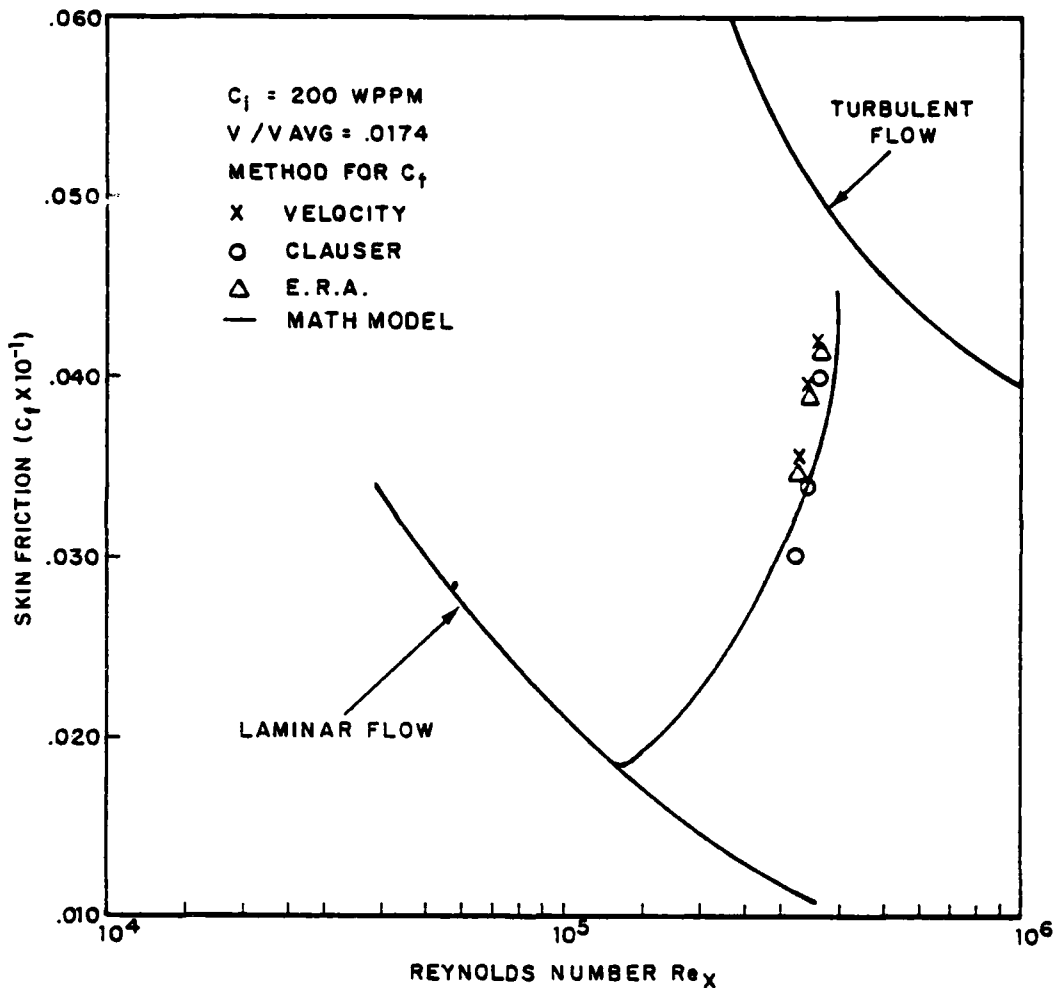


Figure 93. Variation of local skin friction along the plate compared with experimental results for injected polymer concentration $C_i = 200$ WPPM

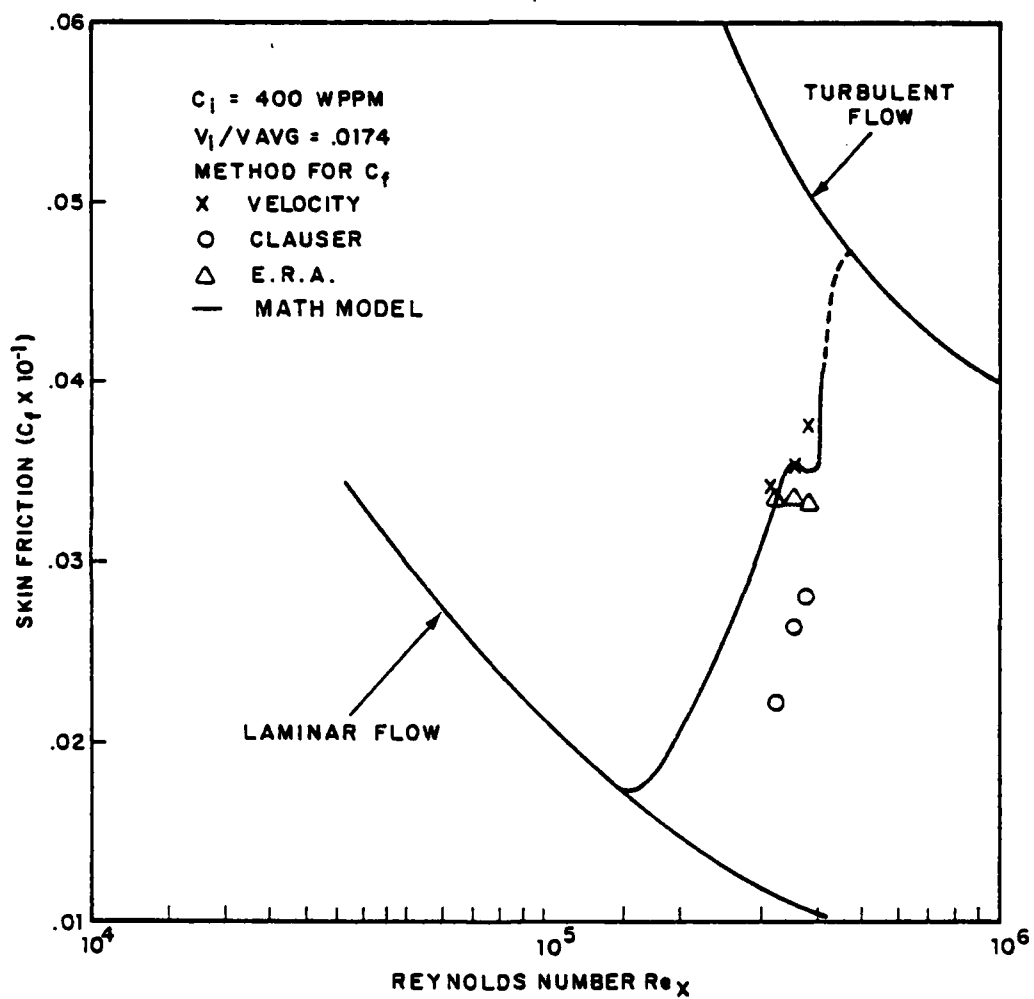


Figure 94. Variation of local skin friction along the plate compared with experimental results for injected polymer concentration $C_i = 400$ WPPM

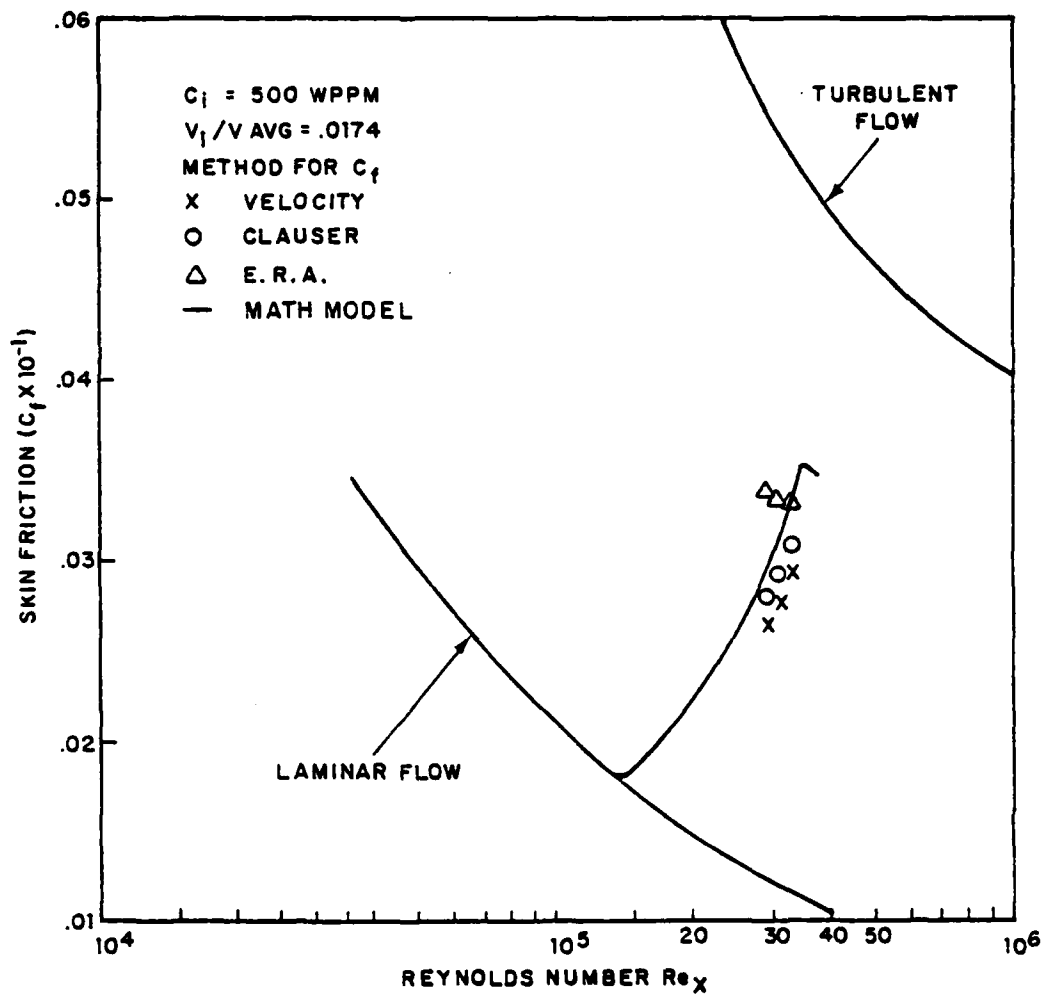


Figure 95. Variation local skin friction along the plate compared with experimental results for injected polymer concentration $C_i = 500$ WPPM

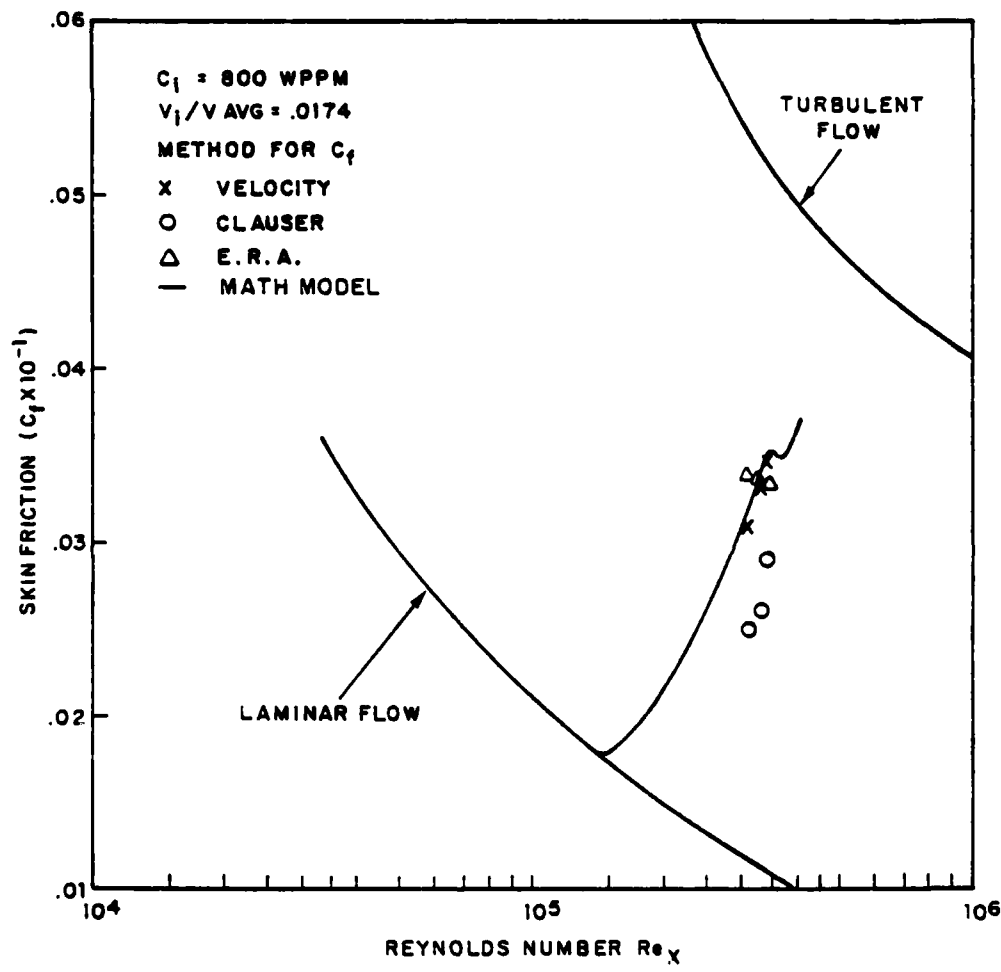


Figure 96. Variation of local skin friction along the plate compared with experimental results for injected polymer concentration $C_1 = 800$ WPPM

is assumed with completion of transition to turbulent flow at $Re_x = 350,000$. The physical limitation of the test setup and the limited length of the plate precluded the taking of additional data at larger length Reynolds numbers. More research in this region with fully-developed turbulent flow is recommended to complete the development of the flow model.

The effective Reynolds number analogy values of the local skin friction agree very well with the values predicted by the analytical model. Figure 97, plotted for the conditions of the 200 WPPM injection case, typically represents the other injection conditions. Curves of C_f versus Re_x are plotted with C as a parameter. To obtain a value for the skin friction, the plot should be entered with the value of Re_x while the value of C_f is taken off at the appropriate value of the polymer wall concentration. Utilization of this technique to aid in the solution of equation (63) has demonstrated its suitability for application to polymer flows.

Polymer Diffusion Patterns

Typical polymer wall concentration distributions normalized with injection concentration and plotted against normalized axial length are shown in figures 98 through 99. The polymer flows injected into the boundary layer showed suppressed diffusion characteristics in the transition region $0.3 < X/L < 0.7$.

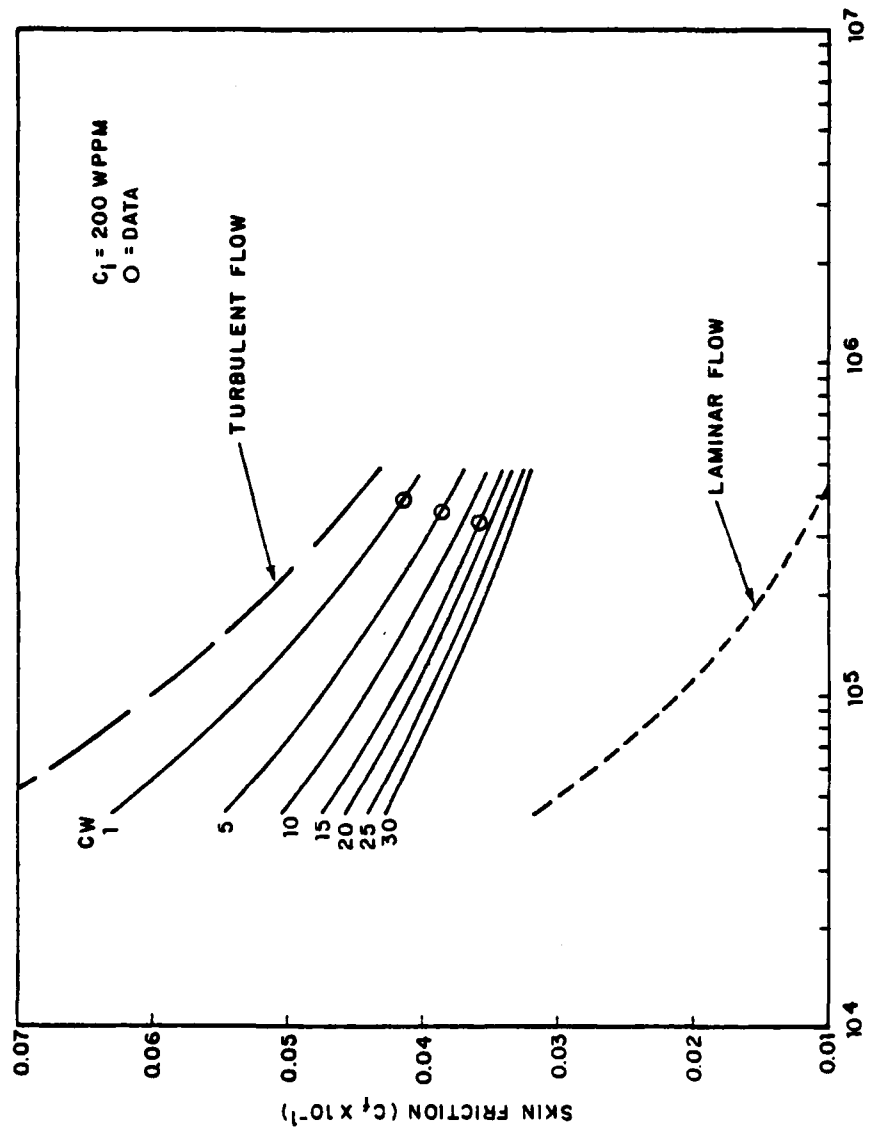


Figure 97. Effective Reynolds number analogy values of local skin friction versus Reynolds number for injected polymer concentration $C_1 = 200$ WPPM

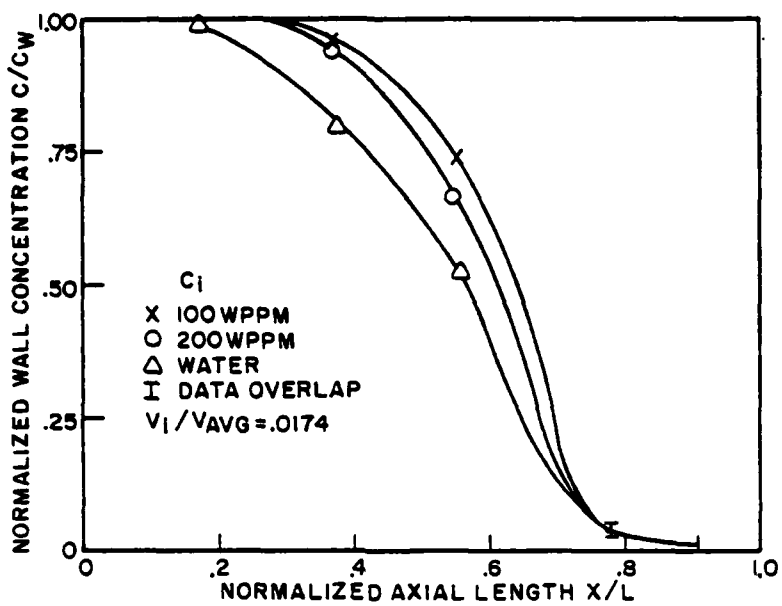


Figure 98. Normalized polymer wall concentration distribution

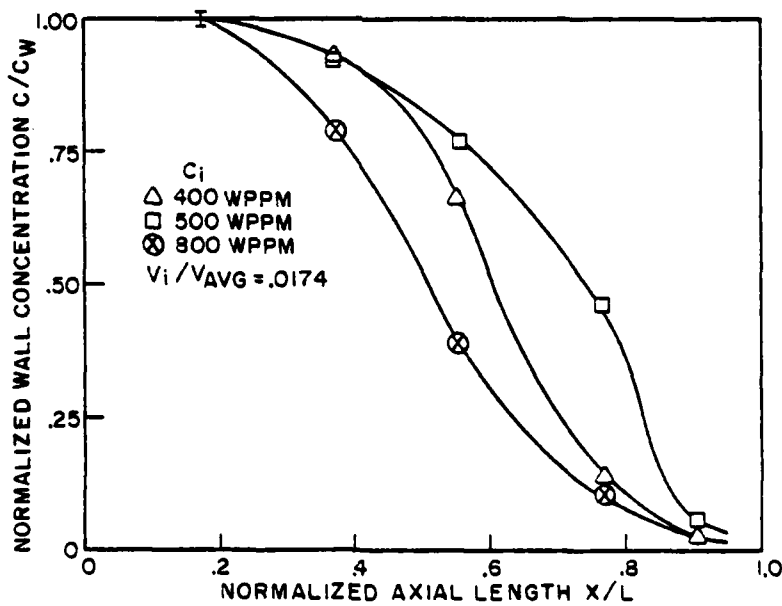


Figure 99. Normalized polymer wall concentration distribution

Higher concentrations of injected polymer resulted in higher plate trailing edge concentrations. The 500 WPPM injection case showed the highest wall concentrations for the largest distance along the plate. It is believed that this distribution was influenced by a Reynolds number effect due to the lower water temperature of this run. The lower temperature produced a higher value of the kinematic viscosity. The resulting lower Reynolds number had an additional delaying effect on transition.

The polymer appears to affect transition by delaying its onset, dampening the turbulent transport of material away from the wall region, and stretching out the transition region.

Figures 100 and 101 show the effect of polymers on transition. The maximum velocity difference between laminar and turbulent velocity profiles occurred at a height of $y = .020$ inch above the plate. Axial velocity distribution profiles at this height along the plate show the characteristic increase in velocity at transition to turbulent flow for the water injection case. Injection of polymer showed no such characteristic increase in velocity indicating delayed transition.

Diffusion patterns normal to the plate were taken at five stations: 1 = 3.75 inches, 2 = 8.5 inches, 3 = 12.5 inches, 4 = 16.5 inches and 5 = 20.5 inches. No concentration measurements were

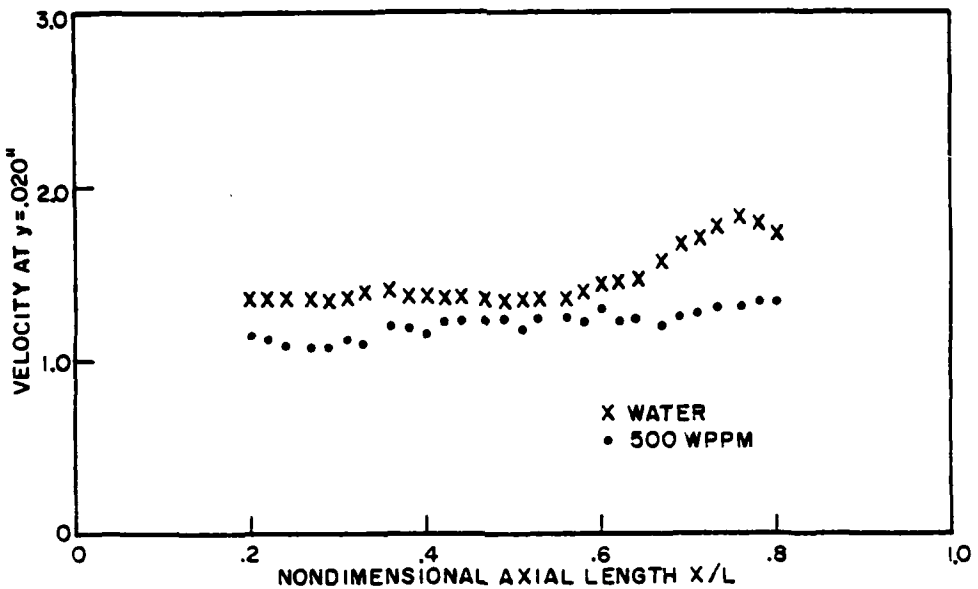


Figure 100. Axial velocity profile at $y = .020$ inches for injected polymer concentration $C_1 = 500$ WPPM compared with water

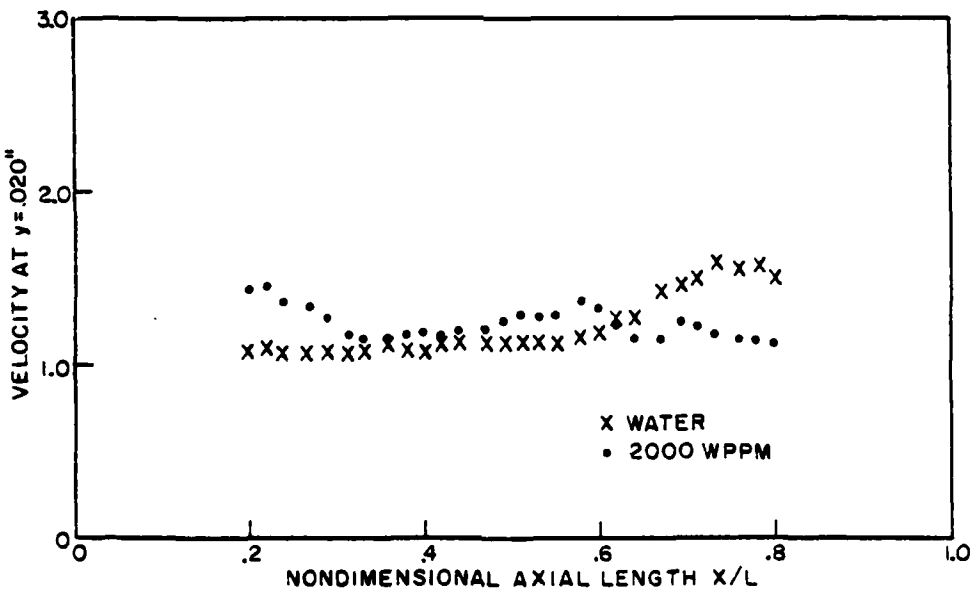


Figure 101. Axial velocity profile at $y = .020$ inches for injected polymer concentration $C_1 = 2000$ WPPM compared with water

generally obtainable above $y = .010$ inch to $.015$ inch above the plate for stations 1 and 2, indicating very little to no diffusion in these laminar regions. Figures 102 through 107, therefore, compare the three concentration measurement stations along the plate at $x = 12.5$, 16.5 and 20.5 inches. The injected polymer concentrations of $C_1 = 100$ and 200 WPPM indicate a continuous gradual decay in concentration at stations 3 and 4, with relatively high concentration levels in the near wall region. The water injected case at these stations shows rapid concentration decay in the near wall region. At station 4, the diffusion pattern above $y = .015$ inch takes on a linear decay characteristic found in the turbulent flow outer region at station 5. The concentration distributions normal to the wall at station 5 for polymer injection of $C_1 = 100$ and 200 WPPM are similar to the water case at the same station. This is due to the very low wall concentration at this station.

The reduced diffusion characteristics of polymer flows may be seen by plotting the growth of the diffusion boundary layer indicated by a characteristic height, λ_c . This characteristic height, λ_c , is defined as that height at which the concentration is equal to one-half of the wall concentration. Increasing concentration of injected polymer reveals a reduced diffusion characteristic away from the wall and a thicker layer of higher

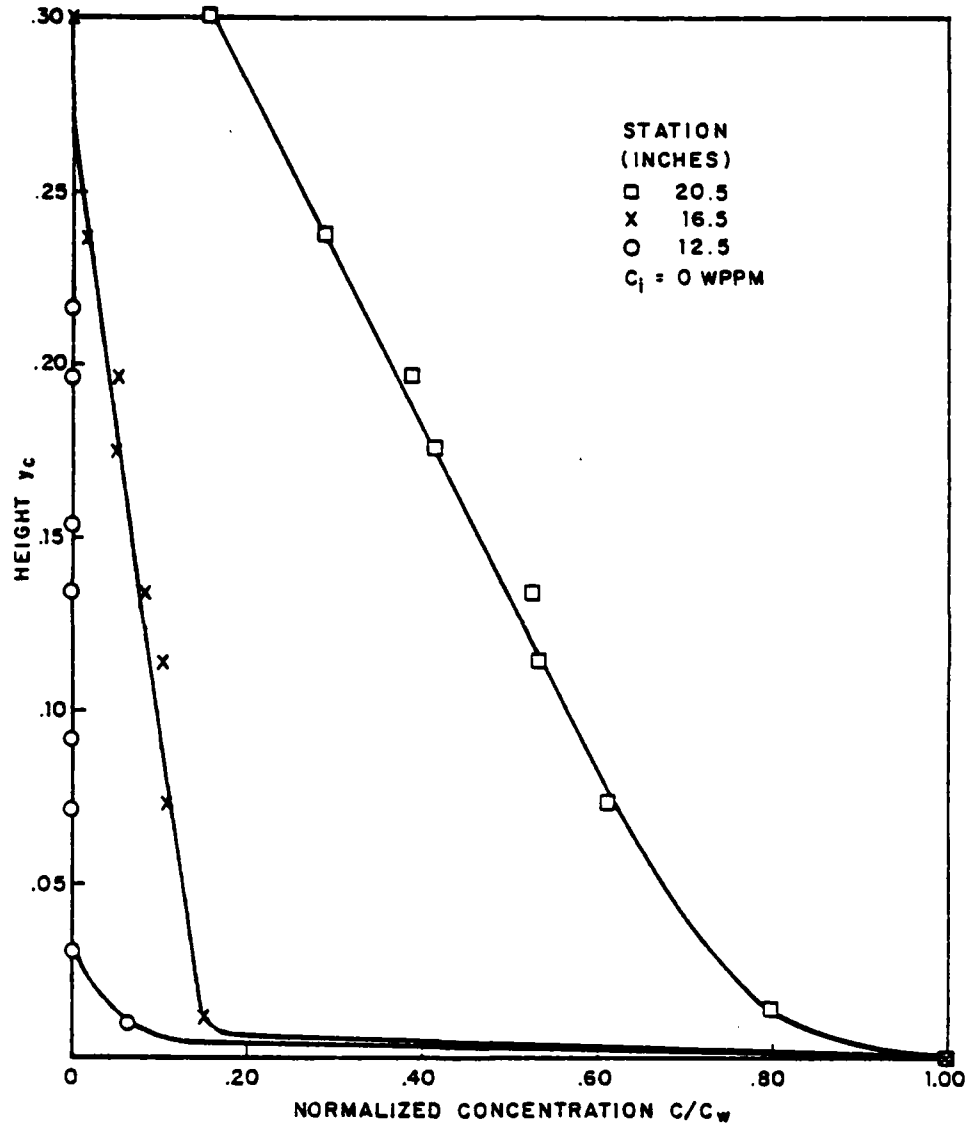


Figure 102. Normalized water diffusion patterns

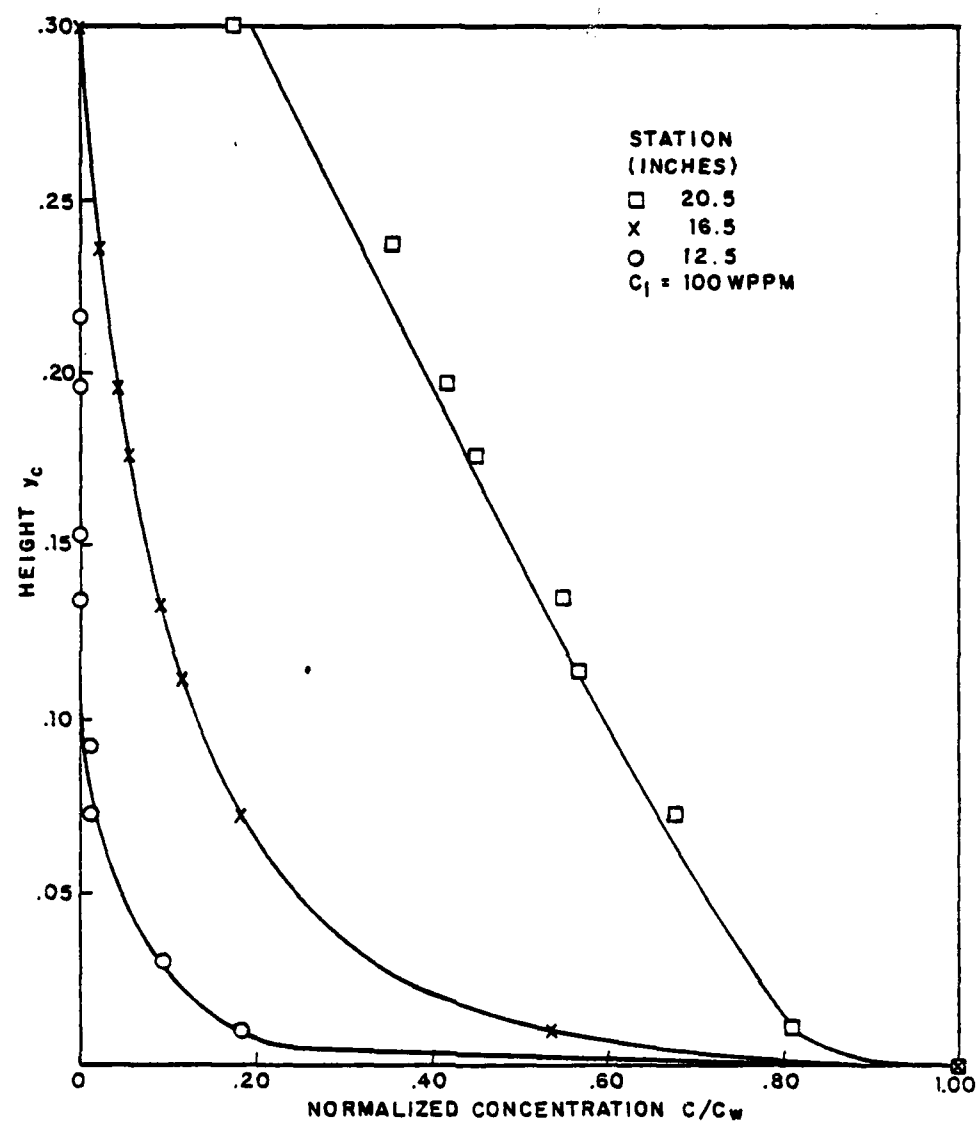


Figure 103. Normalized polymer diffusion pattern for injected polymer concentration $C_1 = 100 \text{ WPPM}$

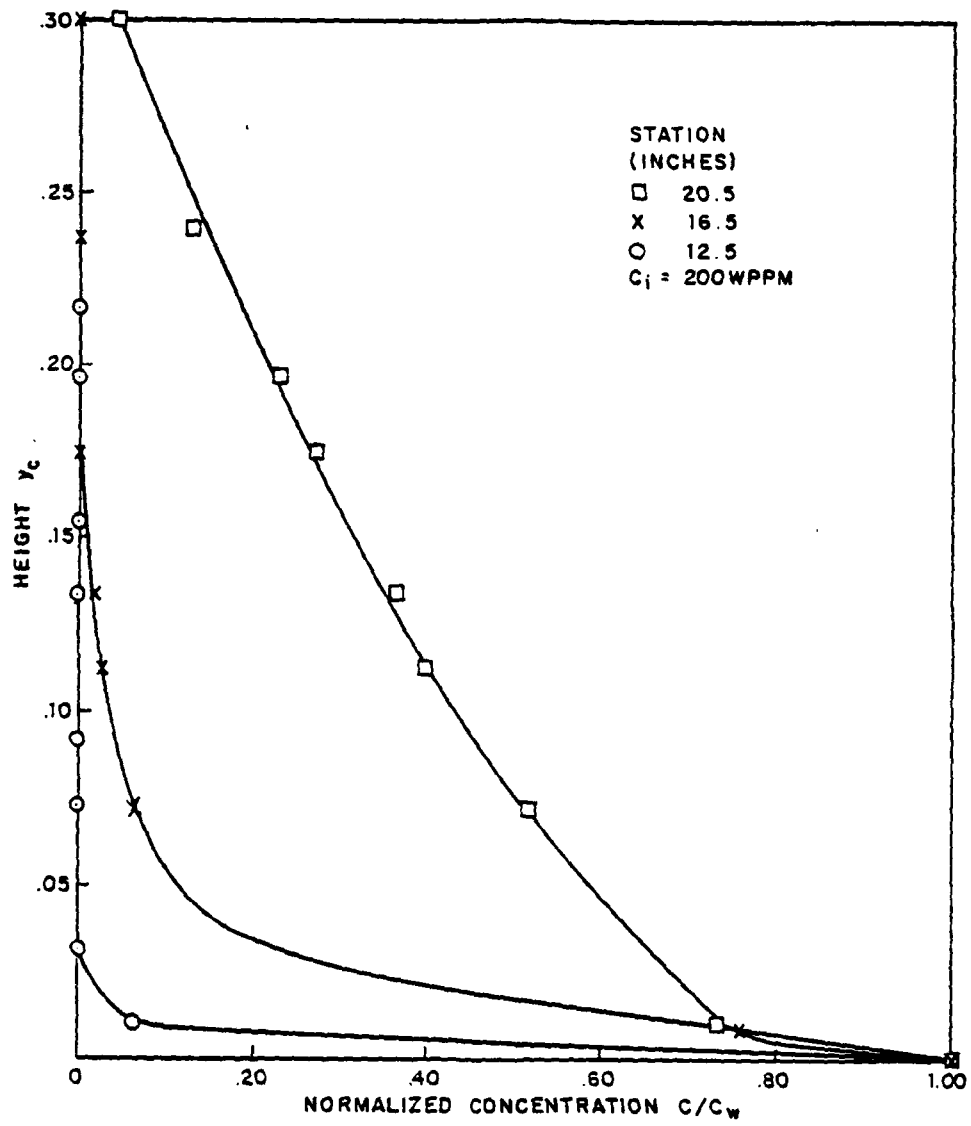


Figure 104. Normalized polymer diffusion pattern for injected polymer concentration $C_i = 200\text{WPPM}$

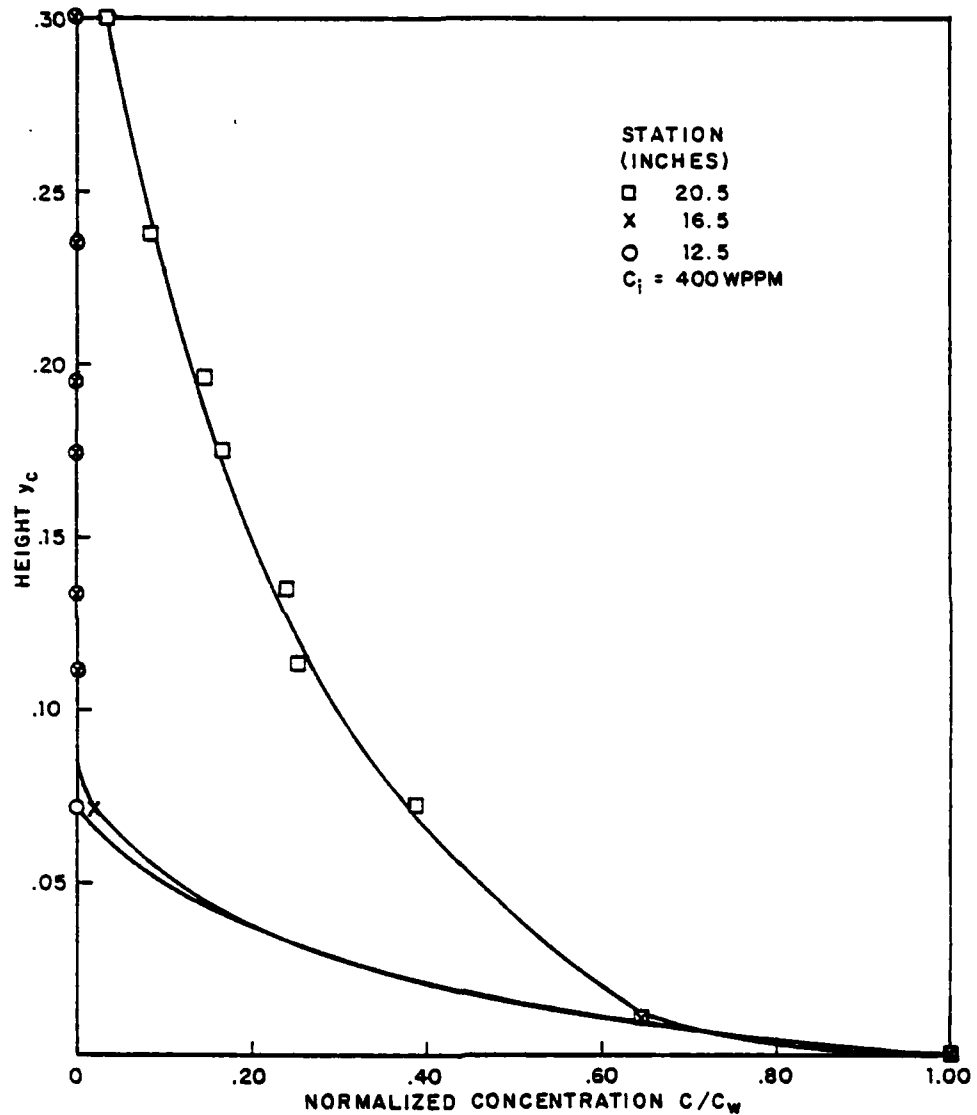


Figure 105. Normalized polymer diffusion pattern for injected polymer concentration $C_i = 400 \text{ WPPM}$

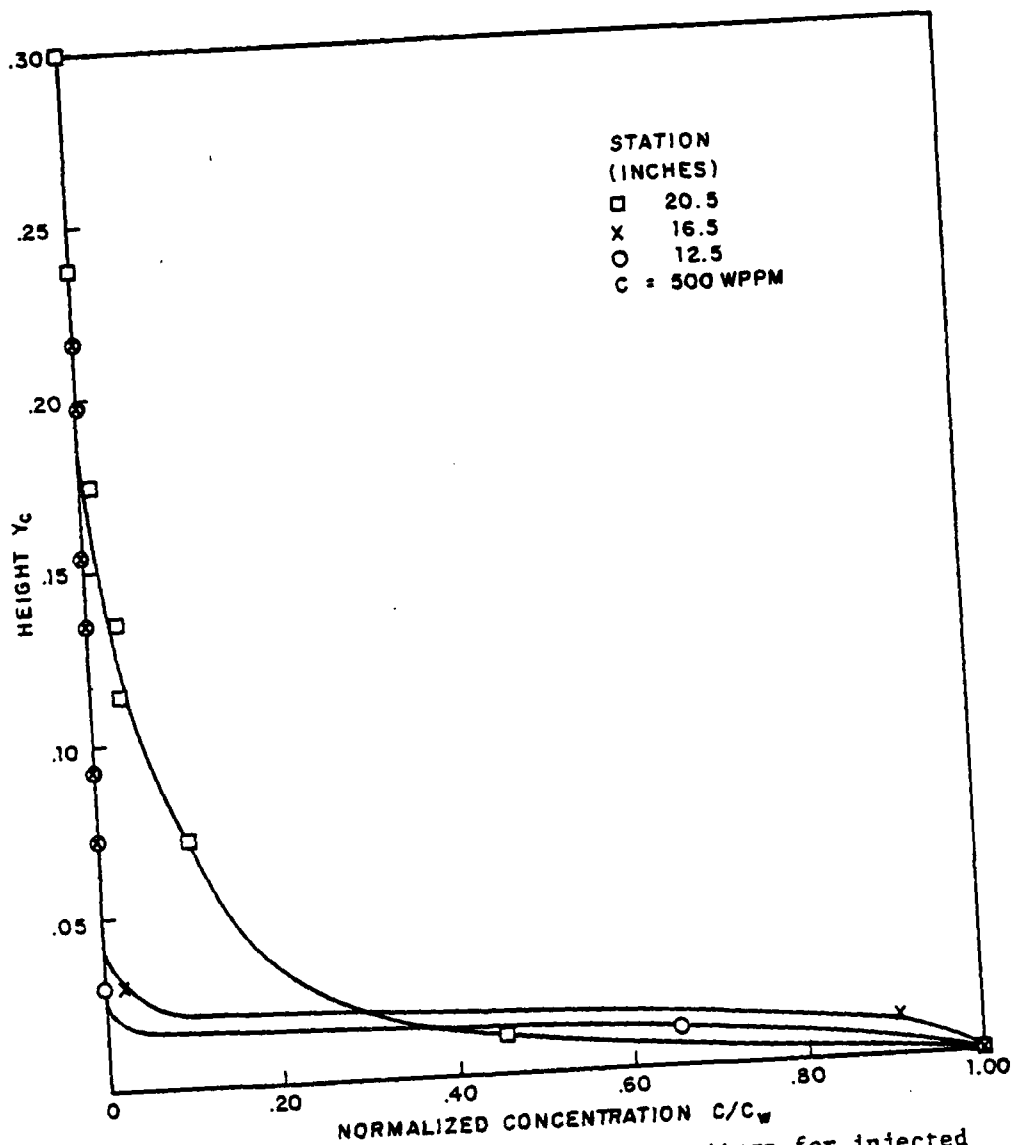


Figure 106. Normalized polymer diffusion pattern for injected polymer concentration $C_1 = 500 \text{ WPPM}$

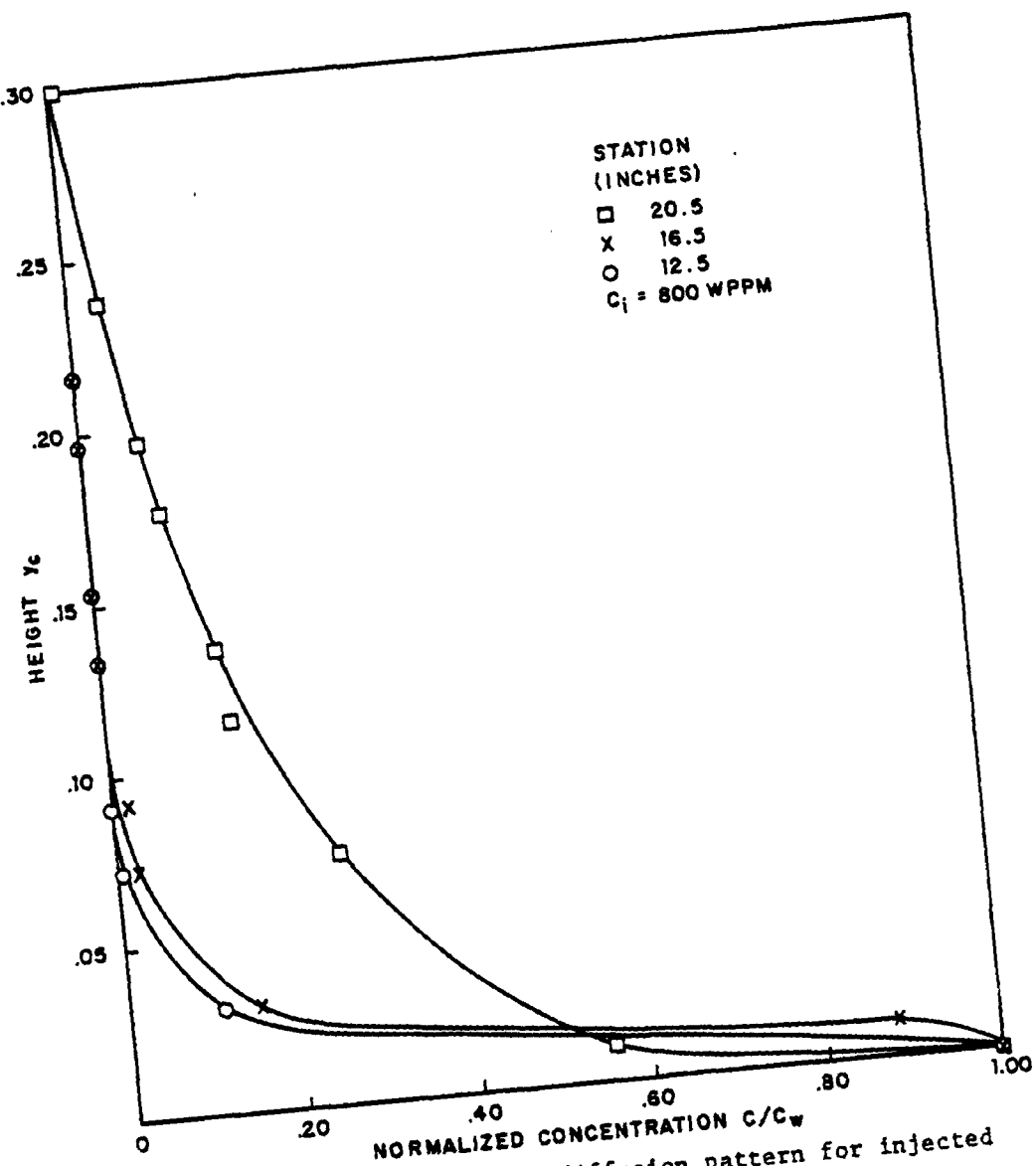


Figure 107. Normalized polymer diffusion pattern for injected polymer concentration $C_i = 800 \text{ WPPM}$

concentration in the near wall region as shown in figure 108.

The quantity of polymer or mass flow rate injected into the boundary layer may be considered to be given by the flow rate of injection times the concentration. Figure 109 is a plot of diffusion boundary layer height versus axial length injected at various flow rates and concentrations in combination to produce a constant quantity of polymer injected into the boundary layer of $Q_1 C_1 = 3,000$. The lowest rate of injection at the highest concentration produces the slowest growth of the diffusion boundary layer. The effect of increasing the quantity of polymer injected into the boundary layer is shown in figure 110 where the value of $Q_1 C_1 = 16,000$. Again, the lowest rate of injection at the highest concentration produces the slowest growth of the diffusion boundary layer. The increased amount of polymer injected into the boundary layer greatly suppressed the diffusion of polymer away from the wall. The effect of increasing injection concentration flux into the boundary layer may be seen in figure 111, which may be considered to present a measure of the injection "displacement" thickness. At constant velocity of injection, increased injection concentration flux greatly suppressed the growth of the diffusion boundary layer. The lowest injection velocity produced the lowest diffusion boundary layer. In the final zone, diffusion was found to vary with an exponent of .6 as shown in figure 112. Sirmalis had predicted that the exponent for similarity profiles would be lower than his value of .75 as he was unable to

obtain data within .01 inch of the wall. Similarity profiles for the growth of the diffusion boundary layer in the transition region are shown in figure 113. Higher injected concentrations are also shown to have reduced diffusion characteristics in this region.

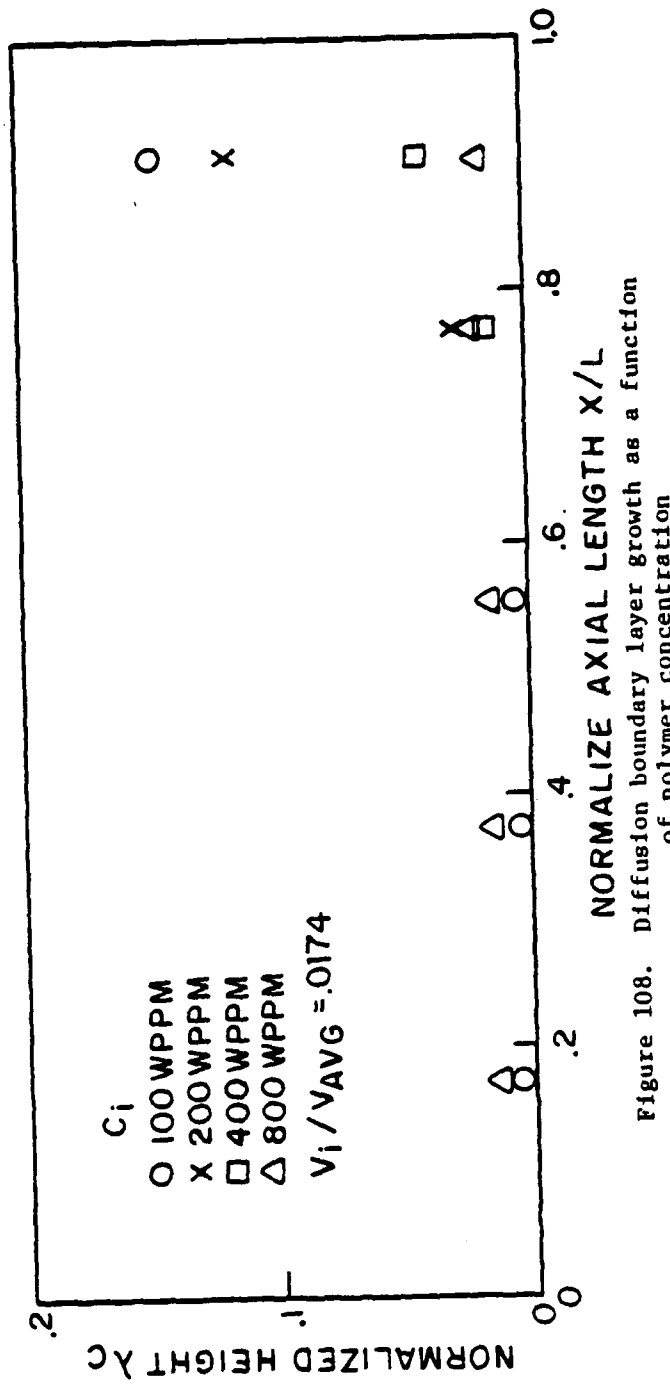


Figure 108. Diffusion boundary layer growth as a function of polymer concentration

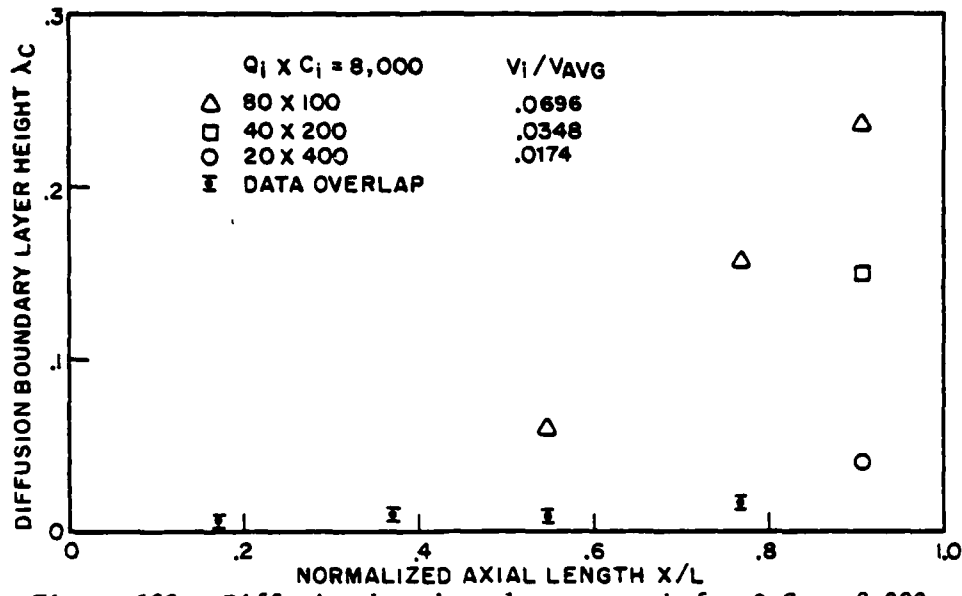


Figure 109. Diffusion boundary layer growth for $Q_1 C_1 = 8,000$

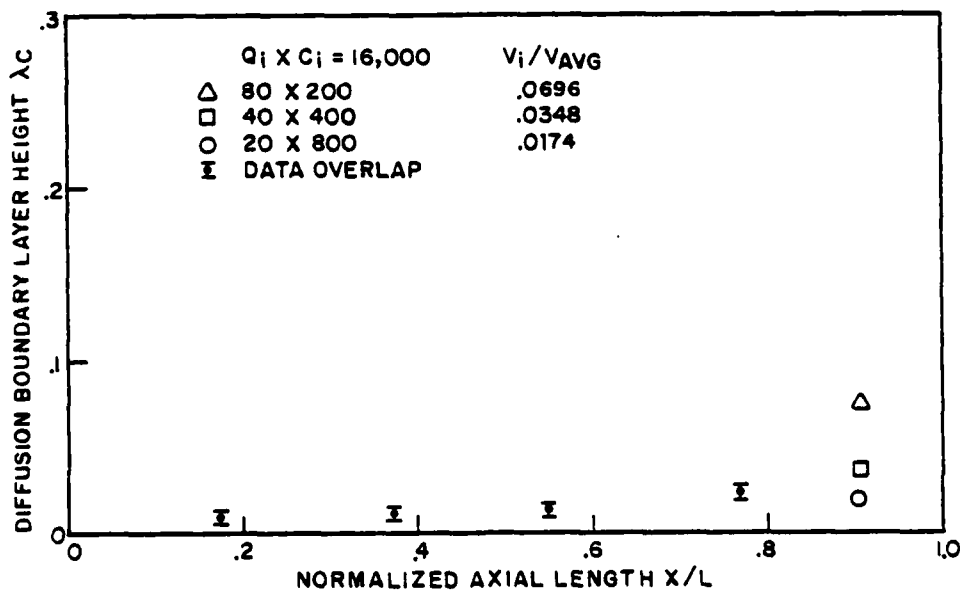


Figure 110. Diffusion boundary layer growth for $Q_1 C_1 = 16,000$

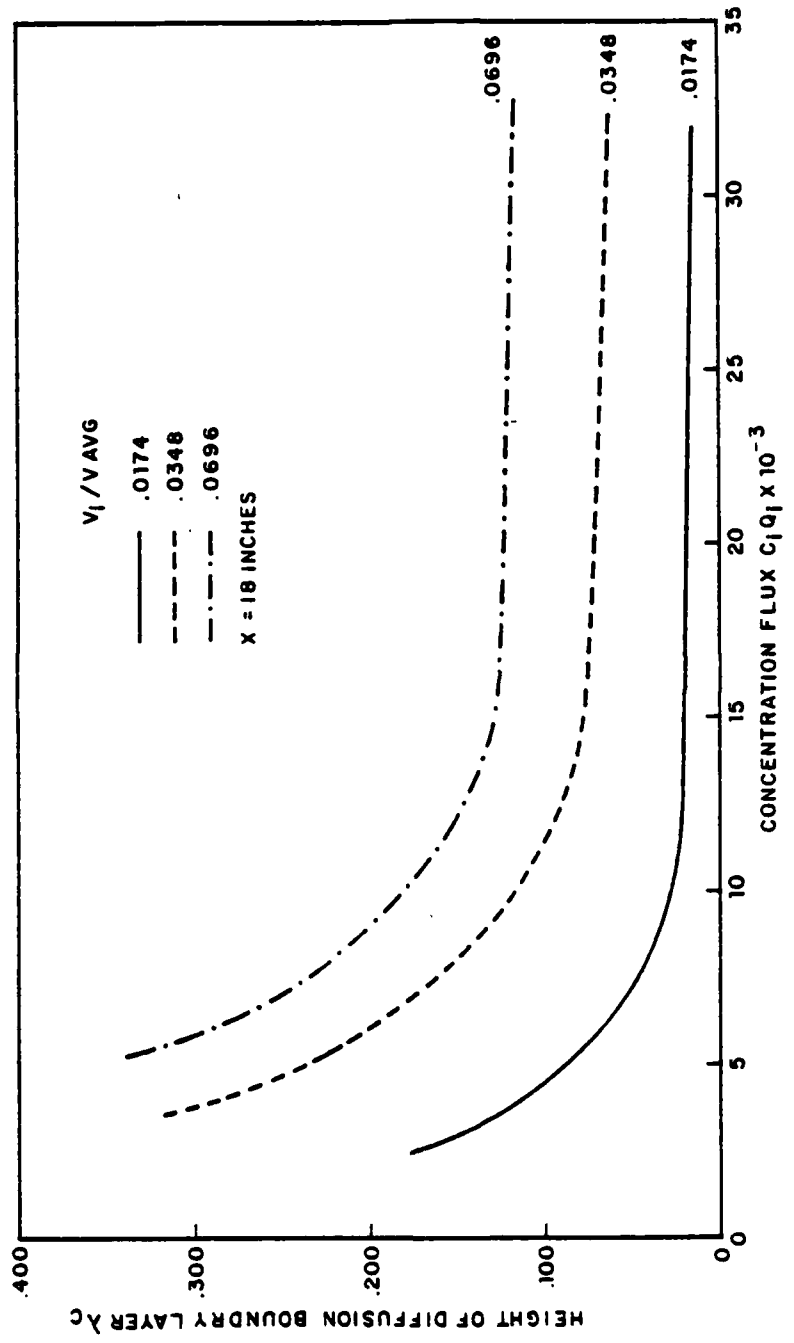


Figure 111. Diffusion boundary layer growth as a function of $Q_i C_i$ and injection velocity ratio

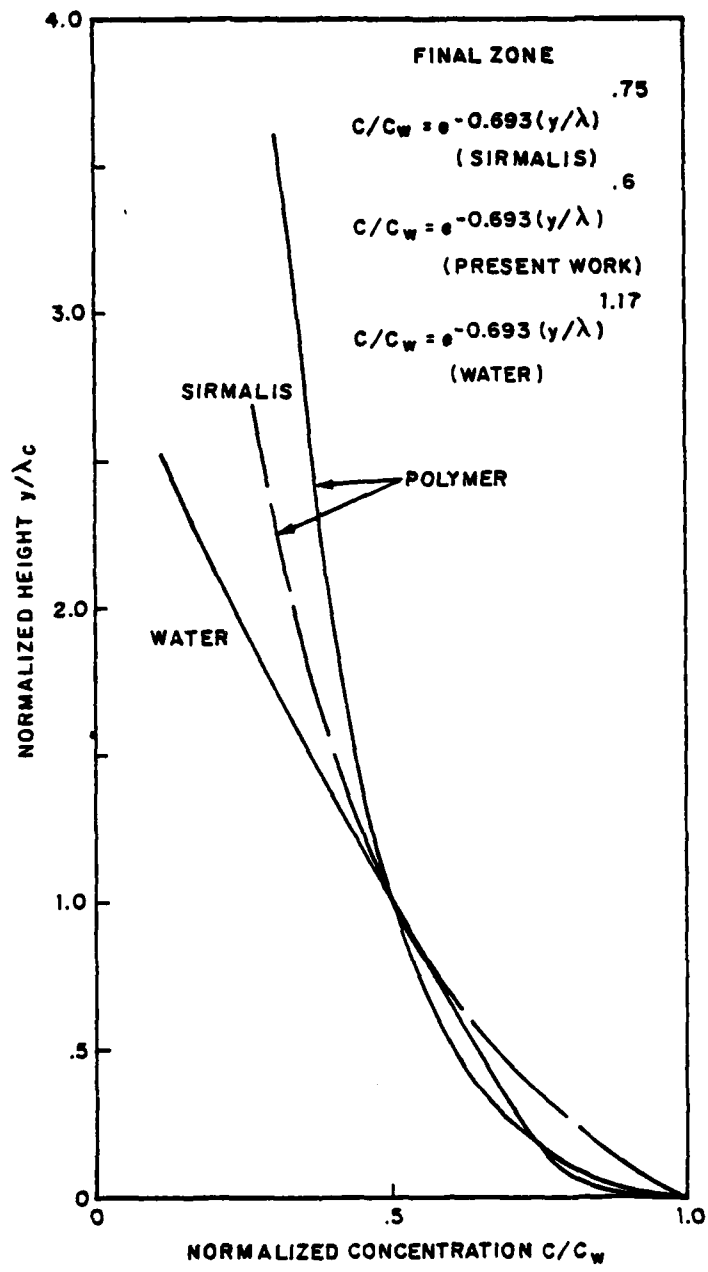


Figure 112. Diffusion boundary layer growth in the final zone

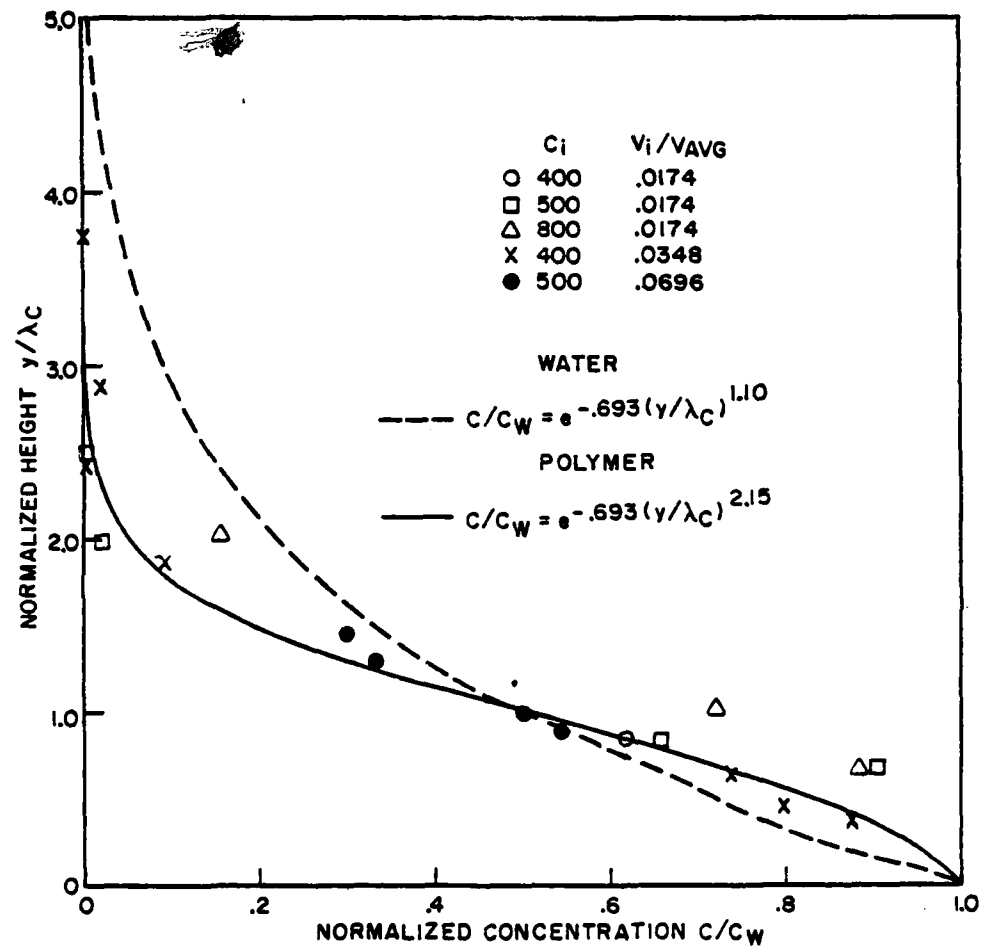


Figure 113. Diffusion boundary layer growth in the transition region

VII. CONCLUSIONS AND RECOMMENDATIONS

General

The object of this research was threefold: (1) to develop an experimental facility and techniques for the study of the effects of drag-reducing polymers on submerged flat plate flow, (2) to qualitatively define the effects of polymers on boundary layers in external flows, and (3) to verify predictive techniques by experiment. A flat plate water tunnel facility was constructed and laser Doppler anemometry techniques were developed for boundary layer velocity measurements. The flow facility is capable of variable injection velocity and concentration of polymer with boundary layer sampling at several heights throughout the boundary layer and at several axial stations. The injection process was unique because injection occurred very close to the leading edge into laminar flow, then developing through transitional to turbulent flow. Application of laser Doppler techniques provided non-disruptive velocity measurements in a low turbulent level facility for a wide range of polymer concentration and velocity of injection.

Analytical Predictive Methods

The case of developing flow with polymer injection has received little attention for external flows. Predictive methods are, therefore, not well developed. Past works on the diffusion of polymer boundary layers have centered on the far downstream region in turbulent flow where the polymer attained the same diffusion characteristics as the medium.

An analytical model was developed for comparison with experimental data. The model is based on integral boundary layer analysis combined with velocity profile relation for flat plate flow at zero pressure gradient and variable polymer wall concentration. Accurate prediction of local skin friction and boundary layer height as a function of variable local wall polymer concentration has been demonstrated over laminar, transitional, and turbulent flow regions by comparison with experimental data.

Polymer Boundary Layer Characteristics

Polymer additives appeared to have no effect in the laminar flow region. However, increasing polymer concentrations delayed and stretched out the transition to turbulent flow. The effect of polymer additives is predominant in the region of maximum turbulence production.

Streamwise turbulence intensity distributions are lower in peak value and displaced further from the wall over a broadened buffer region near the wall than found in comparable solvent flows. Near-wall velocity measurements have shown that the laminar sublayer thickens with the introduction of polymer. A thicker velocity profile sublayer reduces the velocity gradient at and near the wall. The wall shear stress, proportional to the velocity gradient at the wall, also decreases, thus reducing the frictional drag of the surface. Although thickening the sublayer, polymers cause the overall boundary layer to become thinner. Skin friction prediction by Clauser's technique has been shown applicable, with modification, to polymer flows.

Diffusion Characteristics

Various polymer concentrations were injected into a laminar flat plate boundary layer at various injection rates. Transition to turbulent flow was delayed and extended. Kowalski's (1974) explanation that polymer molecules seem to act as barriers restricting communication across the boundary layer, forcing the liquid to flow in a semi-laminar manner is most appropriate here. The growth of the diffusion boundary layer, indicated by a characteristic height, decreased with increasing concentration and quantity of polymer injected into the boundary layer.

The increased concentration of polymer showed reduced diffusion in the transition region resulting in an extended initial mixing zone. This effect is also supported by the work of Sirmalis (1976).

Conclusion Summary

An experimental facility has been developed that allows laboratory measurements of polymer drag reduction concentration profile distribution for various injector geometries, velocities of injection, and injection concentrations. Hydrodynamic properties of the boundary layers were measured using laser Doppler anemometry techniques. Experiments indicated thickening sublayers and overall thinning of the boundary layer with polymer concentration. Turbulence intensity distributions were lower in peak value and distributed over a broad region. Diffusion of polymer injected into the laminar flow at the leading edge of the flat plate delayed transition and spread the transition region out. Very little diffusion occurred in the laminar region. Diffusion in the turbulent region indicated by a characteristic height of the diffusion boundary layer decreased with increasing concentration and quantity of polymer. Predictive methods were developed building on reliable theories and techniques for the prediction of local skin friction as a function of polymer wall concentration. Comparison with experiment has been performed and good agreement achieved.

Recommendations

1. Additional testing should be performed at boundary layer heights between values of y^+ equal to 7 to 50. This region would supply additional data to define the increasing height of the sublayer with polymer concentration, as well as the polymer-induced ΔB shift. Low concentrations of injected polymer below 50 WPPM should also be tested.
2. Application of the modified Clauser skin friction calculation technique to polymer flows should be continued and will require additional data in the above-mentioned region.
3. Application of traversing laser Doppler techniques should be extended to include rotation of the measuring volume by 90° to obtain distribution of the v' turbulence intensity distribution allowing computation of Reynolds stress.
4. Reduction of flow noise indicates that frequency spectrum analysis should be performed to determine which frequencies are attenuated by various polymer concentrations.
5. The experimental facility should be lengthened to allow a more gradual and natural transition to turbulent flow.

6. Multiple horizontal injection stations along the plate should be tested with lower concentration of injection to verify the disentanglement theory. Optimization of the injection system should also include pulsed low concentration injection to determine persistence and possible time scale correlation.

7. Modification of the tunnel passage will allow the study of polymer effects in boundary layers with adverse pressure gradients. The capability for acoustic modulation of the laser beams should be added to the test setup to measure flow reversals using non-disruptive laser Doppler anemometer techniques.

Appendix A
DEVELOPMENT OF SKIN FRICTION RELATIONS

The law of the wall incorporating a polymer term, according to Meyer (1966), is given by

$$u^+ = \left(\frac{1}{K}\right) \ln y^+ + B + \alpha \left(C_w^\gamma\right) \ln \left(\frac{V^*}{V_0^*}\right) \quad (A1)$$

where $\alpha = 2.3$, $\gamma = .5$.

The conservation of mass and the momentum equations for flow over a flat plate are given by

$$\frac{\partial}{\partial x} (\rho u) + \frac{\partial}{\partial y} (\rho v) = 0 \quad (A2)$$

and

$$\rho u \left(\frac{\partial u}{\partial x} \right) + \rho v \left(\frac{\partial u}{\partial y} \right) = - \frac{\partial p}{\partial x} + \frac{\partial \tau}{\partial y}. \quad (A3)$$

For a flat plate, it may be assumed that the pressure gradient is negligible, such that

$$\frac{\partial p}{\partial x} = 0. \quad (A4)$$

Therefore, equation (A3) becomes

$$\rho u \left(\frac{\partial u}{\partial x} \right) + \rho v \left(\frac{\partial u}{\partial y} \right) = \frac{\partial \tau}{\partial y}. \quad (A5)$$

It may further be assumed that $u = f$, $\rho = f$, and $v = f = \frac{u}{\rho}$ are all constants. (A6)

Equation (A2) becomes

$$\frac{\partial u}{\partial x} + \frac{\partial v}{\partial y} = 0. \quad (A7)$$

An expression for v becomes

$$\begin{aligned} \frac{\partial v}{\partial y} &= - \frac{\partial u}{\partial x} \\ dv &= - \frac{\partial u}{\partial x} dy \\ v(y) &= v = - \int_0^y \frac{\partial u}{\partial x} dy. \end{aligned} \quad (A8)$$

Changing to law of the wall variables we have

$$u^+ = \frac{u}{v^*} \quad (A9)$$

$$u = v^* u^+ \quad (A10)$$

$$\frac{\partial u}{\partial x} = \frac{\partial (v^* u^+)}{\partial x} \quad (A11)$$

$$y^+ = \frac{y v^*}{v} \quad (A12)$$

$$dy^+ = \frac{v^*}{v} dy \quad (A13)$$

$$dy = \frac{v}{v^*} dy^+ \quad (A14)$$

$$v^* = v^*(x) = \sqrt{\frac{\tau_w}{\rho}} \quad (A15)$$

Combining equations (A8, A11, A14), equation (A8) becomes

$$v = - \int_0^{y^+} \frac{d(v^* u^+)}{dx} \left(\frac{v}{v^*} \right) dy^+. \quad (A16)$$

Changing equation (A5) into law of the wall variables using equations (A9) thru (A16) we have

$$\begin{aligned} & \rho (v^* u^+) \frac{\partial}{\partial x} (v^* u^+) + \rho \left[- \int_0^{y^+} \frac{\partial (v^* u^+)}{\partial x} \left(\frac{v}{v^*} \right) dy^+ \right] \frac{\partial (v^* u^+)}{\partial y} \\ &= \frac{\partial \tau}{\partial y}. \end{aligned} \quad (A17)$$

The derivatives with respect to x must be handled by the chain rule, because the parameters y^+ and C_w are functions of x in the law of the wall. We are changing independent variables from x and y to x , y^+ and C_w , where $C_w = C_w(x)$ and $y^+ = y^+(x, y)$.

Thus we substitute

$$\frac{\partial}{\partial x} = \frac{\partial y^+}{\partial x} \frac{\partial}{\partial y^+} + \frac{\partial C_w}{\partial x} \frac{\partial}{\partial C_w}. \quad (\text{A18})$$

Now

$$u(x, y) = v^*(x) u^+(y^+, C_w). \quad (\text{A19})$$

Differentiating we have

$$\begin{aligned} \frac{\partial u}{\partial x} &= \frac{\partial(v^* u^+)}{\partial x} \\ &= u^+ \frac{\partial v^*}{\partial x} + v^* \frac{\partial u^+}{\partial x} \\ &= u^+ \frac{\partial v^*}{\partial x} + v^* \left[\frac{\partial y^+}{\partial x} \left(\frac{\partial u^+}{\partial y^+} \right) + \frac{\partial C_w}{\partial x} \left(\frac{\partial u^+}{\partial C_w} \right) \right] \\ &= u^+ \frac{\partial v^*}{\partial x} + v^* \frac{\partial y^+}{\partial x} \left(\frac{\partial u^+}{\partial y^+} \right) + v^* \frac{\partial C_w}{\partial x} \left(\frac{\partial u^+}{\partial C_w} \right). \end{aligned} \quad (\text{A20})$$

Substituting equation (A20) into equation (A18),

$$\rho(v^* u^+) \left[u^+ \frac{\partial v^*}{\partial x} + v^* \frac{\partial y^+}{\partial x} \left(\frac{\partial u^+}{\partial y^+} \right) + v^* \frac{\partial C_W}{\partial x} \left(\frac{\partial u^+}{\partial C_W} \right) \right] - \rho \left[\int_0^{y^+} \frac{\partial}{\partial x} (v^* u^+) \frac{v}{v^*} dy^+ \right] \frac{\partial}{\partial y} (v^* u^+) = \frac{\partial \tau}{\partial y}. \quad (A21)$$

Obtaining an expression for $\frac{\partial u}{\partial y}$ we have

$$\begin{aligned} \frac{\partial u}{\partial y} &= \frac{\partial (v^* u^+)}{\partial y} \\ &= u^+ \frac{\partial v^*}{\partial y} + v^* \frac{\partial u^+}{\partial y}. \end{aligned} \quad (A22)$$

However,

$$v^* = v^*(x) \quad (A23)$$

and hence

$$\frac{\partial v^*}{\partial y} = 0. \quad (A24)$$

Equation (A22) then becomes

$$\frac{\partial (v^* u^+)}{\partial y} = v^* \frac{\partial u^+}{\partial y}. \quad (A25)$$

Changing ∂y to ∂y^+ we have

$$\frac{\partial(v^+ u)}{\partial y} = v^* \frac{\partial u^+}{\partial y} = v^* \left[\frac{\partial u^+}{\partial y} \left(\frac{\partial y^+}{\partial y} \right) + \frac{\partial u^+}{\partial C_W} \left(\frac{\partial C_W}{\partial y} \right) \right] \quad (A26)$$

but

$$\frac{\partial y^+}{\partial y} = \frac{v^*}{v} \text{ and } \frac{\partial C_W}{\partial y} = 0$$

and therefore

$$\frac{\partial(v^* u^+)}{\partial y} = \frac{(v^*)^2}{v} \left(\frac{\partial u^+}{\partial y^+} \right).$$

Equation (A21) becomes

$$\rho (v^* u^+) \left[u^+ + \frac{\partial v^*}{\partial x} + v^* \frac{\partial y^+}{\partial x} \frac{\partial u^+}{\partial y^+} + v^* \frac{\partial C_W}{\partial x} \left(\frac{\partial u^+}{\partial C_W} \right) \right] - \rho \left[\int_0^{y^+} \frac{\partial}{\partial x} (v^* u^+) \frac{v}{v^*} dy^+ \right] \frac{(v^*)^2}{v} \left(\frac{\partial u^+}{\partial y^+} \right) = \frac{\partial \tau}{\partial y}. \quad (A27)$$

As $v = t$, equation (A6) and $v^* = v^*(x)$, equation (A23) may then be removed from within the integral yielding

$$\rho (v^* u^+) \left[u^+ + \frac{\partial v^*}{\partial x} + v^* \frac{\partial y^+}{\partial x} \left(\frac{\partial u^+}{\partial y^+} \right) + v^* \frac{\partial C_W}{\partial x} \left(\frac{\partial u^+}{\partial C_W} \right) \right] - \rho \left[\int_0^{y^+} \frac{\partial(v^* u^+)}{\partial x} dy^+ \right] v^* \left(\frac{\partial u^+}{\partial y^+} \right) = \frac{\partial \tau}{\partial y}. \quad (A28)$$

After substitution of equation (A20) with equation (A28) we have

$$\rho(v^* u^+) \left[u^+ \left(\frac{\partial v^*}{\partial x} \right) + v^* \left(\frac{\partial y^+}{\partial x} \right) \frac{\partial u^+}{\partial y^+} + v^* \left(\frac{\partial C_w}{\partial x} \right) \frac{\partial u^+}{\partial C_w} \right]$$

$$-\rho \left\{ \int_0^{y^+} \left[u^+ \left(\frac{\partial v^*}{\partial x} \right) + v^* \left(\frac{\partial y^+}{\partial x} \right) \frac{\partial u^+}{\partial y^+} + v^* \left(\frac{\partial C_w}{\partial x} \right) \frac{\partial u^+}{\partial C_w} \right] dy^+ \right\} v^* \left(\frac{\partial u^+}{\partial y^+} \right) = \frac{\partial \tau}{\partial y}. \quad (A29)$$

Converting $\frac{\partial \tau}{\partial y}$ to law of wall variables we have

$$\frac{\partial \tau}{\partial y} = \frac{\partial \tau}{\partial y^+} \left(\frac{\partial y^+}{\partial y} \right)$$

$$= \frac{v^*}{v} \left(\frac{\partial \tau}{\partial y^+} \right).$$

Substituting into equation (A29) we have

$$\rho(v^* u^+) \left[u^+ \left(\frac{\partial v^*}{\partial x} \right) + v^* \left(\frac{\partial y^+}{\partial x} \right) \frac{\partial u^+}{\partial y^+} + v^* \left(\frac{dC_w}{dx} \right) \frac{du^+}{dC_w} \right]$$

$$-\rho \left[\int_0^{y^+} \left(u^+ \left(\frac{\partial v^*}{\partial x} \right) + v^* \left(\frac{\partial y^+}{\partial x} \right) \frac{\partial u^+}{\partial y^+} + v^* \left(\frac{\partial C_w}{\partial x} \right) \frac{\partial u^+}{\partial x} \right) dy^+ \right] v^* \left(\frac{\partial u^+}{\partial y^+} \right) = \frac{v^*}{v} \left(\frac{\partial \tau}{\partial y^+} \right).$$

Dividing then by ρv^* and remembering that $v = \frac{\mu}{\rho}$

$$\begin{aligned}
& u^+ \left[u^+ \left(\frac{\partial v^*}{\partial x} \right) + v^* \left(\frac{\partial y^+}{\partial x} \right) \frac{\partial u^+}{\partial y^+} + v^* \left(\frac{\partial C_w}{\partial x} \right) \frac{\partial u^+}{\partial C_w} \right] \\
& - \left\{ \int_0^{y^+} \left[u^+ \left(\frac{\partial v^*}{\partial x} \right) + v^* \left(\frac{\partial y^+}{\partial x} \right) \frac{\partial u^+}{\partial y^+} + v^* \left(\frac{\partial C_w}{\partial x} \right) \frac{\partial u^+}{\partial C_w} \right] dy^+ \right\} \frac{\partial u^+}{\partial y^+} \\
& = \frac{1}{\rho v} \left(\frac{\partial \tau}{\partial y^+} \right) = \frac{1}{\mu} \left(\frac{\partial \tau}{\partial y^+} \right). \tag{A30}
\end{aligned}$$

Multiplying by dy^+ , expanding terms and integrating we have

$$\begin{aligned}
& \int_0^{y^+} (u^+)^2 \left(\frac{\partial v^*}{\partial x} \right) dy^+ + \int_0^{y^+} v^* u^+ \left(\frac{\partial y^+}{\partial x} \right) \frac{\partial u^+}{\partial y^+} dy^+ + \int_0^{y^+} u^+ v^* \left(\frac{\partial C_w}{\partial x} \right) \frac{\partial u^+}{\partial C_w} dy^+ \\
& - \int_0^{y^+} \left\{ \left[\int_0^{y^+} u^+ \left(\frac{\partial v^*}{\partial x} \right) + v^* \left(\frac{\partial y^+}{\partial x} \right) \frac{\partial u^+}{\partial y^+} + v^* \left(\frac{\partial C_w}{\partial x} \right) \frac{\partial u^+}{\partial C_w} dy^+ \right] \frac{\partial u^+}{\partial y^+} \right\} dy^+ \\
& = \int_0^{y^+} \frac{1}{\mu} \left(\frac{\partial \tau}{\partial y^+} \right) dy^+. \tag{A31}
\end{aligned}$$

From equation (A6) and (A22) upon rearranging equation (A31) and integrating through the boundary layer such that $\tau(y^+) = 0$, we have

$$\frac{\partial v^*}{\partial x} \int_0^{y^+} (u^+)^2 dy^+ + v^* \int_0^{y^+} u^+ \left(\frac{\partial y^+}{\partial x} \right) \frac{\partial u^+}{\partial y^+} dy^+ + \int_0^{y^+} u^+ \left(\frac{\partial C_w}{\partial x} \right) \frac{\partial u^+}{\partial C_w} dy^+$$

$$-\int_0^{y^+} \left\{ \left[\int_0^{y^+} (u^+ \left(\frac{\partial v^*}{\partial x} \right) + v^* \left(\frac{\partial y^+}{\partial x} \right) \frac{\partial u^+}{\partial y^+}) dy^+ \right] \right\} \frac{\partial u^+}{\partial y^+} dy^+ = \frac{1}{\mu} \tau_w. \quad (A32)$$

Defining groups of terms we have

$$G = \int_0^{y^+} (u^+)^2 dy^+ \quad (A33)$$

$$H = \int_0^{y^+} u^+ \left(\frac{\partial y^+}{\partial x} \right) \frac{\partial u^+}{\partial y^+} dy^+ \quad (A34)$$

$$J = \int_0^{y^+} u^+ \left(\frac{\partial C_w}{\partial x} \right) \frac{\partial u^+}{\partial C_w} dy^+ \quad (A35)$$

$$M = \int_0^{y^+} \left[u^+ \left(\frac{\partial v^*}{\partial x} \right) + v^* \left(\frac{\partial y^+}{\partial x} \right) \frac{\partial u^+}{\partial y^+} + v^* \left(\frac{\partial C_w}{\partial x} \right) \frac{\partial u^+}{\partial C_w} \right] dy^+ \quad (A36)$$

$$N = \int_0^{y^+} M \left(\frac{\partial u^+}{\partial y^+} \right) dy^+. \quad (A37)$$

Therefore equation (A32) becomes

$$\frac{\partial v^*}{\partial x} (G) + v^* H + v^* J - N = - \frac{1}{\mu} \tau_w. \quad (A38)$$

Recalling the law of the wall equation, (A33) becomes

$$\begin{aligned}
 G &= \int_0^{y^+} \left(\frac{1}{K} \ln y^+ + 5.5 + 2.3 C_w^{.57} \ln \left(\frac{v^*}{v_0} \right) \right) dy^+ \\
 &= \int_0^{y^+} \left\{ \frac{1}{K^2} (\ln y^+)^2 + (5.5)^2 + (2.3)^2 C_w^{1.14} \ln \left(\frac{v^*}{v_0} \right) + 2(5.5) \frac{1}{K} \ln y^+ \right. \\
 &\quad \left. + 2(2.3) \frac{1}{K} \ln y^+ C_w^{.57} \ln \frac{v^*}{v_0} + 2(5.5)(2.3) C_w^{.57} \ln \frac{v^*}{v_0} \right\} dy^+. \quad (A39)
 \end{aligned}$$

$$\begin{aligned}
 G &= \frac{1}{K^2} \int_0^{y^+} (\ln y^+)^2 dy^+ + (5.5)^2 y^+ + (2.3)^2 C_w^{1.14} \ln^2 \left(\frac{v^*}{v_0} \right) y^+ \\
 &\quad + \frac{2(5.5)}{K} \int_0^{y^+} \ln y^+ (dy^+) + \frac{2(2.3)}{K} C_w^{.57} \ln \left(\frac{v^*}{v_0} \right) \int_0^{y^+} \ln(y^+) dy^+ \\
 &\quad + 2(5.5)(2.3) C_w^{.57} \ln \left(\frac{v^*}{v_0} \right) y^+. \quad (A40)
 \end{aligned}$$

Note: $(\ln x)^2 dx = x(\ln x)^2 - 2[x(\ln x - 1)] = x[\ln^2 x - 2 \ln x + 2]$

$$= x[\ln^2 x - 2(\ln x - 1)] \quad (A41)$$

hence

$$G = \frac{1}{K^2} \left\{ y^+ [\ln^2 y^+ - 2(\ln y^+ - 1)] \right\} + (5.5)^2 y^+$$

$$\begin{aligned}
 & + (2.3)^2 C_w^{1.14} \ln^2 \left(\frac{v^*}{v_0^*} \right) y^+ \\
 & + \frac{2(5.5)}{K} [y^+ (\ln y^+ - 1)] + \frac{2(2.3)}{K} C_w^{.57} \ln \left(\frac{v^*}{v_0^*} \right) y^+ (\ln y^+ - 1) \\
 & + 2(5.5) (2.3) C_w^{.57} \ln \left(\frac{v^*}{v_0^*} \right) y^+ - 2
 \end{aligned} \tag{A42}$$

$$G = y^+ \left\{ \frac{1}{K^2} [\ln^2 y^+ - 2(\ln y^+ - 1)] + \frac{2}{K} (\ln y^+ - 1) \left[5.5 + 2.3 C_w^{.57} \ln \left(\frac{v^*}{v_0^*} \right) \right] \right.$$

$$\left. + 2.3 C_w^{.57} \ln \left(\frac{v^*}{v_0^*} \right) \left[2(5.5) + 2.3 C_w^{.57} \ln \left(\frac{v^*}{v_0^*} \right) \right] + (5.5)^2 \right\} \tag{A43}$$

Evaluating term H, we have

$$H = \int_0^{y^+} u^+ \left(\frac{\partial y^+}{\partial x} \right) \frac{u^+}{\partial y^+} dy^+ \tag{A44}$$

$$\frac{\partial y^+}{\partial x} = \frac{\partial}{\partial x} \left(y \frac{v^*}{v} \right) = \frac{y}{v} \left(\frac{\partial v^*}{\partial x} \right) \tag{A45}$$

$$\frac{\partial u^+}{\partial y^+} = \frac{\partial}{\partial y^+} \left[\frac{1}{K} \ln y^+ + 5.5 + 2.3 C_w^{.57} \ln \left(\frac{v^*}{v_0^*} \right) \right] = \frac{1}{Ky^+} \tag{A46}$$

$$H = \int_0^{y^+} \frac{1}{K} \ln y^+ + 5.5 + 2.3 C_W^{.57} \ln \left(\frac{v^*}{v_0^*} \right) \left[\frac{y}{v} \frac{\partial v^*}{\partial x} \left[\frac{1}{Ky^+} \right] \right] dy^+. \quad (A47)$$

Now since

$$y^+ = y \frac{v^*}{v},$$

$$\frac{y}{v} = \frac{y^+}{v^*}. \quad (A48)$$

Substitute into equation (A47)

$$H = \int_0^{y^+} \left[\frac{1}{K} \ln y^+ + 5.5 + 2.3 C_W^{.57} \ln \left(\frac{v^*}{v_0^*} \right) \right] \left[\frac{y^+}{v^*} \frac{dv^*}{dx} \right] \left[\frac{1}{Ky^+} \right] dy^+ \quad (A49)$$

$$H = \int_0^{y^+} \left[\frac{1}{K} \ln y^+ + 5.5 + 2.3 C_W^{.57} \ln \left(\frac{v^*}{v_0^*} \right) \right] \left[\frac{1}{v^* K} \frac{\partial v^*}{\partial x} \right] dy^+$$

$$= \frac{1}{v^* K} \frac{\partial v^*}{\partial x} \int_0^{y^+} \left[\frac{1}{K} \ln y^+ + 5.5 + 2.3 C_W^{.57} \ln \left(\frac{v^*}{v_0^*} \right) \right] dy^+$$

$$= \frac{1}{v^* K} \left(\frac{\partial v^*}{\partial x} \right) y^+ \left[\frac{1}{K} (\ln y^+ - 1) + 5.5 + 2.3 C_W^{.57} \ln \left(\frac{v^*}{v_0^*} \right) \right]. \quad (A50)$$

Evaluating term J:

$$J = \int_0^{y^+} u^+ \left(\frac{\partial u^+}{\partial C_W} \right) \frac{\partial C_W}{\partial x} dy^+ \quad (A51)$$

$$\frac{\partial u^+}{\partial C_W} = \frac{\partial}{\partial C_W} \left\{ \frac{1}{K} \ln y^+ + 5.5 + 2.3 C_W^{.57} \ln \left(\frac{v^*}{v_0^*} \right) \right\}$$

$$= (.57)(2.3) C_W^{-0.43} \ln \left(\frac{v^*}{v_0^*} \right). \quad (A52)$$

$$J = \frac{\partial C_W}{\partial x} \int_0^{y^+} \left[\frac{1}{K} \ln y^+ + 5.5 + 2.3 C_W^{.57} \ln \left(\frac{v^*}{v_0^*} \right) \right] \left[(.57)(2.3) C_W^{-0.43} \ln \left(\frac{v^*}{v_0^*} \right) \right] dy^+$$

$$= (.57)(2.3) C_W^{-0.43} \ln \left(\frac{v^*}{v_0^*} \right) \frac{\partial C_W}{\partial x} \int_0^{y^+} \left(\frac{1}{K} \ln y^+ + 5.5 + 2.3 C_W^{.57} \ln \frac{v^*}{v_0^*} \right) dy^+$$

$$= .57(2.3) C_W^{-0.43} \ln \left(\frac{v^*}{v_0^*} \right) \left(\frac{\partial C_W}{\partial x} \right) y^+ \left[\frac{1}{K} (\ln y^+ - 1) + 5.5 \right. \\ \left. + 2.3 C_W^{.57} \ln \left(\frac{v^*}{v_0^*} \right) \right]. \quad (A53)$$

Evaluating term M, we have:

$$M = \int_0^{y^+} \left[u^+ \left(\frac{\partial v^*}{\partial x} \right) + v^* \left(\frac{\partial y^+}{\partial x} \right) \frac{\partial u^+}{\partial y} + v^* \frac{\partial C_w}{\partial x} \left(\frac{\partial u}{\partial C_w} \right) \right] dy^+. \quad (A54)$$

Let

$$1 = \int_0^{y^+} u^+ \left(\frac{\partial v^*}{\partial x} \right) dy^+ \quad (A55)$$

$$2 = \int_0^{y^+} v^* \left(\frac{\partial y^+}{\partial x} \right) \frac{\partial u^+}{\partial y} dy^+ \quad (A56)$$

$$3 = \int_0^{y^+} v^* \left(\frac{\partial C_w}{\partial x} \right) \frac{\partial u^+}{\partial C_w} dy^+. \quad (A57)$$

Term 1 becomes

$$\begin{aligned} \int_0^{y^+} u^+ \left(\frac{\partial v^*}{\partial x} \right) dy^+ &= \frac{\partial v^*}{\partial x} \int_0^{y^+} \left[\frac{1}{K} \ln y^+ + 5.5 + 2.3 C_w^{.57} \ln \left(\frac{v^*}{v_{0^*}} \right) \right] dy^+ \\ &= \frac{\partial v^*}{\partial x} y^+ \left\{ \frac{1}{K} (\ln y^+ - 1) + 5.5 + 2.3 C_w^{.57} \ln \left(\frac{v^*}{v_{0^*}} \right) \right\}. \end{aligned} \quad (A58)$$

Term 2 becomes

$$\begin{aligned}
 & \int_0^{y^+} v^* \left(\frac{\partial y^+}{\partial x} \right) \frac{\partial u^+}{\partial y^+} dy^+ = v^* \int_0^{y^+} \left(\frac{y}{v} \frac{\partial v^*}{\partial x} \right) \left(\frac{1}{Ky^+} \right) dy^+ \\
 & = v^* \int_0^{y^+} \frac{y^+}{v^*} \frac{\partial v^*}{\partial x} \frac{1}{Ky^+} dy^+ \\
 & = \frac{dv^*}{dx} \frac{1}{K} \int_0^{y^+} dy^+ \\
 & = \frac{1}{K} \frac{dv^*}{dx} y^+. \tag{A59}
 \end{aligned}$$

Term 3 becomes

$$\begin{aligned}
 & \int_0^{y^+} v^* \left(\frac{\partial C_W}{\partial x} \right) \frac{\partial u^+}{\partial C_W} dy^+ = v^* \left(\frac{\partial C_W}{\partial x} \right) \int_0^{y^+} \frac{\partial u^+}{\partial C_W} dy^+ \\
 & = v^* \left(\frac{dC_W}{dx} \right) \int_0^{y^+} (2.3)(.57) C_W^{-0.43} \ln \left(\frac{v^*}{v_{0*}} \right) dy^+ \\
 & = v^* \left(\frac{dC_W}{dx} \right) (2.3)(.57) C_W^{-0.43} \ln \left(\frac{v^*}{v_{0*}} \right) y^+. \tag{A60}
 \end{aligned}$$

Now evaluate term N :

$$N = \int_0^{y^+} M \left(\frac{\partial u^+}{\partial y^+} \right) dy^+$$

$$\begin{aligned}
 &= \int_0^{y^+} \left\{ \frac{\partial v^*}{\partial x} y^+ \left[\frac{1}{K} (\ln y^+ - 1) + 5.5 + 2.3 C_w^{.57} \ln \left(\frac{v^*}{v_{0*}} \right) \right] + \frac{1}{K} \frac{\partial v^*}{\partial x} y^+ \right. \\
 &\quad \left. + v^* \left(\frac{\partial C_w}{\partial x} \right) (2.3)(.57) C_w^{-4.3} \ln \left(\frac{v^*}{v_{0*}} \right) y^+ \frac{\partial u^+}{\partial y^+} dy^+ \right\} \quad (A61)
 \end{aligned}$$

such that

$$\frac{du^+}{dy^+} = \frac{1}{Ky^+} \quad (A62)$$

therefore

$$\begin{aligned}
 N &= \int_0^{y^+} \left\{ \frac{\partial v^*}{\partial x} \left(\frac{1}{K} (\ln y^+ - 1) + 5.5 + 2.3 C_w^{.57} \ln \left(\frac{v^*}{v_{0*}} \right) \right) + \frac{1}{K} \frac{\partial v^*}{\partial x} \right. \\
 &\quad \left. + v^* \left(\frac{\partial C_w}{\partial x} \right) (2.3)(.57) C_w^{-4.3} \ln \left(\frac{v^*}{v_{0*}} \right) \right\} dy^+ \quad (A64)
 \end{aligned}$$

Now

$$N = \int_0^{y^+} [3 + 4 + 5] dy^+ \quad (A65)$$

where

$$3 = \frac{1}{K} \frac{\partial v^*}{\partial x} \left[\frac{1}{K} (\ln y^+ - 1) + 5.5 + 2.3 C_w^{.57} \ln \left(\frac{v^*}{v_0^*} \right) \right] \quad (A66)$$

$$4 = \frac{1}{K^2} \frac{\partial v^*}{\partial x} \quad (A67)$$

$$5 = \frac{1}{K} v^* \left(\frac{\partial C_w}{\partial x} \right) (2.3)(.57) C_w^{-43} \ln \left(\frac{v^*}{v_0^*} \right). \quad (A68)$$

And we then have

$$\begin{aligned} \int_0^{y^+} 3 dy^+ &= \frac{1}{K} \frac{\partial v^*}{\partial x} \int_0^{y^+} \frac{1}{K} (\ln y^+ - 1) + 5.5 + 2.3 C_w^{.57} \ln \left(\frac{v^*}{v_0^*} \right) dy^+ \\ &= \frac{1}{K} \frac{\partial v^*}{\partial x} \left[\frac{1}{K} (y^+ \ln y^+ - 2y^+ + 5.5 y^+ + 2.3 C_w^{.57} \ln \left(\frac{v^*}{v_0^*} \right) y^+) \right] \end{aligned}$$

$$= \frac{1}{K} \frac{\partial v^*}{\partial x} y^+ \left[\frac{1}{K} (\ln y^+ - 2) + 5.5 + 2.3 C_w^{.57} \ln \left(\frac{v^*}{v_0^*} \right) \right] \quad (A69)$$

$$\int_0^{y^+} 4 \partial y^+ = \frac{1}{K^2} \frac{\partial v^*}{\partial x} \int_0^{y^+} dy^+$$

$$= \frac{1}{K^2} \frac{\partial v^*}{\partial x} y^+ \quad (A70)$$

$$\int_0^{y^+} 5 \partial y^+ = \int_0^{y^+} \left[\frac{1}{K} v^* \left(\frac{\partial C_w}{\partial x} \right) (2.3)(.57) C_w^{-43} \ln \left(\frac{v^*}{v_0^*} \right) \right] dy^+$$

$$= \frac{1}{K} v^* \left(\frac{\partial C_w}{\partial x} \right) (2.3)(.57) C_w^{-43} \ln \left(\frac{v^*}{v_0^*} \right) y^+ \quad (A71)$$

$$N = \left\{ \frac{1}{K} \frac{\partial v^*}{\partial x} y^+ \left[\frac{1}{K} (\ln y^+ - 2) + 5.5 + 2.3 C_w^{.57} \ln \left(\frac{v^*}{v_0^*} \right) \right] \right.$$

$$+ \frac{1}{K^2} \frac{\partial v^*}{\partial x} y^+$$

$$\left. + \frac{1}{K} v^* \frac{\partial C_w}{\partial x} (2.3)(.57) C_w^{-43} \ln \frac{v^*}{v_0^*} y^+ \right\} \quad (A72)$$

$$\begin{aligned}
 \frac{\partial v^*}{\partial x} (G) = & \frac{\partial v^*}{\partial x} y^+ \left\{ \frac{1}{K^2} \ln^2 y^+ - 2(\ln y^+ - 1) \right. \\
 & + \frac{2}{K} (\ln y^+ - 1) \left[5.5 + 2.3 C_W^{.57} \ln \left(\frac{v^*}{v_0^*} \right) \right] \\
 & \left. + 2.3 C_W^{.57} \ln \left(\frac{v^*}{v_0^*} \right) \left[2(5.5) + 2.3 C_W^{.57} \ln \left(\frac{v^*}{v_0^*} \right) \right] + (5.5)^2 \right\} \quad (A73)
 \end{aligned}$$

$$\begin{aligned}
 v^*(H) = & v^* \left[\frac{1}{v^* K} \left(\frac{\partial v^*}{\partial x} \right) y^+ + \frac{1}{K} (\ln y^+ - 1) + 5.5 \right. \\
 & \left. + 2.3 C_W^{.57} \ln \left(\frac{v^*}{v_0^*} \right) \right] \\
 = & \frac{1}{K} \frac{\partial v^*}{\partial x} y^+ + \left[\frac{1}{K} (\ln y^+ - 1) + 5.5 + 2.3 C_W^{.57} \ln \left(\frac{v^*}{v_0^*} \right) \right] \quad (A74)
 \end{aligned}$$

$$\begin{aligned}
 v^*(J) = & v^* (.57) (2.3) C_W^{-.43} \ln \left(\frac{v^*}{v_0^*} \right) \frac{\partial C_W}{\partial x} y^+ + \frac{1}{K} (\ln y^+ - 1) + 5.5 \\
 & + 2.3 C_W^{.57} \ln \left(\frac{v^*}{v_0^*} \right). \quad (A75)
 \end{aligned}$$

$$-N = -\left\{ \frac{1}{K} \frac{\partial V^*}{\partial x} y^+ - \frac{1}{K} (\ln y^+ - 2) + 5.5 + 2.3 C_W^{.57} \ln \left(\frac{V^*}{V_0} \right) \right.$$

$$+ \frac{1}{K^2} \left(\frac{\partial V^*}{\partial x} \right)^2 y^+$$

$$\left. + \frac{1}{K} V^* \frac{\partial C_W}{\partial x} (2.3) (.57) C_W^{-0.43} \ln \left(\frac{V^*}{V_0} \right) y^+ \right\} \quad (A76)$$

Combining into equation (A37) we have

$$-\frac{1}{u} \tau_w = 2.3 C_W^{.57} \ln \left(\frac{V^*}{V_0} \right) \left\{ y^+ \frac{\partial V^*}{\partial x} \left[\frac{2}{K} (\ln y^+ - 1) + 2(5.5) \right. \right.$$

$$\left. \left. + 2.3 C_W^{.57} \ln \left(\frac{V^*}{V_0} \right) + \frac{1}{K} \right] \right.$$

$$\left. + V^* y^+ (.57)(2.3) C_W^{-0.43} \ln \frac{V^*}{V_0} \left(\frac{\partial C_W}{\partial x} \right) - \frac{1}{K} \left(\frac{\partial V^*}{\partial x} \right) y^+ \right\}$$

$$+ \frac{(\ln y^+ - 1)}{K} y^+ \left\{ \frac{\partial V^*}{\partial x} - \frac{2}{K} + 2(5.5) + \frac{1}{K} V^* (.57)(2.3) C_W^{-0.43} \ln \left(\frac{V^*}{V_0} \right) \frac{\partial C_W}{\partial x} \right\}$$

$$+ y^+ \frac{\partial v^*}{\partial x} \left\{ \frac{1}{k^2} (\ln y^+)^2 + (5.5)^2 - (2.3)(.57)^{-4.3} \ln \frac{v^*}{v_0} \right\}$$

$$+ (2.3)(.57) C_w^{-4.3} \ln \left(\frac{v^*}{v_0} \right) \frac{\partial C_w}{\partial x} v^* y^+ \left[5.5 - \frac{1}{k} \right]. \quad (A77)$$

Now

$$-\frac{1}{\mu} \tau_w = -\frac{1}{\rho v} \left(\frac{\rho v}{\lambda^2} \right) = -\frac{U^2}{v \lambda^2} \quad (A78)$$

since

$$\tau_w = C_f \left(\frac{1}{2} \rho U^2 \right) \quad (A79)$$

$$\text{and letting } \lambda = \frac{U}{V}, \quad (A80)$$

Recalling equation (A15)

$$v^* = \sqrt{\frac{\tau_w}{\rho}}$$

$$= \sqrt{\frac{1_{20} U^2 C_f}{\rho}}$$

resulting in

$$v^* = U \sqrt{\frac{C_f}{2}}. \quad (A81)$$

from equation (A80)

$$\lambda = \frac{U}{U \sqrt{C_f/2}} = \frac{\sqrt{2}}{C_f} \quad (A82)$$

$$C_f = \frac{2}{\lambda^2}. \quad (A83)$$

Therefore equation (A79) becomes

$$\tau_w = \frac{\rho U}{\lambda^2}. \quad (A84)$$

Also

$$\frac{\partial v^*}{\partial x} = - \frac{U}{\lambda^2} \left(\frac{\partial \lambda}{\partial x} \right). \quad (A85)$$

Substituting equations (A78) and (A85) into equation (A77) and combining terms we have

$$\begin{aligned}
 -\frac{U}{v} = & y^+ \frac{\partial \lambda}{\partial x} \left\{ 2.3 C_w^{.57} \ln\left(\frac{V^*}{V_0}\right) \left[\frac{2}{k} (\ln y^+ - 1) + 2(5.5) \right. \right. \\
 & \left. \left. + 2.3 C_w^{.57} \ln\left(\frac{V^*}{V_0}\right) \right] + \frac{2}{k} (\ln y^+ - 1)(5.5 - \frac{1}{k}) \right. \\
 & \left. + \frac{1}{k^2} (\ln y^+)^2 + (5.5)^2 \right\} \\
 - & y^+ \lambda \frac{\partial C_w}{\partial x} (.57)(2.3) C_w^{-0.43} \ln\left(\frac{V^*}{V_0}\right) \left[1 + \frac{1}{k^2} (\ln y^+ - 1) \right. \\
 & \left. + 5.5 - \frac{1}{k} \right]. \tag{A86}
 \end{aligned}$$

The value of y^+ in equation (A86) is the value of y^+ at the edge of the boundary layer.

Therefore at the edge of the boundary layer we have

$$u = U \tag{A87}$$

and

$$y^+ = \delta^+$$

hence

$$\frac{u^+}{v^*} = \frac{u}{v} = \frac{U}{V} \quad . \quad (A88)$$

Recalling equation (A80) ,

$$\lambda = \frac{U}{V}$$

$$\lambda = \frac{U}{V} = \frac{u^+}{v^*}, \text{ at } y^+ = \delta^+ \quad . \quad (A89)$$

Whence equation (A1) becomes at $y^+ = \delta^+$

$$\lambda = \frac{1}{k} \ln \delta^+ + B + \alpha C_w^\gamma \ln \left(\frac{v^*}{v_0} \right) \quad (A90)$$

where $\alpha = 2.3$ and $\gamma = .5$

and

$$\ln \delta^+ = K\lambda - KB - \left[\ln \left(\frac{v^*}{v_0} \right) \right] \quad K2 \quad (A91)$$

where

$$z = \alpha C_w^{\gamma} \quad (A92)$$

and

$$\delta^+ = e^{K(\lambda-B)} \left[\frac{v^*}{v_0^*} \right]^{-Kz}. \quad (A93)$$

Equation (A86) then becomes

$$\begin{aligned} -\frac{U}{V} &= \delta^+ \left\{ z \ln \frac{v^*}{v_0^*} \left[\frac{2}{K} (\ln \delta^+ - 1) + 2B + z \ln \frac{v^*}{v_0^*} \right] \right. \\ &\quad \left. + \frac{2}{K} (\ln \delta^+ - 1) (B - \frac{1}{K}) + \frac{1}{K^2} (\ln \delta^+)^2 + B^2 \right\} \frac{\partial \lambda}{\partial x} \\ &- \delta^+ \lambda \left\{ \frac{C_w}{C_w^*} \ln \frac{v^*}{v_0^*} \left[1 + \frac{1}{K^2} (\ln \delta^+ - 1) + \frac{1}{K} \right] \right\} \frac{\partial C_w}{\partial x}. \quad (A94) \end{aligned}$$

Multiplying by dx and integrating, we have

$$\begin{aligned} R_e(x) - R_e(x_0) &= \int_{\lambda(x_0)}^{\lambda(x)} \delta^+ \left\{ z \ln \frac{v^*}{v_0^*} \left[\frac{2}{K} (\ln \delta^+ - 1) + 2B + z \ln \frac{v^*}{v_0^*} \right] \right. \\ &\quad \left. + \frac{2}{K} (\ln \delta^+ - 1) (B - \frac{1}{K}) + \frac{1}{K^2} (\ln \delta^+)^2 + B^2 \right\} d\lambda \end{aligned}$$

AD-A103 070

NAVAL UNDERWATER SYSTEMS CENTER NEWPORT RI
AN EXPERIMENTAL STUDY OF POLYMER DRAG REDUCTION AND BOUNDARY LA--ETC(U)

F/6 20/4

UNCLASSIFIED

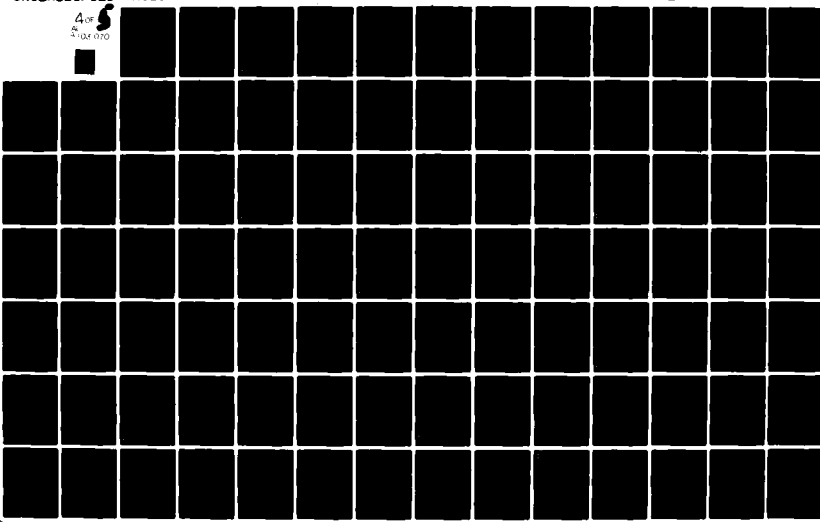
AUG 79

J MIGUEL

NUSC-TD-5656

NL

4 of 5
510X070



$$-\int_{C_w(X_0)}^{C_w(X)} \delta^+ \lambda \left\{ \frac{\gamma z}{C_w} \ln \left(\frac{V^*}{V_0} \right) \left[1 + \frac{1}{K^2} (\ln \delta^+ - 1) + B - \frac{1}{K} \right] \right\} dC_w. \quad (A95)$$

For injection of polymer at or close to the leading edge we may assume $X_0 = 0$, hence $Re(X_0) = 0$ and $C_w(X_0) = C_i$. Equation (A95) is numerically integrated in the flow model described in chapter V.

APPENDIX B

COMPUTER PROGRAM DATAPAC AND SAMPLE LISTING

SEQUENCED LISTING

PROGRAM DATBAC

```

OVERLAY(98)
COMMON/A098/M,N,S,KMALL,KBLAS
COMMON/IOVER/IENO,IPASS
COMMON_YLAM(L1,L2),XC(L1,L2)
COMMON CI,GI,UI,CW,SLOT
COMMON DELTA,DELTA1,DELTA2,XYDTA1,H12,H12,TENT,LI,UF,VH,NPLOT,EE
10ELT4,REDELTA1,REDELTA2,REHYOIA,REX,UF5,XIN
COMMON IF,I1I01,NCASE(I1I01,NYCHAR(I1I01,NYCHAR(I1I01,NCASE(I1I01
120),I(31)
COMMON XAX(9,121,YAX(9,121),TITLE(9,121,CHARAC(12,201
COMMON AETA(-8,2),DUUTAU(31,2),REYL(31,2),U(31,2),UPLUS(31,2),URA
ITTD,L,21,URATD(31,21,Y(31,21,XDELT1(I1,21,XDELT1(I1,21,YDELT1(I1,21
22,Y(31,21),VPLUSL(31,2)
COMMON_CCH(31,2)
DIMENSION CNU(31),O1(31),O2(31),O3(31),FREQ(31),REY(31),TX(31),UM
14311,URATIO2(31),U2(31),U3(31),X(31),XF(31),YM(31),YM(31),YY(31),Y2
2(31),NNN(12,2),YMM(31,2),YPLUS(31,2)
DIMENSION CONC(31),Z(31),FLW(31)
DIMENSION WCCH(31),WY(31)
REAL_LAMBDA
REWIND 1
IF(IPASS.EQ.1) GO TO 30
IPASS=1
READ 10,KBLAS,KMALL
READ 10,NPLOT,NCH,(NCASE(I),I=1,11)
10 FORMAT(1I15)
READ 20,(IFMT(IJK),JK=1,10)
20 FORMAT(1CA8)
READ IFMT,(URATIO(I,2),I=1,KBLAS)
READ IFMT,(LAET(I,2),I=1,KBLAS)
READ 30,(VPLUSL(I,2),I=1,KMALL)
READ 30,(UPLUS(I,2),I=1,KMALL)
30 FORMAT(6F10.5)
DO -D K1,NPLOT
    READ 50,(XAX(JK,K),JK=1,9),NYCHAR(K)
    READ 50,(YAX(JK,K),JK=1,9),NYCHAR(K)
    50 READ 50,(TITLE(JK,K),JK=1,9),NTCHAR(K)
    50 FORMAT(19A3,1B3)
    DO 60 K=1,NCH
    60 READ 50,(CHARAC(JK,K),JK=1,9),NCHAR(K)
    READ 70,M,N,S
    70 FORMAT(1I10,5)
    SLOT=S
    80 READ 90,IDENT,CI,O1
    90 FORMAT (8,-X,2F10.5)
    IF (IDENT=01790) Z90=100
    100 CONTINUE
    M=1
    IF(IQI.LE.1.E-10) GO TO 170
    J=1
    110 READ 120,CONC(J),YC(J,MN),OUM,XC,IC,ISTOP
    120 FORMAT(4E13.3,1I2,15)
    IF(ISTOP.GT.J) GO TO 130
    J=J+1
    GO TO 110
    130 JCNC=J
    CW=CONC(1)
    CONC=CW/C1

```

```

00 1>0 K=1,JCONC          000056
140 CCW(K,MN)=CONC(K1,MN) 000055
00 150 K=1,JCONC          000056
 35K
    IF(CCW(K,MN).GE.0.5) GO TO 160 000056
150 CONTINUE                1000149
160 N2=M-2                  300060
  NPLOT=11                  000061
  GO TO 180                  0003062
170 NPLOT=9                  100061
180 I=1                      000061
190 READ 200,Y(I,MN),V(I,I),FREQ(I,I),X(I,I),T(I,I),FLOW(I,I) 000075
200 FORMAT(8F10.3)           000356
  IF(T(I).LE.EL=101.GO TO 210 1000147
  I=I+1                      000068
  GO TO 190                  1000149
210 CONTINUE                1000070
  QFLOW=FLCH(I),             000071
  QVOL=QFLOW*8.33/(60.*62.+) 000072
  N=L-1                      000073
  30 730 LL=1,NPLOT          000074
  1C3MGASE(I,LL)            100075
  30 780 NM=1,MN              000076
  IF((NM.EQ.2 .AND. _KBLAS.NE.0) .AND. LL.EQ.6) GO TO 750 100077
  IF((NM.EQ.2 .AND. _KHALL.NE.0) .AND. LL.EQ.7) GO TO 760 100078
  IF(LL.NE.1) GO TO 770      100079
  VFS=V(1)                   000083
  UFS=FREQ(I,I)*VFS         100081
  UFSM=UFS*12.*2.3**.01     000082
  SF=S/12.                     200083
  ASLOT=S**4                  000084
  ASLOTF=ASLOT/144.           100085
  UI=OI*.0810237/(ASLOT*12.*50.) 100086
  30 223 J=1,N
    CNU(I,J)=3.60901355E-05-(7.17973811E-07)*(T(J))+(7.15890612E-0 100087
    31*(T(J)**2)-(3.30477156E-11)*(T(J)**3)+(6.62377978E-14)*(T(J)**4) 100088A
  2   JI=46
    U(I,MN)=FREQ(JI)*V(JI) 100088
    URATIO(I,J,MN)=U(I,MN)/UFS 100089
  220 CONTINUE                100089
  30 230 K=1,N
    IF(URATIO(K,MN)<.99) 240,240,230 100092
  230 CONTINUE                000093
  240  DELTA=V(K-1,MN)        100094
  J=N+1
  30 250 J=1,N
    L=J+1
    Y2(N)=Y(L,MN)           100095
    U2(M)=U(L,MN)           100100
    URATIO2(M)=URATIO(L,MN) 100101
  250 CONTINUE                100102
  30 260 J=1,N
    Y(I,MN)=Y2(I)           100103
    U(I,MN)=U2(I)           100105
    URATIO(I,MN)=URATIO2(I) 100106
    UM(I)=U(I,MN)*12.92*54**.01 100107
    YM(I)=Y(I,MN)*2.54       100108
    REY(I)=UFS*Y(I,MN)/(12.92*UM(I)) 100109
    REYL(I,MN)=ALCG10(REY(I)) 100110
  260 CONTINUE                100111
    J1(1)=1
    J2(1)=1,E=10

```

```

03(I)=1.2=10 000114
00 220 L=2,N 000115
01(I)=(1.-URATIO(L,MN)) 000116
22(I)=URATIO(L,MN)*(1.-URATIO(L,MN)) 000117
33(I)=URATIO(L,MN)*(1.-(URATIO(L,MN)**2.)) 000118
270 GOMINUE 000119
00 280 L=2,N 000120
YY(1)=Y(I,MN) 000121
280 CONTINUE 000122
YY(1)=1.2=10 000123
00 290 L=1,4 000124
MCCM1=CCM(M2,MN) 000125
YY(I)=YC(M2,MN) 000126
290 M2=M2+1 000127
CALL INTEGRAL(N,YY,01,DELTAA)
CALL INTEGRAL(N,YY,02,DELTAB)
CALL INTEGRAL(N,YY,03,DELTAC)
00 300 TRL,N
YDELTAA(I,MN)=Y(I,MN)/DELTAA 000128
YDELTAB(I,MN)=Y(I,MN)/DELTAB 000129
YDELTAC(I,MN)=Y(I,MN)/DELTAC 000130
DELTADZ(MMN)=YDELTAA(I,MN)*1.7 000131
300 CONTINUE 000132
AREA=(M2*H1/1.4) 000133
UAVG=QVOL/AREA 000134
UAVGM=UAVG*12.42*0.01 000135
PERIM=((2.*H1+(2.*W1))/12. 000136
HYCIA=4.*AREA/PERIM 000137
HYDIA=HYCIA*.304 000138
H12=DELTAA/DELTAB 000139
H32=DELTAB/DELTAC 000140
REX=UFS*X(I)/(CNU(I)*12.*L 000141
REHALF=UFS*(H/24.)/CNU(I) 000142
REDELTAA=UFS*DELTAA/CNU(I) 000143
REDELTAB=UFS*DELTAB/CNU(I) 000144
REDELTAC=UFS*DELTAC/CNU(I) 000145
REHVOIA=UAVG*HYDIA/CNU(I) 000146
CFW=0.459/( ALOG(0.03*REX)**2.) 000147
DELTAA=DELTAA*2.54 000148
DELTAB=DELTAB*2.54 000149
DELTAC=DELTAC*2.54 000150
XIN=X(I)
XH=XIN*2.54 000151
00 310 I=1,N 000152
YM(I)=Y(I,MN)/12. 000153
XF(I)=X(I)/12. 000154
AETA(I,MN)=YM(I)*SGRT(UFS/ICNU(I)*XF(I).I) 000155
310 CONTINUE 000156
00 320 I=1,N 000157
UTAU=UFS*SORT(CFW/2.)
QUUTAU(L,MN)=UFS*U(I,MN)/UTAU 000158
UPLUS(I,MN)=U(I,MN)/UTAU 000159
YPLUS(I,MN)=Y(I,MN)*UTAU/(12.*CNU(I)) 000160
YPLUSL(I,MN)=ALOG10(YPLUS(I,MN)) 000161
YMH(I,MN)=Y(I,MN)/(H*.5) 000162
320 CONTINUE 000163
IF(01.LE.1.2=10) GO TO 340 000164
CALL POLY(LAMBDA,WCCH,4Y,2) 000165
00 330 I=1,JCONC 000166
YLAM(I,MN)=YC(I,MN)/LAMBDA 000167
340 PRINT 350,IDENT 000168

```

```

380 FORMAT(1M1.20H TEST NUMBER ,I5) 000175
PRINT 380,XIN,XM 000177
PRINT 500, UFS,UF5M 000178
PRINT 510,UAVG,UAVGM 000179
PRINT 370,DELTA1,DELTA1M 000180
PRINT 380,DELTA1,DELTA1M 000181
PRINT 390,DELTA2,DELTA2M 000182
PRINT 400,DELTA1,DELTA1M 000183
PRINT 520,MYOIA ,MYOIAM 000184
PRINT 610,M12 000185
PRINT -20,M32 000186
PRINT 630,REX 000187
PRINT 560,REHALF 000188
PRINT 530,REHYOIA 000189
PRINT 460,REDELT A 000190
PRINT 460,REDELT A 000191
PRINT -60,REDELT A2 000192
PRINT 480,T(1) 000193
PRINT 490,CWU(1) 000194
PRINT 530,CFFW 000195
C UTAU IS BASED ON FRANK WHITE'S FORMULA 000196
PRINT 560,UTAU 000198
PRINT 570,CI 000199
PRINT 580,QI 000200
PRINT 510,QFLOW 000201
PRINT 620,QVOL 000202
PRINT 590,UVI 000203
PRINT 600,S 000204
PRINT 630,CW 000205
PRINT 540,CWC1 000206
PRINT 550,LAMBOA 000207
360 FORMAT (1X,11H X= ,F9.3,-M IN.,F9.3,-M CM.) 000208
370 FORMAT (1X,11H DELTA = ,F9.3,-M IN.,F9.3,-M CM.) 000209
380 FORMAT (1X,11H DELTA1 = ,F9.3,-M IN.,F9.3,-M CM.) 000210
390 FORMAT (1X,11H DELTA2 = ,F9.3,-M IN.,F9.3,-M CM.) 000211
400 FORMAT (1X,11H DELTA3 = ,F9.3,-M IN.,F9.3,-M CM.) 000212
-10 FORMAT (1X,11H M12 = ,F9.3) 000213
-20 FORMAT (1X,11H M32 = ,F9.3) 000214
-30 FORMAT (1X,11H REX = ,F9.0) 000215
-40 FORMAT (1X,11H REDELT A = ,F9.0) 000216
-50 FORMAT (1X,11H REDELT A1 = ,F9.0) 000217
-60 FORMAT (1X,11H REDELT A2 = ,F9.0) 000218
-70 FORMAT (1X,11H TEMP = ,F9.3) 000219
-80 FORMAT (1X,11H T WALL = ,F9.3) 000220
-90 FORMAT (1X,11H NU = ,F9.3) 000221
500 FORMAT (1X,11H UFS = ,F9.2,-M FT/SEC ,F9.3,-M M/SEC ) 000222
510 FORMAT (1X,11H UAVG = ,F9.3,-M FT/SEC ,F9.3,-M M/SEC ) 000223
520 FORMAT (1X,11H HYOIA = ,F9.3,-M FT.,F9.3,-M M.) 000224
530 FORMAT (1X,11H REHYOIA = ,F9.1) 000225
540 FORMAT (1X,11H REHALF = ,F9.0) 000226
550 FORMAT (1X,11H CF = ,F9.0) 000227
560 FORMAT (1X,11H UTAUPW = ,F9.0) 000228
570 FORMAT (1X,11H CONC_IN = ,F9.2,-M PPM) 000229
580 FORMAT (1X,11H POLYFLOW = ,F9.2,-M CC/MIN) 000230
590 FORMAT (1X,11H POLY_UIN = ,F9.4,-M FT/SEC) 000231
600 FORMAT (1X,11H SLOT = ,F9.4,-M IN) 000232
610 FORMAT (1X,11H QFLOW = ,F9.3,-M PPM) 000233
620 FORMAT (1X,11H QVOL = ,F9.3,-M FT3/SEC) 000234
630 FORMAT (1X,11H CHALL = ,F9.2,-M PPM) 000235
640 FORMAT (1X,11H CW/CI = ,F9.0) 000236
650 FORMAT (1X,11H LAMBOA = ,F9.0) 000237

```

```

PRINT 350,IDENT
PRINT 662
660 FORMAT(//, Y(IN.) Y(CH.) U(FT/S) U(M/S) U/UFS Y/
DELTA Y/DELTA2 REY LOG REY Y/DELTA1 LET1 XIN 1
2 Z(IN,1)*1
DO 670 I=1,N
670 PRINT 680,Y(I,NM),YH(I),U(I,NM),UN(I),URATIO(I,NM),YOELTA1(I,M
1 MH, YOELTAZ(I,MH),REYLIT,MH),YOELTA11(MH,LET1,MH),YI
2 IJ,Z(I)
END FORMAT(1X,1F10.3)
PRINT 680
680 FORMAT(//, Y(CLIN) Y/DELTA U/UFS (S/7) UPLUS
1YPLUS DEL UTAU Y/HALFH LOG(YPLUS)/)
DO 710 I=1,N
PRINT 700,Y(I,NM),YOELTA1(NM),URATIO(I,NM),URATIO7(I,NM),U
1 PLUS(I,NM),YPLUS(I,MH),QWHTQWHT(MH),YHM(I,MH),YPLUS(I,MH)
700 FORMAT(1X,3F10.3)
710 CONTINUE
PRINT 720
720 FORMAT(//, Y(CLIN) CONCPRM1 C/C Y/L,MHD1 YC7/1
DO 730 J=1,JCONC
730 PRINT 740,YC11,MH,CONC11,CCH11,MH,Y14Y1,MH,YC
740 FORMAT(1X,3F10.3)
GO TO 770
750 NNN(LL,MH)*KBLAS
GO TO 780
760 NNN(LL,MH)*KHALL
GO TO 780
770 NNN(LL,MH)*N
IF(LL.EQ.10 .OR. LL.EQ.11) NNM(LL,MH)*JCINC
780 CONTINUE
CALL PNPLOT(NNN)
CNC0.
CNCL0.
QIS0.
IIS0.
REWNO 1
GO TO 880
790 CONTINUE
END*99
880 CONTINUE
END

```

RESEQUENCED LISTING

```

510B,W3330,T2,CATARAC1,T-2,PRGRM,OVERLAY,SCB=10,CLASS=AC,B,M,T2T,GSBT,DAT1,TA
1C1,31,TG,3G,4LL1,A,M,I2TAGS83,DATAPAC1,01,TG,06,1280,710,771230,,S 100000
2,3211,C,M,TAIG1,I2TAGS83,DATARAC1,01,TG,01,0,4,PLCB,MASTER,LIBRARY,
3C2,****,I) 3,M,POIR,MASTER,LIBRARY= DIRECTORY,G2,****,I) L,XJ 100000
PROGRAM MAIN 100000
OVERLAY(C) 100002
COMMON/ABSA/CH1,S,KHALL,XBL15 100003
COMMON/IOVER/IEND,IPASS 100004
IENDFL 100005
IPASS#0 100006
10 CONTINUE 100007
CALL UFORVER(98,4HTAG1) 000303
IE(IEND,F2,331 GO TO 27 111423
CALL UFORVER(99,4HTAG1) 1003010
GO TO 10 100011
20 CONTINUE 100012
END 111311

```

RESEQUENCED LISTING

```

      DATA (IND(I),I=1,20)/0.,+3.3+0.5+3,1.3,1,2+3/
      DATA (XNUM(I),I=1,3)/3+2.425/, (XNUM(I),I=4,10)/5+4,773/, (XNUM(I),
      I=11,15)/5+6.675/, (XNUM(I),I=16,20)/5+6.675/
      P(1)=IDENT
      P(2)=XIN
      P(3)=WFS
      P(4)=T(I)
      P(5)=REHYDIA
      P(6)=REX
      P(7)=Z1REHYDIA
      P(8)=REDELTA
      P(9)=REDELTA1
      P(10)=REDLT12
      P(11)=OELTA
      P(12)=OELTA1
      P(13)=OELTA2
      P(14)=M12
      P(15)=M32
      P(16)=CI
      P(17)=QI
      P(18)=CW
      P(19)=AUI
      P(20)=S
      DO 11 I=1,NPLOT
      *C=MCASE(I)
      DO 11 M=1,NC
      ISZ=IZ(I,M)
      20 10 J=1,ISZ
      PL(J,I,M)=U(J,M)
      Q1(J,1,M)=Y(J,M)
      P1(J,2,M)=YDELTA1(J,M)
      Q1(J,2,M)=URATIO(J,M)
      P1(J,3,M)=YDELTA1(J,M)
      Q1(J,3,M)=URATIO(J,M)
      P1(J,4,M)=YDELTA2(J,M)
      Q1(J,4,M)=URATIO(J,M)
      P1(J,5,M)=REYL(J,M)
      Q1(J,5,M)=URATIO(J,M)
      P1(J,6,M)=URATIO(J,M)
      Q1(J,6,M)=AETA(J,M)
      P1(J,7,M)=YPLUS(J,M)
      Q1(J,7,M)=YPLUS(J,M)
      P1(J,8,M)=YDELTA(J,M)
      Q1(J,8,M)=YOUTAU(J,M)
      P1(J,9,1)=URATIO(J,1)
      P1(J,9,2)=URATIO(J,1)
      Q1(J,9,1)=YDELTA(J,1)
      P1(J,10,M)=CCW(J,M)
      Q1(J,10,M)=YCC(J,M)
      P1(J,11,M)=CCW(J,M)
      Q1(J,11,M)=YLAH(J,M)
      10 CONTINUE
      DO 20 I=1,NCM
      20 YNUM(I)=YCL(I)
      WRITE(1,70) NPLOT
      DO 60 I=1,NPLOT
      *C=MCASE(I)
      30 30 M=1,NC
      30 IPZ(M)=IZ(I,M)
      XNTCHAR=XNTCHAR(I)
      XC=.5*(XB1(I)-MGT*XNTCHAR)
      YC=1.625

```

```

      WRITE(1,40) FACT(I),XGRID(I),YGRID(I)          300111
      WRITE(1,70) XLABEL(I),YLABEL(I),GRDX(I),GRDY(I),NLCC 300112
  1  Y(I),NLGZ(I),LGRDX(I),LGRDY(I)              300112
      IF(LABEL(I),EQ,0) GO TO 50                  300113
  30  DO 40 J=1,NCN                            300114
      WRITE(1,901) XC1(I,J),YC1(I,J),XNUM(I,J),YNUM(I,J) 300115
      WRITE(1,1001) (CHARC(IJK,J),JK=1,9),NCHAR(J)       300116
  40  WRITE(1,1101) P(I),HG(I),NL(I)                300117
  50  CONTINUE                                     300118
      WRITE(1,1201) MCASE(I),NYT(I),NYT(I),HG(I)        300119
      WRITE(1,130) PX(I),PY(I),XAXL(I),YAXL(I),XUNIT(I),YUNIT(I),XCF( 300120
  1  I,I,YOELI)
      WRITE(1,130) XEND(I),YEND(I),XB1(I),XB2(I),YB1(I),YB2(I),XC,YC 300121
      WRITE(1,1401) (XAX(L,I),L=1,9),NCHAR(I)           300122
      WRITE(1,1400) (YAX(L,I),L=1,9),NCHAR(I)           300123
      WRITE(1,1401) (TITLE(L,I),L=1,3),NTCHAR(I)         300124
      WRITE(1,150) (KSYM(I,M),M=1,MC)                 300125
      WRITE(1,150) (IZ(I,L),L=1,ISZ)                  300126
      WRITE(1,150) (IPZ(I),L=1,MC)                   300127
      WRITE(1,160) (IEH(I,L),L=1,10)                  300128
  60  DO 60 M=1,MC                            300129
      ISZ=IZ(I,M)
      WRITE(1,IFMT) (P(I,J,M),J=1,ISZ)               300130
      WRITE(1,IFMT) (Q(I,J,M),J=1,ISZ)               300131
      IF(KSYM(I,M).EQ.0) GO TO 60                  300132
      WRITE(1,I=M) NSYM(I,M),NSINTL,M               300133
  60  CONTINUE                                     300134
  70  FORMAT(9I5)                                300135
  80  FORMAT(3F10.5)                            300136
  90  FORMAT(4F10.5)                            300137
 100  FORMAT(9A8,I3)                           300138
 110  FORMAT(F12.5,F10.5,I5)                   300139
 120  FORMAT(3I5,F3.3)                          300140
 130  FORMAT(4F10.3)                           300141
 140  FORMAT(9,I5,F3.3)                         300142
 150  FORMAT(16I5)                            300143
 160  FORMAT(10A8)                            300144
      RETURN
      END                                         300145

```

INPUT LISTING

```

SUBROUTINE INTEGRAL(NGATA1,XDATA,YDATA,SUM)
DOUBLE PRECISION A,B
DIMENSION A(4,3,11),B(3,11),REA(29,29),AV(29)
DIMENSION XDATA(31),YDATA(31)
K=0
K1=0
NOATA1=NOATA2=1
DO 10 I=1,3
K1=K1+1
A(I,1)=XDATA(K1)**2
A(I,2)=XDATA(K1)
A(I,3)=1
10 A(I,:)=YDATA(K1)
K1=K1+2
CALL GAUSJ(A,3,:)
K=K+1
DO 20 I=1,3
20 A(I,:)=A(I,:)/I
KP1=K
KP2=KP1+1
AREA(KP1,K1=8(1,1)+(XDATA(KP2)**2-XDATA(KP1)**2)*3/7.+6(2,11)*(XDATA(KP2)**2-XDATA(KP1)**2)/2.+8(3,1)*(XDATA(KP2)-XDATA(KP1)))
30 KP1=KP1+1
IF(K.LT.NOATA2) GO TO 1
DO 50 I=2,K
50 AV(I)=(AREA(I,I-1)+AREA(I,I))*5
AV(1)=REA(1,1)
AV(NOATA1)=AREA(NOATA1,NOATA2)
SUM=0.
DO 60 I=1,NOATA1
60 SUM=SUM+AV(I)
RETURN
END
END CARD DETECTED

```

RESEQUENCED LISTING

```

SUBROUTINE INTEGRAL (NOATA1,XDATA1,YDATA1,SUM)
DOUBLE PRECISION A,B
DIMENSION A(6,-31,31),B(3,11),AREA1(29,29),X(129)
DIMENSION XDATA1(31),YDATA1(31)
KAO
K1=0
NOATA1=XDATA1-1
NOATA2=NOATA1-2
10 DO 20 I=1,3
   K1=K1+1
   A(I,1)=XDATA1(K1)
   B(I,1)=YDATA1(K1)
20 A(I,:)=YDATA1(K1)
   K1=K1+2
   CALL GAUSJ(A,3,:)
   KPK=1
   DO 30 I=1,3
30 B(I,1)=A(I,KPK)
   KPK=KPK+1
   DO 40 I=1,2
40 B(I,2)=KPK+1
   AREA1(KPK,1)=B(1,1)*(XDATA1(KP2)**3-XDATA1(KP1)**3)+B(2,1)*(XDATA1(KP2)**2-XDATA1(KP1)**2)/2.+B(3,1)*(XDATA1(KP2)-XDATA1(KP1))
   40 KPK=KPK+1
   IF(KPK.LT.NOATA2) GO TO 10
   50 SJ,I=2,K
   AV(I)=(AREA1(I,I-1)+AREA1(I,I))/5.
   AV(1)=AREA1(1,1)
   AV(NOATA1)=AREA1(NOATA1,NOATA2)
   SUM=0.
   DO 60 I=1,NOATA1
60 SUM=SUM+AV(I)
   RETURN
END

```

RESEQUENCED LISTING

SUBROUTINE POLY(8,X,Y,NK)	101051
DOUBLE PRECISION A	000002
DIMENSION_1(4,5),X(31),Y(31)	101003
K=3	003004
CO_10_I=1,3	102005
K=K+1	000006
A(I,1)=X(K)**3	101007
A(I,2)=X(K)**2	003008
A(I,3)=X(K)	101009
I(I,+)=1.	000010
10 A(I,3)=Y(K)	102011
CALL GAUSJ(A,4,5)	300012
GQ_T3_(20,30),NK	000013
20 X2=X(2)/2.	103014
P=A(I,5)**X2**3+A(2,5)**X2**2+A(3,5)**X2+A(4,5)	103015
B=A(2,5)*(P-Y(1))/(X2-Y(1))	300016
GQ_T3_=0	103017
30 B=A(I,5)**3+A(2,5)**3**2+A(3,5)**3+A(4,5)	103018
-0 RETURN	102019
END	000020

SEQUENCED LISTING

SUBROUTINE GAUS1(M,N,NP1)	100001
DOUBLE PRECISION M	100002
DIMENSION M(1:N)	100003
DO 10 I=1,N	000004
XXAKS1	100005
DO 13 J=K,NP1	000006
M(K,J)=M(K,J)/M(K,K)	100007
DO 10 I=1,N	000008
IF (K=I) GO TO 10	100009
M(I,J)=M(I,J)-M(I,K)*M(K,J)	000010
10 CONTINUE	000011
RETURN	100012
END	100013

SEQUENCED LISTING

PROGRAM PLOTIN	000001
OVERLAY (93)	133002
COMMON/LCVERA/ENO,IPASS	000003
COMMON/G/PX,PY	000004
COMMON/KSYM/ISZ(16),KSYM(16)	000005
COMMON/SIM/XLIM1(12),XLIM2(12),YLIM1(12),YLIM2(12),KML	101006
COMMON/LLOG/LOGY,YAX,XAX,NCHAR,NLOG1,NLOG2,LGRIDX,LGRIDY	000007
DIMENSION ISZ(16),IPZ(16),KSYM(16)	000008
DIMENSION XAX(49),YAX(49),TITLE(69),LIM(69)	000009
C...NPLT IS THE NUMBER OF SEPARATE PLOTS	000010
C...FACT IS A FACTOR BY WHICH THE ENTIRE PLOT IS TO BE MULTIBLED	100011
C...XGRID,YGRID ARE THE GRID WIDTHS	101012
C...KLABEL INDICATES WHETHER SPECIFIC VALUES OF XAX/NYL ARE TO BE DRAWN	100013
C...ON THE PLOT	000014
C...NLABEL IS THE NUMBER OF LABELED VARIABLES	000015
C...IF KGRID = 1, A GRID WILL BE PLOTTED	000016
C...NLGDX IS THE HIGHEST POWER OF THE LOG-X-AXIS	102017
C...NLGDL IS THE LOWEST POWER OF THE LOG-X-AXIS	000018
C...NLGDY IS THE HIGHEST POWER OF THE LOG-Y-AXIS	000019
C...NLGDL IS THE LOWEST POWER OF THE LOG-Y-AXIS	000020
C...LGRIDX,LGRIDY INDICATE WHETHER LOG GRIDS ARE TO BE DRAWN	100021
C...MCASE=NUMBER OF FIGURES ON THE PLOT	000022
C...NXT,NYT ARE NUMBER OF TICK MARKS	000023
C...HGT=HEIGHT OF THE CHARACTERS TO BE PRINTED IN TITLE	000024
C...PX,PY ARE BEGINNING COORDINATES OF THE AXES	111025
C...XAXL,YAXL ARE THE AXIS LENGTHS IN INCHES	000026
C...XUNIT,YUNIT ARE THE SCALED LENGTHS OF THE AXES	100027
C...XOF,YOF ARE THE OFFSETS	000028
C...XEND,YEND ARE THE COORDINATES OF ENPLT	100029
C...XB1,XB2,YB1,YB2 ARE THE BORDER LENGTHS IN INCHES	000030
C...XG,YC ARE THE BEGINNING COORDINATES OF THE TITLE	100031
C...XAX IS THE TITLE OF THE X-AXIS	000032
C...NCHAR IS THE NUMBER OF CHARACTERS IN XAX	102033
C...YAX IS THE TITLE OF THE Y-AXIS	000034
C...NCHAR IS THE NUMBER OF CHARACTERS IN YAX	100035
C...TITLE IS THE TITLE OF THE PLOT	000036
C...NCHAR IS THE NUMBER OF CHARACTERS IN THE TITLE	100037
C...KSYM=1 INDICATES THAT SYMBOLS AND LINES ARE TO BE PLOTTED	000038
C...KSYM=2 INDICATES THAT ONLY SYMBOLS ARE TO BE PLOTTED	100039
C...ISZ IS THE NUMBER OF POINTS TO BE READ	100040
C...IPZ IS THE NUMBER OF POINTS TO BE PLOTTED	200041
C...IFMT IS THE FORMAT OF THE X,Y DATA TO BE READ	100042
CALL PLOTS(0,0,10)	100043
READ(1,20) NPLT	000044
DO 110 KLM=N1,NPLT	100045
KML=LML	100046
READ(1,101) FACT,XGRID,YGRID	100047
10 FORMAT(3F10.5)	200048
CALL FACT(FACT)	100049
READ(1,20) KLABEL,NLABEL,KGRID,NLGDX,NLOG1,NLOGY,NLG2,LGRIDX, L	100050
1 GRIDY	000050
20 FORMAT(9I9)	000051
IF(KLABEL.EQ.1) CALL LABEL(NLABEL)	200052
READ(1,30) MCASE,NXT,NYT,HGT	101053
30 FORMAT(3I5,F5.3)	200054
READ(1,-0) PX,PY,XAXL,YAXL,XUNIT,YUNIT,XOF,YOF	000055
READ(1,-0) XEND,YEND,XB1,XB2,YB1,YB2,XG,YC	101056
40 FORMAT(8F10.5)	100057
READ(1,50) (XAX(I),I=1,9),NCHAR	100058

```

      READ(1,30) (YAX(L),L=1,9),NYCHAR          300059
      READ(1,31) (TITLE(L),L=1,31,NCHAR)          300060
  50 FORMAT(9A8,1D)
  51 FORMAT(1H)
  52 FORMAT(1H)
      READ(1,60) (KSYM(L),L=1,M)               300063
      READ(1,60) (ISZ(L),L=1,M)                 300064
      READ(1,60) (IPZ(L),L=1,M)                 300065
  60 FORMAT(16I5)
      READ(1,70) (IFMT(L),L=1,10)               300067
  70 FORMAT(10A4)
      XLIM1(KLN)=XOF                           300069
      XLIM2(KLN)=XUNIT+XOF,0.001              300070
      YLIM1(KLN)=YOF                           300071
      YLIM2(KLN)=YUNIT+YOF,0.001              300072
      CALL PLOT(X82,Y81,3)                      300073
      CALL PLOT(X81,Y81,2)                      300074
      CALL PLOT(X82,Y82,2)                      300075
      CALL PLOT(X82,Y82,2)                      300076
      CALL PLOT(X82,Y81,2)                      300077
      IF(KGRID.EQ.11) CALL GRID(XAXL,YAXL,XGRID,YGRID) 300078
      CALL CHAR(XC,YC,0.,HGT,TITLE,NTCHAR)       300079
      IF(NLOGX.NE.0) CALL LOGAXS(NLOGX,PX,PY,XAXL,YAXL) 300080
  80 1 X,NXCHAR,NLOG1)                         300080
      XSF=XAXL/XUNIT                          300081
      YSF=YAXL/YUNIT                          300082
      CALL PLOT(PX,PY,-3)                      300083
      CALL OFFST(XOF,YOF,1)                     300084
      CALL SCALE(XSF,YSF,1)                     300085
      IF(INLOGX.NE.0) GO TO 80                300086
      CALL AXIS(0.,0.,XAX,NXCHAR,XAXL,NXT,1,0,1) 300087
  80  IF(INLOGY.NE.0) GO TO 90                300088
      CALL AXIS(0.,0.,YAX,NYCHAR,YAXL,NYT,0,1,16*19/2) 300089
  90  DO 100 J=1,M                            300090
      ISZ(J)
      IZ=IPZ(J)
      READ(1,IPMT) (U(I,J),I=1,N)             300093
      READ(1,IPMT) (V(I,J),I=1,N)             300094
      KSYM9=KSYM(J)
      IF(KSYM9.EQ.0) CALL SYM8CM(IZ,J)        300095
      IF(KSYM9.EQ.2) GO TO 100                300097
      CALL PLOT(U(1,J),V(1,J),3)              300098
  100  DO 100 I=1,IZ
          IF(U(I,J).LT.XLIM1(KLN)) OR. U(I,J).GT.XLIM2(KLN)) GO TO 300100
  100  100  IF(V(I,J).LT.YLIM1(KLN)) OR. V(I,J).GT.YLIM2(KLN)) GO TO 300101
  100  100  CALL PLOT(U(I,J),V(I,J),2)        300102
  100  CONTINUE
      CALL RESET
  110  CALL PLOT(XEND,YEND,-3)
      CALL RESET
      CALL ENPLT(XEND,YEND)
  END

```

-RESEQUENCED LISTING-

RESEQUENCED LISTING

SUBROUTINE LABELINI	100001
... XC, YC ARE THE BEGINNING COORDINATES OF THE VARIABLES	000002
... XNUM, YNUM ARE THE BEGINNING COORDINATES OF THE NUMBERS	100003
... CHARAC IS THE ALPHABETIC CHARACTERS	100004
... NCHAR IS THE NUMBER OF CHARACTERS IN CHARAC	000005
... VALUE IS THE VALUE OF THE VARIABLE	100006
... HGT IS THE HEIGHT OF THE CHARACTERS	000007
... NO IS THE NUMBER OF DIGITS TO THE RIGHT OF THE DECIMAL POINT	100008
... DIMENSION CHARAC(9)	100009
DO 40 I=1,N	000010
2540(I,1,10) XC, YC, XNUM, YNUM	100011
10 FORMAT(4F10.5)	100012
READ(I,20) (CHARAC(I,J),J=1,9),NCHAR	100013
20 FORMAT(9A8,I8)	000014
READ(I,30) VALUE,HGT,NO	000015
30 FORMAT(F12.5,F10.5,I3)	000016
CALL CHAR(XC,YC,0.,HGT,CHARAC,NCHAR)	000017
40 CALL NUMPLT(XNUM,YNUM,0.,HGT,VALUE,NO)	100018
RETURN	100019
END	000020

RESEQUENCED LISTING

<u>SUBROUTINE SYMBOML7,J1</u>	100001
C...NSYM IS THE SYMBOL	000002
C...XSINT IS THE INTERVAL AT WHICH SYMBOLS ARE TO BE PLOTTED	100217
C...H IS THE HEIGHT OF THE SYMBOLS	000004
COMMON/SYM/U(50,-2),V(50,-2)	000005
COMMON/SIM/XLIN1(12),XLIN2(12),YLIN1(12),YLIN2(12),KML	000306
READ(1,101)NSYM,XSINT,H	102227
10 FORMAT(1A5,15,F5.3)	100008
100 20 I1,I2,XSINT	100009
IF(U(I1,J1).LT.XLIN1(KML)) .OR. U(I1,J1).GT.XLIN2(KML)) GO TO 20	000010
IF(V(I1,J1).LT.YLIN1(KML)) .OR. V(I1,J1).GT.YLIN2(KML)) GO TO 20	100011
CALL VECTOR(U(I1,J1),V(I1,J1),I1,I,-1,NSYM)	000012
20 CONTINUE	100013
RETURN	000014
END	100015

RESEQUENCED LISTING

```

SUBROUTINE LOGAXIS(NLOGX,PX,PY,XAXL,XAX,NCHAR,NLOG)
COMMON/LCG/NLOG,YAXL,YAX,NYCHAR,NLOG2,LGRIDX,LGRIDY
DIMENSION TAX(91),LOG(10)
DIMENSION XLOG(10),IX(1),XAX(9)
C...PRINT X-AXIS POWERS OF 10
PX=X=PX
PY=Y=PY
IF(NLOGX.EQ.0) GO TO 70
XAX=PX*XAXL
CALL PLOT(PX,PY,3)
CALL PLOT(IXAX,PY,2)
PXX=PX
PY3=PY
PX=PX-.1
PY=PY-.25
X1=X*XL+1.E-5
NL0G=NLOG12**.2
XNLOG=XLOG-XLOG1
XZ=XL/XNLOG
PX2=PX+.25
PY2=PY+.07
IF(NLOG1.LT.10) NL=1
IF(NLOG1.GE.10) NL=2
CALL CHAR(PX,PY,0.,.10,2H10,2)
CALL CHAR(PX2,PY2,0.,.07,NLOG,NL)
NL0G1=NLOG1+1
GO 10 I=NLOGX1,NLOGX
IF(I.LT.10) NL=1
IF(I.GE.10) NL=2
IX(1)=I*2**42
PX=PX+X2
X2=PX+.25
CALL CHAR(PX,PY,0.,.10,2H10,2)
10 CALL CHAR(PX2,PY2,0.,.07,IX,NL)
C...DRAW X-AXIS TICK MARKS UNLESS GRID IS TO BE DRAWN
PY=PY+.25
IF(LGRIDX,EQ.1) GO TO 60
PY1=PY-.075
PY3=PY-.1
DO 50 I=NLOGX1,NLOGX
50 XJ=J+1
CALL PLOT(PXX,PY,3)
IF(J.NE.1 .AND. J.NE.13) GO TO 20
CALL PLOT(PXX,PY3,2)
GO TO 30
20 CALL PLOT(PXX,PY1,2)
30 XLOG(J)=ALOG10(XJ)
IF(J.EQ.10) GO TO 50
40 PXX=PX3+XLOG(J)*X2
50 PX3=PXX
C...LABEL X-AXIS
61 PX=PXAX
PY=PYAX
NXCHAR=IASINXCHAR
NXN=NXCHAR
PX3=.5*(XAXL-(.14*XB11+EX)
PY5=PY-.15
CALL CHAR(PX3,PY5,1.,.15,XAX,NXCHAR)

```

```

70 IF(NLOGY.EQ.0) GO TO 140
    YAX=PXY*YAXL
    CALL PLOT(PX,PY,3)
    CALL PLOT(PY,YAX,2)
C...PRINT Y-AXIS POWERS OF 10
    PY3=PY
    PX3=PXL
    Y1=YAXL*10^-3
    NL1G=NLOG2*200*2
    YNLGY=YLOGY-NLOG2
    Y2=Y1*YNLOGY
    PX2=PX*10^2
    PY2=PY*10^2
    IF(NLOG2.LT.10) NL=1
    IF(NLOG2.GE.10) NL=2
    CALL CHAR(PX,PY,0,..,10,2H10,2)
    CALL CHAR(PX2,PY2,0,..,22,NLCG-NL)
    NLOGV1=NLOG2+1
    GO TO 30 I=NLGY1,YNLOGY
    IF(I.LT.10) NL=1
    IF(I.GE.10) NL=2
    IX(1)=I*200*2
    PY3=PY*2
    PY2=PY*10^2
    PY3=PY*10^2
    CALL CHAR2(PX,PY,0,..,10,2H10,2)
    80 CALL CHAR(PX2,PY2,0,..,07,IX,NL)
C...DRAW Y-AXIS TICK MARKS UNLESS GRID IS TO BE DRAWN
    PX=PX*..0
    IF(ILGRIOD.EQ.1) GO TO 130
    PY1=PX*..375
    PX3=PX*..1
    CO 120 I=NLCG1,I=NLGY
    10 110 J=1,12
        YJ=XJ+1
        CALL PLOT(PX,PY,J)
    IF(J.NE.1 .AND. J.NE.10) GO TO 90
        CALL PLOT(PX3,PY,YJ)
        GO TO 100
    90 CALL PLOT(PX1,PY,YJ)
    100 YLCG(J)=ALCG10(YJ)
    IF(J.EQ.10) GO TO 120
    110  PY3=PY3+YLCG(J)*Y2
    120 PY3=PY
C...LABEL Y-AXIS
    130 PX=PXY
    PY=PYAX
    NYCHAR=1188(NYCHAR)
    YNY=NYCHAR
    PX3=PX*..5
    PY5=.5*(YAXL-(10^YNY))+PY
    CALL CHAR(PX3,PY5,1,16*5/2,..14,YAX,NYCHAR)
    140 IF(ILGRIOD.NE.1) GO TO 170
C...DRAW X-GRID
    PYAX=PXY*YAXL
    PY5=PXY
    PY6=PY
    PX7=PX
    PY7=PY
    CALL PLOT(PY6,PY6,3)
    NXLOG=NLCGX-NLOG1
    GO 130 I=1,NXLOG

```

```

XJ=1.
DO 150 J=1,5
  XJ=XJ+1.
  PX6=PX7*X2*ALOG10(XJ)
  CALL PLOT(PX6,PY6,3)
  CALL PLOT(PX6,2YAX,2)
  XJ=XJ+1.
  IF(J.EQ.3) GO TO 150
  PX6=PX7*X2*ALOG10(XJ)
  CALL PLOT(PX6,PYAX,3)
  CALL PLOT(PX6,PY6,2)
150  CONTINUE
160 PY7=PY7+X2
170 IF(LSRDY.NE.1) RETURN
...DRAW Y=GRID
  PX4=X*PX+XA1
  PX6=PX
  PY6=PY
  CALL PLOT(PX6,PY6,3)
  NYLOG=NLOGY-NLOGZ
  DO 190 I=1,NYLOG
    YJ=Y1
    DO 180 J=1,5
      YJ=YJ+1.
      PY6=PY7+Y2*ALOG10(YJ)
      CALL PLOT(PX6,PY6,3)
      CALL PLOT(PXAX,PY6,2)
      YJ=YJ+1.
      IF(J.EQ.3) GO TO 180
      PY6=PY7+Y2*ALOG10(YJ)
      CALL PLOT(PXAX,PY6,3)
      CALL PLOT(PX6,PY6,2)
180  CONTINUE
190 PY7=PY7+Y2
  RETURN
END

```

TEST NUMBER 51206

X =	16.000 IN.	25.400 CM.
UFS =	2.62 FT/SEC	0.797 M/SEC
UAVG =	2.206 FT/SEC	0.672 M/SEC
DELTA =	0.146 IN.	0.355 CM.
DELTAI =	0.032 IN.	0.083 CM.
DELTIA2 =	0.016 IN.	0.040 CM.
DELTIA3 =	0.026 IN.	0.066 CM.
HYDRA =	0.071 FT.	0.022 M.
H112 =	2.685	
H32 =	1.676	
REX =	180584.	
REHALF =	4742.	
REHYDIA =	12927.9	
REDELTA =	30295.	
REDELTA1 =	2040.	
REDELTA2 =	3377.	
T WALL =	160.63	
H2, TEMP =	60.000	
HU =	0.0001207	
CF =	0.005271	
UTAUFH =	0.1343	
CONC IN =	800.00 PPM	
POLYFLOW =	20.00 CC/MIN	
QFLOW =	0.10 GPM	
QVOL =	0.010 FT ³ /SEC	
POLY QIN =	0.0303 FT/SEC	
SLOT =	0.6200 IN	
CWALL =	0.00 PPM	
CW/CI =	0.000	
LAMDDA =	0.0116	

TEST NUMBER 512.6

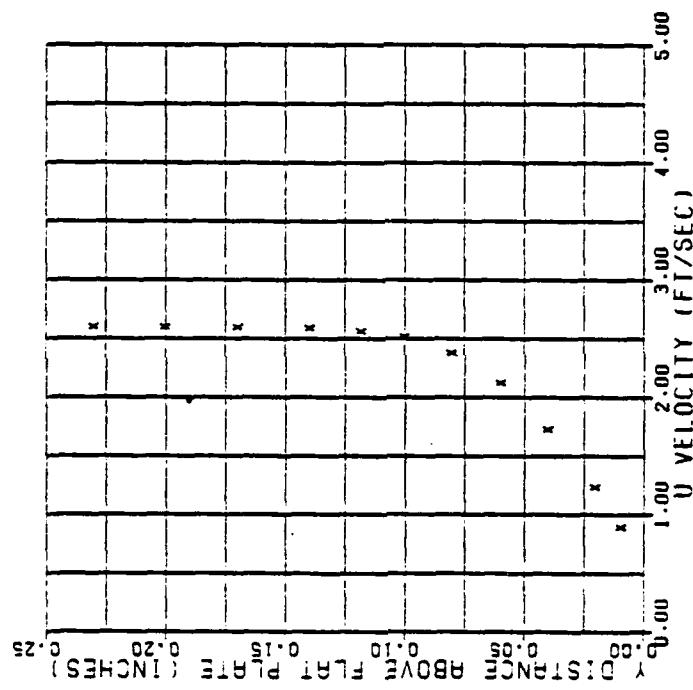
VINH.1	X(CHR.1)	Y(CHR.1)	Z(CHR.1)	U(CHR.1)	V(CHR.1)	W(CHR.1)	S/HEX	Y/DELTA1	Z/DELTA2	REV.	LOG REV	Y/DELTA	AETA	X(IN.)	Z(IN.)
6.310	0.4624	6.912	6.276	8.159	0.236	0.616	173.361	2.239	8.069	0.438	10.003	1.105			
6.320	0.453	6.253	6.361	6.476	0.632	1.296	366.781	2.562	0.146	0.450	10.030	1.116			
6.334	6.312	1.766	0.532	0.667	1.231	2.567	722.339	2.459	0.286	1.766	10.005	1.105			
6.350	6.152	2.143	0.653	0.419	1.857	3.956	1763.507	3.135	0.423	2.556	10.005	1.136			
6.353	6.224	2.395	1.736	0.716	2.472	5.153	1650.093	3.161	0.576	3.412	10.052	1.136			
6.315	2.254	2.531	6.771	6.768	3.178	6.417	1635.844	3.257	0.715	4.253	10.000	1.116			
6.118	6.310	2.581	6.787	6.967	3.639	7.585	2134.538	3.229	0.845	5.923	10.003	1.116			
6.148	6.355	2.607	6.795	4.383	7.945	6.971	2524.579	3.402	1.003	6.944	10.003	1.116			
6.176	6.431	2.613	6.796	6.999	5.227	17.896	3366.324	3.467	1.215	7.216	10.039	1.136			
6.210	6.519	2.616	6.797	6.999	6.163	12.847	3615.300	3.556	1.432	8.508	10.003	1.116			
6.230	6.565	2.616	6.252	1.003	2.086	14.772	4157.053	3.619	1.647	9.782	10.003	1.136			

VINH.1	Y/DELTA1	U/UPS1	U/UTAU	YPLUS	YPLUS	DEL UTAU	Y/HALFH	LOG(YPLUS)
6.310	0.369	0.449	0.662	6.791	8.988	12.680	0.037	8.469
6.320	0.446	0.476	0.759	9.132	14.728	13.171	0.977	1.372
6.334	0.286	0.667	0.636	13.000	37.046	6.478	0.152	1.569
6.350	0.629	1.819	0.866	15.956	55.626	1.522	0.228	1.745
6.353	0.514	0.916	0.922	17.633	74.447	1.646	0.316	1.972
6.118	0.715	0.966	0.953	18.865	32.711	0.633	0.361	1.967
6.148	0.645	1.987	0.976	19.210	119.594	0.261	0.451	2.040
6.176	1.666	0.991	1.010	19.511	129.616	1.367	0.532	2.113
6.170	1.215	0.999	1.028	19.456	157.023	0.922	0.647	2.197
0.231	1.332	0.999	1.053	19.463	105.007	3.015	0.762	2.269
0.235	1.617	1.001	1.076	19.479	213.420	2.030	0.877	2.329

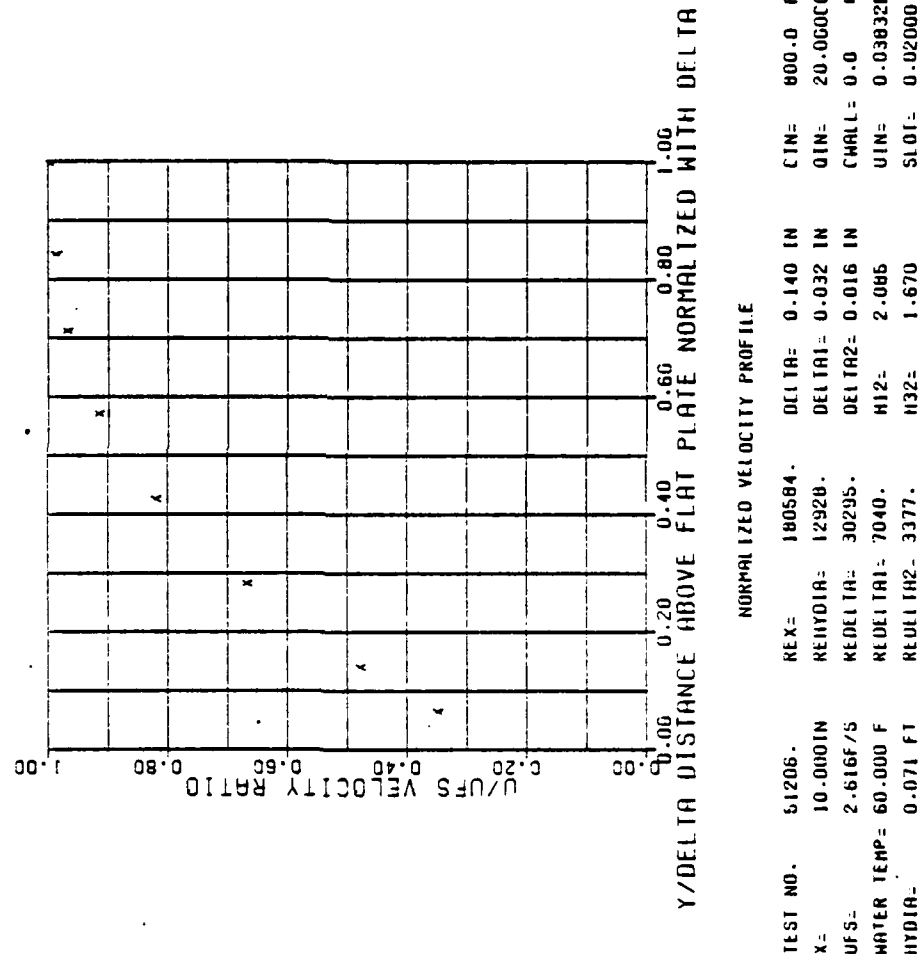
Y/INH.1 — CONC(EPHM) — C/GN — Y/LA70DA — XC
6.310 J.610 2.006 0.010 0.630

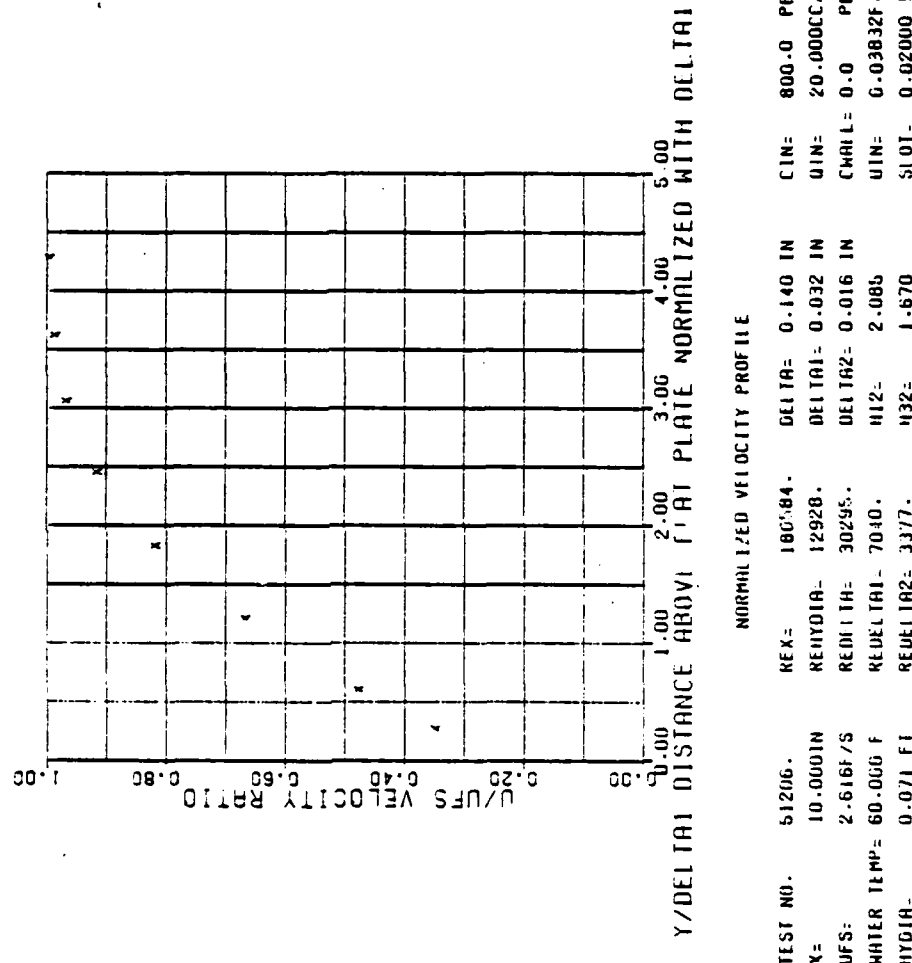
APPENDIX C

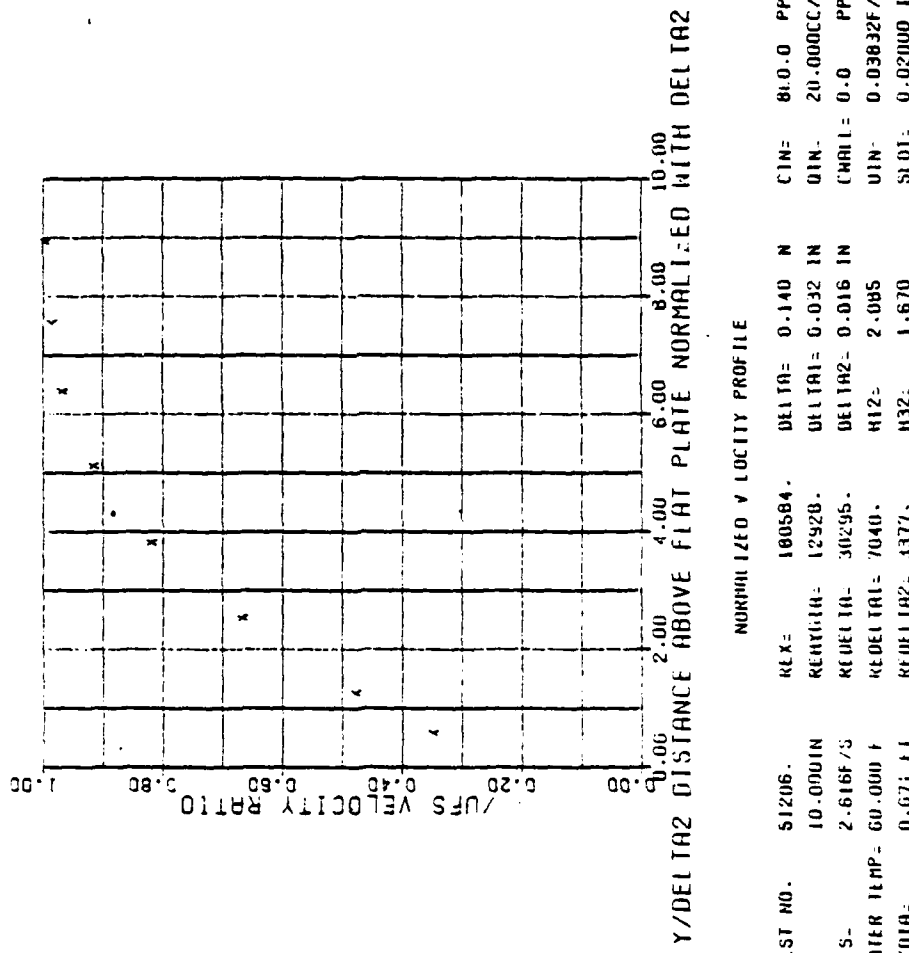
COMPUTER PROGRAM DATAPAC OUTPUT CURVES

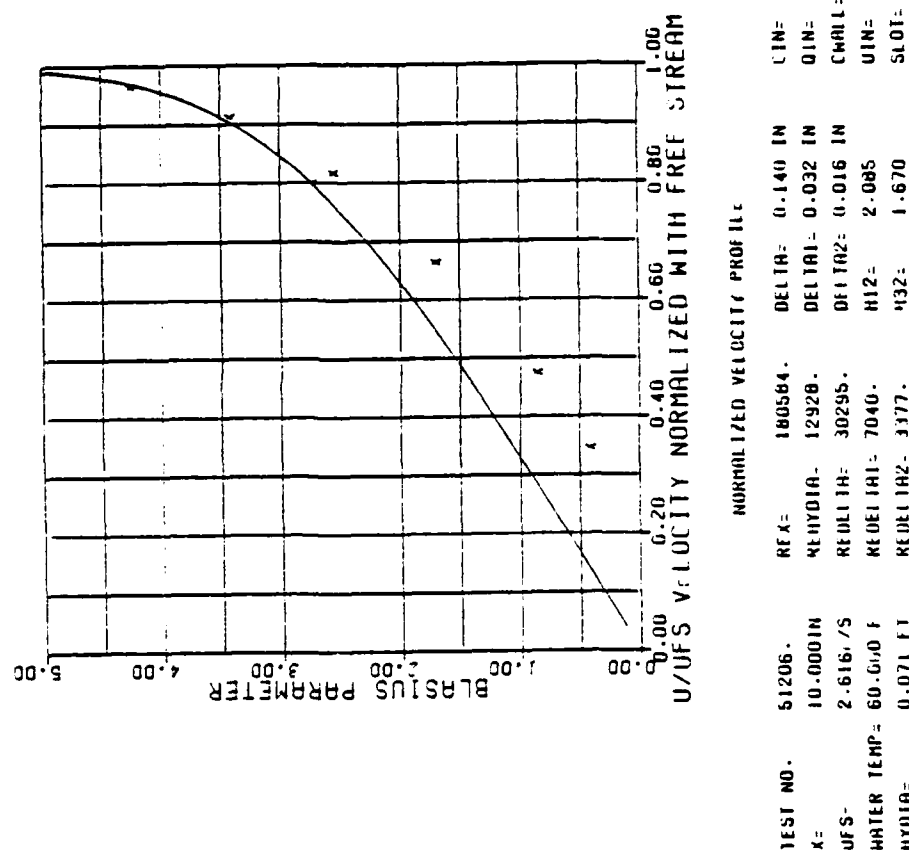


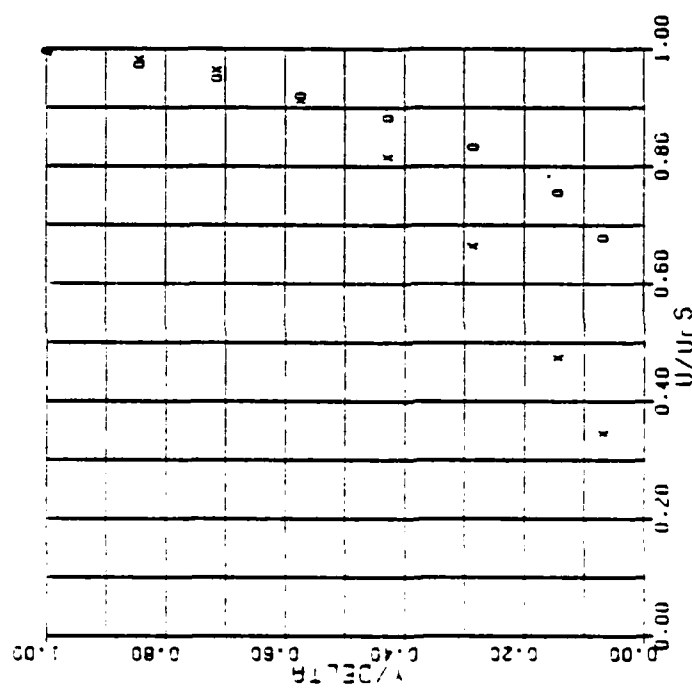
T.L. NO.: 51206. REFLX= 180504. DEL10= 0.140 IN CIN= 000.0 PPM
 X= 10.0001N REHYDRA= 12928. DEL11A= 0.032 IN QIN= 20.000CC/M
 UFS= 2.616F/S REDEL1A= 30295. DEL102= 0.016 IN CWALL= 0.0 PPM
 WALTER RPM= 60.000 F REDELI1A= 7040. H12= 2.085 VIN= 0.03832F/S
 HYDRA= 0.071 FT REDEL1A2= 3377. H132= 1.670 S101= 0.02000 IN





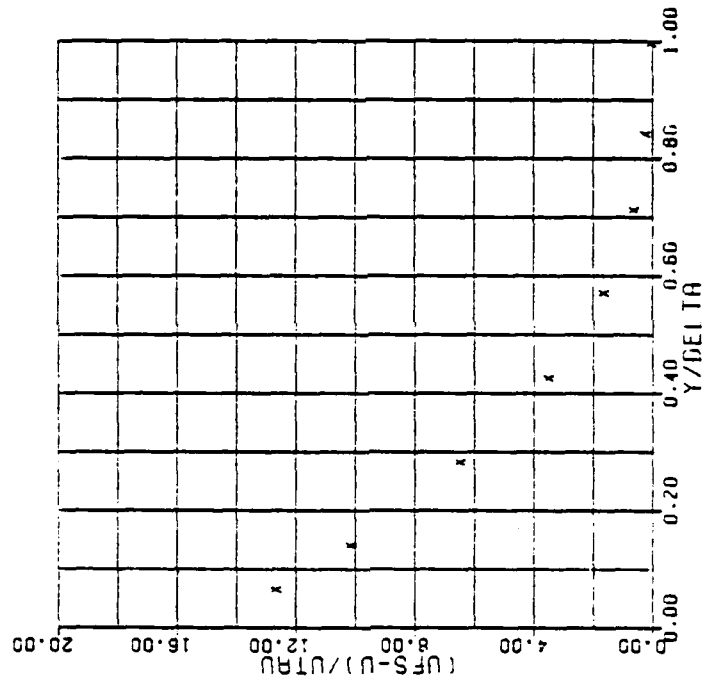






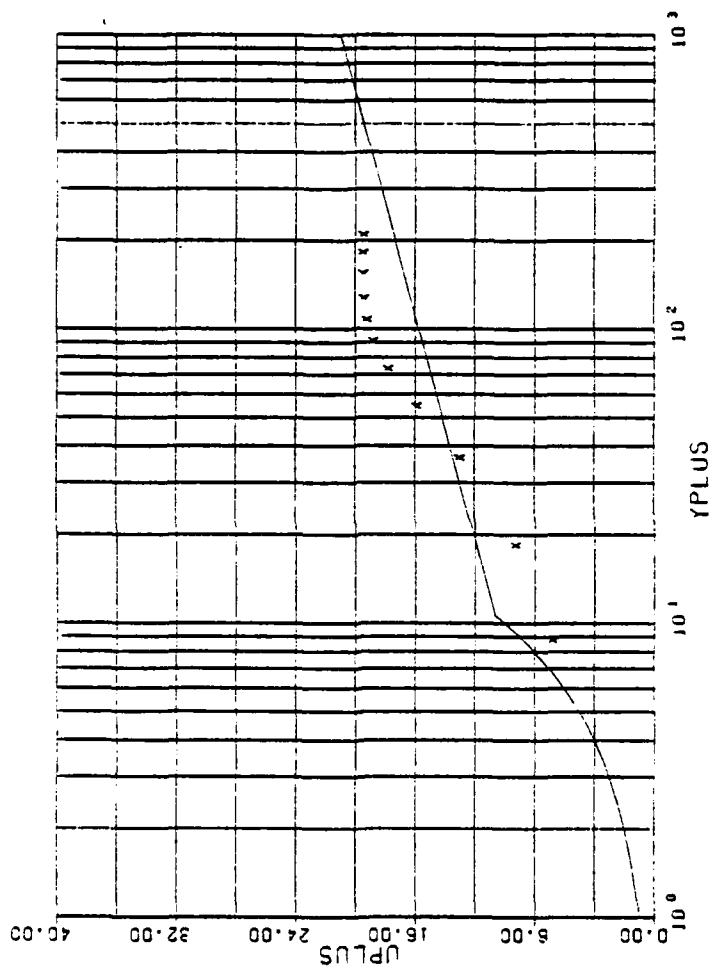
NORMALIZED VELOCITY PROFILES

T, ST NO.	51206.	R _t x=	18064.	DELT _A =	0.140 IN	C _{IN} =	800.0 PPM
ζ =	10.000 IN	RE _{DELTA} _A =	12928.	DELT _{A1} =	0.032 IN	Q _{IN} =	20.0000CC/H
UF S=	2.616 ft / s	RE _{DELTA} _A	30295	DELT _{A2} =	0.016 IN	C _{WALL} =	0.0 PPM
WATER TEMP=	60.000 F	RE _{DELTA} _{A1} =	7040.	H12=	2.085	U _{IN} =	0.13832F/S
HYDIA=	0.071 F1	RE _{DELTA} _{A2} =	3377.	H32=	1.670	SI ₀₁ =	0.02000 IN



WATER DEFICIT

TEST NO.	RDX-	DELTAt=	CIN=
X=	10.000IN	100584.	860.0 PPM
HYDIA=	REHYDIA=	12928.	QIN= 20.000CC/M
UF S=	2.616f /S	REDFI TA=	CWALL= 0.0 PPM
WATER T, MP=	60.000 F	REDFI TA1=	UIN= 0.03822F/S
HYDIA=	0.071 F1	REDFI TA2=	SI01= 0.02010 IN



FM OF THE WALL

TEST NO.	51206.	REYNOLDS=	106684.	DELTA=	0.140 IN	CIN=	0.00 PPM
L=	10.000IN	REHYDRA=	12928.	DELTA1=	0.032 IN	QIN=	20.000FC/M
UFS=	2.616/s	REDEFLA=	30295.	DELTA2=	0.016 IN	FWALL=	0.0 PPM
WATER TEMP=	60.000 F	REDEFLA1=	7040.	W12=	2.085	WIN=	0.038125/S
HYDRA=	0.671 FT	REDEFLA2=	3377.	W32=	1.670	SLOT=	0.02060 N

APPENDIX D

HYDRODYNAMIC PARAMETER TABULATIONS

TABLE 20
BOUNDARY LAYER PARAMETERS FOR WATER INJECTED AT $V_1 = .0383$ FT/SEC

$C_1 = 0.0$ WPPM		$Q_1 = 20$ cc/min		$Q_W = 8.00$ gal/min		$S = .02$ in.					
X	Re_x	δ	δ_1	δ_2	Re_H	Re_δ	$Re_{\delta 1}$	$Re_{\delta 2}$	H_{12}	H_{32}	
3.75	2.575	75761	.080	.022	.009	14693	19395	5343	2217	2.410	1.659
6.00	2.651	124795	.099	.027	.012	14693	24759	6783	2872	2.362	1.632
8.00	2.691	168904	.099	.030	.013	14693	25082	7670	3332	2.302	1.634
10.00	2.731	214268	.160	.027	.019	14693	41088	6931	4893	1.416	1.590
14.00	2.795	307005	.179	.026	.018	14693	47051	6850	4701	1.457	1.808
15.00	2.787	327992	.220	.029	.020	14693	57674	7547	5295	1.425	1.813
16.00	2.822	354252	.200	.033	.021	14693	53085	8749	5450	1.605	1.816
17.00	2.825	376793	.158	.027	.017	14693	42023	7102	4494	1.580	1.764
18.00	2.847	402064	.200	.033	.019	14693	53662	8766	5183	1.691	1.784

TABLE 21
BOUNDARY LAYER PARAMETERS FOR WATER INJECTED AT $V_1 = .0766$ FT/SEC

$c_1 = 0.0$	WPPM	$Q_1 = 40$	cc/min	$Q_w = 8.00$	gal/min	$S = .02$	in.				
X	U_{FS}	Re_x	δ	δ_1	δ_2	Re_H	Re_δ	$Re_{\delta 1}$	$Re_{\delta 2}$	H_{12}	H_{32}
3.75	2.563	73373	.080	.023	.010	14297	18807	5480	2322	2.360	1.658
6.00	2.641	120970	.140	.034	.014	14297	33872	7657	3434	2.229	1.652
8.00	2.681	163736	.170	.036	.017	14297	41704	8861	4234	2.093	1.671
10.00	2.722	207800	.119	.034	.015	14297	29774	8431	3789	2.225	1.630
14.00	2.802	299470	.159	.037	.018	14297	40711	9471	4654	2.035	1.662
15.00	2.822	323151	.180	.037	.021	14297	46430	9640	5338	1.806	1.724
16.00	2.825	345061	.179	.036	.022	14297	46428	9311	5763	1.616	1.719
17.00	2.804	363902	.230	.037	.023	14297	59081	9600	5825	1.648	1.777
18.00	2.842	390530	.220	.035	.023	14297	57278	9073	6077	1.493	1.774

TABLE 22
BOUNDARY LAYER PARAMETERS FOR WATER INJECTED AT $V_1 = .1532 \text{ FT/SEC}$

$C_1 = 0.0$		$WPPM$	$Q_1 = 80$	cc/min	$Q_W = 8.00$		gal/min	$S = .02 \text{ in.}$			
X	UFS	Re_x	δ	δ_1	δ_2	Re_H	Re_f	Re_{f1}	Re_{f2}	H_{12}	H_{32}
3.75	2.574	70643	.090	.026	.012	13706	20390	5787	2623	2.206	1.607
6.00	2.638	115840	.110	.030	.013	13706	25485	6913	3038	2.276	1.636
8.00	2.677	156736	.120	.031	.014	13706	28213	7232	3332	2.171	1.652
10.00	2.704	197896	.140	.036	.016	12706	33223	8448	3866	2.185	1.638
14.00	2.786	235456	.180	.037	.020	13706	44042	9104	5010	1.817	1.718
15.00	2.796	306944	.230	.039	.023	14706	56576	9568	5674	1.686	1.751
16.00	2.813	329398	.230	.040	.025	13706	56772	9822	6088	1.613	1.779
17.00	2.817	350483	.263	.042	.027	13706	65116	10347	6640	1.558	1.796
18.00	2.810	370177	.266	.041	.026	13706	65595	10159	6457	1.573	1.794

TABLE 23
BOUNDARY LAYER PARAMETERS FOR WATER INJECTED AT $V_1 = .3074$ FT/SEC

$C_1 = 0.0$		$WPPM$	$Q_1 = 40$	cc/min	$Q_W = 8.00$		gal/min	$S = .005$	$in.$		
X	UFS	Re_x	δ	δ_1	δ_2	Re_H	Re_δ	$Re_{\delta 1}$	$Re_{\delta 2}$	H_{12}	H_{32}
3.75	2.570	70533	.120	.028	.012	13706	27085	6331	2611	2.425	1.612
6.00	2.640	115927	.120	.032	.014	13706	27776	7476	3271	2.286	1.634
8.00	2.677	156736	.120	.035	.016	13706	28165	8217	3654	2.249	1.627
10.00	2.703	197823	.120	.032	.015	13706	28534	7628	3574	2.135	1.658
14.00	2.784	285252	.160	.033	.017	13706	39071	8052	4158	1.937	1.703
15.00	2.801	307493	.179	.034	.018	13706	44131	8312	4496	1.849	1.725
16.00	2.825	330803	.200	.035	.020	13706	49620	8624	5019	1.718	1.764
17.00	2.836	352847	.220	.036	.022	13706	54745	8903	5393	1.651	1.777
18.00	2.839	373997	.220	.035	.022	13706	54853	8805	5460	1.613	1.800

TABLE 24
BOUNDARY LAYER PARAMETERS FOR WATER INJECTED AT $V_1 = .6148 \text{ FT/SEC}$

$C_1 = 0.0$	WPPM	$Q_1 = 80 \text{ cc/min}$	$Q_w = 8.00 \text{ gal/min}$	$S = .005 \text{ in.}$			
X	UFS	Re_x	δ	δ_1	δ_2	Re_H	Re_f
3.75	2.578	70753	.100	.030	.013	13706	22573
6.00	2.634	115664	.120	.034	.015	13706	27759
8.00	2.671	156385	.120	.035	.016	13706	28149
10.00	2.705	197969	.120	.036	.016	13706	28508
14.00	2.789	285764	.170	.038	.020	13706	41591
15.00	2.804	307822	.180	.035	.019	13706	44277
16.00	2.830	331388	.200	.037	.022	13706	49708
17.00	2.833	352473	.220	.037	.023	13706	54687
18.00	2.890	380716	.220	.038	.024	13706	55838

TABLE 25
BOUNDARY LAYER PARAMETERS FOR 100 WPPM POLYMER INJECTED AT $V_1 = .0383$ FT/SEC

$C_1 = 100$		$WPPM$	$Q_1 = 20$	cc/min	$Q_W = 8.00$			gal/min			$S = .02$ in.		
X	UFS	Re_x	δ	δ_1	δ_2	Re_H	Re_δ	$Re_{\delta 1}$	$Re_{\delta 2}$	H_{12}	H_{32}		
3.75	2.581	71342	.080	.027	.011	13804	18218	60676	2549	2.384	1.636		
6.00	2.658	117553	.100	.032	.014	13804	23464	7479	3216	2.325	1.624		
8.00	2.693	158801	.118	.032	.015	13804	28155	7728	3518	2.197	1.643		
10.00	2.737	201745	.140	.035	.017	13804	33845	8403	4030	2.085	1.659		
14.00	2.802	289151	.190	.039	.021	13804	47065	9624	5092	1.890	1.700		
15.00	2.813	311020	.180	.038	.021	13804	44812	9496	5246	1.810	1.720		
16.00	2.805	330312	.205	.035	.021	13804	50862	8808	5289	1.665	1.777		
17.00	2.817	352991	.220	.040	.025	13804	54768	10020	6147	1.630	1.767		
18.00	2.828	375215	.263	.040	.025	13804	65738	9994	6352	1.573	1.794		

TABLE 26
BOUNDARY LAYER PARAMETERS FOR 100 WPPM POLYMER INJECTED AT $V_1 = .0766$ FT/SEC

$C_1 = 100$	WPPM	$Q_1 = 40$	cc/min	$Q_w = 8.00$	gal/min	$S = .02$	in.				
X	UFS	Re_x	δ	δ_1	δ_2	Re_H	Re_δ	$Re_{\delta 1}$	$Re_{\delta 2}$	H_{12}	H_{32}
3.75	2.426	74280	.070	.023	.009	15291	16639	5490	2188	2.509	1.596
6.00	-----	-----	-----	-----	-----	-----	-----	-----	-----	-----	-----
8.00	-----	-----	-----	-----	-----	-----	-----	-----	-----	-----	-----
10.00	-----	-----	-----	-----	-----	-----	-----	-----	-----	-----	-----
14.00	2.669	305087	.169	.024	.024	15291	44299	6252	4101	1.524	1.771
15.00	2.668	326756	.170	.025	.014	15291	44439	6516	3575	1.823	1.801
16.00	2.676	349585	.170	.022	.015	15291	63043	8090	5851	1.441	1.814
17.00	2.676	371434	.180	.023	.016	15291	47194	5962	4308	1.384	1.816
18.00	2.681	394018	.240	.031	.022	15291	44572	5716	3967	1.383	1.813

TABLE 27
BOUNDARY LAYER PARAMETERS FOR 200 WPPM POLYMER INJECTED AT $V_1 = .0383$ FT/SEC

$C_1 = 200.0$ WPPM	$Q_1 = 20$ cc/min	$Q_W = 8.00$ gal/min			$S = .02$ in.						
X	Re_x	δ	δ_1	δ_2	Re_H	Re_δ	$Re_{\delta 1}$				
						H_{12}	H_{32}				
3.75	2.570	69526	.080	.021	.009	13510	17843	4601	1915	2.403	1.676
6.00	2.631	113883	.100	.025	.011	13510	22731	5665	2328	2.334	1.656
8.00	2.664	153748	.100	.028	.012	13510	22970	6349	2820	2.251	1.652
10.00	2.705	195143	.100	.029	.013	13510	23417	6688	3048	2.195	1.661
14.00	2.792	281987	.140	.031	.016	13510	33838	7468	3763	1.984	1.702
15.00	---	---	---	---	---	---	---	---	---	---	---
16.00	2.818	345601	.160	.034	.018	13510	39033	8203	4457	1.840	1.730
17.00	2.823	346215	.200	.035	.021	13510	48877	8442	5029	1.679	1.776
18.00	2.817	365801	.200	.032	.019	13510	48822	7682	4644	1.654	1.805

TABLE 28

BOUNDARY LAYER PARAMETERS FOR 200 WPPM POLYMER INJECTED AT $V_1 = .0766$ FT/SEC

$C_1 = 200$ WPPM		$Q_1 = 40$ cc/min		$Q_W = 8.00$ gal/min		$S = .02$ in.					
X	UFS	Re_{λ}	δ	δ_1	δ_2	Re_H	Re_{δ}	$Re_{\delta 1}$	$Re_{\delta 2}$	H_{12}	H_{32}
3.75	2.581	69824	.080	.027	.010	13510	17875	5926	2313	2.562	1.589
6.00	2.642	114359	.100	.029	.012	13510	22872	6534	2731	2.392	1.623
8.00	2.677	154498	.100	.029	.013	13510	23128	6792	2942	2.308	1.634
10.00	2.716	195937	.120	.031	.014	13510	28215	7260	3268	2.221	1.644
14.00	2.807	283502	.180	.034	.018	13510	43740	8321	4436	1.876	1.715
15.00	2.815	304618	.160	.031	.017	13510	38991	7614	4228	1.801	1.750
16.00	2.810	324348	.180	.033	.019	13510	43787	8102	4713	1.719	1.772
17.00	2.819	345724	.200	.036	.022	13510	48833	8783	5354	1.640	1.789
18.00	2.834	368009	.220	.037	.022	13510	53975	8967	5510	1.628	1.788

TABLE 29
BOUNDARY LAYER PARAMETERS FOR 200 WPPM POLYMER INJECTED AT $V_1 = .1532$ FT/SEC

$C_1 = 200$ WPPM		$Q_1 = 80$ cc/min		$Q_w = 8.00$ gal/min		$S = .02$ in.					
X	UFS	Re_x	δ	δ_1	δ_2	Re_H	Re_δ	$Re_{\delta 1}$	$Re_{\delta 2}$	H_{12}	H_{32}
3.75	2.42	73620	.080	.024	.009	15691	19497	5934	2118	2.801	1.593
6.00	---	---	---	---	---	---	---	---	---	---	---
8.00	---	---	---	---	---	---	---	---	---	---	---
10.00	---	---	---	---	---	---	---	---	---	---	---
14.00	2.657	311656	.140	.032	.016	15691	37452	8564	4163	2.057	1.705
15.00	2.671	335677	.170	.029	.018	15691	45652	7869	4936	1.594	1.230
16.00	2.690	360602	.180	.029	.020	15691	48735	7802	5364	1.455	1.764
17.00	2.698	284279	.240	.030	.021	15691	65101	8133	5829	1.395	1.793
18.00	2.716	409598	.238	.032	.023	15691	64935	8653	6306	1.372	1.797

TABLE 30
BOUNDARY LAYER PARAMETERS FOR 400 WPPM POLYMER INJECTED AT $V_1 = .0383$ FT/SEC

$C_1 = 400$ WPPM		$Q_1 = 20$ cc/min		$Q_W = 8.00$ gal/min		$S = .02$ in.					
X	UFS	Re_x	δ	δ_1	δ_2	Re_H	Re_δ	$Re_{\delta 1}$	$Re_{\delta 2}$	H_{12}	H_{32}
3.75	2.451	68231	.080	.029	.011	13902	17467	6286	2364	2.659	1.582
6.00	---	---	---	---	---	---	---	---	---	---	---
8.00	---	---	---	---	---	---	---	---	---	---	---
10.00	---	---	---	---	---	---	---	---	---	---	---
14.00	2.684	278945	.170	.035	.019	13902	40551	8445	4631	1.823	1.663
15.00	2.702	300874	.170	.038	.021	13902	40919	9058	5057	1.791	1.658
16.00	2.715	322476	.180	.038	.022	13902	43438	9138	5439	1.680	1.682
17.00	2.720	343262	.200	.038	.022	13902	48485	9298	5434	1.711	1.746
18.00	2.734	365325	.210	.037	.024	13902	51145	9004	5956	1.512	1.758

TABLE 31
BOUNDARY LAYER PARAMETER FOR 400 WPPM POLYMER INJECTED AT $V_1 = .766$ FT/SEC

$C_1 = 400$ WPPM	$Q_1 = 40$ cc/min	$Q_W = 8.00$ gal/min		$S = .02$ in.	
X	Re_x	δ	δ_1	δ_2	Re_{δ}
3.75	2.484	64302	.080	.022	.010
					12928
					16461
					4506
					2051
					2.197
					1.624
6.00	---	---	---	---	---
8.00	---	---	---	---	---
10.00	---	---	---	---	---
14.00	2.714	262289	.200	.036	.019
					12928
					44919
					8013
					4362
					1.837
					1.648
15.00	2.731	282784	.160	.037	.020
					12928
					36151
					8315
					4455
					1.866
					1.672
16.00	2.729	304116	.160	.031	.019
					12928
					36125
					7029
					4199
					1.674
					1.754
17.00	2.732	320606	.200	.034	.021
					12928
					45353
					7651
					4799
					1.594
					1.747
18.00	2.746	341205	.200	.033	.022
					12928
					45494
					7563
					4926
					1.535
					1.767

TABLE 32

BOUNDARY LAYER PARAMETERS FOR 400 WPPM POLYMER INJECTED AT $V_1 = .1532 \text{ FT/SEC}$

$C_1 = 400 \text{ WPPM}$			$Q_1 = 80 \text{ cc/min}$			$Q_w = 8.00 \text{ gal/min}$			$S = .02 \text{ in.}$		
X	UFS	Re_x	δ	δ_1	δ_2	Re_H	Re_δ	$Re_{\delta 1}$	$Re_{\delta 2}$	H_{12}	H_{32}
3.75	2.468	64844	.100	.030	.011	13121	20708	6172	2312	2.670	1.582
6.00	2.538	106693	.100	.031	.014	13121	21339	6657	2910	2.288	1.629
8.00	2.578	144499	.140	.028	.015	13121	30345	6052	3168	1.910	1.738
10.00	2.610	182866	.180	.029	.018	13121	39499	6264	3915	1.600	1.750
14.00	2.673	262191	.200	.031	.021	13121	44947	6991	4718	1.482	1.789
15.00	2.680	281655	.220	.032	.022	13121	49616	7290	4900	1.488	1.776
16.00	2.675	299871	.219	.032	.021	13121	49164	7236	4832	1.498	1.780
17.00	2.666	317541	.218	.033	.022	13121	48864	7309	4918	1.486	1.786
18.00	2.670	336725	.220	.034	.022	13121	49499	7522	4936	1.524	1.780

TABLE 33

BOUNDARY LAYER PARAMETERS FOR 400 WPPM POLYMER INJECTED AT $V_1 = .6148 \text{ FT/SEC}$

$C_1 = 400 \text{ WPPM}$			$Q_1 = 80 \text{ cc/min}$			$Q_w = 8.00 \text{ gal/min}$			$S = .005 \text{ in.}$		
X	UFS	Re_x	δ	δ_1	δ_2	Re_H	Re_δ	$Re_{\delta 1}$	$Re_{\delta 2}$	H_{12}	H_{32}
3.75	2.603	71439	.199	.027	.009	13706	45584	6157	2078	2.963	1.463
6.00	2.660	116806	.120	.029	.014	13706	27987	6807	3325	2.047	1.691
8.00	2.695	157790	.170	.028	.015	13706	40284	6584	3647	1.805	1.778
10.00	2.730	199799	.200	.030	.018	13706	47856	7304	4352	1.678	1.799
14.00	2.799	286788	.263	.036	.023	13706	64749	8875	5531	1.605	1.806
15.00	2.790	306285	.230	.034	.021	13706	56257	8243	5175	1.593	1.820
16.00	2.779	325416	.230	.031	.019	13706	56134	7463	4695	1.589	1.835
17.00	2.775	345257	.230	.031	.020	13706	56060	7630	4771	1.599	1.832
18.00	2.798	368596	.240	.032	.020	13706	58975	7886	4891	1.612	1.832

TABLE 34
BOUNDARY LAYER PARAMETERS FOR 500 WPPM POLYMER INJECTED AT $V_1 = .0383$ FT/SEC

X	C1 = 500 WPPM	$Q_1 = 20$ cc/min	$Q_W = 8.00$ gal/min			S = .02 in.					
X	UFS	Re_x	δ	δ_1	δ_2	Re_H	Re_δ	$Re_{\delta 1}$	$Re_{\delta 2}$	H_{12}	H_{32}
3.75	2.485	61468	.080	.023	.010	12353	15736	4600	1982	2.321	1.671
6.00	2.561	101357	.100	.025	.012	12353	20231	5091	2338	2.177	1.690
8.00	2.608	137623	.119	.029	.013	12353	24607	5911	2782	2.124	1.679
10.00	2.713	178955	.119	.031	.016	12353	25398	6589	3439	1.916	1.718
14.00	2.724	251553	.140	.038	.019	12353	30186	8285	3996	2.073	1.656
15.00	2.744	271500	.160	.039	.019	12353	34708	8448	4212	2.006	1.658
16.00	2.765	291816	.160	.041	.020	12353	35062	8925	4308	2.071	1.650
17.00	2.780	311736	.160	.037	.020	12353	35252	8143	4417	1.843	1.711
18.00	2.790	331261	.180	.033	.019	12353	39707	7261	4089	1.775	1.756

TABLE 35
BOUNDARY LAYER PARAMETERS FOR 500 WPPM POLYMER INJECTED AT $V_1 = .0766$ FT/SEC

$C_1 = 500$ WPPM		$Q_1 = 40$	cc/min	$Q_w = 8.00$			gal/min			$S = .02$	$in.$
X	UFS	Re_x	δ	δ_1	δ_2	Re_H	Re_δ	$Re_{\delta 1}$	$Re_{\delta 2}$	H_{12}	H_{32}
3.75	2.474	64043	.100	.026	.011	12928	20535	5273	2194	2.404	1.636
6.00	2.550	105617	.120	.033	.014	12928	25306	6900	2888	2.389	1.613
8.00	2.596	143363	.120	.033	.015	12928	25762	7021	3197	2.196	1.644
10.00	2.633	181758	.040	.032	.015	12928	30535	6913	3379	2.046	1.681
14.00	2.717	262579	.160	.038	.019	12928	35921	8504	4309	1.973	1.680
15.00	2.736	283302	.180	.040	.021	12928	40796	8982	4682	1.918	1.692
16.00	2.759	304729	.200	.040	.022	12928	45709	9161	5077	1.804	1.680
17.00	2.769	324948	.200	.042	.023	12928	45875	9579	5182	1.849	1.704
18.00	2.786	346175	.199	.042	.023	12928	45972	9627	5314	1.812	1.713

TABLE 36

BOUNDARY LAYER PARAMETERS FOR 500 WPPM POLYMER INJECTED AT $V_1 = .1532 \text{ FT/SEC}$

$C_1 = 500 \text{ WPPM}$		$Q_1 = 80 \text{ cc/min}$			$Q_W = 8.00 \text{ gal/min}$				$S = .02 \text{ in.}$		
X	Re_x	δ	δ_1	δ_2	Re_H	Re_δ	$Re_{\delta 1}$	$Re_{\delta 2}$	H_{12}	H_{32}	
3.75	-----	-----	-----	-----	-----	-----	-----	-----	-----	-----	
6.00	2.611	129581	.120	.029	.024	15491	31048	7567	3570	2.119	1.673
8.00	2.633	174231	.169	.169	.028	15491	44272	7415	4301	1.724	1.725
10.00	2.674	221180	.200	.200	.027	15491	53030	7226	4819	1.500	1.795
14.00	2.752	318684	.220	.220	.031	15491	60095	8353	5806	1.439	1.800
15.00	2.751	341324	.220	.220	.031	15491	60128	8508	5886	1.446	1.799
16.00	2.753	364343	.220	.032	.022	15491	60117	8744	5954	1.469	1.794
17.00	2.736	384724	.240	.051	.015	15491	65122	13864	4191	3.308	1.885
18.00	2.760	410928	.219	.034	.021	15491	60105	9276	5793	1.601	1.814

TABLE 37

BOUNDARY LAYER PARAMETERS FOR 500 WPPM POLYMER INJECTED AT $V_1 = .6148 \text{ FT/SEC}$

X	UFS	Re_x	δ	δ_1	δ_2	Re_H	Re_δ	$Re_{\delta 1}$	$Re_{\delta 2}$	H_{12}	H_{32}	S = .005 in.
3.75	2.596	71247	.100	.030	.012	13706	22708	6789	2804	2.421	1.572	
6.00	2.648	116279	.120	.027	.014	13706	27860	6336	3286	1.928	1.730	
8.00	2.689	157439	.180	.028	.016	13706	42485	6724	3798	1.770	1.785	
10.00	2.719	198994	.201	.030	.018	13706	48045	7142	4203	1.699	1.805	
14.00	2.794	286276	.230	.033	.021	13706	56388	8042	5072	1.586	1.821	
15.00	2.809	308371	.263	.035	.022	13706	64783	8669	5473	1.584	1.814	
16.00	2.802	328110	.230	.033	.021	13706	56550	8077	5091	1.587	1.828	
17.00	2.785	346501	.230	.033	.020	13706	56256	7988	4969	1.608	1.823	
18.00	---	---	---	---	---	---	---	---	---	---	---	

TABLE 38
BOUNDARY LAYER PARAMETERS FOR 800 WPPM POLYMER INJECTED AT $V_1 = .0383$ FT/SEC

$C_1 = 800$	WPPM	$Q_1 = 20$	cc/min	$Q_W = 8.00$	gal/min	$S = .02$	in.				
X	UFS	Re_x	δ	δ_1	δ_2	Re_H	Re_δ	$Re_{\delta 1}$	$Re_{\delta 2}$	H_{12}	H_{32}
3.75	2.461	63707	.080	.025	.010	12928	16309	5063	2118	2.391	1.641
6.00	2.534	104954	.100	.030	.013	12928	20929	6307	2731	2.309	1.636
8.00	2.581	142535	.120	.032	.015	12928	25613	6836	3140	2.177	1.649
10.00	2.616	180584	.140	.032	.016	12928	30295	7040	3377	2.085	1.670
14.00	2.696	260550	.160	.036	.019	12928	35733	8501	4298	1.978	1.679
15.00	2.715	281128	.160	.040	.020	12928	35984	8928	4485	1.991	1.674
16.00	2.734	301968	.200	.040	.021	12928	45250	8978	4714	1.905	1.694
17.00	2.740	321545	.180	.038	.021	12928	40855	8560	4864	1.760	1.733
18.00	2.748	341454	.220	.037	.022	12928	50080	8444	4961	1.702	1.759

TABLE 39
BOUNDARY LAYER PARAMETERS FOR 800 WPPM POLYMER INJECTED AT $V_1 = .0766$ FT/SEC

$C_1 = 800$ WPPM		$Q_1 = 80$ cc/min		$Q_w = 8.00$ gal/min		$S = .02$ in.					
X	UFS	Re_X	δ	δ_1	δ_2	Re_{δ}	$Re_{\delta 1}$	$Re_{\delta 2}$	H_{12}	H_{32}	
3.75	2.467	61023	.100	.031	.012	12352	19566	5974	2343	2.550	1.597
6.00	2.539	100486	.120	.030	.014	12353	24117	6109	29090	2.100	1.670
8.00	2.582	136251	.140	.030	.016	12353	28613	6102	3202	1.906	1.728
10.00	2.611	172227	.160	.031	.018	12353	33068	6493	3658	1.775	1.760
14.00	2.687	248136	.230	.036	.022	12353	48833	7676	4609	1.665	1.778
15.00	2.706	267740	.220	.038	.023	12353	47122	8096	4922	1.645	1.778
16.00	2.721	287172	.220	.039	.023	12353	47383	8336	5059	1.648	1.779
17.00	2.729	306017	.240	.039	.024	12353	51843	8515	5264	1.618	1.784
18.00	2.747	326156	.262	.039	.024	12353	57055	8509	5187	1.640	1.780

TABLE 40
BOUNDARY LAYER PARAMETERS FOR 800 WPPM POLYMER INJECTED AT $V_1 = .1532$ FT/SEC

$C_1 = 800$ WPPM	$Q_1 = 40$ cc/min	$Q_W = 8.00$ gal/min				$S = .02$ in.					
X	UFS	Re_x	δ_1	δ_2	Re_H	Re_δ	$Re_{\delta 1}$	$Re_{\delta 2}$	H_{32}		
3.75	2.544	75861	.100	.025	.013	14892	24276	61754	3245	1.903	1.665
6.00	---	---	---	---	---	---	---	---	---	---	---
8.00	2.654	168836	.200	.032	.020	14892	50701	8105	5143	1.576	1.753
10.00	2.677	212873	.220	.035	.023	14892	56147	8908	5965	1.493	1.774
14.00	2.697	300249	.240	.037	.026	14892	61766	1.455	1.782	1.455	1.782
15.00	2.698	321815	.240	.035	.024	14892	61788	1.436	1.792	1.436	1.792
16.00	2.686	341742	.240	.034	.022	14892	51514	1.589	1.819	1.589	1.819
17.00	2.724	368238	.240	.035	.023	14892	62332	1.569	1.817	1.569	1.817
18.00	2.726	390186	.022	.034	.021	14892	57279	1.638	1.803	1.638	1.803

TABLE 41
BOUNDARY LAYER PARAMETERS FOR 800 WPPM POLYMER INJECTED AT $V_1 = .6148$ FT/SEC

$C_1 = 800$ WPPM		$Q_1 = 40$ cc/min			$Q_W = 8.00$ gal/min			$S = .02$ in.			
X	UFS	Re_x	δ	δ_1	δ_2	Re_H	Re_δ	$Re_{\delta 1}$	$Re_{\delta 2}$	H_{12}	H_{32}
3.75	2.606	71521	.100	.033	.014	13706	22887	7664	3158	2.427	1.593
6.00	2.668	117157	.170	.032	.017	13706	39833	7554	3958	1.909	1.722
8.00	2.704	158317	.200	.034	.019	13706	47471	8159	4503	1.812	1.743
10.00	2.733	200019	.200	.034	.020	13706	47908	8338	4747	1.757	1.759
14.00	2.823	289248	.262	.037	.023	13706	64957	9198	5672	1.622	1.792
15.00	2.823	309908	.220	.037	.023	13706	54494	9171	5621	1.631	1.791
16.00	2.844	333028	.230	.039	.024	13706	57397	9709	6011	1.615	1.784
17.00	2.820	351354	.230	.036	.022	13706	57093	8929	5550	1.609	1.800
18.00	2.822	371758	.236	.036	.022	13706	58589	8986	5506	1.632	1.795

TABLE 42

BOUNDARY LAYER PARAMETERS FOR 2000 WPPM POLYMER INJECTED AT $V_1 = .6148 \text{ FT/SEC}$

$C_1 = 2000 \text{ WPPM}$		$Q_1 = 80 \text{ cc/min}$		$Q_w = 8.00 \text{ gal/min}$		$S = .02 \text{ in.}$					
X	UFS	Re_x	δ	δ_1	δ_2	Re_H	Re_δ	$Re_{\delta 1}$	$Re_{\delta 2}$	H_{12}	H_{32}
3.75	2.598	71302	.160	.032	.017	13706	36552	7257	3880	1.870	1.734
6.00	2.653	116498	.220	.039	.021	13706	51259	9124	4952	1.842	1.728
8.00	2.696	157849	.240	.043	.023	13706	56778	10085	5545	1.819	1.725
10.00	2.719	198994	.262	.044	.025	13706	62611	10438	6006	1.738	1.709
14.00	2.790	285866	.263	.047	.026	13706	64442	11575	6392	1.811	1.715
15.00	2.808	308261	2.40	.045	.026	13706	59186	11089	6322	1.754	1.730
16.00	2.820	330217	.239	.045	.026	13706	59291	11097	6317	1.757	1.727
17.00	2.813	349985	.240	.045	.026	13706	59390	11193	6354	1.763	1.726
18.00	2.819	371363	.240	.042	.025	13706	59319	10709	6182	1.732	1.739

APPENDIX E

VELOCITY PROFILE SAMPLES

TABLE 43
VELOCITY PROFILES FOR WATER INJECTED AT $V_1 = .0383$ FT/SEC

X Inches	3.75	6.00	8.00	10.00	14.00	15.00	16.00	17.00	18.00
Y Inches	VELOCITY (FT/SEC)								
.010	.880	.728	.763	.973	1.785	1.750	1.787	1.495	1.465
.020	1.410	1.217	1.172	---	1.996	1.998	1.970	1.830	1.807
.040	2.118	1.954	1.856	---	2.204	2.193	2.175	---	2.122
.060	2.510	2.426	2.348	2.402	2.351	2.311	2.304	2.341	2.291
.080	2.570	2.608	2.590	---	2.449	2.412	2.382	2.521	2.441
.100	2.580 ⁻¹⁰	2.648	2.667	2.560	2.520	2.470	2.469	2.638	2.561
.120	2.581 ⁻¹⁰	2.642	2.685	2.622	2.639	2.552	2.556	2.752	2.655
.140	2.577	2.652	2.686	2.683	2.701	2.627	2.649	2.758	2.737
.160	2.574 ⁺¹⁰	2.650	2.685	2.708	2.744	2.682	2.682	2.693	2.764
.180	---	2.650	2.687	2.719	2.769	2.728	2.749	2.817	2.810
.200	2.569	2.649	2.689	2.729	2.791	2.757	2.799	2.825	2.833
.220	2.570 ⁺¹⁰	2.650	---	2.731	2.793	2.782	2.822	2.825	---

NOTE: +10 - add .010 inches to y value

TABLE 44
VELOCITY PROFILES FOR 100 WPPM POLYMER INJECTED AT $V_1 = .0383$ FT/SEC

X Inch	3.75	6.00	8.00	10.00	14.00	15.00	16.00	17.00	18.00
Y Inches	VELOCITY (FT/SEC)								
.010	.741	.707	.793	.882	.965	1.128	1.414	1.308	1.127
.020	1.197	1.110	1.180	1.280	1.332	1.477	1.762	1.739	1.1795
.040	1.948	1.748	1.778	1.778	1.799	1.853	2.062	1.985	2.095
.060	2.412	2.229	2.237	2.172	2.119	2.134	2.179	2.135	2.229
.080	2.558	2.558	2.509	2.455	2.349	2.342	2.351	2.234	2.293
.100	2.571	2.635	2.631	2.623	2.559	2.511	2.497	2.359	2.385
.120	---	2.647	2.676	2.685	2.666	2.628	2.545	2.474	2.476
.140	2.571	2.653	2.691	2.715	2.726	2.714	2.644	2.590	2.553
.160	2.570	1.651 ⁺¹⁰	2.687 ⁺¹⁰	2.730	2.725	2.766	2.716	2.667	2.651
.180	---	---	---	2.737	2.777 ⁺¹⁰	2.793	2.751	2.732	2.704
.200	2.574	2.658	2.693	2.737	---	2.794	2.804	2.776	2.743
.220	2.572	---	---	---	2.802 ⁺¹⁰	2.813 ⁺¹⁰	2.805	2.817	2.775
.240	---	---	---	---	---	---	2.805	2.817	2.789

NOTE: +10 - add .010 inches to y value; +15 - add .015 inches to y value

TABLE 45
VELOCITY PROFILES FOR 200 WPPM POLYMER INJECTED AT $V_1 = .0383$ FT/SEC

X inches	3.75	6.00	8.00	10.00	14.00	15.00	16.00	17.00	18.00
Y inches	VELOCITY (FT/SEC)								
.010	.998	.875	.832 ⁻²	.943	1.092	----	1.209	1.360	1.565
.020	1.469	1.345	1.284	1.318	1.437	1.435	1.543	1.762	1.913
.040	2.203	2.046	1.942	1.927	1.956	1.922	1.958	2.038	2.157
.060	2.514	2.460	2.385	2.379	2.304	2.290	2.244	2.232	2.277
.080	2.565	2.603	2.590	2.595	2.570	2.544	2.462	2.384	2.418
.100	2.567	2.630	2.651	2.683	2.693	2.682	2.606	2.515	2.540
.120	2.569	2.631	2.662	2.696	2.754	2.756	2.697	2.606	2.604
.140	2.570	2.624	2.664	2.702	2.772	2.787	2.751	2.681	2.679
.160	2.570	2.631 ⁺¹⁰	2.662	2.705	2.775 ⁺¹⁰	2.795	2.794	2.742	2.733
.180	2.570	----	2.660	2.704	----	2.804	2.795	2.779	2.788
.200	2.570	2.630	2.664	2.704	2.777	2.807	2.816	2.809	2.803
.220	2.570	2.630	2.663	2.700	2.87 ⁺¹⁰	2.808	2.818	2.817	2.815

NOTE: +10 - Add .010 inches to y value; -2 - subtract .002 inches from y value

TABLE 46
VELOCITY PROFILES FOR 400 WPPM POLYMER INJECTED AT $V_1 = .0383$ FT/SEC

X Inches	3.75	6.00	8.00	10.00	14.00	15.00	16.00	17.00	18.00
Y Inches	VELOCITY (FT/SEC)								
.010	.645 ⁺⁵	---	---	---	---	.949	1.004	1.138	1.458 ⁺⁵
.020	.916	---	---	---	---	1.046 ⁻⁵	1.285	1.369	1.559
.040	1.801	---	---	---	---	1.679	1.674	1.723	1.873
.060	2.285	---	---	---	---	2.063	2.034	2.019	2.063
.080	2.429	---	---	---	---	2.311	2.261	2.246	2.237
.100	2.447	---	---	---	---	2.491	2.451	2.400	2.365
.120	2.445	---	---	---	---	2.594	2.566	2.531	2.481
.140	2.449	---	---	---	---	2.648	2.643	2.617	2.572
.160	2.449	---	---	---	---	2.676 ⁺¹⁰	2.693 ⁺¹⁰	----	2.626
.180	2.449	---	---	---	---	----	----	2.704	2.678
.200	2.450	---	---	---	---	2.684	2.701	2.715	2.711

NOTE: +15 - add .005 inches to y value; +10 - add .010 inches to y value

TABLE 47

VELOCITY PROFILES FOR 500 WPPM POLYMER INJECTED AT $V_1 = .0383 \text{ FT/SEC}$

X inches	3.75	6.00	8.00	10.00	14.00	15.00	16.00	17.00	18.00
Y inches	VELOCITY (FT/SEC)								
.010	.851	.994	.935	1.083	.883	.787	.804	1.109	.830
.020	1.326	1.380	1.313	1.522	1.140	1.297	1.136	1.402	1.619
.040	2.018	1.993	1.879	1.883	1.658	1.606	1.540	1.924	2.097
.060	2.355	2.337	2.270	2.229	2.063	----	2.068	2.098	2.235
.080	2.465	2.497	2.477	2.443	----	2.330	----	2.299	2.391
.100	2.480	2.541	2.566	2.582	----	2.528	2.527	2.490	2.526
.120	2.482	2.554	2.596	2.694	2.644	2.652	2.647	2.639	2.643
.140	2.481	2.557	2.603	2.692	2.714	2.711	2.720	2.716	2.708
.160	2.480	2.558	2.605	2.691	2.715	2.734	2.746	2.754	2.756
.180	2.481	2.556	2.604	2.708	2.723	2.738	2.761	2.769	2.782
.200	2.483	2.560	2.605	2.709	2.723	2.740	2.760	2.775	2.786

TABLE 48
VELOCITY PROFILES FOR 800 WPPM POLYMER INJECTED AT $V_1 = .0383$ FT/SEC

X Inches	3.75	6.00	8.00	10.00	14.00	15.00	16.00	17.00	18.00
Y Inches	VELOCITY (FT/SEC)								
.010	.713	.652	.742	.912	.875	.869	.952	1.194	1.175
.020	1.200	1.109	1.163	1.250	1.240	1.181	1.288	1.522	1.633
.040	1.940	1.772	1.725	2.746	1.679	1.686	1.717	1.826	1.931
.060	2.315	2.217	2.141	2.143	2.050	2.023	2.054	2.079	2.125
.080	2.441	2.433	2.409	2.395	2.311	2.277	2.288	2.277	2.255
.100	2.459	2.511	2.526	2.531	2.494	2.487	2.463	2.431	2.401
.120	2.460	2.529	2.568	2.581	2.597	2.588	2.579	2.540	2.513
.140	2.460	2.530	2.578	2.607	2.634	2.658	2.668 ⁺¹⁰	2.625	2.607
.160	2.460	2.531	2.581	-----	2.677	2.689	2.693	2.677	2.669
.180	2.460	2.532	2.581	2.613 ⁺¹⁰	2.684	2.698	2.705	2.715	2.709
.200	2.460	2.534	2.581	2.614	2.689	2.709	2.727	2.724	2.720
.240	2.460	2.534	2.581	2.616	2.694	2.715	2.733	2.740	2.748

NOTE: +10 - add .010 inches to y value

APPENDIX F

COMPUTER PROGRAM SKINFRIC

```

SCHED,CORE=48,SCR=4,CLASS=E
SFTNU(L,X,S)
PROGRAM SKINFRIC
REAL K,L,LAMBDA,INTGND1,INTGND2,INTGRL1,INTGRL2
DIMENSION LAMBDA(256),X(256),CWX(256),YINTG1(256),YINTG2(256)
DIMENSION Y1(50),Y2(50),DREX(50),QIFINT(50),CF(256),DELTA(256)
DIMENSION REX(256),REXL(256),VVO(256),UTAU(256),DELTABL(256)
DIMENSION CFT(256)
COMMON K,B,VOS,ALPHA,GAMMA,U,RE,CX,XCT,DELT,CXL
1 FORMAT(8F5.0,3F10.0,E10.0)
2 FORMAT(1I10,3F10.0,6F5.0)
3 FORMAT(1H1,9X,'CI=',F7.2,/,10X,'XCT=',F6.3,/,10X,'VOS=',F5.3,/,,
A   10X,'ALPHA=',F5.3,/,10X,'GAMMA=',F5.3,/,10X,'B=',F5.3,/,,
B   10X,'K=',F5.3,/,10X,'NU=',E12.5,/,10X,'TEMP=',F5.1,/,,
C   10X,'REXT=',E12.5,/,10X,'XTRANS=',F6.3)
4 FORMAT(' NO ROOT IN GIVEN RANGE')
5 FORMAT(9X,'X',9X,'REX',8X,'REXL',8X,'CW',5X,'DELTA',8X,'CF',
X   4X,'LAMBDA',4X,'VS/VOS',6X,'UTAU',5X,'DELTABL',7X,'CFT')
6 FORMAT(F10.2,2F12.2,F10.2,F10.3,F10.5,F10.3,2F10.4,F12.6,F10.5)
7 FORMAT(1H1,18X,'X',11X,'INT1-INT2',16X,'DREX')
8 FORMAT(5X,'(',F6.2,',',F6.2,',',2E20.8)
C
C      INPUTS
C
9 CONTINUE
READ 1,U,VOS,L;CI,ALPHA,GAMMA,B,K,T,XCT,CXL,REXT
IF(U.EQ.0.0)GO TO 99
READ 2,NITER,EPS,RES,EDREX,XB,XF,XINC,STEPX,XCTL,XCTH
C
C      INITIALIZATIONS
C
V=3.60901355E-5+T*(-7.17973611E-7+T*(7.15890612E-9+
1   T*(-3.50677166E-11+T*6.62377978E-14)))+
NSTEPS=(XF-XB)/STEPX+1.1
UV=U/(V-12.1)
XTRANS=REXT/UV
UVS=U/VOS
NPT=XINC/STEPX+1.1
GM=GAMMA
AL=ALPHA
IF(NPT.EQ.2.0*(NPT/2))NPT=NPT+1
DELEX=(NPT-1)*STEPX
NINT=(XF-XB)/DELEX+.00001
REX0=UV*XB
PREDIF=0.0
DO 15 I=1,NSTEPS
  X(I)=XB+(I-1)*STEPX
  CWX(I)=C(CI,X(I),L)
15 CONTINUE
10 CONTINUE
GAMMA=0.0
ALPHA=1.0
JS=1
SIGX=XB
INTGRL1=0.0
INTGRL2=0.0
C
C      GENERATE A TABLE OF X,CW,LAMBDA AND INTEGRANDS
C

```

```

DO 30 I=1,NSTEPS
CX=CWX(I)
REX(I)=UV*X(I)
IF(X(I).LE.XCT) GO TO 27
REXL(I)=UV*(X(I)-XCT)
RE=REXL(I)
GAMMA=GM
ALPHABAL
XL=5.
F1=F(XL)
DO 28 J=6,400
XH=j
F2=F(XH)
IF(F1*F2.LT.0.01) GO TO 29
F1=F2
XL=XH
20 CONTINUE
PRINT 6
GO TO 99
25 CONTINUE
CALL FALPOS(XL,XH,NITER,RES,EPS,LAMBDA(I))
GO TO 29
27 CONTINUE
REXL(I)=REX(I)
LAMBDA(I)=1.735525336*REX(I)**.25
29 CONTINUE
RE=REXL(I)
YINTG2(I)=INTGN02(LAMBDA(I),X(I))
YINTG1(I)=INTGN01(LAMBDA(I),X(I))
VVO(I)=UV/(LAMBDA(I))
CF(I)=2.0/(LAMBDA(I)*LAMBDA(I))
DELTA(I)=DELT
UTAU(I)=VVO(I)*VQS
DELTA8L(I)=V*DELT*12./UTAU(I)
30 CONTINUE
C
C      PERFORM INTEGRATION
C
DO 60 I=1,NINT
BIGX=BIGX+DEIX
OREX(I)=BIGX*UV-REX0
JE=JS+NPT-1
M=0
DO 55 J=JS,JE
M=M+1
Y1(M)=YINTG1(J)
Y2(M)=YINTG2(J)
55 CONTINUE
JS=JE
CALL SIMPSON(NPT,STEPX,Y1,Y2,YIN1,YIN2)
INTGRL1=INTGRL1+YIN1
INTGRL2=INTGRL2+YIN2
DIFINT(I)=INTGRL1-INTGRL2
60 CONTINUE
RELER=(DIFINT(NINT)-PREDIF)/DIFINT(NINT)
IF(ABSRELER).LT.EOREX(GO TO 79
DEL=DIFINT(NINT)-OREX(NINT)
PREDIF=DIFINT(NINT)
IF(DEL.GT.0.0) GO TO 65
XCTH=XCT
XCT=.5*(XCTL+XCTH)
GO TO 10

```

```

65  CONTINUE
    XCTL=XCT
    XCT=.5*(XCTL+XCTH)
    GO TO 10
75  CONTINUE
    PRINT 3,CI,XCT,VOS,ALPHA,GAMMA,B,K,V,T,REXT,XTRANS
    PRINT 5
    DO 79 I=1,NSTEPS
        IF(X(I).GT.XTRANS) GO TO 76
        CFT(I)=CF(I)
        GO TO 78
76  CONTINUE
    IF(X(I).GT.XTRANS) GO TO 77
    GM=(X(I)-XCT)/(XTRANS-XCT)
    XLL=1.735525336*REX(I)**.25
    CFL=2.0/(XLL*XLL)
    CFT(I)=(1.-GM)*CFL+GM*CF(I)
    GO TO 78
77  CONTINUE
    CFT(I)=CFT(I)
78  CONTINUE
    PRINT 6,X(I),REX(I),REXL(I),CMX(I),DELTA(I),CF(I),LAMBOA(I),
    X          VVO(I),UTAU(I),DELTABL(I),CFT(I)
    79  CONTINUE
    PRINT 7
    BIGX=XB
    DO 80 I=1,NINT
        BIGX=BIGX+DELX
        PRINT 8,XB,BIGX,DIFINT(I),DREX(I)
    80  CONTINUE
    GO TO 9
99  CONTINUE
ENO
SUBROUTINE FALPOS(XL,XH,N,R,E,X3)
C SUBROUTINE FALPOS USES THE METHOD OF FALSE POSITION TO FIND THE ROOT OF
C A NONLINEAR EQUATION . THE USER SUPPLIES THE NONLINEAR EQUATION IN THE
C FORM OF A FUNCTION ROUTINE F(X)=0.0
C XL = LOW ESTIMATE OF ROOT
C XH = HIGH ESTIMATE OF ROOT
C N = NUMBER OF ITERATIONS
C R = RESIDUAL,ABS(F(ANS)).LT. R
C E = TOLERANCE BETWEEN SUCCESSIVE APPROXIMATIONS , ABS(X1-X2) .LT.E
C BOTH R AND E HAVE TO BE SATISFIED FOR CONVERGENCE
C X3 = ROOT OF THE NONLINEAR EQUATION
1 FORMAT(' SOLUTION DOES NOT CONVERGE IN',I5,' ITERATIONS')
X1=XL
X2=XH
DO 10 I=1,N
    X21=X2-X1
    X3=X1+F(X1)*(F(X2)-F(X1))/X21
    Z=F(X3)
    IF(ABS(Z).GT.R)GO TO 7
    IF(Abs(X21).LT.E)RETURN
7   IF(Z*(X2/X1).EQ.1)GO TO 9
    X1=X3
    GO TO 10
9   X2=X3
10  CONTINUE
    PRINT 1,N
    RETURN
ENO
SUBROUTINE SIMPSON(N,H,Y1,Y2,YINT1,YINT2)

```

```

DIMENSION Y1(1), Y2(1)
YINT1=Y1(1)+Y1(N)+6.*Y1(N-1)
YINT2=Y2(1)+Y2(N)+6.*Y2(N-1)
H=N/3
DO 10 I=2,M,2
  YINT1=YINT1+6.*Y1(I)+2.*Y1(I+1)
  YINT2=YINT2+6.*Y2(I)+2.*Y2(I+1)
10 CONTINUE
YINT1=H*YINT1/3.
YINT2=H*YINT2/3.
RETURN
END
FUNCTION CW(CI,X,L)
REAL L
XL=X/L
K=.01*CI+.0001
GO TO (100,200,990,400,500,990,990,800),K
100 CONTINUE
CW=CI*(.97187+XL*(1.4495+XL*(-6.403+3.96539*XL)))
IF(XL.GT..65)CW=.007*CI
GO TO 900
200 CONTINUE
CW=CI*(.96372+XL*(1.5801+XL*(-5.84557+3.17897*XL)))
IF(XL.GT..87)CW=.007*CI
GO TO 900
400 CONTINUE
CW=CI*(.97238+XL*(1.2537+XL*(-4.6849+2.3182*XL)))
IF(XL.GT..88)CW=.014*CI
GO TO 900
500 CONTINUE
CW=CI*(1.00126+XL*(-.177746+XL*(-.535748-1.6046*XL)))
IF(XL.GT..93)CW=.008*CI
GO TO 900
800 CONTINUE
CW=CI*(1.99383+XL*(1.02215+XL*(-5.9056+3.9775*XL)))
IF(XL.GT..89)CW=.025*CI
900 CONTINUE
IF(CM.GT.CY.OR.X.LY..4)CW=CI
RETURN
990 CONTINUE
STOP
END
FUNCTION F(LAMBDA)
COMMON K,B,VOS,ALPHA,GAMMA,U,REX,CX,XCT,DELTA,CXL
REAL LAMBDA,K
ULV=U/LAMBDA/VOS
IF (CX.GT. CXL) GO TO 20
XK*K*ALPHA*CX**GAMMA
GO TO 30
20 CONTINUE
XK*K*ALPHA*CXL**GAMMA
30 CONTINUE
F=LAMBDA*LAMBDA-4.395604396* ALOG(.06*REX*ULV**XK)**2
RETURN
END
FUNCTION INTGND(LAMBDA,X)
REAL INTGND1,LAMBDA,K
COMMON K,B,VOS,ALPHA,GAMMA,U,REX,CX,XCT,DELTA,CXL
VV=U/LAMBDA/VOS
ALV=ALOG(VV)
IF (CX.GT. CXL) GO TO 20
Z=ALPHA*CX**GAMMA

```

```

GO TO 30
20 CONTINUE
Z=ALPHA*CXL**GAMMA
30 CONTINUE
IFIX.GT.XCT GO TO 10
DELTA=5.*X/SQRT(REX)
GO TO 15
10 CONTINUE
DELTA=EXP(K*(LAMBDA-B)) *VV**(-K*Z)
15 CONTINUE
ADEL=ALOG(DELTA)
ADL1=ADEL-1.
F1=Z*ALV*(2./K*AOL1+2.*B+Z*ALV)
F2=2./K*AOL1*(B-1./K)+1./(K*K)*ADEL-ADEL+B*B
INTGND1=DELTA*(F1+F2)
RETURN
END
FUNCTION INTGND2(LAMBDA,X)
REAL INTGND2,LAMBDA,K
COMMON K,B,VOS,ALPHA,GAMMA,U,REX,CX,XCT,DELTA,CXL
VVU/LAMBDA/VOS
ALV=ALOG(VV)
IF (CX.GT. CXL) GO TO 20
Z=ALPHA*CXL**GAMMA
GO TO 30
20 CONTINUE
Z=ALPHA*CXL**GAMMA
30 CONTINUE
IFIX.GT.XCT GO TO 10
DELTA=5.*X/SQRT(REX)
GO TO 15
10 CONTINUE
DELTA=EXP(K*(LAMBDA-B)) *VV**(-K*Z)
15 CONTINUE
ADEL=ALOG(DELTA)
ADL1=ADEL-1.
F1=DELTA*LAMBDA*GAMMA*Z/CX*ALV
F2=1.+1./(K*K)*AOL1+B-1./K
INTGND2=F1+F2
RETURN
END
FINIS
SX,LGO
2.8 .03 22.5 100. 2.3 .6 7.2 .4 64.5 5. 30. 3.5E5
25 .001 .01 .01 2. 20. 1. .1 1. 10. 3.5E5
2.8 .08 22.5 200. 2.3 .6 7.2 .4 63.0 5. 30. 3.5E5
25 .001 .01 .01 2. 20. 1. .1 1. 10. 3.5E5
2.8 .03 22.5 400. 2.3 .6 7.2 .4 65.0 5. 30. 3.5E5
25 .001 .01 .01 2. 20. 1. .1 1. 10. 3.5E5
2.8 .08 22.5 500. 2.3 .6 7.2 .4 57.0 5. 30. 3.5E5
25 .001 .01 .01 2. 20. 1. .1 1. 10. 3.5E5
2.8 .08 22.5 900. 2.3 .6 7.2 .4 68.0 5. 30. 3.5E5
25 .001 .01 .01 2. 20. 1. .1 1. 10. 3.5E5

```

EOF ON IMP

BIBLIOGRAPHY

Achia, B. U., and Thompson, D. W., "Laser Holographic Measurement of Wall Turbulence Structures in Drag-Reducing Pipe Flow," International Conference on Drag Reduction, September 4-6, Paper A2, 1974.

Adrian, R. J., "Statistics of Laser Doppler Velocimeter Signals: Frequency Measurement," Journal of Physics E: Scientific Instruments, vol. 5, 1972.

Adrian, R. J., and Goldstein, R. J., "Analysis of a Laser Doppler Anenometer," Journal of Physics E: Scientific Instruments, vol. 4, 1971, pp. 505-511.

Angus, J. C., and French, M. J., "Measurements of Movements of Microscopic Objects: The Laser Doppler Meter," Industrial and Engineering Chemistry, vol. 61, no. 2, 1969.

Angus, J. C., Edwards, R. V., and Dunning, J. W., Jr., "Signal Broadening in the Laser Doppler Velocimeter," AIChE Journal, vol. 17, no. 6, November 1971, pp. 1509-1510.

Angus, J. C., Morrow, D. L., Dunning, J. W., Jr., and French, M. J., "Motion Measurement by Laser Doppler Techniques," Industrial and Engineering Chemistry, vol. 61, no. 2, February 1969, pp. 9-20.

Anyiwo, J. C., and Meroney, R. N., "A Semi-Empirical Transition Criterion for Laminar Wall Boundary Layers," ASME Publication, no. 75-FE-27, February 1976.

Aquino, H., and Lamontagne, R., "A Method of Measuring the Sub-layer Velocity-Profile of a Liquid with Polymer Additive," AIAA 9th Annual Meeting and Technical Display, AIAA Paper No. 73-79, Washington, D. C., January 1973.

Asher, J. A., "Odds and Ends Relating to Application of a Laser Velocimeter," Proceedings of a Workshop: The Use of the Laser Doppler Velocimeter for Flow Measurements, Purdue University, 9-10 March 1972, p. 147.

Astarita, G., Greco, G., Jr., and Nicodemo, L., "A Phenomenological Interpretation and Correlation of Drag Reduction," AIChE Journal, vol. 15, no. 4, July 1969, pp. 564.

Bark, F. H., Hinch, E. J., and Landahl, M. T., "Drag Reduction in Turbulent Flow Due to Additives: A Report on Euromech 52," Journal of Fluid Mechanics, vol. 68, part 1, 1971, pp. 129-138.

Barker, S. J., "Radiated Noise From Turbulent Boundary Layers in Dilute Polymer Solutions," Physics of Fluids, vol. 16, no. 9, California Institute of Technology, Pasadena, California, September 1973.

_____, "Laser-Doppler Measurements on a Round Turbulent Jet in Dilute Polymer Solutions," Journal of Fluid Mechanics, vol. 60, no. 4, October 1973, pp. 721-731.

Barnes, H. A., Townsend, P., and Walters, K., "Measurements Made on a Drag Reduction Solution with a Laser Velocimeter," Department of Applied Mathematics, University College of Wales, Aberystwyth, Nature, vol. 224, 8 November 1969.

Batchelor, G. K., "Diffusion in Free Turbulent Shear Flows," Cavendish Laboratory, Cambridge, 1957.

Beattie, H., "Drag Reduction Phenomena in Gas-Liquid Systems," International Conference on Drag Reduction, September 4-6, Paper D3, 1974.

Bedi, P. S., "A Simplified Optical Arrangement for the Laser Doppler Velocimeter," Journal of Physics E: Scientific Instruments, vol. 4, 1971, pp. 27-28.

Berman, N. S., and Cooper, E. E., "Laser Doppler Measurements of the Decay of Velocity Fluctuations in Dilute Polymer Solutions," Proceedings of Symposium on Turbulence Measurements in Liquids, University of Missouri at Rolla, 1969.

Berman, N. S., and Santos, V. A., "Laminar Velocity Profiles in Developing Flows Using a Laser Doppler Technique," AIChE Journal, vol. 15, no. 3, pp. 323-327, 1968.

Berman, N. S., Gurney, G. B., and George, W. K., "Pitot Tube Errors in Dilute Polymer Solutions," Physics of Fluids, vol. 16, no. 9, September 1973, pp. 1526-1528.

Black, T. J., "Viscous Drag Reduction Examined in the Light of a New Model of Wall Turbulence," Viscous Drag Reduction, ed. C. S. Wells, New York: Plenum Press, 1969.

Blake, K. A., "New Developments of the NEL Laser Velocimeter and the Treatment of Data," Opto-Electronics, vol. 5, 1973, pp. 27-39.

Blick, E. F., "Skin Friction Drag Reduction by Compliant Coatings," International Conference on Drag Reduction, September 4-6, Paper F2, 1974.

Boley, B. A., and Friedman, M. B., "On the Viscous Flow Around the Leading Edge of a Flat Plate," Journal of Acoustical Society of America, vol. 26, 1959, pp. 453-454.

Bossel, H. H., and Orloff, K. L., "Laser Doppler Anemometer for Water Tunnel Application," Journal of Hydraulics, vol. 6, no. 2, July 1972, pp. 101-105.

Bowlus, D. A., and Brighton, J. A., "Incompressible Turbulent Flow in the Inlet Region of a Pipe," Journal of Basic Engineering, September 1968, pp. 431-433.

Brady, J. F., "An Experimental Study of the Vibration, Noise, and Drag of a Cylinder Rotating in Water and Certain Polymer Solutions," Ph.D. Dissertation, University of Rhode Island, 1973.

Brand, R., and Persen, L., "Implications of the Law of Wall for Turbulent Boundary Layers," Acta Polytechnica Scandinavica, Ph 30, Trondheim, Norway, 1964.

Brayton, D. B., and Goethart, W. H., "A New Dual-Scatter Laser Doppler Shift Velocity Measuring Technique," ISA Transactions, vol. 10, no. 1, 1971, p. 40.

Brayton, D. B., Kalb, H. T., and Crossway, F. L., "A Two-Component Dual-Scatter Laser Doppler Velocimeter With Frequency Burst Signal Readout, in the Use of the Laser Doppler Velocimeter for Flow Measurements," Proceedings of a Workshop at Purdue University, March 1972.

Brennen, C., and Gadd, G. E., "Aging and Degradation in Dilute Polymer Solutions," Nature, vol. 215, 1967.

Brighton, J. A., "Incompressible Turbulent Flow in Inlet Region of a Pipe," Transactions of the ASME, vol. 90, series D, September 1968, pp. 431-433.

Broadbent, J. M., Kaye, A., Lodge, A. S., and Vale, D. G., "Possible Systematic Error in the Measurement of Normal Stress Differences in Polymer Solutions in Steady Shear Flow," Nature, vol. 217, 1968, pp. 55-56.

Bryson, A. W., Arunachalam, V. R., and Fulford, G. D., "A Tracer Dispersion Study of the Drag Reduction Effect in a Turbulent Pipe Flow," Journal of Fluid Mechanics, vol. 47, no. 2, 1971, pp. 209-230.

Butson, J., and Glass, D. H., "Mass-Transfer Measurements in the Turbulent Pipe Flow of a Solution of Drag Reduction Polymer," International Conference on Drag Reduction, September 4-6, Paper A3, 1974.

Carey, G. F., Chlupsa, J. E., and Schloemer, H. H., "Acoustic Turbulent Water-Flow Tunnel," Journal of Acoustical Society of America, 5 October 1966, pp. 373-379.

Carrier, G. F., and Lin, C. C., "On the Nature of the Boundary Layer Near the Leading Edge of a Flat Plate," Quarterly of Applied Mathematics, vol. 6, no. 1, 1948, pp. 63-68.

Castro, W., and Squire, W., "The Effect of Polymer Solutions on Transition in Pipe Flow," Applied Scientific Research, vol. 18, 1967, pp. 81-96.

Cebeci, T., Moninskis, G. J., and Smith, A. M. O., Calculation of Viscous Drag and Turbulent Boundary-Layer Separation on Two-Dimensional and Axisymmetric Bodies in Incompressible Flows, Report No. MDC J0973-01, Douglas Aircraft Company, November 1970.

Cermak, J. E., "Lagrangian Similarity Hypothesis Applied to Diffusion in Turbulent Shear Flow," College of Engineering, Colorado State University, 1962.

Cess, R. D., A Survey of the Literature in Heat Transfer in Turbulent Tube Flow, Westinghouse Research Report 8-0529-R24, Westinghouse Corp., 1958.

Chase, D. M., "Mean Velocity Profile of a Thick Turbulent Boundary Layer Along a Circular Cylinder," AIAA Journal, vol. 10, no. 7, July 1972.

Chatterton, N. E., Lewis, R. D., and George, E. W., "Two-Dimensional Laser-Doppler Velocimetry in Turbulent Flows," Proceedings of Symposium on Turbulent Movements in Liquids, University of Missouri at Rolla, ed. G. K. Patterson and J. L. Zaki, September 1969.

Christman, R. A., "Evaluation of the Quarter-Scale Water Tunnel Nozzle in Air," USC Technical Memorandum 2112-8-69, University of Southern California, 28 January 1969.

Chung, J. S., and Graebel, W. P., "Laser Anemometer Measurements of Turbulence in Non-Newtonian Pipe Flows," Physics of Fluids, vol. 15, no. 4, April 1972, pp. 546-554.

Clark, J. A., "A Study of Incompressible Turbulent Boundary Layers in Channel Flow," Journal of Basic Engineering, vol. 90, December 1968, pp. 455-468.

Clarke, W. B., Fluid Velocity Measurement by Doppler Shift of Scattered Light, AD-68421, Massachusetts Institute of Technology, 1968.

Clauser, F. H., "Turbulent Boundary Layers in Adverse Pressure Gradients," Journal of Aeronautical Sciences, vol. 21, no. 2, February 1954.

Coles, D., "The Problem of the Turbulent Boundary Layer," Journal of Applied Mathematics and Physics, vol. 5, 1954, pp. 181-201.

Coles, D., "The Law of the Wake in the Turbulent Boundary Layer," Journal of Fluid Mechanics, vol. 1, part 2, July 1956.

Comte-Bellot, G., "Coefficients de Dissymetrie et D'aplatissement, Spectres et Correlations en Turbulence de Conduits," Journal de Mecanique, vol. 11, no. 2, 1963.

Coriloni, E. R., and Brodkey, R. S., "A Visual Investigation of the Wall Region in Turbulent Flow," Journal of Fluid Mechanics, vol. 37, 1969.

Crawford, H. R. and Pruitt, G. T., Rheology and Drag Reduction of Some Dilute Polymer Solutions, Final Report, Contract No. N605306899 (NOTS), Westco Research, Dallas, Texas, July 1962.

Davis, D. T., "Analysis of a Laser Doppler Velocimeter," ISA Transactions, vol. 7, no. 1, 1968, pp. 43-51.

Denham, M. K.; The Use of Laser Anemometry for Fluid Flow Measurements, Report No. CA 13, Department of Chemical Engineering, University of Exeter, May 1971.

Dimant, Y., and Poreh, M., "Momentum and Heat Transfer in Flows With Drag Reduction," Technion, Israel Institute of Technology, Faculty of Civil Engineering Publication No. 203, 1974.

Dobrodjichi, G. A., Flow Visualization in the National Aero-nautical Establishments Water Tunnel, Report No. LR-557 NRC-12506-N72-29369, National Aeronautical Establishment, Ottawa, Ontario, February 1972, p. 56.

Dodge, D. W., and Metzner, A. B., "Turbulent Flow of Non-Newtonian Systems," AICHE Journal, vol. 5, no. 2, June 1959, pp. 189.

Donohue, G. L., "The Effect of a Dilute, Drag-Reducing Macro-Molecular Solution on the Turbulent Bursting Process," University Microfilms, Ann Arbor, Michigan, no. 73-15, 094, 1972.

Donohue, G. L., and Tiederman, W. G., "The Effect of a Dilute, Drag-Reducing Macro-Molecular Solution in the Viscous Sublayer of a Turbulent Channel Flow," ASME/ESL Film Library, New York, 1971.

Donohue, G. L., McLaughlin, D. K., and Tiederman, W. G., "Turbulence Measurements With a Laser Anemometer Measuring Individual Realizations," Physics of Fluids, vol. 15, 1972, p. 1920.

Donohue, G. L., Tiederman, W. G., and Reischman, M. M., "Flow Visualization of the Near-Wall Region in a Drag Reduction Channel Flow," Journal of Fluid Mechanics, vol. 56, no. 3, 1972, pp. 559-575.

Drain, L. E., "Coherent and Noncoherent Methods in Doppler Optical Heat Velocity Measurement," Journal of Physics D: Applied Physics, vol. 5, 1972, pp. 481-495.

Dryden, H. L., and Schubauer, G. B., "The Use of Dumping Screens for the Reduction of Wind-Tunnel Turbulence," Journal of Aeronautical Science, April 1947, pp. 221-228.

Dunning, J. W., and Berman, N. S., "Pipe Flow Measurements of Turbulence and Ambiguity Using Laser-Doppler Velocimetry," Journal of Fluid Mechanics, vol. 61, no. 2, 1973, pp. 289-299.

Durst, F., "Introduction to Laser Doppler Shift Anemometry," Technica, 408, 1971, pp. 47-61.

_____, "Scattering Phenomena and Their Application in Optical Anemometry," University of Karlsruhe, August 1972.

Durst, F., and Keller, R. J., "Structural Changes in Turbulent Conduit Flows by Polymer Additives," Fifth Australian Conference on Hydraulics and Fluid Mechanics, December 9-13, 1974.

Durst, F., and Whitelaw, J. H., "Theoretical Considerations of Significance to the Design of Optical Anemometers," ASME Paper No. 72-HT-7, 1972.

Durst, F., and Whitelaw, J. H., "Light Source and Geometrical Requirements for the Optimization of Optical Anemometry Signals," Opto-Electronics, vol. 5, 1973, pp. 137-151.

Durst, F., Melling, A., and Whitelaw, J. H., "Laser Anemometry: A Report on EUROMECH 36," Journal of Fluid Mechanics, vol. 56, no. 1, 1972, pp. 143-160.

Durst, F., Melling, A., and Whitelaw, J. H., Principles and Practices of Laser-Doppler Anemometry, Academic Press, 1976.

Eckelman, L. D., Fortuna, F., and Hanratty, T. J., "Drag Reduction and the Wavelength of Flow-Oriented Wall Eddies," Nature: Physical Science, 236:67, 10 April 1972, pp. 94-96.

Ecklemann, H., and Relchardt, H., "An Experimental Investigation in a Turbulent Channel Flow With a Thick Viscous Sublayer," Proceedings of the Symposium on Turbulence in Liquids, University of Missouri at Rolla, 1971.

Edwards, R. V., and Angus, J. C., "Spectral Analysis of the Signal From the Laser Doppler Flowmeter: Time Independent Systems," Journal of Applied Physics, vol. 42, no. 2, February 1971, pp. 837-850.

Einstein, H. A., and Li, H., "The Viscous Sublayer Along a Smooth Boundary," ASChE Journal of Engineering Mechanics, 1956, p. 945.

Elatia, R., Lehrer, J., and Kahanovitz, A., "Turbulent Shear Flow of Polymer Solutions," Israel Journal of Technology, vol. 4 1966, pp. 87-95.

Ellis, A. T., "Effects of Shear Treatment of Drag-Reducing Polymer Solutions and Fibre Suspensions," Nature, vol. 226, April 25, 1970.

Ellis, A. T., Ting, R. Y., and Nadolink, R. H., "Some Storage and Shear History Effects on Polymeric Friction Rediction," Journal of Hydraulics, vol. 6, no. 2, July 1972, pp. 66-69.

Ellis, A. T., Waugh, J. G., and Ting, R. Y., "Cavitation Suppression and Stress Effects in High-Speed Flows of Water With Dilute Macro-Molecule Additives," Journal of Basic Engineering, September 1970.

Ellison, T. H., "Turbulent Diffusion," Meteorology Science Progress, vol. 47, 1959, p. 495.

Ernst, W. D., "Investigation of the Turbulent Shear Flow of Dilute Aqueous CMC Solutions," AICHE Journal, vol. 12, 1966, p. 581.

_____, "Turbulent Flow of an Elasticoviscous Non-Newtonian Fluid," AIAA Journal, vol. 5, no. 5, 1967, pp. 906-909.

Fabula, A. G., "The Toms Phenomenon in the Turbulent Flow of Very Dilute Polymer Solutions," Proceedings of the Fourth International Congress of Rheology, part 3, ed. E. H. Lee, 1964, pp. 455-479.

_____, "An Experimental Study of Grid Turbulence in Dilute High Polymer Solutions," Ph.D. Dissertation, Pennsylvania State University, 1966, unpublished.

_____, "Fire Fighting Benefits of Polymeric Friction Reduction," Journal of Basic Engineering, September 1971, pp. 453-455.

Fenter, F. W., The Turbulent Boundary Layer on Uniformly Rough Surfaces at Supersonic Speeds, Report No. RE-E9R, Vought Research Center, Chance Vought Aircraft Inc., December 1959.

Fingerson, L. M., "Laser Doppler Anemometers," Measurements and Data, May-June 1976, pp. 78-65.

Fitzgerald, P. D., "Laser Doppler Velocimeter Evaluation and Measurements in a Flow With Drag Reduction," Ph.D. Dissertation, University of Michigan, 1974.

Foreman, J. W., Lewis, R. D., Thornton, J. R., and Watson, H. J., "Laser Doppler Velocimeter for Measurement of Localized Flow Velocities in Liquids," Proceedings of the IEEE, March 1966, pp. 424-425.

Foreman, J. W., George, E. W., Jetton, J. L., Lewis, R. D., Thornton, J. R., and Watson, H. J., "Fluid Flow Measurement With a Laser Doppler Velocimeter," IEEE Journal of Quantum Electronics, vol. QE-2, no. 8, 1966, pp. 260-266.

Fortuna, G., and Hanratty, T. J., "Use of Electromechanical Techniques to Study the Effect of Drag-Reducing Polymers on Flow in the Viscous Sublayer," Symposium Series, Drag Reduction, vol. 67, no. 11, 1971.

Fortuna G., and Hanratty, J. J., "The Influence of Drag-Reducing Polymers on the Viscous Sublayer," Journal of Fluid Mechanics, vol. 53, 1972, pp. 575-586.

Friehe, C. A., "Velocity Measurements in Dilute Polymer Solutions," Ph.D. Dissertation, Stanford University, 1968, unpublished.

Freihe, G. A., and Schwarz, W. H., "The Use of Pitot Static Tubes and Hot-Film Anemometers in Dilute Polymer Solutions," Proceedings of the Symposium on Viscous Drag Reduction, ed. C. S. Wells, New York: Plenum Press, 1969, p. 281.

Fruman, D. H., and Tulin, M. P., "Diffusion of a Tangential Drag-Reducing Polymer Injection on a Flat Plate at High Reynolds Numbers," Paper presented at the Hydroballistics Advisory Committee, 9-11 October 1974.

Fruman, D. H., Sundaram, T. R., and Daugard, S. J., "Effect of Drag-Reducing Polymer Injection on the Lift and Drag of a Two-Dimensional Hydrofoil," International Conference on Drag Reduction, September 4-6, Paper E2, 1974.

Gadd, G. E., "Turbulence Damping and Drag Reduction Produced by Certain Additives in Water," Nature, vol. 206, 1965, p. 463.

_____, "Differences in Normal Stress in Aqueous Solutions of Turbulent Drag-Reducing Additives," Nature, vol. 212, 1966, pp. 1348-1352.

George, W. K., "Analysis of Turbulent Flow Measurements from LDV Data, in the Use of Laser Doppler Velocimeter for Flow Measurements," Proceedings of a Workshop at Purdue University, March 1972.

_____, "The Measurement of Turbulence Intensities Using Real-Time Laser Doppler Velocimetry," Paper presented at the 2nd International Workshop on Laser Velocimetry, Purdue University, March 1974.

George, W. K., and Lumley, J. L., "Doppler Ambiguity and the Measurement of Turbulence, in The Use of the Laser Doppler Velocimeter for Flow Measurements," Proceedings of a Workshop at Purdue University, March 1972.

George, W. K., and Lumley, J. L., "The Laser-Doppler Velocimeter," Journal of Fluid Mechanics, vol. 60, no. 2, 4 September 1973, pp. 321-362.

George, W. K., Gurney, G. B., and Berman, N. S., "Technique for Rapid Friction Factor Fluid Characterization," Journal of Hydraulics, vol. 9, no. 1, January 1975, pp. 36-38.

Giles, W. B., "Similarity Laws of Friction-Reduced Flows," Journal of Hydraulics, vol. 2, no. 1, 1968, pp. 34-40.

Giles, W. B., and W. T. Petit, "Stability of Dilute Viscoelastic Flows," Nature, vol. 216, 1967, p. 470.

Goethert, W. H., Frequency Broadening in Reference Beam Laser Doppler Velocimeter Data, ARO, Inc. Report AEDC-TR-163, September 1971.

Goldstein, R. J., and Adrian, R. J., "Measurement of Fluid Velocity Gradients Using Laser-Doppler Techniques," Review of Scientific Instruments, vol. 42, no. 9, 1971.

Goldstein, R. J., and Kreid, D. K., "Measurement of Laminar Flow Development in a Square Duct Using a Laser Doppler Flowmeter," Journal of Applied Mechanics, vol. 34, 1967, p. 813.

Goldstein, R. J., and Hagen, W. F., "Turbulent Flow Measurements Using a Laser-Doppler Velocimeter," Physics of Fluids, vol. 10, 1967, pp. 1349-1352.

Goldstein, R. J., and Kreid, D. K., Fluid Velocity Measurement From the Doppler Shift of Scattered Laser Radiation, Mechanical Engineering Department, University of Minnesota, HTL TR No. 85, 1966.

Goldstein, R. J., Adrian, R. J., and Kreid, D. K., "Turbulent and Transition Pipe Flow of Dilute Aqueous Polymer Solutions," I&EC Fundamentals, vol. 8, no. 3, 1969, pp. 498-502.

Gordon, R. J., "Mechanism for Turbulent Drag Reductions in Dilute Polymer Solutions," Nature, vol. 227, August 1970, p. 599.

Goren, Y., and Norbury, J. F., "Turbulent Flow of Dilute Aqueous Polymer Solutions," Journal of Basic Engineering, 1967, pp. 814-822.

Glushko, G. S., "Turbulent Boundary Layer Near Flat Plates in Incompressible Fluids," Izvestiya Akademii Nauk SSSR, Mekhanika, no. 4, 1965, pp. 13-23.

Granville, P. S., "Frictional-Resistance and Velocity Similarity Forms of Drag-Reducing Dilute Polymer Solutions," Journal of Ship Research, vol. 12, no. 3, 1968, p. 201.

Created, C., "An Improved Method of Flow Measurements in Water," La Houille Blanche, no. 6, 1969, pp. 631-633.

_____, "Statistical Ambiguity in Laser Anemometry," Disa Information Bulletin, no. 12, November 1971.

Greene, H. L., Thomas L. C., Mostard, R. A., and Nokes, R. F.,
"Potential Biomedical Application of Drag-Reducing Agents,"
International Conference on Drag Reduction, September 4-6,
Paper H2, 1974.

Guenterberg, G. L., "Laser-Doppler Anemometer Measurements of
Turbulence in Drag-Reducing Flows," University of Michigan
Department of Engineering Mechanics, College of Engineering,
ORA Project 065050, December 1972.

Gupta, M. K., Metzner, A. B., and Hartnett, J. P., "Turbulent
Heat-Transfer Characteristics of Viscoelastic Fluids,"
International Journal of Heat Mass Transfer, vol. 10, 1967,
pp. 1211-1224.

Halleen, R. M., and Johnston, J. P., The Influence of Rotation
on Flow in a Long Rectangular Channel - An Experimental
Study, Report MD-18, Department of Mechanical Engineering,
Stanford University, 1967.

Han, L. S., "Hydrodynamic Entrance Lengths for Incompressible
Laminar Flow in Rectangular Ducts," Journal of Applied
Mechanics, September 1960, pp. 403-408.

Hanratty, T. J., "Study of Turbulence Close to a Solid Wall,"
Physics of Fluids (Supplement), 1967.

_____, "Use of Electromechanical Techniques to Study the
Influence of Drag-Reducing Polymers on Turbulence Close to a
Wall," Presented at Symposium on Turbulence in Liquids,
University of Missouri at Rolla, 1971.

Hansen, R. J., Little, R. C., Reischman, M. M., and Kelleher,
M. D., "Stability and the Laminar-to-Turbulent Transition in
Pipe Flows of Drag-Reducing Polymer Solutions," International
Conference on Drag Reduction, September 4-6, Paper B4, 1974.

Hanson, C. E., The Design and Construction of a Low-Noise, Low-
Turbulence Wind Tunnel, Report 79611-1, Massachusetts
Institute of Technology, January 13 1969.

Harys. J. L., Hoehne, V. O., Allen, J. M., and Whitacre, G. R.,
"Water Tunnel Design, Related Instrumentation Considerations
and a Selected Bibliography of Incompressible Internal Fluid
Flow," Contract No. DA-D1-021-AMC-203 (2) AD-457-110,
Battelle Memorial Institute, November 1964.

Hassid, S., and Poreh, M., "A Turbulent Energy Model for Flows With Drag Reduction," Journal of Fluids Engineering, no. 210 August 1974.

Hassid, S., and Poreh, M., "Boundary Layer Development of Polymer Solutions in Pressure Gradients," International Conference on Drag Reduction, September 4-6, Paper B-1, 1974.

Hassid, S., and Poreh, M., "A Turbulent Energy Model for Flows With Drag Reduction," Journal of Fluids Engineering, June 1975, pp. 241, 324.

Hatton, A. P., and Woolley, N. H., "Heat Transfer in Two-Dimensional Turbulent Confined Flows," Proceedings of Institute of Mechanical Engineers, 1972, pp. 625-633.

Head, M. R., and Rechenberg, I., "The Preston Tube as a Means of Measuring Skin Friction," Journal of Fluid Mechanics, vol. 14, 1962.

Hecht, A. M., "A Turbulent Mixing Length Formulation for Non-Newtonian Power Law Fluids," General Electric Co., Philadelphia, Penn.

Hershey, H. C., and Zakin, J. L., "A Molecular Approach to Predicting the Onset of Drag Reduction in the Turbulent Flow of Dilute Polymer Solution," Chemical Engineering Science, vol. 22, 1967, p. 1847.

Hetzner, A. B., and Astarita, G., "External Flow of Viscoelastic Materials: Fluid Property Restrictions on the Use of Velocity-Sensitive Probes," AIChE Journal, vol. 13, 1967, p. 550.

Hjelmfelt, A. T., Jr., and Mockros, L. F., "Motion of Discrete Particles in a Turbulent Fluid," Applied Science, Research, vol. 16, 1965, pp. 149-161.

Hoyt, J. W., "Drag Reduction Effectiveness of Polymer Solutions in the Turbulent-Flow Rheometer: A Catalog," Polymer Letters, vol. 9, 1971, pp. 851-862.

_____, "The Effects of Additives on Fluid Friction," Freeman Review, Journal of Basic Engineering, vol. 94, 1972, pp. 258-285.

Hsu, K. S., "Diffusion of Polymers in a Developing Boundary Layer," Masters Thesis, University of Iowa, January 1971.

Huang, T. T., "Similarity Laws for Turbulent Flow of Dilute Solutions of Drag-Reducing Polymers," Physics of Fluids, 1974.

Hussain, A. K., and Reynolds, W. C., The Mechanics of a Perturbation Wave in Turbulent Shear Flow, Report No. FM-6, Department of Mechanical Engineering, Stanford University, 1970.

Jackson, D. A., and Paul, D. M., "Measurement of Supersonic Velocity and Turbulence by Laser Anemometry," Journal of Physics E, Scientific Instrumentation, vol. 4, 1971, pp. 173-177.

Jenkins, F. A., and White, H. E., Fundamentals of Optics, New York: McGraw-Hill Book Company, Inc., 1957.

Johnson, B., and Barchi, R. H., "The Effect of Drag-Reducing Additives on Boundary Layer Turbulence," AIAA 3rd Propulsion Joint Specialist Conference, Report No. 67-459, 17-21 July 1967.

Jonsson, L., "Laser-Velocity Meter," Journal of Hydraulic Research, vol. 9, no. 4, 1971.

Journal of the Hydraulics Division Proceedings of the American Society of Civil Engineers Discussion, Paper 6988, January 1970, pp. 251-305.

Kadykov, I. F., and Lyanshev, L. M., "Influence of Polymer Additives on the Pressure Fluctuations in a Boundary Layer," Soviet Physics-Acoustics, vol. 16, no. 1, 1970, p. 59.

Karpuk, M. E., "A Laser Doppler Anemometer for Viscous Sublayer," Masters Thesis, Oklahoma State University, 1974.

Katisibas, P., Bulakrishman, D., White, D., and Gordon, R. J., "Drag Reduction Correlations," International Conference on Drag Reduction, September 4-6, Paper B-2, 1974.

Keller, A., Yilmaz, E., and Hammitt, F. G., Comparative Investigations of the Scattered Light Counting Method for the Registration of Cavitation Nuclei and the Coulter Counter, Report No. UMICH 01357-36-T, University of Michigan, Department of Mechanical Engineering, Ann Arbor, Michigan, 1974.

Killen, J. M., and Almo, J., "Experimental Study of Effects of Dilute Solutions of Polymer Additives on Boundary Layer Characteristics," Viscous Drag Reduction, ed. C. S. Wells, New York: Plenum Press, 1969.

Kim, H. T., Kline, S. J., and Reynolds, W. C., An Experimental Study of Turbulence Production Near a Smooth Wall in the Turbulent Boundary Layer With Zero Pressure Gradient, Report MD-20, Department of Mechanical Engineering, Stanford University, 1968.

Kim, S., and Tagori, T., "A Correlation of the Toms Phenomenon," International Conference on Drag Reduction September 4-6, Paper B-3, 1974.

Kline, S. J., "On the Nature of Stall," Journal of Basic Engineering, September 1959, pp. 305-320.

Kline, S. J., and McClintock, F. A., "Uncertainties in Single-Sample Experiments," Mechanical Engineering, January 1953.

Kline, S. J., and Schraub, F. A., A Study of the Turbulent Boundary Layer With and Without Longitudinal Pressure Gradients, Report MD-12, Department of Mechanical Engineering, Stanford University, 1965.

Kline, S. J., Rundtadler, P. W., and Reynolds, W. C., An Experimental Investigation of the Flow Structure of the Turbulent Boundary Layer, Report MD-8, Department of Mechanical Engineering, Stanford University, 1963.

Kline, S. J., Morkovin, M. V., Sovran, G., and Cockrell, D. J., "Computation of Turbulent Boundary Layers - 1986," Proceedings on AFOSR-IEP Stanford Conferences 1 and 2, Stanford University, California, 1968.

Kline, S. J., Reynolds, W. C., Schraub, F. A., and Runstadler, P. W., "The Structure of Turbulent Boundary Layers," Journal of Fluid Mechanics, vol. 30, 1967, p. 741.

Kobets, G. F., Matjukhov, A. P., and Migirenko, G. S., "Connection Between Synthetic and Natural Polymer Solutions Physical Properties With Drag Reduction in Turbulent Flow," International Conference on Drag Reduction, September 4-6, Paper D4, 1974.

Kowalski, T., "Turbulence Suppression and Viscous Drag Reduction by Non-Newtonian Additives," Transactive Royal Institute of Naval Architecture, vol. 2, April 1968, pp. 207-219.

Kowalski, T., and Brundrett, E., "Macromolecular Entanglement Hypothesis in Drag Reduction Flows," International Conference on Drag Reduction, September 4-6, Paper C1, 1974.

Kreid, D. K., "Measurements of the Developing Laminar Flow in a Square Duct: An Application of the Laser Doppler Flow Meter," Masters Thesis, University of Minnesota, 1966.

Kumor, S. M., and Sylvester, N. D., "Effects of a Drag-Reducing Polymer on the Turbulent Boundary Layer," AICHE Symposium, Series 130, vol. 69, no. 1, 1973, pp. 1-13.

Latto, B., and Czaban, J., "On the Performance of Turbomachinery in the Presence of Aqueous Polymer Solutions," International Conference on Drag Reduction, September 4-6, Paper G1, 1974.

Latto, B., and Middleton, J. A., "Effect of Dilute Polymer Solutions on External Boundary Layers," Proceedings of the Symposium on Turbulence in Liquids, University of Missouri at Rolla, 1971.

Latto, B., and Shen, C. H., "Effect of Dilute Polymer Solution Injection on External Boundary Layer Phenomena," Canadian Journal of Chemical Engineering, vol. 48, February 1970.

Laufer, J., Investigation of Turbulent Flow in a Two-Dimensional Channel, NACA Report No. 1053, National Advisory Committee on Aeronautics, 1951.

Launder, B. E., and Spalding, D. G., Mathematical Models of Turbulence, London: Academic Press, 1972.

Lennert, A. E., et al., Summary Report of the Development of a Laser Velocimeter to be Used in AEDC Wind Tunnels, AEDC-RT-70-101, July 1970.

Leonard, J. W., "Linearized Compressible Flow by the Finite Element Method," Bell Aerosystems, December 1969.

Lezius, D. K., and Johnston, J. P., The Structure and Stability of Turbulent Wall Layers in Rotating Channel Flow, Report MD29, Department of Mechanical Engineering, Stanford University, August 1971.

Lighthill, M. J., "On Sound Generated Aerodynamically," Proceedings of Royal Society, London, vol. 222, 23 February 1954.

Lin, C. C., Turbulent Flows and Heat Transfer, Princeton: Princeton University Press, 1959.

Little, R. C., and Wiegard, M., "Drag Reduction and Structural Turbulence in Flowing Polyox Solutions," Naval Research Laboratory, Journal of Applied Polymer Science, vol. 11, 1970.

Logan, S. E., "Laser Velocimeter Measurements of Reynolds Stress and Turbulence in Polymer Solutions," AIAA Journal, vol. 10, 1972, pp. 962-964.

_____, "Laser Velocimeter Measurement of Reynolds Stress and Turbulence in Dilute Polymer Solutions," Ph.D. Dissertation, California Institute of Technology, 1972, unpublished.

Loof, J., "A Synthesis on Drag Reduction Experiment at Berlin From Compliant Surfaces and Gas Film at Polymers," International Conference on Drag Reduction, September 4-6, Paper F3, 1974.

Lumley, J. L., "The Toms Phenomenon: Anomalous Effects in Turbulent Flow of Dilute Solutions of High Molecular Weight Linear Polymers," Applied Mechanics Review, vol. 20:1139, 1967.

_____, "Drag Reduction by Additives," Annual Review of Fluid Mechanics, vol. 1, 1969.

_____, "Drag Reduction in Turbulent Flow by Polymer Additives," Journal of Polymer Sciences, vol. 7, 1973, pp. 263-290.

Lumley, J. L., and McMahon, J. F., "Reducing Water Tunnel Turbulence by Means of Honeycomb," Pennsylvania State University ORL 271750, Journal of Basic Engineering, December 1967, pp. 764-770.

Lumley, J. L., George, W. K., and Kobashi, Y., "The Influence of Ambiguity and Noise on the Measurement of Turbulent Spectra by Doppler Scattering," Proceedings of Symposium on Turbulence Measurements in Liquids, University of Missouri at Rolla, 1969.

Mans, J. R., and Wilhelm, L. R., "Effect of Polymer Injection on Frictional Drag in Turbulent Pipe Flow," Journal of Hydraulics, vol. 4, no. 1, January 1970.

Mazumder, M. K., and Wankum, D. L., "SNR and Spectral Broadening in Turbulence Structure Measurements Using a CW Laser," Applied Optics, vol. 9, no. 3, March 1970.

Mayo, W. T., Jr., Riter, S., and Shag, M. T., "An Introduction to the Estimation of Power Spectra From Single Particle LDV Data," LDA Workshop, Oklahoma State University, 11-13 June 1973.

Mazumder, M. K., and Wankum, D. L., "SNR and Spectral Broadening in Turbulence Structure Measurement Using a CW Laser," Applied Optics, vol. 9 no. 3, March 1970, pp. 633-637.

Mazumder, M. K., McLeod, P. D., and Testerman, M. K., "Application of a Laser Doppler Velocity Meter in Turbulence Characterization in the Use of the Laser Doppler Velocimeter for Flow Measurements," Proceedings From a Workshop at Purdue University, March 1972.

McCarthy, J. H., "Flat-Plate Frictional Drag Reduction with Polymer Injection," Journal of Ship Research, December 1971.

McIlroth, J. C., "Continuous Degradation of Polymer Solutions in Simulated Pipe Flow," International Conference on Drag Reduction, September 4-6, Paper C3, 1974.

McLaughlin, D. K., and Tiederman, W. G., "Statistical Biasing in Individual Realization Laser Anemometry," Physics of Fluids, (to be published).

Melling, A., Scattering Particles for Laser Anenometry in Air: Selection Criteria and Then Realization, Report ET/TN/B/7, Imperial College, London, England, April, 1971.

Mellor, G. L., "The Effects of Pressure Gradients on Turbulent Flow Near a Smooth Wall, Journal of Fluid Mechanics, vol. 24, part 2, 1966, pp. 255-274.

Mellor, G. S., and Herring, H. G., "Two Methods of Calculating Turbulent Boundary Layer Development Based on Numerical Solutions of the Equations of Motion," AFOSR - API Conference on Turbulent Boundary Layer, Stanford University, vol. 1, 1968, pp. 331-365.

Merrill, E. W., Smith, K. A., and Chung, R. Y. C., "Drag Augmentation by Polymer Addition," Massachusetts Institute of Technology, Cambridge, Massachusetts, 1964.

Merrill, E. W., Smith, K. A., Shin, H., and Mickley, H. S., "Study of Turbulent Flows of Dilute Polymer Solutions in a Couette Viscometer," Transactions of the Society of Rheology, vol. 10, no. 1, 1966, p. 335.

Metzner, A. D., and Astarita, G., "Effects of Local Injection of a Drag-Reducing Fluid into Turbulent Pipe Flow of a Newtonian Fluid," Physics of Fluids, vol. 10, no. 9, 1967, p. 1890.

Meyer, W. A., "A Correlation of the Frictional Characteristics for Turbulent Flow of Dilute Viscoelastic Non-Newtonian Fluids in Pipes," AIChE Journal, vol. 12, no. 3, May 1966, pp. 522-525.

Meyer, W. A., and Kline, S. J., A Visual Study of the Flow Model in the Later Stages of Laminar-Turbulent Transition on a Flat Plate, Report MD-7, Department of Mechanical Engineering, Stanford University, 1961.

Middleman, S., The Flow of High Polymers, John Wiley & Sons, 1968.

Millward, A., and Lilley, G. M., "Turbulent Pressure Fluctuations in Water With Drag-Reducing Additives," International Conference on Drag Reduction, September 4-6, Paper Al, 1974.

Mollo-Christense, E., "Physics of Turbulent Flow," AIAA Journal, vol. 9, no. 7, 1971, p. 1217.

Mongia, H., and Russell, G. A., "Preliminary Design of an Acoustic Water Tunnel," AD-682-232, University of Massachusetts, January 1969.

Morel, T., "Comprehensive Design of Axisymmetric Wind Tunnel Contractions," ASME Publication, no. 75-FE-17, February 1976.

Moretti, P. M., and Keys, W. M., Heat Transfer Through an Incompressible Turbulent Boundary Layer With Varying Free-Stream Velocity and Varying Surface Temperature, Report No. PG-1, Stanford University, 1964.

Morkovin, M. V., "On Eddy Diffusivity, Quasi-Similarity and Diffusion Experiment in Turbulent Boundary Layers," Journal of Heat Mass Transfer, vol. 8, 1963.

Morse, H. L., Tullis, B. J., Seifert, H. S., and Babcock, W., "Development of a Laser-Doppler Particle Sensor for the Measurement of Velocities in Rocket Exhausts," Journal of Spacecraft, vol. 6, no. 3, 1969, pp. 264-272.

Mysel, K., "Flow of Thickened Fluids," U.S. Patent 2, 492, 173, 1949.

Narahari Rao, K., Narasimha, R., and Badri Narayana, M. A., "The 'Bursting' Phenomenon in a Turbulent Boundary Layer," Journal of Fluid Mechanics, vol. 48, 1971, p. 339.

Nash-Webbler, J. L., and Oates, G. C., "An Instrument for Skin Friction Measurements in Thin Boundary Layers," Journal of Basic Engineering, December 1971, pp. 571-575.

Nicodemo, L. D., and Astarita, G., "Velocity Profiles in Turbulent Pipe Flow of Drag-Reducing Liquids," Chemical Engineering Science, vol. 24, 1969, p. 1241.

Novak, B. M., "Effect on Drag Forces on the Activated Sludge Flocs," International Conference on Drag Reduction, September 4-6, Paper H3, 1974.

Oldaker, D. K., and Tiederman, W. G., "The Effect of Drag Reduction Upon Flow in the Near The Wall Region," Scenario, Film Department of Mechanical and Aerospace Engineering, Oklahoma University, 1973.

Oldroyd, J. G., Proceedings of the First International Congress on Rheology, Amsterdam: North Holland Publishing Co., 1949, p. 130.

Oliver, D. R., "The Expansion/Contraction Behavior of Laminar Liquid Jets," Canadian Journal of Chemical Engineering, vol. 44, 1966, p. 100.

Olsen, J. H., and Liv, H. T., Construction and Operation of a Water Tunnel in Application to Flow Visualization Studies of an Oscillating Airfoil, Report No. NASA-CR-114696, Report 13, Contract NASA-6927, Flow Research Inc., Kent, Washington, May 1973.

Orloff, K. L., and Logan, S. E., "Confocal Backscatter Laser Velocimeter With On-Axis Sensitivity," Paper presented at LDA Workshop, Oklahoma State University, 11-13 June 1973.

Palyvos, J. A., Drag Reduction and Associated Phenomena Internal and External Liquid Flows, Report No. 741, Thermodynamics and Transport Helo, Schod of Chan. England, National Technical University, Athens 147, Greece, September 1974.

Pasquill, F., "Lagrangian Similarity and Vertical Diffusion From a Source at Ground Level," Quarterly Journal of the Royal Meteorological Society, vol. 92, no. 392, April 1966.

Patel, V. C., "Calibration of the Preston Tube and Limitations in its Use in Pressure Gradients," Journal of Fluid Mechanics, vol. 23, 1965, p. 185.

_____, A Unified View of the Law of the Wall Using Mixing-Length Theory, HHR Report No. 137, Iowa Institute of Hydraulic Research, University of Iowa, April 1972.

Patel, V. C., and Head, R. M., "Some Observations of Skin Friction and the Velocity Profile in Fully Developed Pipe and Channel Flow," Journal of Fluid Mechanics, vol. 38, 1969, pp. 181-201.

Patel, V. C., Nakayama, A., and Damian, R., "Measurements in the Thick Axisymmetric Turbulent Boundary Layer Near the Tail of a Body of Revolution," Journal of Fluid Mechanics, vol. 63, part 2, 1974, pp. 345-367.

Patel, V. C., and Head, M. R., "Some Observations on Skin Friction and Velocity Profiles in Fully Developed Pipe and Channel Flows," Journal of Fluid Mechanics, vol. 38, part 1, 1969, pp. 181-201.

Patterson, G. K., and Florez, G. L., "Velocity Profiles During Drag Reduction," Viscous Drag Reduction, ed. C. S. Wells, New York: Plenum Press, 1969.

Person, L. N., "Boundary Layer Theory," Tapin, Forlag, Trantherin, 1972.

Peterlin, A., "Molecular Model of Drag Reduction by Polymer Solutes," Nature, vol. 227, August 1970, p. 598.

Pfeifer, H. J., "Realization Time of Small Particles," Proceedings of a Workshop on the Use of the Laser-Doppler Velocimeter for Flow Measurements, Purdue University, 1972, p. 534.

Pfeffer, R., and Kane, R. S., "A Review of Drag Reduction in Dilute Gas-Solids Suspension Flow in Tubes," International Conference on Drag Reduction, September 4-6, Paper F1, 1974.

Piair, M., "Flow of Dilute Polymer Solutions," Laboratories at Aerodynamics Batiment 502, Lentre Universities, Orsay, France, Film, 1974.

Pope, R. J., "Skin-Friction Measurements in Laminar and Turbulent Flows Using Heated Thin-Film Gages," AIAA Journal, vol. 10, no. 6, June 1972, pp. 729-730.

Poreh, M., and Germak, J. E., "Study of Diffusion From a Line Source in a Turbulent Boundary Layer," International Journal of Heat Mass Transfer, vol. 7, 1964.

Poreh, M., and Crunblatt, L., "Phenomenological Models of Boundary Layer Flow With Drag Reduction," Publication No. 196, Technion, Israel Institute of Technology, 1973.

Poreh, M., and Dimant, Y., "Velocity Distribution and Friction Factors in Pipe Flows With Drag Reduction, Publication No. 175, Technion, Israel Institute of Technology, 1972.

Poreh, M., and Hsu, K. S., Diffusion of Drag-Reducing Polymers in a Turbulent Boundary Layer, HHR Report No. 125, Iowa Institute of Hydraulic Research, University of Iowa, April 1971.

Preston, J. H., "The Determination of Turbulent Skin Friction by Means of Pitot Tubes," Journal of Royal Aerodynamic Society, vol. 58, 1954, p. 109.

Quarmby, A., "Fully-Developed Turbulent Flow in the Circular Tube and Parallel Plate Channel," Transactions of the ASME, March 1969, pp. 124-127.

Rao, G. N. V., "The Law of the Wall in a Thick Axisymmetric Turbulent Boundary Layer," Journal of Applied Mechanics, March 1967.

Reischmann, M. M., "Laser Anemometer Measurements in Drag-Reducing Channel Flow," Ph.D. Dissertation, Oklahoma State University, 1973.

Reischmann, M. M., and Tiederman, W. G., "Laser-Doppler Anemometer Measure in Drag-Reducing Channel Flows," Journal of Fluid Mechanics, part 2, 1975, pp. 369-392.

Reneau, L. R., Johnston, J. P., and Kline, S. J., "Performance and Design of Straight, Two-Dimensional Differentials," Journal of Basic Engineering, March 1967.

Ribeiro, M. M., and Whitelaw, J. H., "Turbulent Mixing of Co-Axial Jets With Particular Reference to the Near-Exit Region," ASME Publication 75-FE-36, 1 February 1976.

Roberts, D. J., Evaluation of a Laser Anemometer for Turbulence Measurements, Research Report No. 01-04-74, Case Western Reserve University, Department of Chemical Engineering, 1974.

Rollin, A., and Seyer, F. A., "Velocity Measurements in Turbulent Flow of Dilute Viscoelastic Solutions," Department of Chemical Engineering, University of Alberta, Edmonton, Ala., 1972.

Rollin, A., and Seyer, F. A., "Statistical Analysis of Instantaneous Velocities in Turbulent Flow of Dilute Viscoelastic Solutions," Presented at Symposium on Turbulence in Liquids, University of Missouri at Rolla, 1973.

Rouse, P. E., Jr., "A Theory of the Linear Viscoelastic Properties of Dilute Solutions of Coiling Polymers," Journal of Chemical Physics, vol. 21, 1953, p. 1272.

Rudd, M. J., "The Laser Dopplermeter - A Practical Instrument," Optics Technology, November 1969.

_____, "Measurements Made on a Drag-Reducing Solution With a Laser Velocimeter," Nature, vol. 224, November 1969, p. 587.

_____, "Measurements on a Drag-Reducing Fluid With a Laser Velocimeter," Guided Weapons Division, British Aircraft Corp., Filton Bristol, 1969.

_____, "A New Theoretical Model for the Laser Dopplermeter," Journal of Scientific Instruments, series 2, 2, 1969, pp. 55-58.

_____, "The Laser Anemometer - A Review," Optics and Laser Technology, vol. 3, no. 4, 1971.

_____, "Laser Dopplermeter and Polymer Drag Reduction," Drag Reduction, Chemical Engineering Progress Symposium Series, vol. 67, 1971.

_____, "Velocity Measurements Made With a Laser Dopplermeter on the Turbulent Pipe Flow of a Dilute Polymer Solution," Journal of Fluid Mechanics, vol. 51, no. 4, 1972, pp. 673-685.

Ryabokon, M. P., and Yelkin, U. S., "Tests of Short Diffusers, at High Supersonic Velocities," Fluid Mechanics-Soviet Research, January-February 1975, pp. 52-59.

Sampson, R. L., "A Study of the Turbulent Non-Newtonian Boundary Layer on a Flat Plate," Ph.D. Dissertation, Notre Dame University, December 1969.

Sarpkaya, T., "On the Performance of Hydrofoils in Dilute Polyox Solutions," International Conference on Drag Reduction, September 4-6, Paper E1, 1974.

Sarpkaya, T., Rainey, P. G., and Kell, R. E., "Flow of Dilute Polymer Solutions About Circular Cylinders," Journal of Fluid Mechanics, vol. 57, part 1, 1973.

Savins, J. G., "Some Comments on Pumping Requirements for Non-Newtonian Fluids," Journal of the Institute of Petroleum, vol. 47, 1961, p. 329.

Sayer, W. W., "Dispersion of Mass in Open-Channel Flow,"
Colorado State University, February 1968.

_____, "Dispersion of Silt Particles in Open-Channel Flow,"
Journal of Hydraulics Div. ASCE vol. 95 Hy-3 1969
1801009-1038.

Schubauer, G. B., Spangenber, W. G., and Kleganoff, P. S.,
"Aerodynamic Characteristics of Damping Screens," 7th International Congress for Applied Mechanics, September 5-11, Technical Note 2001, 1948.

Seban, R. A., "Heat Transfer and Effectiveness for a Turbulent Boundary Layer With Tangential Fluid Injection," Journal of Heat Transfer, November 1960, pp. 303-312.

Sedov, L. I., Vassetkaya, N. G., and Ioselevich, V. A.,
"Calculation of Turbulent Boundary Layers With Polymer Additives," International Conference on Drag Reduction, September 4-6, Paper 06, 1974.

Sellin, R. H. J., "Experiments With Polymer Additives in a Long Pipeline," International Conference on Drag Reduction, September 4-6, Paper G2, 1974.

Seyer, F. A., and Metzner, A. B., "Turbulence Phenomena in Drag-Reductin Systems," AICHE Journal, vol. 15, no. 3, May 1969, pp. 426-434.

Seyer, F. A., and Metzner, A. B., "Drag Reduction in Large Tubes and the Behavior of Annular Films of Drag-Reducing Fluids," Canadian Journal of Chemical Engineering, vol. 47, December 1969, pp. 525-529.

Shankar, P. N., Laser Doppler Velocity Profile Measurements in Laminar and Turbulent Pipe Flow, Report No. 69-C-396, General Electric Research and Development Center, Schenectady, N. Y., 1969.

Shaver, R. G., and Merrill, E. W., "Turbulent Flow of Pseudo-Plastic Solution in Straight Cylindrical Tubes," AICHE Journal, vol. 5, 1959, pp. 181-187.

AD-A103 070

NAVAL UNDERWATER SYSTEMS CENTER NEWPORT RI
AN EXPERIMENTAL STUDY OF POLYMER DRAG REDUCTION AND BOUNDARY LA--ETC(U)

F/6 20/4

5 IF 5
A-03 E70

UNCLASSIFIED

NUSC-TD-5656

NL

END
DATE
FORMED
9-81
DTIC

Shulman, Z. P., Pikryuailo, N. A., Kaberdians, E. B., and Nestrov, A. K., "Effect of Polymer Additives on Intensity and Spectrum of Velocity Gradient Fluctuations Close to a Solid Surface," International Conference on Drag Reduction, September 4-6, Paper A4, 1974.

Sirmalis, J. W., "A Study of the Drag Characteristics and Polymer Diffusion in the Boundary Layer of an Axisymmetric Body," Ph.D. Dissertation, University of Rhode Island, 1975.

Smith, C. R., "A Note on a Diffuser Generated Flow Unsteadiness," Journal of Fluids Engineering, September 1975, pp. 377-379.

Smith, K. A., Merrill, E. W., Mickley, H. S., and Virk, P. S., "Anomalous Pitot Tube and Hot Film Measurements in Dilute Polymer Solutions," Chemical Engineering Sciences, vol. 22, 1967, p. 619.

Spalding, D. B., "A Single Formula for the Law of the Wall," Journal of Applied Mechanics, vol. 28, vol. 86, series E, no. 3, September 1961.

_____, "A Model and Calculation Procedure for the Friction and Heat Transfer Behavior of Dilute Polymer Solutions in Turbulent Pipe Flow," Progress in Heat Transfer, vol. 5, London: Pergamon Press, 1972, pp. 275-283.

Spangler, J. G., "Studies of Viscous Drag Reduction With Polymers Including Turbulence Measurements and Roughness Effects," Viscous Drag Reduction, ed. C. S. Wells, New York: Plenum Press, 1969.

Stevenson, W. H., et al., "The Use of the Laser Doppler Velocimeter for Flow Measurements," Project Squid-Workshop held at Purdue University, 9-10 March 1972.

Stevenson, W. H., Pudigo, M. K., and Zamnot, R. E., "Bibliography on Laser Doppler Velocimeters, Theory, Design, and Application," NTIS No. AD-746-634, National Technical Information Service, July 1972.

Stow, F. S., and Elliott, J. H., "Drag on a Tethered Ball in Solution of Drag Reducing Polymers," Polymer Letters, vol. 8, 1970, pp. 611-615.

Sylvester, N. D., and Kumar, S. M., "Degradation of Dilute Polymer Solutions in Turbulent Tube Flow," AICHE Symposium Series 130, vol. 69, 1973, pp. 69-81.

Tanner, R. I., and Pipkin, A. C., "Intrinsic Errors in Pressure-Hole Measurements," Transactions of the Society of Rheology, vol. 13, no. 4, 1969, pp. 471-484.

Tassinari, P. J., and Durgin, W. W., "An Investigation of the Errors Associated With the Westinghouse System for the Blue Plains Water Pollution Control Plant, Flow Measurements in Rectangular Ducts," Alden Research Laboratory, November 1975.

_____, "Analytical Production of the Influence of Polymer Additives on the Shear Drag Bodies of Revolution," Journal of Hydronautics, vol. 8, 1974, p. 45.

Thompson, D. H., "The Use of Digs for Water Tunnel Flow Visualization," ARL/A-Note-339, Aeronautical Research Laboratory, Melbourne, Australia, February 1973.

_____, "Summary of Water Tunnel Flow Visualization Technology," ARL/A-Note-335, Aeronautical Research Laboratory, Melbourne, Australia, January 1972.

Thompson, E. R., and Snyder, W. T., "Drag Reduction of a Non-Newtonian Fluid by Fluid Injection at the Wall," Journal of Hydronautics, vol. 2, no. 4, October 1968.

Tiederman, W. G., and Reynolds, W. C., Stability of Turbulent Poiseuille Flow With Application to the Malkus Theory of Turbulence, Report No. FM-2, Department of Mechanical Engineering, Stanford University, 1965.

Tomita, Y., "Pipe Flows of Dilute Aqueous Polymer Solutions," Bulletin of Journal of Ship and Marine Engineers, vol. 13, no. 61, 1970, pp. 926-942.

Toms, B. A., "Some Observations on the Flow of Linear Polymer Solutions Through Straight Tubes at Large Reynolds Numbers," Proceedings 1st International Congress on Rheology 1948, vol. II, Amsterdam: North Holland Publishing Co., 1949, p. 135.

Townsend, A. A., The Structure of Turbulent Shear Flow, Cambridge: University Press, 1954.

Thorne, P. F., "Drag Reduction in Fire-Fighting," International Conference on Drag Reduction, September 4-6, Paper H1, 1974.

Tullis, J. P., and Ramu, K. L. V., Viscous Drag Reduction in Developing Pipe Flow, Report No. 34, Hydro-Machinery Laboratory, Colorado State University, November 1973.

Tullis, J. P., and Ramu, K. L. U., "Drag Reduction in Developing Pipe Flow With Polymer Injection," International Conference on Drag Reduction September 4-6, Paper C3, 1974.

Treacy, E. B., "Analysis of Some Factors Affecting the Laser Doppler Velocimetry," Instrumentation of Aerospace Industry, Instrumentation Society of America Proceedings of May 1971, vol. 17, 1971, pp. 165-173.

Turner, G. K., Associates, "Fluorometry in Studies of Pollution and Movements of Fluids," Palo Alto, California, Bulletin, no. 9941B, May 1971.

Turner, G. K., Associates, "Laboratory Instruments" Bulletin, Palo Alto, California, 1972.

Uzkan, T., and Reynolds, W. C., A Turbulent Boundary Layer on a Wall Moving at the Free Stream Velocity, Report No. MD-14, Department of Mechanical Engineering, Stanford University, 15 August 1965.

Vlachos, N., A Statistical Analysis of Error in Laser Doppler Measurements Due to Velocity Gradients, International Report, Imperial College, Department of Mechanical Engineering, 1973.

Van den Berg, K., The Law of the Wall in Two- and Three-Dimensional Turbulent Boundary Layers, NLR TR 72111 U, National Aerospace Laboratory, The Netherlands, 3 January 1973.

Van Driest, E. R., "On Turbulent Flow Near a Wall," Journal of Aeronautical Science, vol. 23, 1956, pp. 1007-1011.

_____, "Turbulent Drag Reduction of Polymeric Solutions," Journal of Hydronautics, vol. 4, no. 3, 1970, pp. 120-126.

Vasetskaya, N. G., and Iosilevitch, V. A., "Semiempirical Turbulence Theory for Dilute Polymer Solutions," Fluid Dynamics Consultants Bureau, Division of Plenum Publishing Corp., N. Y., 1972.

Virk, P. S., "An Elastic Sublayer Model for Drag Reduction by Dilute Solutions of Linear Macromolecules," Journal of Fluid Mechanics, vol. 45, part 3, 1971, pp. 417-440.

Virk, P. S., and Merrill, E. W., "The Onset of Dilute Polymer Solution Phenomena," Viscous Drag Reduction, ed. C. S. Wells, New York: Plenum Press, 1969.

Virk, P. S., Mickley, H. S., and Smith, K. A., "The Ultimate Asymptote and Mean Flow Structure in Toms' Phenomenon," ASME Publication, 1971.

Virk, P. S., Merrill, E. W., Mickley, H. S., Smith, K. A., and Mollo-Christensen, E. L., "The Toms Phenomena: Turbulent Pipe Flow of Dilute Polymer Solutions," Journal of Fluid Mechanics, vol. 30, 1967, pp. 305-328.

Vlachos, N., A Statistical Analysis of Error in Laser Doppler Measurements Due to Velocity Gradients, International Report, Imperial College, Department of Mechanical Engineering, 1973.

Vogel, W. M., and Patterson, A. M., An Experimental Investigation of the Effect of Additives Injected into the Boundary Layer of an Underwater Body, Pacific Naval Laboratory Report, Victoria, British Columbia, Canada.

Wagner, W. B., and Pyczarek. J. A., "An Investigation of the Corner Secondary Flows Generated in Planar Nozzles," Journal of Fluids Engineering, September 1974, pp. 234-245.

Wallace, J. M., Eckelmann, H., and Brodkey, R. S., "The Wall Region in Turbulent Shear Flow," Submitted for publication in the Journal of Fluid Mechanics, July 1971.

Walsh, M., "On the Turbulent Flow of Dilute Polymer Solutions," Ph.D. Dissertation, California Institute of Technology, 1967, unpublished.

_____, "Theory of Drag Reduction in Dilute High-Polymer Flows," International Shipbuilding Progress, vol. 14, 1967, pp. 134-139.

Walters, R. R., Drag-Reducing Polymer Molecular Weight Effects on Turbulent Diffusion for Uniformly Distributed Polymer Injection, Report No. B-94300/4CR-11, Advanced Technology Center, Inc., Dallas, Texas, March 1974.

Walters, R. R., and Wells, C. S., Effects of Distributed Injection of Polymer Solutions of Turbulent Diffusion, Report No. B-94000/1CR-7, Advanced Technology Center, Inc., Dallas, Texas, March 1971.

Wang, C. P., and Snyder, D., "Laser Doppler Velocimetry: Experimental Study," Applied Optics, vol. 13, no. 1, January 1974, pp. 98-102.

Watson, H. J., Lewis, R. D., and Thornton, J. R., "Laser Doppler Velocimeter Measurements of Velocity Profile in Liquids," Technical Note R-224, Brown Engineering Research Labs, 1966.

Wells, C. S., "Anomalous Turbulent Flow of Non-Newtonian Fluids," AIAA Journal, vol. 3, no. 10, October 1965, pp. 1800-1805.

_____, "An Analysis of Uniform Injection of a Drag-Reducing Fluid into a Turbulent Boundary Layer," Paper presented at Symposium on Viscous Drag Reduction, Report No. 0-71100/8R-14, September 1968.

_____, "Turbulent Heat Transfer in Drag Reducing Fluids," AICHE Journal, vol. 14, no. 3, 1968, pp. 406-410.

_____, "The Use of Pipe Flow Correlations to Predict Turbulent Skin Friction for Drag-Reducing Fluids," Paper presented at the AIAA 2nd Advanced Marine Vehicles and Propulsion Meeting, Seattle, Washington, 21-23 May 1969.

Wells, C. S., and Spangler, J. G., "Effects of Local Injection of a Drag-Reducing Fluid in Turbulent Pipe Flow of a Newtonian Fluid," Physics of Fluids, vol. 10, no. 9, 1967, p. 1890.

Wells, C. S., and Spangler, J. G., "Injection of a Drag-Reducing Fluid into Turbulent Pipe Flow of a Newtonian Fluid," Physics of Fluids, vol. 10, no. 9, 1967, p. 91890.

Wells, C. S., Harkness J., and Meyer, W. A., "Turbulence Measurements in Pipe Flow of a Drag-Reducing Non-Newtonian Fluid," AIAA Journal, vol. 6, no. 2, February 1968, pp. 250-257.

Wetzel, J. M., and Ripken, J. P., Shear and Diffusion in a Large Boundary Layer Injected With Polymer Solution, Project Report No. 114, University of Minnesota, St. Anthony Falls Hydraulic Laboratory, February 1970.

Wetzel, J. M., and Tsai, F. Y., "Impact Tube Measurements in Dilute Solutions," AICHE Journal, vol. 14, 1968, p. 663.

Wetzel, J. M., Almo, J. A., and Killen, J. M., "Turbulence Measurements in Dilute Polymer Flows," University of Minnesota, Minneapolis, Minnesota, Proceedings of Symposium Turbulence Measurements in Liquids, University of Missouri at Rolla, 1969.

White, A., "Some Observations on the Flow Characteristics of Certain Dilute Macromolecular Solutions," Hendon College of Technology, London, 1966.

_____, "Turbulence and Drag Reduction With Polymer Additives," Research Bulletin, no. 4, Hendon College of Technology, London, January 1967.

White, F. M., "An Analysis of Flat-Plate Drag With Polymer Additives," Journal of Hydraulics, vol. 2, no. 4, October 1968.

_____, "Limitations on the Drag Reduction of External Bodies by Polymer Additives," AIAA 6th Aerospace Sciences Meeting, AIAA Paper No. 68-127, 1968.

_____, "Theory of Boundary-Layer Flow Noise With Applications to Pressure Gradients and Polymer Solutions," Journal of Hydraulics, vol. 3, no. 2, April 1969, pp. 95-99.

_____, "A New Integral Method for Analyzing the Turbulent Boundary Layer With Arbitrary Pressure Gradient," Journal of Basic Engineering, vol. 91, no. 3, September 1969, pp. 371-378.

_____, Viscous Fluid Flow, McGraw Hill Book Co., 1974.

White, F. M., and Christoph, G. H., "A Simple Theory for the Two-Dimensional Compressible Turbulent Boundary Layer," Transactions of the ASME, September 1972.

White, F. M., and Christoph, G. H., "A Simple Analysis of Two-Dimensional Turbulent Skin Friction With Arbitrary Wall and Freestream Conditions," Conference on Turbulent Shear Flows, Reprint No. 93, NATO, 1974.

White, F. M., Christoph, G. H., and Lessmann, R. C., "A Three-Dimensional Integral Method for Calculating Incompressible Turbulent Skin Friction," ASME Publication, no. 75-FE-26, February 1976.

White, F. M., Lessman, R. C., and Christoph, G. H., "A Simplified Approach to the Analysis of Turbulent Boundary Layers in Two and Three Dimensions," URI Contract No. F33615-71-C-1585, University of Rhode Island, 1971.

White, F. M., and Lessmann, R. C., and Christoph, G. H., "A Three-Dimensional Integral Method for Calculating Incompressible Turbulent Skin Friction," ASME Publication, no. 75-FE-26, February 1976.

White, F. M., Lessman, R. C., and Christoph, G. H., "Analysis of Turbulent Skin Friction in Thick Axisymmetric Boundary Layers," University of Rhode Island, Kingston, R. I., 1972.

White, W. D., and McEligot, E. M., "Transition of Mixtures of Polymers in a Dilute Aqueous Solution," Journal of Basic Engineering, vol. 92, 1970, pp. 411-418.

Whitelaw, J. H., "Measurement in Turbulent Water Flows by Laser Anemometry," Lecture presented at the Symposium on Turbulence in Liquids, University of Missouri at Rolla, 1973.

Whitsitt, N. F., Harrington, L. J., and Crawford, H. R., "Effect of Wall Shear Stress on Drag Reduction of Viscoelastic Solutions," Viscous Drag Reduction, ed. C. S. Wells, New York: Plenum Press, 1969.

Willmarth, W. W., and Lu, S. S., "Structure of the Reynolds Stress Near the Wall," Journal of Fluid Mechanics, vol. 55, no. 1, 1972, pp. 65-92.

Wilmhurst, T. H., "A Signal Simulator for Testing Laser-Doppler Fluid-Flow Velocimeter Systems," Journal of Physics E: Scientific Instruments, vol. 5, 1972, pp. 1205-1208.

Wolfshtein, M., "The Velocity and Temperature Distribution on One-Dimensional Flow With Turbulence Augmentation and Pressure Gradient" International Journal of Heat-Mass Transfer, vol. 12, 1967, pp. 301-318.

Wu, J., Drag Reduction in External Flows of Additive Solutions,
Technical Report 353-6, Hydronautics Incorporated, 1965.

_____, Suppressed Diffusion of Drag-Reducing Polymer in a
Turbulent Boundary Layer, Technical Report 353-8,
Hydronautics Incorporated, 1965.

Wu, J., and Tulin, M. P., Drag Reduction by Ejecting Additive
Solutions into a Pure-Water Boundary Layer, Technical Report
353-7, Hydronautics Incorporated, June 1970.

Wyler, J. S., "Probe Blockage Effects in Free Jets and Closed
Tunnels," Journal of Engineering for Power, October 1975, pp.
509-515.

Yanta, W. J., and Smith, R. A., "Measurements of Turbulent
Transport Properties With a Laser Doppler Velocimeter," AIAA
11th Aerospace Science Meeting, AIAA Paper 73-169, 10-12
January, 1973.

Yeh, Y., and Cummins, H. A., "Localized Fluid Flow Measurement
With an HeNe Laser Spectrometer," Applied Physics Letters vol.
4, 1964, pp. 176-178.

Young, A. D., The Calculation of the Total and Skin Friction
Drags of Bodies of Revolution at Zero Incidence, Report No.
B. A. 1533, Royal Aircraft Establishment, Farnborough, April
1939.

Zagustin, K., "Drag Reduction in Pipes and Channels Due to
Suspended Sediment," International Conference on Drag
Reduction, September 4-6, 1974.

Zakin, J. L., and Chang, J. L., "Polyoxyethylene Alcohol Non-
Ionic Surfactants as Drag-Reducing Additives," International
Conference on Drag Reduction, September 4-6, Paper D1, 1974.

